Biological therapy and tissue engineering approaches for the treatment of osteoarthritis

Inaugural dissertation

to

be awarded the degree of Dr. sc. med.
presented at
the Faculty of Medicine
of the University of Basel

by

Reihane Ziadlou

from Gorgan, Iran

2020

Approved by the Faculty of Medicine

On application of

Prof. Dr. Ivan Martin	(first supervisor)
PD Dr. Sibylle Grad	(second supervisor)
Dr. Laura Creemers	(external expert)
Prof. Dr. Mauro Alini	(further advisor)
Prof. Dr. Andrea Barbero	(further advisor)

Basel, June 22, 2020

Prof. Dr. Primo Leo Schär
Dean of the Medical Faculty

Table of Contents

Chapter 1

General introduction & thesis aims

1. General introduction

1.1 Cartilage and Osteoarthritis

Cartilage is a type of connective tissue that is abundantly present throughout different parts of the body and consists of chondrocyte cells embedded in a specifically composed extracellular matrix (ECM). Different classes of cartilage such as elastic cartilage, hyaline cartilage, fibrocartilage and articular cartilage are present at specific locations in the body where they perform a multitude of functions. All types of cartilage possess several key characteristics such as avascularity and slow tissue turnover rate. These properties severely impair the regenerative capacity of cartilage in cases of trauma [1]. Articular cartilage is a type of cartilage that is located at the interface of bones that are part of diarthrodial joints (Fig. 1A). The function of articular cartilage is to provide smooth movement of the joints through transmission of loads and for lubrication purposes [1]. The ability of articular cartilage to provide easy joint movement can be severely impaired when damage occurs by means of acute trauma (focal lesions) or by age-related degeneration (degenerative lesions). Due to the poor intrinsic regenerative capabilities that are characteristic to all types of cartilage, the preservation and health of articular cartilage are vital. Under normal conditions, healthy chondrocytes maintain a dynamic equilibrium between synthesis and degradation of extracellular matrix components. This equilibrium is characterized by a slow turnover of matrix synthesis and breakdown which is mediated by anabolic factors (growth factors) and matrix degrading enzymes, e.g. matrix metalloproteinases (MMPs). Additional regulators include tissue inhibitors of metalloproteinases (TIMPs), which balance the action of the MMPs.

In case of aberrant metabolic activity, ECM degradation occurs faster than ECM deposition by chondrocytes, resulting in damaged articular cartilage and developing into osteoarthritis (OA) [2,3]. Other genetic and environmental factors that contribute or promote the development of OA include obesity, ageing, and inflammation, which cause an imbalance between chondrocyte anabolism and catabolism and primarily affect articular cartilage in load bearing joints [4-6]. OA is the cause of approximately 50% of all musculoskeletal disease burdens and is affecting 30% of the elderly population [7,8]. Critically degenerating OA results in an increased friction between two opposing bones within the joint and generally leads to inflammation and pain upon movement or loading of the joints in general. Progressive OA can eventually lead to disabilities and complete loss of function of the affected joint [9].

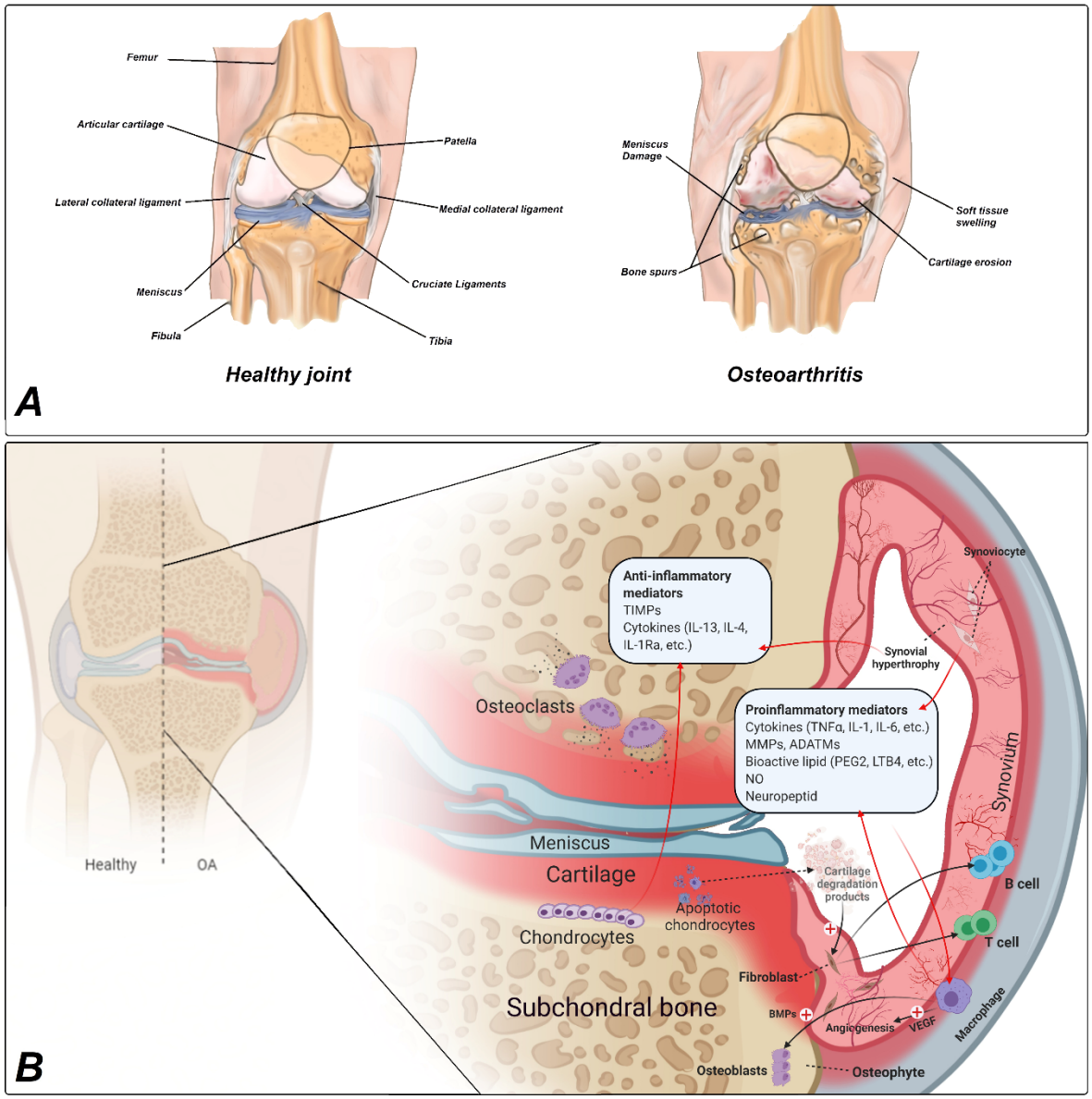

Figure 1. (A) Anatomy of a healthy and osteoarthritic knee joint. (B) Biochemical environment of an osteoarthritic joint showing the pro- and anti-inflammatory mediators involved in OA.

1.2 Pathophysiology of OA

Multiple pathological processes and phenotypes contribute to OA development [10]. Currently, inflammation is the primary factor associated with pathophysiology of OA which can cause cartilage loss alongside pain, swelling and stiffness [11]. Inflammation can be observed in the joints at the macroscopic level which is characterized by the enlargement of the synovial membrane due to infiltration of inflammatory cells [12]. Pro-inflammatory cytokines including interleukin 1 beta (IL1-β) and tumor necrosis factor alpha (TNF-α) produced by the

chondrocytes, synovial cells and osteoblasts (OB), are extensively abundant in OA joints; therefore these cytokines have also widely been used in vitro for mimicking the in vivo catabolic response [13-18]. It is known that these two cytokines and mechanical stress, activate several different signaling pathways including the Nuclear factor kappa-light-chain-enhancer of activated B cells (NF-κB), high-mobility group box 1 (HMGB1), interleukin-1 receptor (IL-1R)/Toll-like receptor (TLR), mitogen-activated protein kinases (MAPKs) and phosphoinositide-3-kinase/protein kinase B or Akt (PI3K/Akt) pathways [19-29]. NF-κB controls the expression of genes involved in several physiological and pathological responses such as inflammatory response. Activation of NF-κB canonical pathway can induce an increased expression of other pro-inflammatory cytokines (IL-6 and IL-8), cyclooxygenease-2 (COX-2), matrix degrading proteins, including MMPs and various types of a disintegrin and metalloproteinase with a thrombospondin type 1 motif (ADAMTS) and chemokines [30-32]. IL1-β and TNF-α also suppress the expression of anabolic cartilaginous markers such as type II collagen and aggrecan favoring the imbalance between the chondrocytes anabolic and catabolic activities [11,33,34].

Elevated catabolism of the ECM can increase the expression of proteolytic enzymes in the joint, including MMP1, -3 and -13, aggrecanase (ADAMTS4 and -5) which are responsible for ECM breakdown. Pro-inflammatory and pro-catabolic mediators, together with mechanical and oxidative stressors, decrease the performance and life cycle of chondrocytes, which can lead to hypertrophic differentiation, and senescence [35]. Products of cartilage breakdown that are released into the synovial fluid are phagocytosed by synovial cells, amplifying synovial inflammation [12]. In turn, inflamed synovium contains activate synovial cells that produce catabolic and proinflammatory mediators that lead to cartilage breakdown due to excessive production of the proteolytic enzymes. This process creates a positive feedback loop in which the inflammatory response is amplified due to the infiltration of macrophages into the synovium. To counteract this inflammatory response, chondrocytes and hypertrophic synovial tissues release anti-inflammatory mediators (i.e., IL-4, IL-13, IL-1Ra) and TIMPs which eventually lead to the modulation of inflammatory responses (Fig. 1B) [36]. However, the mechanism by which the inflammatory process is initiated in osteoarthritis is still unknown.

In order to treat degenerative OA, current treatment options are limited. While few pharmacological treatments are currently implemented to alleviate symptoms of early stage OA,

surgical intervention by means of allowing bone marrow intrusion into an articular defect or even a total joint replacement is considered the only treatment option for progressed OA joints. Total joint replacement is a common orthopaedic procedure with 1.26 million surgeries projected to take place in the U.S. in 2030 and associated costs of 50 billion US dollars [37]. Therefore, preservation of healthy articular cartilage and prevention of onset of OA are clinically relevant goals that would alleviate healthcare costs and improve the patient's quality of life.

1.3 Bioactive factors for treatment or alleviation of OA

Administration of non-steroidal anti-inflammatory drugs (NSAIDs) is considered to be mainly a short-term palliative treatment with adverse gastrointestinal and cardiovascular effects and a high variation of patient responses [38-40]. Intraarticular injection of glucocorticoids is another method to reduce pain symptoms with short term effects [41]. Growth factors (GFs) including transforming growth factor beta (TGF-β) and insulin-like growth factor 1 (IGF-1) also have shown positive anabolic effects in several studies [42,43]. However, the use of growth factors has several limitations, including enzymatic disruption, degradation due to its short half-life, inhibition of its function by binding proteins, their relatively large size, their potential toxicity and lack of cost effective methods for producing recombinant GFs at the required doses [44]. In addition, the optimal dose and delivery to ensure both safety and efficacy of growth factors are still a matter of debate. Also, the use of some supplements like glucosamine and chondroitin in clinical studies showed inconsistent and non-significant effects in the treatment of OA [45,46]. It is known that many of the anti-inflammatory drugs in our current pharmacopoeia have originated from herbal extracts [47,48]. In the recent years, several herbal and synthetic small molecules which were more potent than natural supplements (glucosamine) and could circumvent the side effects of NSAIDs, have been attributed a great potential for OA therapy (Fig. 2) [49-52]. Some of these compounds with herbal origins can act through specific signaling pathways and inhibit inflammation or increase matrix synthesis [53-56]. In addition, extracts of Traditional Chinese Medicine (TCM) herbs have been investigated for their anti-inflammatory, anti-catabolic and anabolic effects through blockage or activation of different signaling pathways including NFκB, TLR4, Wnt/β-catenin, MAPK and TGF-β/Smads signaling listed in the Table 1.

Table 1. TCM small molecules and their anti-inflammatory, anti-catabolic and anabolic effects through inhibition or activation of different signaling pathways.

Compound (TCM)	Pathways/Mechanisms	References
Curcumin	TLR4/MyD88/NF-κB	[57]
Resveratrol	NF-κB and AP-1	[58]
Amurensin H	TLR4/Syk/NF-κB	[59]
Paeonol	PI3K/Akt/NF-κB	[60]
Trans-Cinnamaldehyde	NF-κB and p38-JNK	[61]
Nobiletin	PI3K/AKT/NF-κB	[62]
Ligustrazine	SOX9/NF-κB	[63]
Crocin	NF-κB	[64]
Piperine	NF-κB	[65]
Leonurine	NF-κB	[66]
Scutellarin	NF-κB and Nrf2/HO-1	[67]
Isofraxidin	NF-κB	[68]
Juglanin	NF-κB	[69]
Oxymatrine	NF-κB and MAPK	[70]
Hinokitiol	Wnt/β-catenin	[71]
Tetrandrine	Wnt/β-catenin	[72]
Polygalacic acid	Wnt/β-catenin and MAPK	[73]
Icariin	Wnt/β-catenin and MAPK	[74]
Zingerone	p38 and JNK/MAPK	[75]
Geniposide	p38/MAPK	[76]
Halofuginone	TGF-β/Smads	[77]
Celastrol	SDF-1/CXCR4	[78]
Wogonin	ROS/ERK/Nrf2	[79]

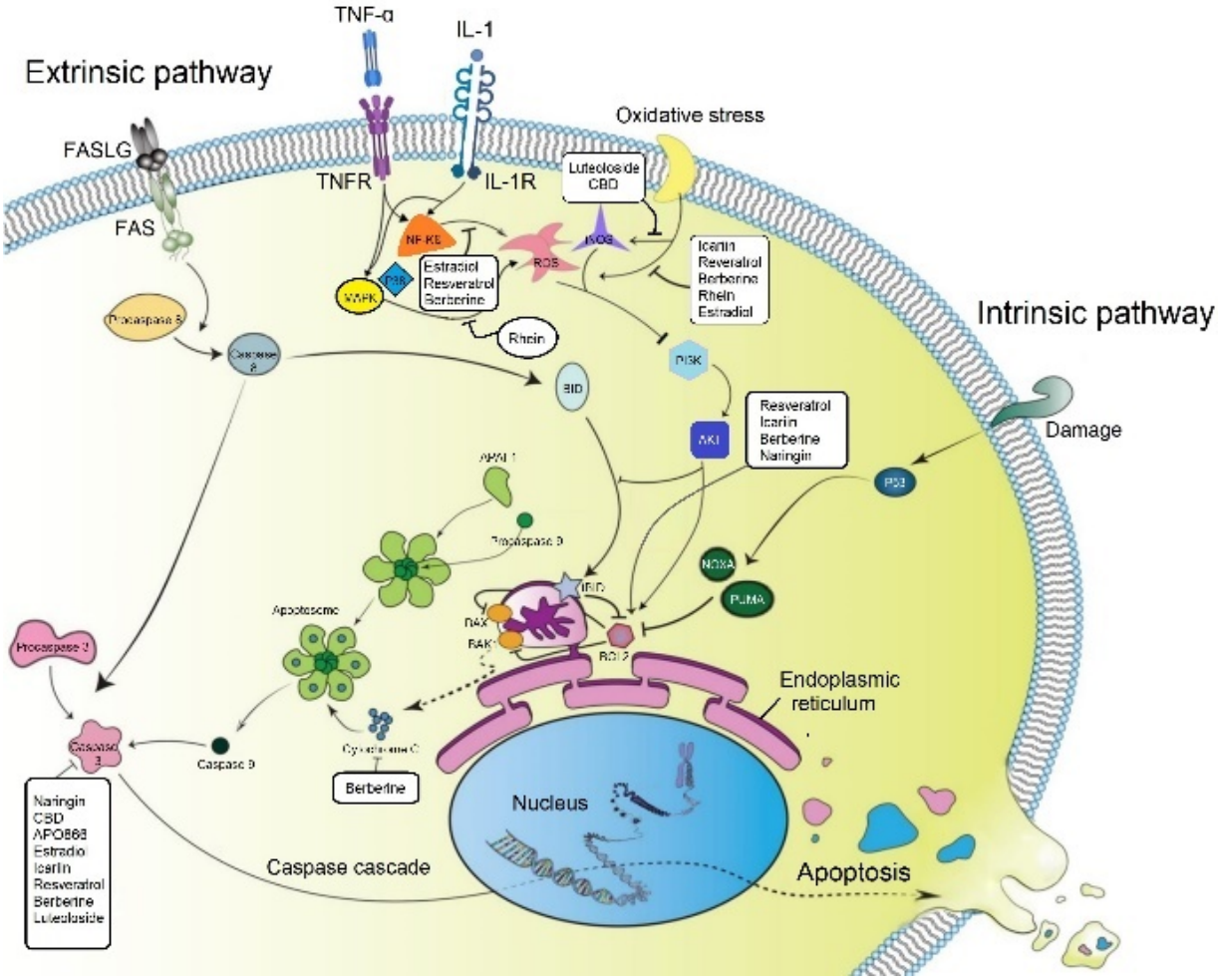

Figure 2. Inhibition of IL-1 and TNF-α induced signaling pathways by small molecules.

1.4 Local delivery for treatments of OA

For avascular tissues such as cartilage, local delivery of the drugs is a highly efficient approach compared to parental or intravenous administrations. Likewise, for cellular therapies, local delivery is also the preferred strategy and is part of the general tissue engineering paradigm. In order to deliver drugs and cells in a minimally invasive manner to OA joints, injectability of the drug- or cell-laden biomaterials is a significant advantage. Biomaterial have been developed to have a sustained and controllable drug release in the joints to reduce the necessity for frequent injections, while showing minimal adverse side effects [80-82]. Furthermore, biomaterials have been used to construct supporting environment for the cells to produce matrix and to regenerate the damaged cartilage [83]. Hydrogels make for an excellent class of biomaterials for local treatment of OA cartilage, representing a good mimicking structure for cartilage tissue as a

hydrated solid [84-86]. The tunability of hydrogel structures in terms of stiffness, degradability and polymer density is considered a major advantage of implementing hydrogel for cartilage drug delivery or cell therapy [87-89]. Hydrogels can also be classified based on the type of polymers incorporated in the hydrogel, namely synthetic or natural hydrogels. Among the synthetic polymers poly-ethylene glycol (PEG) have been extensively utilized in cartilage regeneration supporting matrix deposition and cartilage tissue engineering [90]. However, these hydrogels are non-biodegradable and do not recapitulate the chemical and biological features of native cartilage ECM. Natural hydrogels are biodegradable and mainly consist of proteins and polysaccharides. Natural polysaccharides such as chitosan, alginate, agarose and hyaluronic acid (HA) and protein-based materials, such as collagen, gelatin and silk-fibroin are used as injectable hydrogels for drug delivery or tissue engineering purposes. Natural hydrogels are very biocompatible and biodegradable, and they can mimic the extracellular environment [91,92].

Hyaluronic acid (HA) is a biopolymer that is abundantly present in articular cartilage and is part of the ECM composition, providing mechanical support in a water rich environment. Since inflammatory cytokines are abundant in the OA joint, having a hydrogel with natural anti-inflammatory properties is of great interest. HA has anti-inflammatory properties and its intraarticular injection showed effective and temporary pain reduction [93,94]. While the effect of HA injection is usually temporary, combining it with anti-inflammatory drugs showed longer term effects [93,95]. HA is very fast degradable and even after functionalizing HA with tyramine, the material was degraded over a month after implantation [96]; furthermore, its mechanical properties are sub-optimal for applications in cartilage tissue engineering [97]. Therefore, combining it with a material with lower degradation rate is hypothesized to improve long-term tissue engineering applications and prolonged drug release in the joints.

Silk-fibroin (SF) as natural protein derived from *Bombyx mori* (*B. mori*) cocoons can form biocompatible hydrogels with adequate mechanical strength and slow rate of degradation which make it a suitable matrix for the long-term drug delivery and tissue engineering approaches [98-101]. However, enzymatic crosslinking of SF is slow, which could result in poor homogeneity of cell encapsulation in tissue engineering hydrogels. Additionally, the mechanical properties of crosslink SF hydrogels are prone to change due to the formation of β-sheet secondary structures making for an unsuitable environment for embedded cells [102]. Thus, the

combination of SF with HA-based materials, such as HA-Tyramine, into a composite hydrogel is expected to make for a good candidate for cartilage tissue engineering and articular drug delivery.

2. Aims of the Thesis

The first aim of this thesis is to investigate the potential of 34 herbal small molecules extracted from Traditional Chinese Medicine (TCM) in attenuation of inflammation and regeneration of cartilage. The second aim is to perform RNA sequencing in order to analyze the transcriptome of gene expression patterns of IL-1β/TNF-α treated OA chondrocytes in presence or absence of the six most potent compounds identified in the first aim of the thesis. These compounds are additionally assayed for their capacity to modulate the transcription and translation of key catabolic and anabolic factors. We then selectively investigate the mechanisms regulating the anti-inflammatory and pro-anabolic effects of the two most effective compounds Vanillic acid (VA) and Epimedin C (Epi C). As the final aim we combine different concentrations of HA-Tyramine (HA) with aqueous silk-fibroin (SF) solutions, establishing a tunable and injectable hydrogel for cartilage tissue engineering and drug delivery purposes. Upon enzymatic crosslinking, the gelation and mechanical properties of cell-free and cell-laden HA/SF hydrogels are characterized over time. The release of encapsulated VA and Epi C in different HA/SF composite hydrogels are assessed in vitro. Chondrocyte embedded in HA/SF composite hydrogels are studied in terms of cell viability, phenotypic behavior and ECM production to find the most suitable HA/SF hydrogels for applications in cartilage tissue engineering.

3. Outline of the Thesis

In **Chapter 2**, the anti-catabolic and anti-inflammatory effects of 34 herbal compounds extracted from XLGB capsules were examined biochemically and histologically. Six herbal compounds were identified that showed significant anti-catabolic and anti-inflammatory effects and increased presence of ECM components in an inflammation induced 3D human chondrocyte pellet culture model.

Chapter 3 describes an *ex-vivo* study in human OA cartilage which the six previously identified herbal compounds were assessed for their capacity to modulate the key catabolic and anabolic factors. The mechanism of action of the two most potent compounds Vanillic acid (VA) and Epimedin C (Epi C) were investigated. Ingenuity Pathway Analysis confirmed that

osteoarthritic signaling pathways were inhibited when VA and Epi C were included in the culture conditions.

In **Chapter 4** the preparation of enzymatically crosslinked HA/SF hydrogels loaded with chondrocytes and herbal compounds is described. The effect of altering HA-Tyr and SF ratios within the hydrogel on gelation time, ECM deposition and cell behavior were tested. The empty and cell loaded hydrogels were mechanically characterized after extensive culture periods. Additionally, HA/SF hydrogels allowed for sustained release of VA and Epi C, showing that the HA/SF hydrogel system could act as a carrier material for cartilage tissue engineering and drug delivery.

Chapter 5 consists of a literature overview of animal models of osteochondral defects that can be utilized to study *in vivo* cartilage regeneration. Parallels with OA *in vivo* models can be made. This chapter acts as a justification for any *in vivo* experiments that might follow from the promising *in vitro* results presented in the previous chapters.

Finally, in **Chapter 6** the findings of this thesis are discussed considering the broader perspective of OA treatment. The future prospective of this work and regenerative cartilage treatments are presented.

4. References

1. Krishnan, Y.; Grodzinsky, A.J. Cartilage diseases. Matrix Biol 2018, 71-72, 51-69, doi:10.1016/j.matbio.2018.05.005.
2. Goldring, M.B.; Marcu, K.B. Cartilage homeostasis in health and rheumatic diseases. Arthritis research & therapy 2009, 11, 224-224, doi:10.1186/ar2592.
3. Wang, M.; Shen, J.; Jin, H.; Im, H.J.; Sandy, J.; Chen, D. Recent progress in understanding molecular mechanisms of cartilage degeneration during osteoarthritis. Ann N Y Acad Sci 2011, 1240, 61-69, doi:10.1111/j.1749-6632.2011.06258.x.
4. Carames, B.; Taniguchi, N.; Otsuki, S.; Blanco, F.J.; Lotz, M. Autophagy is a protective mechanism in normal cartilage, and its aging-related loss is linked with cell death and osteoarthritis. Arthritis Rheum 2010, 62, 791-801, doi:10.1002/art.27305.
5. Loeser, R.F. Age-related changes in the musculoskeletal system and the development of osteoarthritis. Clin Geriatr Med 2010, 26, 371-386, doi:10.1016/j.cger.2010.03.002.
6. Clockaerts, S.; Bastiaansen-Jenniskens, Y.M.; Runhaar, J.; Van Osch, G.J.; Van Offel, J.F.; Verhaar, J.A.; De Clerck, L.S.; Somville, J. The infrapatellar fat pad should be considered as an active osteoarthritic

joint tissue: a narrative review. Osteoarthritis and cartilage 2010, 18, 876-882, doi:10.1016/j.joca.2010.03.014.

7. Kotlarz, H.; Gunnarsson, C.L.; Fang, H.; Rizzo, J.A. Insurer and out-of-pocket costs of osteoarthritis in the US: evidence from national survey data. Arthritis Rheum 2009, 60, 3546-3553, doi:10.1002/art.24984.

8. Pereira, D.; Peleteiro, B.; Araujo, J.; Branco, J.; Santos, R.A.; Ramos, E. The effect of osteoarthritis definition on prevalence and incidence estimates: a systematic review. Osteoarthritis and cartilage 2011, 19, 1270-1285, doi:10.1016/j.joca.2011.08.009.

9. Martel-Pelletier, J.; Barr, A.J.; Cicuttini, F.M.; Conaghan, P.G.; Cooper, C.; Goldring, M.B.; Goldring, S.R.; Jones, G.; Teichtahl, A.J.; Pelletier, J.-P. Osteoarthritis. Nature Reviews Disease Primers 2016, 2, 16072, doi:10.1038/nrdp.2016.72.

10. Mobasheri, A.; Batt, M. An update on the pathophysiology of osteoarthritis. Annals of physical and rehabilitation medicine 2016, 59, 333-339.

11. Goldring, M.B.; Otero, M. Inflammation in osteoarthritis. Curr Opin Rheumatol 2011, 23, 471-478, doi:10.1097/BOR.0b013e328349c2b1.

12. Scanzello, C.R.; Goldring, S.R. The role of synovitis in osteoarthritis pathogenesis. Bone 2012, 51, 249-257, doi:10.1016/j.bone.2012.02.012.

13. Wojdasiewicz, P.; Poniatowski Ł, A.; Szukiewicz, D. The role of inflammatory and anti-inflammatory cytokines in the pathogenesis of osteoarthritis. Mediators of inflammation 2014, 2014, 561459, doi:10.1155/2014/561459.

14. Melchiorri, C.; Meliconi, R.; Frizziero, L.; Silvestri, T.; Pulsatelli, L.; Mazzetti, I.; Borzi, R.M.; Uguccioni, M.; Facchini, A. Enhanced and coordinated in vivo expression of inflammatory cytokines and nitric oxide synthase by chondrocytes from patients with osteoarthritis. Arthritis Rheum 1998, 41, 2165-2174, doi:10.1002/1529-0131(199812)41:12<2165::aid-art11>3.0.co;2-o.

15. de Lange-Brokaar, B.J.; Ioan-Facsinay, A.; van Osch, G.J.; Zuurmond, A.M.; Schoones, J.; Toes, R.E.; Huizinga, T.W.; Kloppenburg, M. Synovial inflammation, immune cells and their cytokines in osteoarthritis: a review. Osteoarthritis and cartilage 2012, 20, 1484-1499, doi:10.1016/j.joca.2012.08.027.

16. Massicotte, F.; Lajeunesse, D.; Benderdour, M.; Pelletier, J.P.; Hilal, G.; Duval, N.; Martel-Pelletier, J. Can altered production of interleukin-1beta, interleukin-6, transforming growth factor-beta and prostaglandin E(2) by isolated human subchondral osteoblasts identify two subgroups of osteoarthritic patients. Osteoarthritis and cartilage 2002, 10, 491-500, doi:10.1053/joca.2002.0528.

17. Farahat, M.N.; Yanni, G.; Poston, R.; Panayi, G.S. Cytokine expression in synovial membranes of patients with rheumatoid arthritis and osteoarthritis. Annals of the rheumatic diseases 1993, 52, 870-875, doi:10.1136/ard.52.12.870.

18. Sebastian Müller, L.A., Xiaomei Wang, M. Zia Karim, Ajay Matta, Arne Mehrkens,; Stefan Schaeren, S.F., Marcel Jakob, Ivan Martin, Andrea Barbero, W. Mark Erwin. Notochordal cell conditioned medium (NCCM) regenerates end-stage human osteoarthritic articular chondrocytes and promotes a healthy phenotype. Arthritis research & therapy 2016, 18.

19. van Loo, G.; Beyaert, R. Negative regulation of NF-kappaB and its involvement in rheumatoid arthritis. Arthritis research & therapy 2011, 13, 221, doi:10.1186/ar3324.

20. Kumar, S.; Boehm, J.; Lee, J.C. p38 MAP kinases: key signalling molecules as therapeutic targets for inflammatory diseases. Nat Rev Drug Discov 2003, 2, 717-726, doi:10.1038/nrd1177.

21. Loeser, R.F.; Erickson, E.A.; Long, D.L. Mitogen-activated protein kinases as therapeutic targets in osteoarthritis. Current opinion in rheumatology 2008, 20, 581-586, doi:10.1097/BOR.0b013e3283090463.

22. Andersson, U.; Erlandsson-Harris, H. HMGB1 is a potent trigger of arthritis. J Intern Med 2004, 255, 344-350, doi:10.1111/j.1365-2796.2003.01303.x.

23. Wang, H.; Bloom, O.; Zhang, M.; Vishnubhakat, J.M.; Ombrellino, M.; Che, J.; Frazier, A.; Yang, H.; Ivanova, S.; Borovikova, L., et al. HMG-1 as a late mediator of endotoxin lethality in mice. Science (New York, N.Y.) 1999, 285, 248-251, doi:10.1126/science.285.5425.248.

24. Taniguchi, N.; Kawahara, K.; Yone, K.; Hashiguchi, T.; Yamakuchi, M.; Goto, M.; Inoue, K.; Yamada, S.; Ijiri, K.; Matsunaga, S., et al. High mobility group box chromosomal protein 1 plays a role in the pathogenesis of rheumatoid arthritis as a novel cytokine. Arthritis Rheum 2003, 48, 971-981, doi:10.1002/art.10859.

25. Biscetti, F.; Flex, A.; Alivernini, S.; Tolusso, B.; Gremese, E.; Ferraccioli, G. The Role of High-Mobility Group Box-1 and Its Crosstalk with Microbiome in Rheumatoid Arthritis. Mediators of inflammation 2017, 2017, 5230374, doi:10.1155/2017/5230374.

26. Thalhamer, T.; McGrath, M.A.; Harnett, M.M. MAPKs and their relevance to arthritis and inflammation. Rheumatology 2008, 47, 409-414, doi:10.1093/rheumatology/kem297.

27. Feng, G.J.; Goodridge, H.S.; Harnett, M.M.; Wei, X.Q.; Nikolaev, A.V.; Higson, A.P.; Liew, F.Y. Extracellular signal-related kinase (ERK) and p38 mitogen-activated protein (MAP) kinases differentially regulate the lipopolysaccharide-mediated induction of inducible nitric oxide synthase and IL-12 in macrophages: Leishmania phosphoglycans subvert macrophage IL-12 production by targeting ERK MAP kinase. J Immunol 1999, 163, 6403-6412.

28. Brennan, F.M.; McInnes, I.B. Evidence that cytokines play a role in rheumatoid arthritis. The Journal of clinical investigation 2008, 118, 3537-3545, doi:10.1172/jci36389.

29. Mariani, E.; Pulsatelli, L.; Facchini, A. Signaling pathways in cartilage repair. International journal of molecular sciences 2014, 15, 8667-8698, doi:10.3390/ijms15058667.

30. Hayden, M.S.; Ghosh, S. NF-kappaB, the first quarter-century: remarkable progress and outstanding questions. Genes Dev 2012, 26, 203-234, doi:10.1101/gad.183434.111.

31. Tak, P.P.; Firestein, G.S. NF-kappaB: a key role in inflammatory diseases. The Journal of clinical investigation 2001, 107, 7-11, doi:10.1172/jci11830.

32. Lawrence, T. The nuclear factor NF-kappaB pathway in inflammation. Cold Spring Harb Perspect Biol 2009, 1, a001651, doi:10.1101/cshperspect.a001651.

33. Maldonado, M.; Nam, J. The role of changes in extracellular matrix of cartilage in the presence of inflammation on the pathology of osteoarthritis. BioMed research international 2013, 2013, 284873, doi:10.1155/2013/284873.

34. Liacini, A.; Sylvester, J.; Li, W.Q.; Huang, W.; Dehnade, F.; Ahmad, M.; Zafarullah, M. Induction of matrix metalloproteinase-13 gene expression by TNF-alpha is mediated by MAP kinases, AP-1, and NF-kappaB transcription factors in articular chondrocytes. Experimental cell research 2003, 288, 208-217, doi:10.1016/s0014-4827(03)00180-0.

35. Mobasheri, A.; Batt, M. An update on the pathophysiology of osteoarthritis. Annals of physical and rehabilitation medicine 2016, 59, 333-339, doi:10.1016/j.rehab.2016.07.004.

36. Sellam, J.; Berenbaum, F. The role of synovitis in pathophysiology and clinical symptoms of osteoarthritis. Nature reviews. Rheumatology 2010, 6, 625-635, doi:10.1038/nrrheum.2010.159.

37. Sloan, M.; Premkumar, A.; Sheth, N.P. Projected Volume of Primary Total Joint Arthroplasty in the U.S., 2014 to 2030. The Journal of bone and joint surgery. American volume 2018, 100, 1455-1460, doi:10.2106/jbjs.17.01617.

38. Wieland, H.A.; Michaelis, M.; Kirschbaum, B.J.; Rudolphi, K.A. Osteoarthritis - an untreatable disease? Nat Rev Drug Discov 2005, 4, 331-344, doi:10.1038/nrd1693.

39. Williams, A.; Kamper, S.J.; Wiggers, J.H.; O'Brien, K.M.; Lee, H.; Wolfenden, L.; Yoong, S.L.; Robson, E.; McAuley, J.H.; Hartvigsen, J., et al. Musculoskeletal conditions may increase the risk of chronic disease: a systematic review and meta-analysis of cohort studies. BMC Med 2018, 16, 167, doi:10.1186/s12916-018-1151-2.

40. Marcacci, M.; Filardo, G.; Kon, E. Treatment of cartilage lesions: what works and why? Injury 2013, 44 Suppl 1, S11-15, doi:10.1016/s0020-1383(13)70004-4.

41. Richter, D.L.; Schenck, R.C., Jr.; Wascher, D.C.; Treme, G. Knee Articular Cartilage Repair and Restoration Techniques: A Review of the Literature. Sports health 2016, 8, 153-160, doi:10.1177/1941738115611350.

42. Ahearne, M.; Kelly, D.J. A comparison of fibrin, agarose and gellan gum hydrogels as carriers of stem cells and growth factor delivery microspheres for cartilage regeneration. Biomed Mater 2013, 8, 035004, doi:10.1088/1748-6041/8/3/035004.

43. Kim, K.; Lam, J.; Lu, S.; Spicer, P.P.; Lueckgen, A.; Tabata, Y.; Wong, M.E.; Jansen, J.A.; Mikos, A.G.; Kasper, F.K. Osteochondral tissue regeneration using a bilayered composite hydrogel with modulating dual growth factor release kinetics in a rabbit model. Journal of controlled release : official journal of the Controlled Release Society 2013, 168, 166-178, doi:10.1016/j.jconrel.2013.03.013.

44. Wakefield, L.M.; Winokur, T.S.; Hollands, R.S.; Christopherson, K.; Levinson, A.D.; Sporn, M.B. Recombinant latent transforming growth factor beta 1 has a longer plasma half-life in rats than active transforming growth factor beta 1, and a different tissue distribution. The Journal of clinical investigation 1990, 86, 1976-1984, doi:10.1172/jci114932.

45. Clegg, D.O.; Reda, D.J.; Harris, C.L.; Klein, M.A.; O'Dell, J.R.; Hooper, M.M.; Bradley, J.D.; Bingham, C.O., 3rd; Weisman, M.H.; Jackson, C.G., et al. Glucosamine, chondroitin sulfate, and the two in combination for painful knee osteoarthritis. N Engl J Med 2006, 354, 795-808, doi:10.1056/NEJMoa052771.

46. Henrotin, Y.; Mobasheri, A. Natural Products for Promoting Joint Health and Managing Osteoarthritis. Curr Rheumatol Rep 2018, 20, 72, doi:10.1007/s11926-018-0782-9.

47. Rainsford, K.D. Anti-inflammatory drugs in the 21st century. Subcell Biochem 2007, 42, 3-27.

48. Kopp, E.; Ghosh, S. Inhibition of NF-kappa B by sodium salicylate and aspirin. Science (New York, N.Y.) 1994, 265, 956-959.

49. Shi, Y.; Hu, X.; Cheng, J.; Zhang, X.; Zhao, F.; Shi, W.; Ren, B.; Yu, H.; Yang, P.; Li, Z., et al. A small molecule promotes cartilage extracellular matrix generation and inhibits osteoarthritis development. Nat Commun 2019, 10, 1914, doi:10.1038/s41467-019-09839-x.

50. Johnson, K.; Zhu, S.; Tremblay, M.S.; Payette, J.N.; Wang, J.; Bouchez, L.C.; Meeusen, S.; Althage, A.; Cho, C.Y.; Wu, X., et al. A stem cell-based approach to cartilage repair. Science (New York, N.Y.) 2012, 336, 717-721, doi:10.1126/science.1215157.

51. Yano, F.; Hojo, H.; Ohba, S.; Fukai, A.; Hosaka, Y.; Ikeda, T.; Saito, T.; Hirata, M.; Chikuda, H.; Takato, T., et al. A novel disease-modifying osteoarthritis drug candidate targeting Runx1. Annals of the rheumatic diseases 2013, 72, 748-753, doi:10.1136/annrheumdis-2012-201745.

52. Cai, G.; Liu, W.; He, Y.; Huang, J.; Duan, L.; Xiong, J.; Liu, L.; Wang, D. Recent advances in kartogenin for cartilage regeneration. J Drug Target 2019, 27, 28-32, doi:10.1080/1061186x.2018.1464011.

53. Zhu, F.; Ma, X.H.; Qin, C.; Tao, L.; Liu, X.; Shi, Z.; Zhang, C.L.; Tan, C.Y.; Chen, Y.Z.; Jiang, Y.Y. Drug discovery prospect from untapped species: indications from approved natural product drugs. PLoS One 2012, 7, e39782, doi:10.1371/journal.pone.0039782.

54. Newman, D.J.; Cragg, G.M.; Snader, K.M. Natural products as sources of new drugs over the period 1981-2002. J Nat Prod 2003, 66, 1022-1037, doi:10.1021/np030096l.

55. Mobasheri, A. The future of osteoarthritis therapeutics: emerging biological therapy. Curr Rheumatol Rep 2013, 15, 385, doi:10.1007/s11926-013-0385-4.

56. Kim, J.H.; Kismali, G.; Gupta, S.C. Natural Products for the Prevention and Treatment of Chronic Inflammatory Diseases: Integrating Traditional Medicine into Modern Chronic Diseases Care. Evid Based Complement Alternat Med 2018, 2018, 9837863, doi:10.1155/2018/9837863.

57. Zhang, Y.; Zeng, Y. Curcumin reduces inflammation in knee osteoarthritis rats through blocking TLR4 /MyD88/NF-kappaB signal pathway. Drug Dev Res 2019, 80, 353-359, doi:10.1002/ddr.21509.

58. Liu, F.C.; Hung, L.F.; Wu, W.L.; Chang, D.M.; Huang, C.Y.; Lai, J.H.; Ho, L.J. Chondroprotective effects and mechanisms of resveratrol in advanced glycation end products-stimulated chondrocytes. Arthritis Res Ther 2010, 12, R167, doi:10.1186/ar3127.

59. Ma, P.; Yue, L.; Yang, H.; Fan, Y.; Bai, J.; Li, S.; Yuan, J.; Zhang, Z.; Yao, C.; Lin, M., et al. Chondroprotective and anti-inflammatory effects of amurensin H by regulating TLR4/Syk/NF-kappaB signals. J Cell Mol Med 2020, 24, 1958-1968, doi:10.1111/jcmm.14893.

60. Lou, Y.; Wang, C.; Tang, Q.; Zheng, W.; Feng, Z.; Yu, X.; Guo, X.; Wang, J. Paeonol Inhibits IL-1beta-Induced Inflammation via PI3K/Akt/NF-kappaB Pathways: In Vivo and Vitro Studies. Inflammation 2017, 40, 1698-1706, doi:10.1007/s10753-017-0611-8.

61. Xia, T.; Gao, R.; Zhou, G.; Liu, J.; Li, J.; Shen, J. Trans-Cinnamaldehyde Inhibits IL-1beta-Stimulated Inflammation in Chondrocytes by Suppressing NF-kappaB and p38-JNK Pathways and Exerts Chondrocyte Protective Effects in a Rat Model of Osteoarthritis. BioMed research international 2019, 2019, 4039472, doi:10.1155/2019/4039472.

62. Xie, L.; Xie, H.; Chen, C.; Tao, Z.; Zhang, C.; Cai, L. Inhibiting the PI3K/AKT/NF-kappaB signal pathway with nobiletin for attenuating the development of osteoarthritis: in vitro and in vivo studies. Food Funct 2019, 10, 2161-2175, doi:10.1039/c8fo01786g.

63. Yu, T.; Qu, J.; Wang, Y.; Jin, H. Ligustrazine protects chondrocyte against IL-1beta induced injury by regulation of SOX9/NF-kappaB signaling pathway. J Cell Biochem 2018, 119, 7419-7430, doi:10.1002/jcb.27051.

64. Ding, Q.; Zhong, H.; Qi, Y.; Cheng, Y.; Li, W.; Yan, S.; Wang, X. Anti-arthritic effects of crocin in interleukin-1beta-treated articular chondrocytes and cartilage in a rabbit osteoarthritic model. Inflamm Res 2013, 62, 17-25, doi:10.1007/s00011-012-0546-3.

65. Ying, X.; Chen, X.; Cheng, S.; Shen, Y.; Peng, L.; Xu, H.Z. Piperine inhibits IL-beta induced expression of inflammatory mediators in human osteoarthritis chondrocyte. Int Immunopharmacol 2013, 17, 293-299, doi:10.1016/j.intimp.2013.06.025.

66. Yin, W.; Lei, Y. Leonurine inhibits IL-1beta induced inflammation in murine chondrocytes and ameliorates murine osteoarthritis. Int Immunopharmacol 2018, 65, 50-59, doi:10.1016/j.intimp.2018.08.035.

67. Luo, Z.; Hu, Z.; Bian, Y.; Su, W.; Li, X.; Li, S.; Wu, J.; Shi, L.; Song, Y.; Zheng, G., et al. Scutellarin Attenuates the IL-1beta-Induced Inflammation in Mouse Chondrocytes and Prevents Osteoarthritic Progression. Front Pharmacol 2020, 11, 107, doi:10.3389/fphar.2020.00107.

68. Lin, J.; Li, X.; Qi, W.; Yan, Y.; Chen, K.; Xue, X.; Xu, X.; Feng, Z.; Pan, X. Isofraxidin inhibits interleukin-1beta induced inflammatory response in human osteoarthritis chondrocytes. Int Immunopharmacol 2018, 64, 238-245, doi:10.1016/j.intimp.2018.09.003.

69. Chen, X.; Zhang, C.; Wang, X.; Huo, S. Juglanin inhibits IL-1beta-induced inflammation in human chondrocytes. Artif Cells Nanomed Biotechnol 2019, 47, 3614-3620, doi:10.1080/21691401.2019.1657877.

70. Jiang, Y.; Sang, W.; Wang, C.; Lu, H.; Zhang, T.; Wang, Z.; Liu, Y.; Xue, B.; Xue, S.; Cai, Z., et al. Oxymatrine exerts protective effects on osteoarthritis via modulating chondrocyte homoeostasis and suppressing osteoclastogenesis. J Cell Mol Med 2018, 10.1111/jcmm.13674, doi:10.1111/jcmm.13674.

71. Li, J.; Zhou, X.D.; Yang, K.H.; Fan, T.D.; Chen, W.P.; Jiang, L.F.; Bao, J.P.; Wu, L.D.; Xiong, Y. Hinokitiol reduces matrix metalloproteinase expression by inhibiting Wnt/beta-Catenin signaling in vitro and in vivo. Int Immunopharmacol 2014, 23, 85-91, doi:10.1016/j.intimp.2014.08.012.

72. Zhou, X.; Li, W.; Jiang, L.; Bao, J.; Tao, L.; Li, J.; Wu, L. Tetrandrine Inhibits the Wnt/ beta -Catenin Signalling Pathway and Alleviates Osteoarthritis: An In Vitro and In Vivo Study. Evid Based Complement Alternat Med 2013, 2013, 809579, doi:10.1155/2013/809579.

73. Xu, K.; Ma, C.; Xu, L.; Ran, J.; Jiang, L.; He, Y.; Adel Abdo Moqbel, S.; Wang, Z.; Wu, L. Polygalacic acid inhibits MMPs expression and osteoarthritis via Wnt/beta-catenin and MAPK signal pathways suppression. Int Immunopharmacol 2018, 63, 246-252, doi:10.1016/j.intimp.2018.08.013.

74. Zeng, L.; Wang, W.; Rong, X.F.; Zhong, Y.; Jia, P.; Zhou, G.Q.; Li, R.H. Chondroprotective effects and multi-target mechanisms of Icariin in IL-1 beta-induced human SW 1353 chondrosarcoma cells and a rat osteoarthritis model. Int Immunopharmacol 2014, 18, 175-181, doi:10.1016/j.intimp.2013.11.021.

75. Ruangsuriya, J.; Budprom, P.; Viriyakhasem, N.; Kongdang, P.; Chokchaitaweesuk, C.; Sirikaew, N.; Chomdej, S.; Nganvongpanit, K.; Ongchai, S. Suppression of Cartilage Degradation by Zingerone Involving the p38 and JNK MAPK Signaling Pathway. Planta Med 2017, 83, 268-276, doi:10.1055/s-0042-113387.

76. Chen, Y.; Shou, K.; Gong, C.; Yang, H.; Yang, Y.; Bao, T. Anti-Inflammatory Effect of Geniposide on Osteoarthritis by Suppressing the Activation of p38 MAPK Signaling Pathway. BioMed research international 2018, 2018, 8384576, doi:10.1155/2018/8384576.

77. Cui, Z.; Crane, J.; Xie, H.; Jin, X.; Zhen, G.; Li, C.; Xie, L.; Wang, L.; Bian, Q.; Qiu, T., et al. Halofuginone attenuates osteoarthritis by inhibition of TGF-beta activity and H-type vessel formation in subchondral bone. Ann Rheum Dis 2016, 75, 1714-1721, doi:10.1136/annrheumdis-2015-207923.

78. Wang, W.; Ha, C.; Lin, T.; Wang, D.; Wang, Y.; Gong, M. Celastrol attenuates pain and cartilage damage via SDF-1/CXCR4 signalling pathway in osteoarthritis rats. J Pharm Pharmacol 2018, 70, 81-88, doi:10.1111/jphp.12835.

79. Khan, N.M.; Ahmad, I.; Ansari, M.Y.; Haqqi, T.M. Wogonin, a natural flavonoid, intercalates with genomic DNA and exhibits protective effects in IL-1beta stimulated osteoarthritis chondrocytes. Chem Biol Interact 2017, 274, 13-23, doi:10.1016/j.cbi.2017.06.025.

80. Wang, Z.; Wang, Z.; Lu, W.W.; Zhen, W.; Yang, D.; Peng, S. Novel biomaterial strategies for controlled growth factor delivery for biomedical applications. NPG Asia Materials 2017, 9, e435-e435, doi:10.1038/am.2017.171.

81. Li, J.; Chen, G.; Xu, X.; Abdou, P.; Jiang, Q.; Shi, D.; Gu, Z. Advances of injectable hydrogel-based scaffolds for cartilage regeneration. Regenerative biomaterials 2019, 6, 129-140, doi:10.1093/rb/rbz022.

82. Burt, H.M.; Tsallas, A.; Gilchrist, S.; Liang, L.S. Intra-articular drug delivery systems: Overcoming the shortcomings of joint disease therapy. Expert opinion on drug delivery 2009, 6, 17-26, doi:10.1517/17425240802647259.

83. Armiento, A.R.; Stoddart, M.J.; Alini, M.; Eglin, D. Biomaterials for articular cartilage tissue engineering: Learning from biology. Acta Biomater 2018, 65, 1-20, doi:10.1016/j.actbio.2017.11.021.

84. Liu, M.; Zeng, X.; Ma, C.; Yi, H.; Ali, Z.; Mou, X.; Li, S.; Deng, Y.; He, N. Injectable hydrogels for cartilage and bone tissue engineering. Bone Research 2017, 5, 17014, doi:10.1038/boneres.2017.14.

85. Vega, S.L.; Kwon, M.Y.; Burdick, J.A. Recent advances in hydrogels for cartilage tissue engineering. Eur Cell Mater 2017, 33, 59-75, doi:10.22203/eCM.v033a05.

86. Toh, W.S.; Spector, M.; Lee, E.H.; Cao, T. Biomaterial-Mediated Delivery of Microenvironmental Cues for Repair and Regeneration of Articular Cartilage. Molecular Pharmaceutics 2011, 8, 994-1001, doi:10.1021/mp100437a.

87. Lee, K.Y.; Mooney, D.J. Alginate: properties and biomedical applications. Progress in polymer science 2012, 37, 106-126, doi:10.1016/j.progpolymsci.2011.06.003.

88. Antoine, E.E.; Vlachos, P.P.; Rylander, M.N. Review of collagen I hydrogels for bioengineered tissue microenvironments: characterization of mechanics, structure, and transport. Tissue engineering. Part B, Reviews 2014, 20, 683-696, doi:10.1089/ten.TEB.2014.0086.

89. Li, L.; Yu, F.; Zheng, L.; Wang, R.; Yan, W.; Wang, Z.; Xu, J.; Wu, J.; Shi, D.; Zhu, L., et al. Natural hydrogels for cartilage regeneration: Modification, preparation and application. Journal of orthopaedic translation 2019, 17, 26-41, doi:https://doi.org/10.1016/j.jot.2018.09.003.

90. Bryant, S.J.; Anseth, K.S. Controlling the spatial distribution of ECM components in degradable PEG hydrogels for tissue engineering cartilage. Journal of biomedical materials research. Part A 2003, 64, 70-79, doi:10.1002/jbm.a.10319.

91. Coviello, T.; Matricardi, P.; Marianecci, C.; Alhaique, F. Polysaccharide hydrogels for modified release formulations. Journal of controlled release : official journal of the Controlled Release Society 2007, 119, 5-24, doi:10.1016/j.jconrel.2007.01.004.

92. Stenzel, K.H.; Miyata, T.; Rubin, A.L. Collagen as a biomaterial. Annual review of biophysics and bioengineering 1974, 3, 231-253, doi:10.1146/annurev.bb.03.060174.001311.

93. Euppayo, T.; Punyapornwithaya, V.; Chomdej, S.; Ongchai, S.; Nganvongpanit, K. Effects of hyaluronic acid combined with anti-inflammatory drugs compared with hyaluronic acid alone, in clinical trials and

experiments in osteoarthritis: a systematic review and meta-analysis. BMC Musculoskeletal Disorders 2017, 18, 387, doi:10.1186/s12891-017-1743-6.

94. Masuko, K.; Murata, M.; Yudoh, K.; Kato, T.; Nakamura, H. Anti-inflammatory effects of hyaluronan in arthritis therapy: Not just for viscosity. International journal of general medicine 2009, 2, 77-81, doi:10.2147/ijgm.s5495.

95. Kon, E.; Mandelbaum, B.; Buda, R.; Filardo, G.; Delcogliano, M.; Timoncini, A.; Fornasari, P.M.; Giannini, S.; Marcacci, M. Platelet-rich plasma intra-articular injection versus hyaluronic acid viscosupplementation as treatments for cartilage pathology: from early degeneration to osteoarthritis. Arthroscopy : the journal of arthroscopic & related surgery : official publication of the Arthroscopy Association of North America and the International Arthroscopy Association 2011, 27, 1490-1501, doi:10.1016/j.arthro.2011.05.011.

96. Kurisawa, M.; Chung, J.E.; Yang, Y.Y.; Gao, S.J.; Uyama, H. Injectable biodegradable hydrogels composed of hyaluronic acid-tyramine conjugates for drug delivery and tissue engineering. Chemical communications (Cambridge, England) 2005, 10.1039/b506989k, 4312-4314, doi:10.1039/b506989k.

97. Abu-Hakmeh, A.; Kung, A.; Mintz, B.R.; Kamal, S.; Cooper, J.A.; Lu, X.L.; Wan, L.Q. Sequential gelation of tyramine-substituted hyaluronic acid hydrogels enhances mechanical integrity and cell viability. Medical & Biological Engineering & Computing 2016, 54, 1893-1902, doi:10.1007/s11517-016-1474-0.

98. Yucel, T.; Lovett, M.L.; Kaplan, D.L. Silk-based biomaterials for sustained drug delivery. Journal of controlled release : official journal of the Controlled Release Society 2014, 190, 381-397, doi:10.1016/j.jconrel.2014.05.059.

99. Partlow, B.P.; Hanna, C.W.; Rnjak-Kovacina, J.; Moreau, J.E.; Applegate, M.B.; Burke, K.A.; Marelli, B.; Mitropoulos, A.N.; Omenetto, F.G.; Kaplan, D.L. Highly tunable elastomeric silk biomaterials. Adv Funct Mater 2014, 24, 4615-4624, doi:10.1002/adfm.201400526.

100. Rockwood, D.N.; Preda, R.C.; Yucel, T.; Wang, X.; Lovett, M.L.; Kaplan, D.L. Materials fabrication from Bombyx mori silk fibroin. Nature protocols 2011, 6, 1612-1631, doi:10.1038/nprot.2011.379.

101. Crivelli, B.; Perteghella, S.; Bari, E.; Sorrenti, M.; Tripodo, G.; Chlapanidas, T.; Torre, M.L. Silk nanoparticles: from inert supports to bioactive natural carriers for drug delivery. Soft Matter 2018, 14, 546-557, doi:10.1039/c7sm01631j.

102. Hasturk, O.; Jordan, K.E.; Choi, J.; Kaplan, D.L. Enzymatically crosslinked silk and silk-gelatin hydrogels with tunable gelation kinetics, mechanical properties and bioactivity for cell culture and encapsulation. Biomaterials 2020, 232, 119720, doi:https://doi.org/10.1016/j.biomaterials.2019.119720.

Chapter 2

Regulation of Inflammatory Response in Human Osteoarthritic Chondrocytes by Novel Herbal Small Molecules

Reihane Ziadlou[1,2,3], Andrea Barbero[2], Martin J. Stoddart[1], Michael Wirth[1], Zhen Li[1], Ivan Martin[2,3], Xin-luan Wang[4], Ling Qin[4,5], Mauro Alini[1] and Sibylle Grad[1,6]

[1] AO Research Institute Davos, Davos Platz, 7270, Switzerland;

[2] Department of Biomedical Engineering, University of Basel, Allschwil, 4123, Switzerland

[3] Department of Biomedicine, University Hospital Basel, University of Basel, Basel, 4001, Switzerland

[4] Translational Medicine R&D Center, Shenzhen Institutes of Advanced Technology, Chinese Academy of Sciences, Shenzhen, 518057, China

[5] Department of Orthopaedics & Traumatology, the Chinese University of Hong Kong, Hong Kong SAR, China

[6] Department of Health Sciences and Technology, ETH Zürich, Zürich, 8092, Switzerland

Published in *International Journal of Molecular Sciences* **2019**, *Nov 15;20(22):5745*

Abstract

In this study, 34 Traditional Chinese Medicine (TCM) compounds were screened for potential anabolic and anti-inflammatory properties on *human* osteoarthritic (OA) chondrocytes. The anabolic effects were assessed by measuring the glycosaminoglycan (GAG) relative to the DNA content using a 3D pellet culture model. The most chondrogenic compounds were tested in an inflammatory model consisting of 3 days of treatment with cytokines (IL-1β/TNF-α) with or without supplementation of TCM compounds. The anti-inflammatory effects were assessed transcriptionally, biochemically and histologically. From the 34 compounds, Vanilic acid (VA), Epimedin A (Epi A) and C (Epi C), 2″-O-rhamnosylicariside II (2-O-rhs II), Icariin, Psoralidin (PS), Protocatechuicaldehyde (PCA), 4-Hydroxybenzoic acid (4-HBA) and 5-Hydroxymethylfurfural (5-HMF) showed the most profound anabolic effects. After induction of inflammation, pro-inflammatory and catabolic genes were upregulated, and GAG/DNA was decreased. VA, Epi C, PS, PCA, 4-HBA and 5-HMF exhibited anti-catabolic and anti-inflammatory effects and prevented the up-regulation of pro-inflammatory markers including metalloproteinases and cyclooxygenase 2. After two weeks of treatment with TCM compounds, the GAG/DNA ratio was restored compared with the negative control group. Immunohistochemistry and Safranin-O staining confirmed superior amounts of cartilaginous matrix in treated pellets. In conclusion, VA, Epi C, PS, PCA, 4-HBA and 5-HMF showed promising anabolic and anti-inflammatory effects.

1. Introduction

Occurrence of age-related musculoskeletal disorders is increasing, with osteoarthritis (OA) being the most prevalent joint disorder. Approximately 20% of the adult population in Europe and the US is expected to be afflicted with OA by 2030 [1–3], resulting in excessive economic burdens on healthcare systems.

Development of OA results from a combination of genetic and environmental factors including obesity, ageing, acute joint trauma and inflammation, which cause an imbalance between chondrocyte anabolism and catabolism and primarily affect articular hyaline cartilage in load bearing joints [4–8]. Furthermore, OA can increase the risk of onset of other chronic diseases, making prevention and early effective treatment of OA a relevant research focus [9]. The

avascular nature of cartilage, combined with low cell density and slow matrix turnover rate, results in a lack of effective methods to prevent or treat OA [7]. If conventional treatment such as physical therapy or weight reduction fails to alleviate symptoms, simple analgesics are initially recommended (e.g., acetaminophen). Additionally, non-steroidal anti-inflammatory drugs (NSAIDs), including specific or non-specific cyclooxygenase 2 (COX-2) inhibitors, are used frequently [10–12]. However, these systemic treatments are often insufficient and bear the risks of gastrointestinal, renal or cardiovascular side effects [13–15]. Alternative anti-inflammatory treatments include the inhibition of inducible nitric oxide synthase (iNOS) or nuclear factor kappa B (NFκB) signaling [16]. Furthermore, anti-cytokine therapy, such as anti-tumor necrosis factor (TNF)-α antibodies, can potentially suppress inflammation and prevent cartilage degradation in OA patients [17]. However, in addition to TNF-α, other pro-inflammatory cytokines such as interleukin (IL)-1, are also involved in the degenerative process [18]. Anti-matrix metalloproteinase (MMP) therapy faces a similar concern, as multiple enzymes contribute to the complex breakdown mechanism of the extracellular matrix. When the disease is progressing (Stage 3), intra-articular injection of hyaluronic acid, glucosamine or corticosteroids can be considered [19]. Though effects are often initially satisfactory, these injections only achieve short-term pain relief, and eventually surgical joint replacement is one of the last options remaining in the Stage 4 of OA [20]. Joint replacement is a highly invasive procedure with an extended rehabilitation period and limited options for revision when necessary [21]. Alternatively, arthroscopic lavage and debridement have been applied in OA patients with variable outcomes [22]. Since conventional treatment approaches aim at symptoms relief and do not address the catabolic component of the destructive OA disease [23], the development of innovative, disease modifying and low risk treatments for OA is an unmet clinical need.

Several plant-derived compounds have been identified that have the potential to inhibit NFκB signaling and inflammation [24–28]. Well known plant-derived compounds used for these purposes are curcumin and resveratrol [29]. In addition, extracts of Traditional Chinese Medicine (TCM) herbs have been investigated for their anti-inflammatory effects. For example, *Caesalpinia sappan* derived extracts were shown to suppress nitric oxide synthesis in osteoarthritic chondrocytes by down-regulating the iNOS mRNA expression. It was concluded that blockage of IL-1 induced NFκB signaling and its down-stream pro-inflammatory targets

by *Caesalpinia sappan* extracts may counteract cartilage breakdown in OA [18]. Similarly, Honokiol, a low molecular weight natural product isolated from *Magnolia officinalis*, was able to prevent IL-1 induced inflammatory reactions and cartilage matrix breakdown in *human* OA chondrocytes [30].

Therapy with herbal Fufang is popular in TCM for prevention and treatment of osteoporosis and related bone diseases. Xianlinggubao formula (XLGB) was formed based on modification of the empirical "Miao minority" medicine, which was commonly used to tone the "kidney system" and nourish bones [31]. XLGB capsule was officially approved by the Chinese State Food and Drug Administration (cFDA) as the over-the-counter drug for treatment of osteoporosis [32], aseptic osteonecrosis [33], osteoarthritis [34] and bone fractures [32]. XLGB is composed of six kinds of herbs containing various compounds [32,33]. A total of 118 compounds were identified from XLGB extract [35]. Some of them, e.g., Icariin, had previously demonstrated extensive bioactivity and anti-inflammatory activity and were used as bioactive factors in tissue engineering for cartilage defect repair [36,37].

We hypothesized that, among the various compounds identified in TCM herbal extracts, there are distinct molecules with potent chondrogenic and anti-inflammatory effects. However, no comprehensive and systematic direct comparison of diverse TCM molecules in terms of combined chondrogenic and anti-inflammatory properties has been performed. The current study assessed the anabolic and anti-inflammatory effects of 34 relevant TCM compounds from XLGB on *human* osteoarthritic chondrocytes. The aim was to identify the most potent compounds in terms of cartilage matrix synthesis and counteraction of inflammatory responses.

2. Materials and Methods

2.1. Drugs Screening on Human Osteoarthritic Chondrocytes

Thirty-four compounds (listed in Table 1) were investigated for their anabolic and/or anti-inflammatory effect (Chengdu Herbpurify Co.LTD and Chengdu Push Bio-Technology Co.LTD, Chengdu, China). The extraction method is shown in supplementary Figure 1 [68]. All compounds were dissolved in dimethyl sulfoxide (DMSO) at a final concentration of 10 mg/mL and stored at 4 °C. Chondrocytes were treated with different concentrations of

compounds (1 μM, 10 μM, 25 μM, 50 μM), as indicated in the specific experiments. These concentrations were selected from previous *in vitro* studies, where positive effects with doses between 1 μM and 50 μM had been reported [36,42].

Table 1. List of 34 tested Traditional Chinese Medicine (TCM) compounds extracted from XLGB with their chemical formula, molecular weight and component herb.

No	Name of the Compound	Molecular Formula	Molecular Weight	Component Herb
1	5-Hydroxymethylfurfural	$C_6H_6O_3$	126	H.E
2	Protocatechuicaldehyde	$C_7H_6O_3$	138	R.S
3	Vanilic acid	$C_8H_8O_4$	168	R.S
4	4-Hydroxybenzoic acid	$C_7H_6O_3$	138	R.S
5	Chlorogenic acid	$C_{16}H_{18}O_9$	354	H.E
6	Cryptochlorogenic acid	$C_{16}H_{18}O_9$	354	H.E
7	Loganic acid	$C_{16}H_{24}O_{10}$	376	R.D
8	Loganin	$C_{17}H_{26}O_{10}$	390	R.D
9	Isobavachalcone	$C_{20}H_{20}O_4$	324	F.P
10	Sweroside	$C_{16}H_{22}O_9$	358	R.D
11	(+)-Cycloolivil	$C_{20}H_{24}O_7$	376	H.E
12	Baohuside I	$C_{27}H_{30}O_{10}$	514	H.E
13	2″-*O*-rhamnosylicariside II	$C_{33}H_{40}O_{14}$	660	H.E
14	Epimedin A	$C_{39}H_{50}O_2$	838	H.E
15	Epimedin B	$C_{38}H_{48}O_{19}$	808	H.E
16	Epimedin C	$C_{39}H_{50}O_{19}$	822	H.E
17	Isobavachin	$C_{20}H_{20}O_4$	324	F.P
18	Bavachin	$C_{20}H_{20}O_4$	324	F.P
19	Bavachinin	$C_{21}H_{22}O_4$	338	F.P
20	Neobavaisoflavone	$C_{20}H_{18}O_4$	322	F.P
21	Corylin	$C_{20}H_{16}O_4$	320	F.P
22	Epimedin A1	$C_{39}H_{50}O_{20}$	838	H.E
23	Psoralen	$C_{11}H_6O_3$	186	F.P
24	Isopsoralen	$C_{11}H_6O_3$	186	F.P
25	(*S*)-Bukuchiol	$C_{18}H_{24}O$	256	F.P
26	Psoralidin	$C_{20}H_{16}O_5$	336	F.P
27	Asperosaponin VI	$C_{47}H_{76}O_{18}$	390	R.D
28	Baohuside II	$C_{26}H_{28}O_{10}$	500	H.E
29	Epimedoside A	$C_{32}H_{38}O_{15}$	662	H.E
30	Baohuside V	$C_{39}H_{50}O_{19}$	822	H.E
31	Corylifol A	$C_{25}H_{26}O_4$	390	F.P
32	4′-Methylbavachalcone	$C_{21}H_{22}O_4$	338	F.P
33	Icaitin	$C_{21}H_{20}O_6$	368	H.E
34	Icariin	$C_{33}H_{40}O_{15}$	676	H.E

H.E.: Herba Epimedi; R.S.: Radix ET Rhizoma Salviae; R.D.: Radix Dipsaci; F.P.: Fructus Psoraleae.

2.2. Isolation of Human Osteoarthritic Chondrocytes and Cell Expansion

Cartilage tissue was obtained from three patients suffering from end stage OA and undergoing total knee arthroplasty (ages 47, 60 and 82 years; all female) at the university hospital of Basel under ethical agreement (Ethikkommission beider Basel, Ref.Nr. EK: 78/07, 20. March 2007). The cells were isolated as described elsewhere [69]. Briefly, tissue samples were minced with a scalpel into small pieces and were digested overnight in 0.2% collagenase II (300 U/mg, Worthington Biochemical Corp, Lakewood, NJ, USA) on an orbital shaker at 37 °C. Then, the isolated chondrocytes were expanded for three passages to 80% confluency in basal medium (BM, Dulbecco's modified Eagle medium, high glucose (DMEM)), 10 mM HEPES, 1 mM sodium pyruvate, 1% penicillin/streptomycin (P/S), 100 µg/mL streptomycin, and 0.29 mg/mL glutamate (all from Gibco, Paisley, UK), supplemented with 10% fetal bovine serum (FBS), 5 ng/mL fibroblast growth factor-2 (FGF-2) and 1 ng/mL transforming growth factor (TGF)ß1 (both from Fitzgerald, Acton, MO, USA) in a humidified incubator (37 °C, 5% CO_2).

2.3. Cell Toxicity Assay

Cytotoxicity of the compounds was assessed using the WST-1 reagent (Roche Applied Science, Mannheim, Germany) [70]. *Human* osteoarthritic chondrocytes were seeded in 96-well plates at a density of 2000 cells per well in 100 µL of DMEM containing 4.5 g/L glucose and supplemented with 5% FBS and 1% penicillin–streptomycin (P/S) (all products from Gibco). Cells were cultured at 37 °C, 5% CO_2, 19% oxygen and 90% humidity. After 24 h of incubation, the cells were treated with TCM compounds in four different concentrations (1 µM, 10 µM, 25 µM, 50µM) or DMSO alone at concentrations of 0.01%, 0.1%, 0.25%, 0.5%, as control vehicle groups. After 48 h of treatment, medium was removed and 100 µL of a 10% *v/v* solution of WST-1 reagent in DMEM supplemented with 2.5% FBS was added to each well. After 4 h of incubation at 37 °C, absorbance of the samples was measured against a background control with a microplate reader (Victor 3, PerkinElmer, Waltham, MA, US) at 490 nm, with reference wavelength of 600 nm [71]. For this assay and further analyses, all treatment groups in different concentrations were normalized to the respective control vehicle group. Since DMSO in these concentrations (lower than 1%) did not show any significant effect on cells metabolism, normalization with the highest concentration of DMSO resulted in similar outputs [72].

2.4. Anabolic Effects of the TCM Compounds on Osteoarthritic Chondrocytes Pellet Cultures

Chondrogenic effect of TCM compounds was assessed by culturing the expanded chondrocytes at passage 3 in pellets. Standard BM (high glucose DMEM) was supplemented with 1.25 mg/mL *human* serum albumin (Gibco, Life Technologies Limited, Paisley, UK), ITS- Premix (Corning, Bedford, MA, USA), 0.1 mM ascorbic acid 2-phosphate (Sigma-Aldrich, St. Louis, MO, USA), and 1% P/S. Since the standard chondrogenic supplements TGF-β and dexamethasone could mask the anabolic effect of the compounds, these two essential components for chondrogenic differentiation were omitted from our culture medium (referred to as chondropermissive medium) and were replaced with the TCM compounds. Briefly, cells were re-suspended in chondropermissive medium as described before [73]. Aliquots of 1.5×10^5 cells/150 µL were centrifuged at 400 g for 5 min in v-bottom non-adherent 96-well plates (Thermo Fisher scientific, Waltham, MA, US). Pellets were cultured for 2 weeks in a humidified incubator (37 °C, 5% CO_2) with a change of medium twice a week. Medium was supplemented with TCM compounds in four different final concentrations (1 µM, 10 µM, 25 µM, 50 µM) or control vehicle group containing 0.01%, 0.1%, 0.25%, 0.5% *v/v* DMSO.

2.5. Anti-Catabolic Effects of the TCM Compounds on Osteoarthritic Chondrocytes Pellet Cultures

Passage 3 chondrocytes were centrifuged at 400 g for 5 min (2.5×10^5 cells per pellet in 250 µL medium) in v-bottom, non-adherent 96-well plates and cultured in pellets using standard chondrogenic medium (chondropermissive medium containing 10 ng/mL TGFβ and 10^{-7} M dexamethasone (Sigma Aldrich)). After one week of culture in chondrogenic medium (short term), pellets were harvested for transcriptional analysis, and after two weeks of culture in chondrogenic medium (long term), pellets were harvested for biochemical and histochemical analysis (phase I). The remaining pellets were exposed to IL-1β and TNF-α (both from Peprotech, London, UK), each at 1 ng/mL, for 72 h (phase II), using an established inflammatory pellet culture model [74]. During this inflammatory phase, pellets were cultured in chondropermissive medium (chondrogenic medium deprived of TGF-β1 and dexamethasone) with or without TCM compound. Pellets were then harvested for analysis (phase II) or cultured two more weeks (phase III) in chondropermissive medium supplemented with TCM compounds or DMSO as control vehicle group. The most potent compounds in terms of their anabolic effects were selected for testing in this inflammatory model, in 3 different

concentrations (1 μM, 10 μM, 25 μM). The positive control (ctr +) group was supplemented with 10 ng/mL TGF-β1 and 10^{-7} M dexamethasone (phase III). Cell pellets were maintained at 37 °C, 5% CO_2, with medium changes twice per week. The different experimental groups are summarized in Table 2.

Table 2. Description of experimental groups.

Pellet Culture	**Group**	**Culture Phase I** (cartilage generation)	**Culture Phase II** (IL-1β/TNFα exposure; inflammatory phase)		**Culture Phase III (Treatment)**	
		Time	Time	Compound	Time	Compound
Short term	Control (IL-1β/TNFα)	1 week	3 days	--	n/a	
	Treatment group (IL-1β/TNFα + compound)	1 week	3 days	+	n/a	
Long term	Control (IL-1β/TNFα)	2 weeks	3 days	--	2 weeks	--
	Treatment group (IL-1β/TNFα - compound)	2 weeks	3 days	+	2 weeks	+

2.6. Biochemical Analysis

Pellets (n = 3) from three donors were digested with 0.5 mL of 1 mg/mL proteinase K at 56 °C for 16 h (Roche, Mannheim, Germany). Using 1,9 dimethylmethylene blue (DMMB) assay, the amount of sulfated glycosaminoglycan (GAG) within the pellets was measured spectrophotometrically with chondroitin sulphate as a standard (Sigma-Aldrich) [75]. The DNA content was measured spectrofluorometrically using PicoGreen (Invitrogene, Eugene, OR, USA) dye with calf thymus DNA (LuBio Science, Zurich, Switzerland) as a standard and according to the manufacturer's instruction. The GAG content was normalized to the DNA content in all samples.

2.7. Gene Expression Analysis

For total RNA extraction, 1 mL of TRI reagent (Molecular Research Center) was added to the pellet. After homogenization by a Tissue Lyser for 3 min and 5 Hz (Qiagen, Hilden, Germany), the RNA was extracted using phase separation by 1-Bromo-3-chloropropane (Sigma) in a

volume ratio of 1:10 with the TRI reagent. Reverse transcription was performed with SuperScript VILO cDNA Synthesis Kit (Life Technologies, Carlsbad, CA). Quantitative real-time PCR (qPCR) was accomplished using TaqMan Universal Master Mix (Applied biosystems, Foster City, CA, USA) and the Quant Studio 6 Flex Instrument and software (Applied biosystems) were used for detection. The gene expression assays and sequences of *human* primers and TaqMan probes for *human 18S rRNA*, *MMP1, MMP3, MMP13, COX-2*, *COL-II* and *ACAN* are shown in Table 3 (a, b). The relative gene expression was calculated using the $2^{-\Delta\Delta CT}$ quantification method [76], with 18S ribosomal RNA as endogenous control.

Table 3. Oligonucleotide primers and probes (*human*) used for Real-Time PCR.

a. Primers and probes (Applied Biosystems).

Gene	Probe Type	Assay ID
MMP-1	5′ FAM-3′ NFQ	Hs00899658_m1
MMP-3	5′ FAM-3′ NFQ	Hs00968305_m1
18s fast	5′ FAM-3′ NFQ	Hs99999901_s1

MMP1: matrix metalloproteinase 1; *MMP3*: matrix metalloproteinase 3; FAM: Carboxyfluorescein; NFQ: nonfluorescent quencher a. *Human* Gene Expression Assays (ThemoFisher Scientific). b.

b. Custom Designed Primer/Probe (Microsynth, Balgach, Switzerland).

Gene	Primer/Probe Type	Sequence
MMP-13	Primer forward (5′-3′)	CGGCCACTCCTTAGGTCTTG
	Primer reverse (5′-3′)	TTTTGCCGGTGTAGGTGTAGATAG
	Probe (5′ FAM/3′ TAMRA)	CTCCAAGGACCCTGGAGCACTCATGT
COX-2	Primer forward (5′-3′)	TTGTACCCGGACAGGATTCTATG
	Primer reverse (5′-3′)	TGTTTGGAGTGGGTTTCAGAAATA
	Probe (5′ FAM/3′ TAMRA)	GAAAACTGCTCAACACCGGAATTTTTGACAA
Col2a1	Primer forward (5′-3′)	GGCAATAGCAGGTTCACGTACA
	Primer reverse (5′-3′)	GATAACAGTCTTGCCCCACTTACC
	Probe (5′ FAM/3′ TAMRA)	CCTGAAGGATGGCTGCACGAAACATAC
ACAN	Primer forward (5′-3′)	AGTCCTCAAGCCTCCTGTACTCA
	Primer reverse (5′-3′)	CGGGAAGTGGCGGTAACA
	Probe (5′ FAM/3′ TAMRA)	CCGGAATGGAAACGTGAATCAGAATCAACT

COL2A1: collagen type II; *MMP13*: matrix metalloproteinase 13; *COX-2*: cyclooxygenase-2; *ACAN:* aggrecan; FAM: Carboxyfluorescein; TAMRA: Tetramethylrhodamine.

2.8. Histological and Immunohistochemical Analysis

Pellets were fixed in 70% methanol and incubated overnight in 5% sucrose solution at 4 °C. Then, the samples were embedded in cryo-compound and were sectioned with cryostat at 8 µm thickness. To visualize cells, proteoglycan and the collagen deposition, slides were first stained with Weigert's Haematoxylin for 10 min. Sections were stained with 0.02% Fast green in ultrapure (ddH_2O) water for 5 min to reveal collagen deposition, then stained with 0.1% Saf-O for 12 min to show proteoglycan deposition, and finally rinsed in dH_2O and sequentially differentiated in 70%, 96% and 100% ethanol. The presence of ACAN and COL-II was identified immunohistochemically using antibodies against ACAN (1-C-6) and COL-II (CIIC1), both from Developmental Studies Hybridoma Bank, University of Iowa). Briefly, after enzyme treatment with hyaluronidase (Sigma-Aldrich, St. Louse, MO, USA) for COL-II and chondroitinase (Sigma-Aldrich) for 1C6, non-specific binding sites were blocked with horse serum (Vector Laboratories, Burlingame, CA, USA) for 1h at RT. The primary antibody (5 µg/mL) was incubated for 30 min and detected using secondary biotinylated anti-*mouse* antibody (Vector Laboratories) followed by incubation with avidin-biotin-peroxidase complex (Vectastain ABC Kit, *Mouse* IgG, Vector Laboratories). Peroxidase activity was visualized using diaminobenzidine (DAB) as a substrate (ImmPACT DAB, Substrate for Peroxidase, Vector Laboratories) [77].

2.9. Statistical Analysis

Statistical comparisons were performed using Graphpad Prism 7. One-way analysis of variance (ANOVA) followed by Dunnett's post hoc test (multiple comparison) or Tukey's post hoc test (multiple comparison) was applied as non-parametric test of three independent experiments with different *human* osteoarthritic chondrocytes. To assess statistical significance among the groups, differences were considered statistically significant at $p < 0.05$. All Graphs are displayed as box plots.

3. Results

3.1. Toxicity Assay for the Compounds on Human Osteoarthritic Chondrocytes

Cytotoxicity assay of monolayer cultures showed that after 48 h of treatment with TCM compounds (1 µM, 10 µM, 25 µM, 50 µM), more than 75% of the cells were viable in all

treatment groups. Furthermore, in different concentrations of dimethyl sulfoxide (DMSO) (0.01%, 0.1%, 0.25%, 0.5% *v/v*) as control vehicle group the numbers of viable cells were consistent. So, DMSO did not show any toxic effect on the cells in these concentrations. Furthermore, the viability of the cells in the un-treated control group was not different from the control vehicle group. All data are normalized to the control vehicle group (Table 4).

Table 4. Relative viable cell count after treatment with the 34 compounds measured by WST-1 assay.

Compound	% Cell numbers (Normalized to control vehicle)				
	Conc.[μM]	1	10	25	50
5-Hydroxymethylfurfural		111.4 ± 6.6	107.0 ± 11.2	110.2 ± 9.4	107.9 ± 3.3
Protocatechuicaldehyde		100.1 ± 4.2	96.0 ± 9.3	94.8 ± 6.4	81.2 ± 5.4
Vanilic acid		102.1 ± 2.4	96.8 ± 3.7	115.7 ± 3.2	112.6 ± 2.1
4-Hydroxybenzoic acid		103.4 ± 2.5	102 ± 9.6	105 ± 3.4	78.6 ± 6.9
Chlorogenic acid		77.8 ± 3.2	78.6 ± 4.8	77.8 ± 5.2	79.8 ± 5.6
Cryptochlorogenic acid		86.2 ± 8.5	86 ± 7.9	93.8 ± 5.2	78.3 ± 8.4
Loganic acid		85.6 ± 3.6	94.7 ± 3	91.5 ± 1.7	93.6 ± 4.9
Loganin		107 ± 5.6	109.2 ± 5.1	110.6 ± 9.8	102.8 ± 3.6
Isobavachalcone		102.1 ± 6.6	108.7 ± 5.7	105.7 ± 0.6	88.4 ± 8.8
Sweroside		110.2 ± 2.3	106.7 ± 4.1	112.5 ± 1.8	107.7 ± 9.8
(+)-Cycloolivil		101.5 ± 1.5	98. ± 2.1	105.6 ± 4.9	103.2 ± 8.2
Baohuoside I		82.8 ± 6.3	76.3 ± 1.8	77.5 ± 0.4	79.8 ± 5.8
2'-O-rhamnosylicariside II		102.1 ± 6.6	105.5 ± 4.7	91.8 ± 3.2	102.9 ± 2.1
Epimedin A		83.9 ± 5.6	84.8 ± 8.1	97.1 ± 6.9	111.3 ± 5.1
Epimedin B		82.7 ± 9.2	88 ± 9.9	87.8 ± 9.1	94. ± 7.9
Epimedin C		87.5 ± 0.6	89.5 ± 6.5	88.1 ± 3.7	89.8 ± 6.4
Isobavachin		87.3 ± 1.3	91.5 ± 8.2	89.2 ± 0.8	85.7 ± 0.1
Bavachin		109.1 ± 2.1	102 ± 8.4	89.2 ± 9.5	91.7 ± 2.1
Bavachinin		96.4 ± 1.1	78.1 ± 6.6	79.9 ± 5.1	79.7 ± 3
Neobavaisoflavone		84.4 ± 8.6	89.6 ± 1.9	99 ± 2.5	76.1 ± 2.2
Corylin		89.6 ± 2.4	94 ± 3.7	87.8 ± 1.6	79.3 ± 3.1
Epimedin A1		95.48 ± 4.3	85.49 ± 0.5	88.21 ± 3.1	95.46 ± 2.4
Psoralen		83.6 ± 5.1	80.3 ± 5.3	85.1 ± 6.4	84.8 ± 8.3
Isopsoralen		86.2 ± 8.6	80.2 ± 1.9	83 ± 2.7	85.4 ± 3.2
(S)-Bukuchiol		89.1 ± 4.4	94.4 ± 3.5	104.7 ± 4.2	88.4 ± 4.2
Psoralidin		106.5 ± 6.3	84.7 ± 1.4	86.4 ± 5.9	85.1 ± 4.8
Asperosaponin VI		93.9 ± 2.8	99 ± 9.2	103.8 ± 4.5	93.9 ± 4.8
Baohuoside II		103.6 ± 5.9	96.4 ± 7.6	95 ± 5.2	79.7 ± 2.9
Epimedoside A		89 ± 4.7	87.9 ± 3.1	90.6 ± 4.4	85.6 ± 3.7
Baohuoside V		98.6 ± 8.7	100 ± 6.5	100.9 ± 7.8	78.5 ± 3.8
Corylifol A		86.1 ± 3.3	85.3 ± 1.8	94.6 ± 0.9	103.8 ± 2.6
4'-O-Methyl-broussochalcone		81.4 ± 2.9	85.4 ± 2.4	95.4 ± 3.6	97.5 ± 2.3
Anhydroicaritin		85.2 ± 2.2	83.4 ± 6.6	86.2 ± 1.5	81.8 ± 2.4
Icariin		95.7 ± 3.6	101.4 ± 3.7	95.5 ± 3.2	101.5 ± 5.7

2.2. Anabolic Effects of Traditional Chinese Medicine (TCM) Compounds on Glycosaminoglycan Production

To determine the anabolic effect of the TCM compounds, all 34 compounds were tested in 3D pellet culture in four different concentrations (1 µM, 10 µM, 25 µM, 50 µM). *Human* OA chondrocytes from three donors were cultured in chondro-permissive medium with supplementation of compounds or with DMSO (0.01%, 0.1%, 0.25%, 0.5% *v/v*) (control vehicle group) for two weeks. Nine compounds, namely Vanilic acid (VA), Epimedin A (Epi A) and C (Epi C), 2″-O-rhamnosylicariside II (2-O-rhs II), Psoralidin (PS), Icariin, Protocatechuicaldehyde (PCA), 4-Hydroxybenzoic acid (4-HBA) and 5-Hydroxymethylfurfural (5-HMF) significantly increased the GAG/DNA ratio compared to the control vehicle group in all three donors. All data are normalized to their respective control vehicle groups, and the compounds which were effective in all the different concentrations are shown in Figure 1 in their most effective dose. The complete data set from all compounds tested in four concentrations is shown in Supplementary Table 1. Epi A, Epi C, 2-O-rhs II and Icariin are all extracts of *Epimedium* medicinal herb with similar chemical structures and positive anabolic effects. Since Epi C showed the highest amount of matrix production among these four compounds, it was chosen as a representative of *Epimedium* herb extract for use in further experiments. Furthermore, VA, PS, PCA, 4-HBA and 5-HMF from the first screening in their most effective dose were selected for further studies in the inflammatory models.

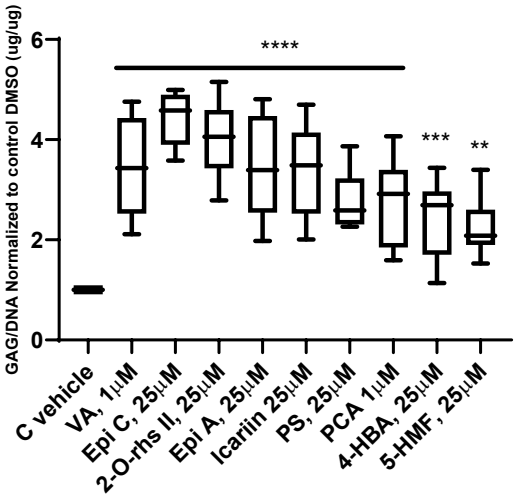

Figure 1. Glycosaminoglycan (GAG) production of 3D *human* osteoarthritic chondrocyte pellet cultures after two weeks in chondro-permissive medium supplemented with Traditional Chinese Medicine (TCM) compounds. Glycosaminoglycan content was normalized to the amount of DNA. The most effective doses of compounds which could promote GAG production versus control vehicle (C vehicle) group in 3/3 donors are shown; for each donor three experimental replicates were analyzed. For statistical analysis using Graphpad Prism, one-way analysis of variance (ANOVA) followed by Dunnett's post hoc test (multiple comparison) was applied. ** $p < 0.001$, *** $p < 0.0005$, **** $p < 0.0001$ versus control vehicle. Vanilic acid (VA), Epimedin A (Epi A) and C (Epi C), 2″-O-rhamnosylicariside II (2-O-rhs II), Icariin, Psoralidin (PS), Protocatechuicaldehyde (PCA), 4-Hydroxybenzoic acid (4-HBA), 5-Hydroxymethylfurfural (5-HMF).

2.3. Effects of TCM Compounds on Pro-Inflammatory and Pro-Catabolic Gene Expression under Inflammatory Conditions

After one week of cartilage generation (short-term) in phase I, the pro-catabolic and pro-inflammatory genes in the pellets treated with IL-1β/TNF-α in phase II were significantly increased. To investigate the inhibitory effects of the selected compounds in phase II, compounds in their most effective dose were simultaneously added with inflammatory cytokines to the chondro-permissive culture media. We observed that after treatment with VA, Epi C, PS, PCA, 4-HBA and 5-HMF, the catabolic marker gene matrix metalloproteinase 13 (*MMP13)* was significantly downregulated in all treatment groups. In the groups treated with VA, Epi C, PCA, 4-HBA and 5-HMF, other catabolic marker genes matrix metalloproteinase 1, 3 (*MMP1, MMP3)* were also significantly inhibited compared with the control DMSO group. Furthermore, *COX-2* was significantly downregulated in all the treatment groups except for PS and 4-HBA. In pellets treated with Epi C, in addition to downregulation of catabolic marker genes, the anabolic marker genes collagen type II (*COL-II)* and aggrecan (*ACAN)* were significantly upregulated (Figure 2a–f).

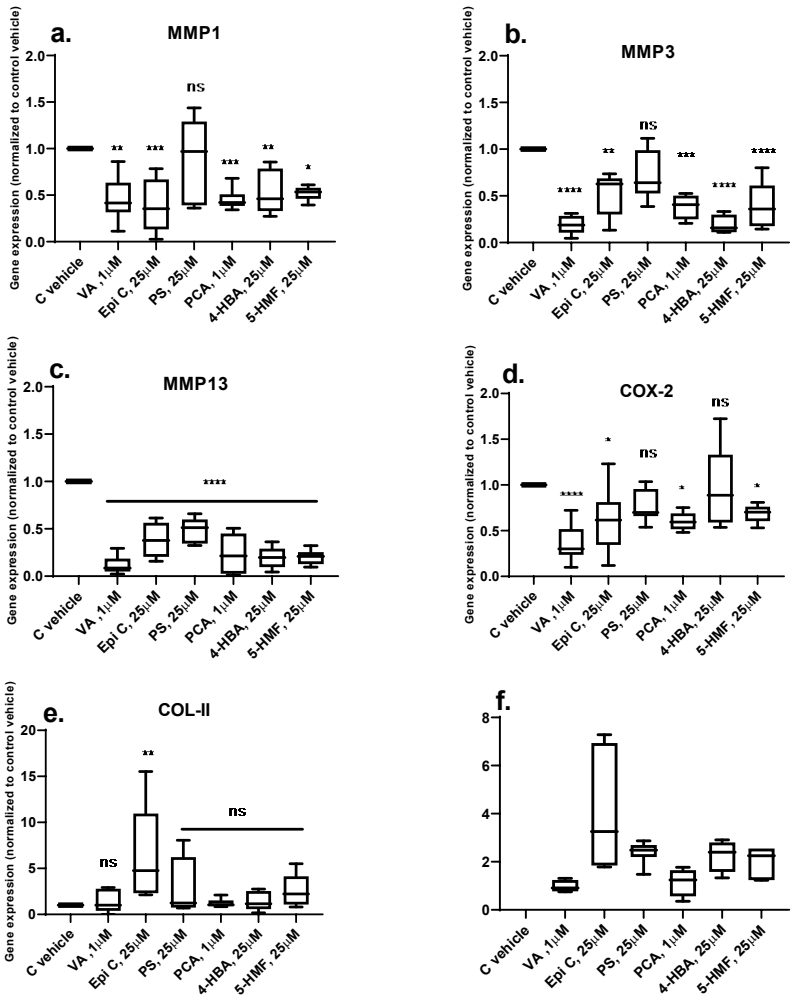

Figure 2. Transcriptional level of catabolic genes matrix metalloproteinase (MMP) a) *MMP1* b) *MMP3* c) *MMP13*, pro-inflammatory gene d) cyclooxygenase 2 *(COX-2)* and anabolic marker genes e) collagen type II (*COL-II)* and f) aggrecan (*ACAN)* in Phase II (short term pellets) simultaneously treated with TCM compounds and IL-1β/TNF-α versus control vehicle (C vehicle) group in *human* OA chondrocytes. $n = 3$; n indicates the number of *human* OA donors; for each donor three experimental replicates were analyzed. Data are normalized to the levels of control groups. For statistical analysis using Graphpad Prism, one-way analysis of variance (ANOVA) followed by Dunnett's post hoc test (multiple comparisons) was applied. * $p < 0.01$, ** $p < 0.001$, *** $p < 0.0005$, **** $p < 0.0001$, ns (non-significant).

2.4. Effect of TCM Compounds on Matrix Production under Inflammatory Conditions

After two weeks of cartilage generation with chondrogenic medium in phase I (long term) the cells produced significant amounts of matrix as assessed by dimethylmethylene blue (DMMB) assay and histology. After induction of inflammation with inflammatory cytokines in phase II (IL-1β/TNF-α), biochemical analysis showed that the GAG/DNA ratio was decreased compared with phase I (Figure 3a). In phase III, after two weeks of treatment (long term), the GAG/DNA ratio did not recover in the control vehicle group in which the cells were treated

with chondro-permissive medium supplemented with 0.01%, 0.1%, 0.25% *v/v* DMSO. In the control positive group (chondrogenic medium) the GAG/DNA ratio reached a similar level as before induction of inflammation (Figure 3a). In the groups treated with VA, Epi C, PS, PCA, 4-HBA and 5-HMF in phase III, the amount of GAG production per DNA increased as compared to the control vehicle group (Figure 3b).

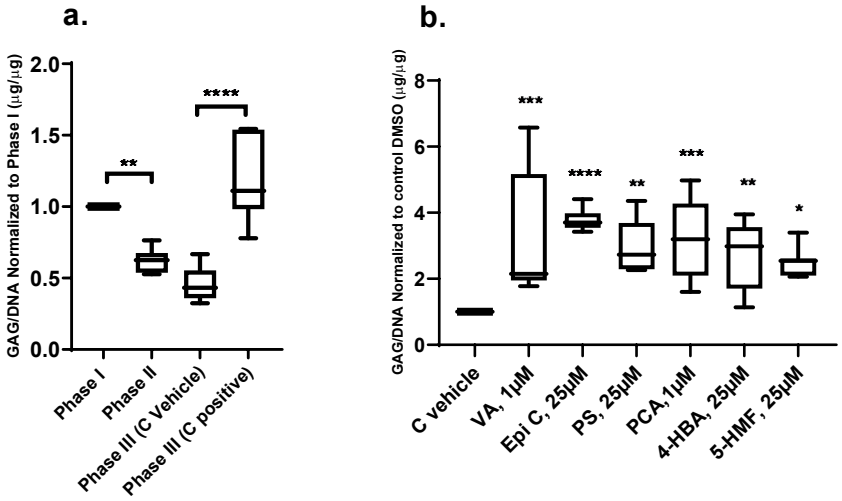

Figure 3. Biochemical analysis of the osteoarthritic chondrocyte pellets (long term) in the inflammatory model. a) GAG production per DNA in three different phases of the inflammatory model. b) The effect of TCM compounds on GAG/DNA ratio in *human* osteoarthritic chondrocytes in phase III after induction of inflammation normalized to control vehicle group (C vehicle). $n = 3$; n indicates the number of *human* OA chondrocytes donors; for each donor three experimental replicates were analyzed. For statistical analysis using Graphpad Prism, one-way analysis of variance (ANOVA) followed by Tukey's post hoc test (multiple comparisons) for Figure 3a and Dunnett's post hoc test (multiple comparisons) for Figure 3b were applied. * $p < 0.01$, ** $p < 0.001$, *** $p < 0.0005$, **** $p < 0.0001$.

Histological analysis confirmed the observed biochemical results. In phase I, after two weeks of pellet culture in chondrogenic medium (long term), cartilage matrix was produced by osteoarthritic chondrocytes (Figure 4a). However, after induction of inflammation (phase II), the intensity of Safranin-O (Saf-O), COL-II and ACAN immunostaining significantly decreased. After two weeks of treatment (long term) in phase III, in the control positive group (chondrogenic medium), high intensity of Saf-O staining and immunostaining for COL-II and ACAN was observed, while staining for extracellular matrix (ECM) proteins in the control DMSO group was not noticeable (Figure 4a). After treatment with the compounds in the recovery phase III (long term), staining intensity for Saf-O, COL-II and ACAN in the groups treated with VA, Epi C, PS, PCA, 4-HBA and 5-HMF was preserved compared to phase II and stronger compared to the control vehicle group; though, the intensity of Saf-O staining and

immunostaining for ECM proteins was still lower compared to phase I, and the compounds did not restore ECM to the same level as before induction of inflammation (Figure 4b).

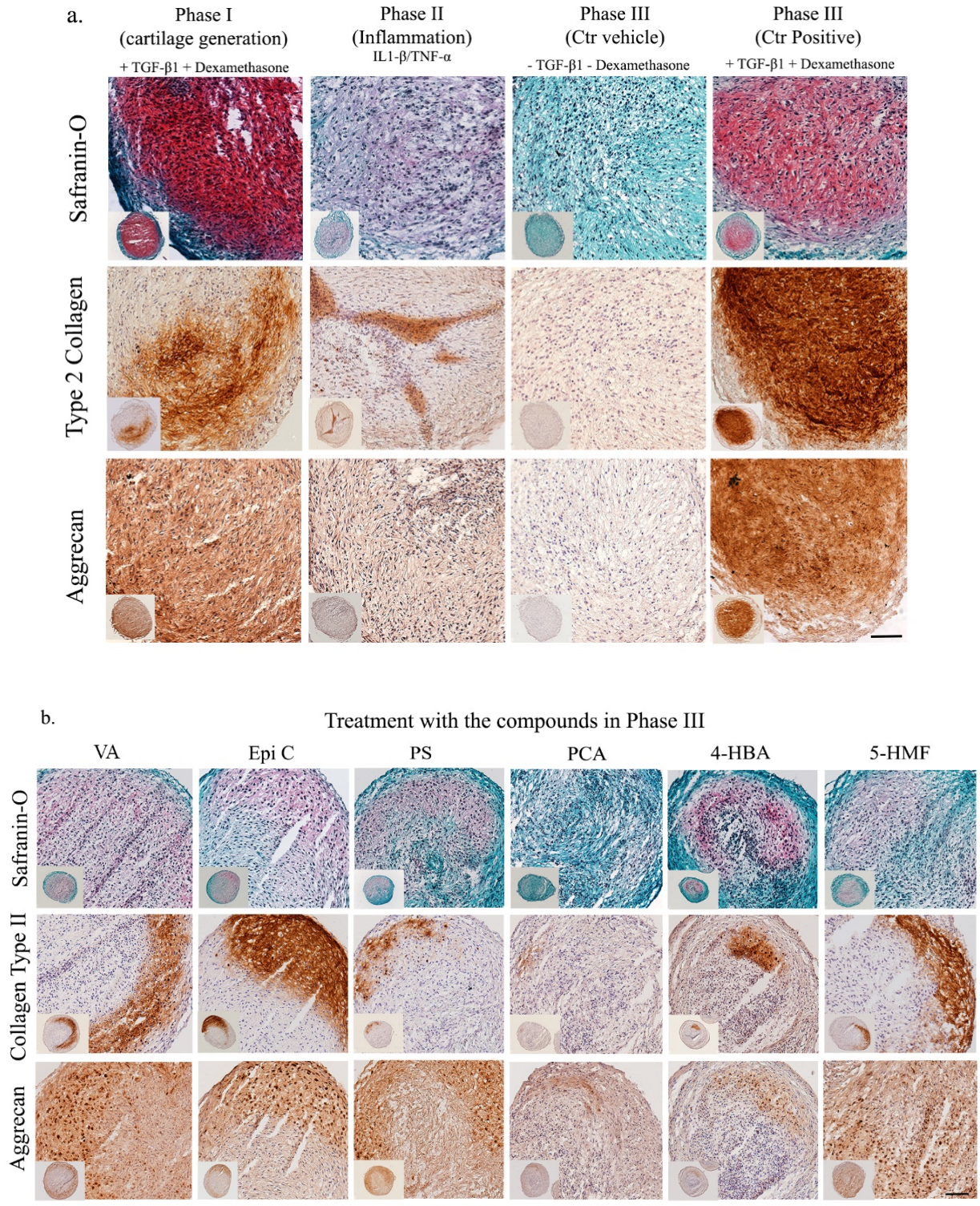

Figure 4. Histological and immunohistochemical characterization of pellets from OA chondrocytes in the inflammatory model (long term). a) Saf-O staining, COL-II and ACAN immunostaining of pellets in three different phases as the control groups (Phase I, Phase II, Phase III). b) and after 14 days of treatment with the TCM compounds in phase III (VA, Epi C, PS, PCA, 4-HBA, 5-HMF). Scale bars = 100 µm.

4. Discussion

For an effective biological therapy against OA, it is essential to counteract elevated catabolism while increasing anabolism. Furthermore, it is necessary to inhibit pro-inflammatory cytokines that are excessively abundant in osteoarthritic joints [18]. In the current study, for the first time, the anabolic and anti-inflammatory effects of 34 bioactive compounds existing in the over-the-counter XLGB formula for the treatment of osteoporosis [32] and osteoarthritis [34] were assessed in 3D pellet culture using *human* OA chondrocytes. Osteoporosis is recognized as one of the most common bone loss conditions in which the elevated amount of pro-inflammatory cytokines can cause a systemic inflammatory condition [38–41]. Since OA is considered an inflammatory disease, we hypothesized that the compounds which could decrease bone resorption and stimulate new bone formation in postmenopausal osteoporosis, could also have the potential for treatment of OA. In fact, a recent clinical study showed both efficacy and safety of XLGB herbal formula for treatment of OA [34].

In our study, the cytotoxicity of the TCM compounds in monolayer culture was tested at four different concentrations (1 μM, 10 μM, 25 μM, 50 μM). Cell viability was more than 75% for all the compounds and even at the highest concentration no cytotoxicity was seen. In previous *in vitro* studies, compounds with positive chondrogenic and anti-inflammatory effects with an optimal dose between 1 μM and 50 μM have been reported [42–45]. In an *in vivo* study in adult *rabbit*s, Icariin which was added to the cell-hydrogel constructs at a final concentration of 10 μM showed potential effect in cartilage tissue regeneration [36]. Furthermore, in a *rat* model of experimental OA, injection of 0.3 mL of 20 μM Icariin reduced the number of cartilage lesions and the expression of MMP-13 [46]. Since most of the tested compounds in our study are novel in the orthopedic field, the reported concentrations of representative compounds from each herbal extract (*Herba Epimedi*, *Radix ET Rhizoma Salviae, Fructus Psoraleae*) were considered [47–51]. Therefore, the anabolic effects of all the compounds in 3D pellet culture in chondropermissive medium (deprived of TGF-β and dexamethasone) and supplemented with compounds in four concentrations (1 μM, 10 μM, 25 μM, 50 μM) were tested. Nevertheless, we cannot exclude that lower or higher concentrations of certain compounds may have shown more pronounced effects. Additional studies will be required to identify the optimal dose for each single drug.

Since TGF-β and dexamethasone could mask the anabolic and anti-inflammatory effect of the compounds, these two essential chondrogenic components were removed from our culture media and replaced with TCM compounds. Among them, we reported bioactivity for Epi A, Epi C, 2-O-rhsII, Icariin, VA, PS, PCA, 4-HBA and 5-HMF, which could increase matrix production in *human* OA chondrocytes at different doses. Furthermore, at the transcriptional level in the inflammatory model, in pellets treated with Epi C, the expression of anabolic marker genes including *COL-II* and *ACAN* was significantly increased compared to the vehicle group. There is limited literature available on the anabolic effect of these compounds on articular chondrocytes. Icariin, as a widely-studied TCM compound with similar chemical structure as Epi C, has been proposed as a potential promoting compound for cartilage repair and can be used as a substitute for growth factors [36].

In contrast, the anti-inflammatory effects of certain TCM compounds are better characterized in the literature. Since IL-1β and TNF-α are key regulators of inflammatory pathways and induce the synthesis of MMPs, prostaglandins, aggrecanases [52] and other pro-inflammatory cytokines, these two cytokines were used to induce inflammation in our *in vitro* inflammatory model. Biochemical characterization of pellets (long term) demonstrated that adding 1 ng/mL of IL-1β and TNF-α significantly decreased extracellular matrix production of the samples. Although a certain donor variation was noticed, the same trend in three independent donors in response to inflammatory cytokines and after treatment with the compounds was observed. We showed that pellets (short term) treated with VA, Epi C, PS, PCA, 4-HBA and 5-HMF could reduce the inflammatory response, and expression of *MMP13*, the critical target gene in OA progression, was significantly inhibited [53,54]. In the groups treated with VA, Epi C, PCA, 4-HBA and 5-HMF, other catabolic marker genes including *MMP1* and *MMP3* were downregulated. Additionally, *COX-2* was inhibited in all the treatment groups except 4-HBA and PS. *COX-2* is recognized as an inflammatory enzyme which can promote other inflammatory mediators including prostaglandins. Inhibition of *COX-2* can provide relief from the symptoms of inflammation and pain [55]. The mechanism of action of acetylsalicylic acid (Aspirin®), the first NSAID, involves the inhibition of COX-2 and NFκB. Aspirin® is developed from salicylates as the active components of natural Willow bark [56,57]. Interestingly, the chemical structures of VA, PCA and 4-HBA which are the extracts of *Radix ET Rhizoma Salviae*, is very similar to salicylates. Hence, these currently investigated small molecules with

anti-inflammatory effects are likely to be active through hindering the NFκB signaling pathway. An *in vivo* study using a murine model of inflammatory pain showed that VA could inhibit pro-inflammatory cytokine production by suppressing NFκB activity [49], which supports our hypothesis on the mechanism of action of VA, PCA and 4-HBA. *O*-Vanilic acid, a derivative of VA, reduced pro-inflammatory cytokine levels by inhibiting LPS-induced degradation of IκBα and nuclear translocation of NFκB in LPS-stimulated macrophages [58]. It has been shown that low daily oral doses of 3- or 4-HBA in mice were acting like Aspirin® and salicylic acids in terms of anti-inflammatory and analgesic effects [59]. PCA demonstrated promising anti-inflammatory and analgesic activity in *rat* models of both acute and chronic inflammation which was comparable with standard anti-inflammatory therapy [60]. Besides these compounds, we also reported Epi C and 5-HMF extracted from *Herba Epimedi*, as potential candidates with anti-inflammatory effects. It was demonstrated 5-HMF could suppress VCAM-1 expression in TNF-α stimulated HUVECs through inhibition of NFκB signaling pathway [45]. The anti-inflammatory effects of *Epimedium* plant extracts, such as Icariin, that act by inhibiting TNF-α and pro-inflammatory cytokines has been previously studied [61–63], and Epi C as a novel extract of this plant showed anti-inflammatory effects in our inflammatory model. Further study will be required to elucidate the exact signaling mechanisms of the compounds in *human* OA chondrocytes.

Histological and immunohistochemical staining showed that, after induction of inflammation by IL-1β/TNF-α, Saf-O staining and the staining intensity of ECM proteins, such as COL-II and ACAN, were significantly reduced. After treating pellets (long term) with VA, Epi C, PS, PCA, 4-HBA and 5-HMF, an increase in intensity for Saf-O, COL-II and ACAN in comparison with the control vehicle group was observed. These observations confirmed our inflammatory model, as well as previous results in which these compounds could preserve chondrogenic phenotype after induction of inflammation. After two weeks of treatment in phase III (recovery phase), the histological data of the control positive group treated with dexamethasone and TGF-β, showed that ECM matrix proteins including COL-II, ACAN and proteoglycans were significantly induced. However, it has been proved that in the presence of dexamethasone and TGF-β, the cells progress towards the hypertrophic phenotype [64]. Furthermore, an *in vivo* study in an osteoarthritic *mouse* model showed that the high concentration of active TGF-β1 in subchondral bone could initiate pathological changes leading to progression of OA, while

inhibition of TGF-β1 activity in subchondral bone reduced the degradation of articular cartilage [65]. Since our compounds are less potent than TGF-β1, the parts of the pellets which were not exposed to the compound supplemented medium (due to culture in non-adherent v-bottom 96-well plates) demonstrated limited matrix production. To have an equal transport of drugs throughout the pellet, a trans-well system allowing all parts of the pellet to be simultaneously exposed to the compounds may be utilized. Additionally, in future studies, we will encapsulate the selected compound(s) in a hydrogel towards development of a local intra-articular delivery system.

In the current study, *human* OA chondrocytes were used, as they are the most clinically relevant source of cells for screening of potential OA treatments. However, due to use of *human* cells isolated from macroscopically evident OA regions of the joint, limited numbers of primary cells were obtained; therefore, passaged chondrocytes were used. Although, to minimize the cell de-differentiation an established expansion medium was used that promotes cell proliferation and maintains cell differentiation ability [66]. In further pre-clinical studies, the efficacy of the compounds will be validated in an osteochondral explant culture model using a cartilage bioreactor under mechanical stimulation [67] and finally tested in an osteoarthritic animal model.

In summary, after screening of anabolic and anti-inflammatory effects of 34 bioactive compounds in different *in vitro* models of *human* OA chondrocytes, VA, Epi C, PS, PCA, 4-HBA and 5-HMF showed anti-inflammatory and anti-catabolic effects and could inhibit matrix degradation after induction of inflammation. Additionally, Epi C also induced an anabolic effect. These bioactive compounds, and combinations thereof, can be considered as anti-inflammatory and anabolic drugs for treatment of early OA. A local drug delivery system will be envisioned, as the permeability and bioavailability of the drugs in the joint are limited.

5. Supplementary information

Supplementary Table 1. Anabolic effects of TCM compounds on glycosaminoglycan production

Compound	GAG/DNA ratio in three human OA chondrocytes donors			
Conc.[µM]	1	10	25	50
5-Hydroxymethylfurfural	2.07 ± 0.43	2.08 ± 0.26	2.79 ± 0.62	2.62 ± 0.36
Protocatechuicaldehyde	3.39± 1.23	2.97 ± 0.66	2.23 ± 0.47	2.05 ± 0.32
Vanillic acid	3.47 ± 0.12	2.58 ± 0.65	3.32 ± 1.22	2.14 ± 0.41
4-Hydroxybenzoicacid	2.01 ± 0.65	1.98 ± 0.33	2.89 ± 0.53	1.34 ± 0.63
Chlorogenic acid	1.53 ± 0.23	2.52 ± 0.97	2.07 ± 0.32	0.88 ± 0.39
Cryptochlorogenic acid	2.26 ± 0.55	1.29 ± 0.42	2.74 ± 0.87	0.91 ± 0.21
Loganic acid	0.85 ± 0.13	0.91 ± 0.26	0.82 ± 0.58	0.93 ± 0.22
Loganin	0.71 ± 0.14	1.69 ± 0.42	2.31 ± 0.37	0.16 ± 0.22
Isobavachalcone	1.70 ± 0.37	2.30 ± 0.75	1.59 ± 0.62	1.16 ± 0.56
Sweroside	2.17 ± 0.33	1.83 ± 0.82	2.07 ± 0.94	1.35 ± 0.22
(+)-Cycloolivil	2.49 ± 0.52	1.18 ± 0.58	1.82 ± 0.32	0.19 ± 0.07
Baohuoside I	2.54 ± 0.68	2.92 ± 0.42	1.65 ± 0.74	0.59 ± 0.04
2'-O-rhamnosylicariside II	3.40 ± 0.65	2.48 ± 0.53	3.65 ± 0.42	2.46 ± 0.23
Epimedin A	2.92 ± 0.64	2.54 ± 0.23	3.64 ± 0.35	2.18 ± 0.48
Epimedin B	2.14 ± 0.46	2.04 ± 0.22	2.75 ± 0.74	1.62 ± 0.26
Epimedin C	2.16 ± 0.54	2.27 ± 0.30	3.82 ± 0.43	3.53 ± 0.32
Isobavachin	1.74 ± 0.64	2.00 ± 0.28	1.50 ± 0.31	1.18 ± 0.46
Bavachin	2.21 ± 0.34	2.05 ± 0.63	2.38 ± 0.83	0.84 ± 0.13
Bavachinin	0.12 ± 0.07	0.32 ± 0.13	0.24 ± 0.02	0.17 ± 0.03
Neobavaisoflavone	1.08 ± 0.12	0.85 ± 0.14	0.91 ± 0.29	0.14 ± 0.05
Corylin	0.59 ± 0.15	0.88 ± 0.12	0.90 ± 0.43	0.53 ± 0.16
Epimedin A1	1.03 ± 0.32	0.88 ± 0.57	0.92 ± 0.14	0.08 ± 0.04
Psoralen	1.47± 0.48	1.31 ± 0.34	1.70 ± 0.63	0.81± 0.38
Isopsoralen	1.15 ± 0.47	0.90 ± 0.29	0.80 ± 0.14	0.84 ± 0.22
(S)-Bukuchiol	1.13 ± 0.35	1.15 ± 0.42	0.79 ± 0.26	0.88 ± 0.12
Psoralidin	2.18 ± 0.57	1.67 ± 0.42	2.56 ± 0.78	1.74 ± 0.85
Asperosaponin VI	0.83 ± 0.18	0.80 ± 0.23	0.79 ± 0.19	0.79 ± 0.34
Baohuoside II	0.59 ± 0.03	0.79 ± 0.24	1.04 ± 0.28	0.77 ± 0.09
Epimedoside A	0.93 ± 0.07	0.82 ± 0.14	0.82 ± 0.04	0.67 ± 0.17
Baohuoside V	0.96 ± 0.08	0.92 ± 0.05	0.88 ± 0.06	0.76 ± 0.03
Corylifol A	1.14 ± 0.42	1.27 ± 0.31	1.03 ± 0.03	0.64 ± 0.07
4'-O-Methyl-broussochalcone	0.95 ± 0.22	0.78 ± 0.14	0.89 ± 0.19	0.89 ± 0.23
Anhydroicaritin	0.93 ± 0.02	0.80 ± 0.26	1.36 ± 0.28	0.93 ± 0.14
Icariin	2.28 ± 0.17	2.25 ± 0.32	2.97 ± 0.53	2.81 ± 0.52

1. Isolation procedure for “Xian-Ling-Gu-Bao” extraction

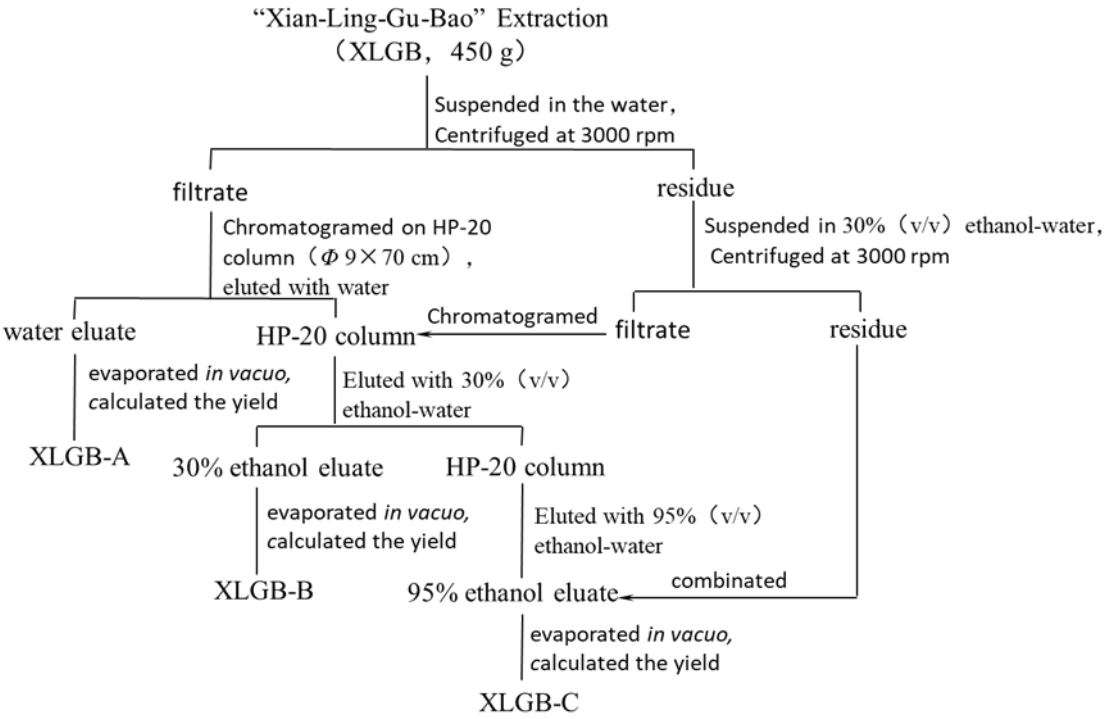

2. Isolation procedure for active fractions XLGB-B and XLGB-C

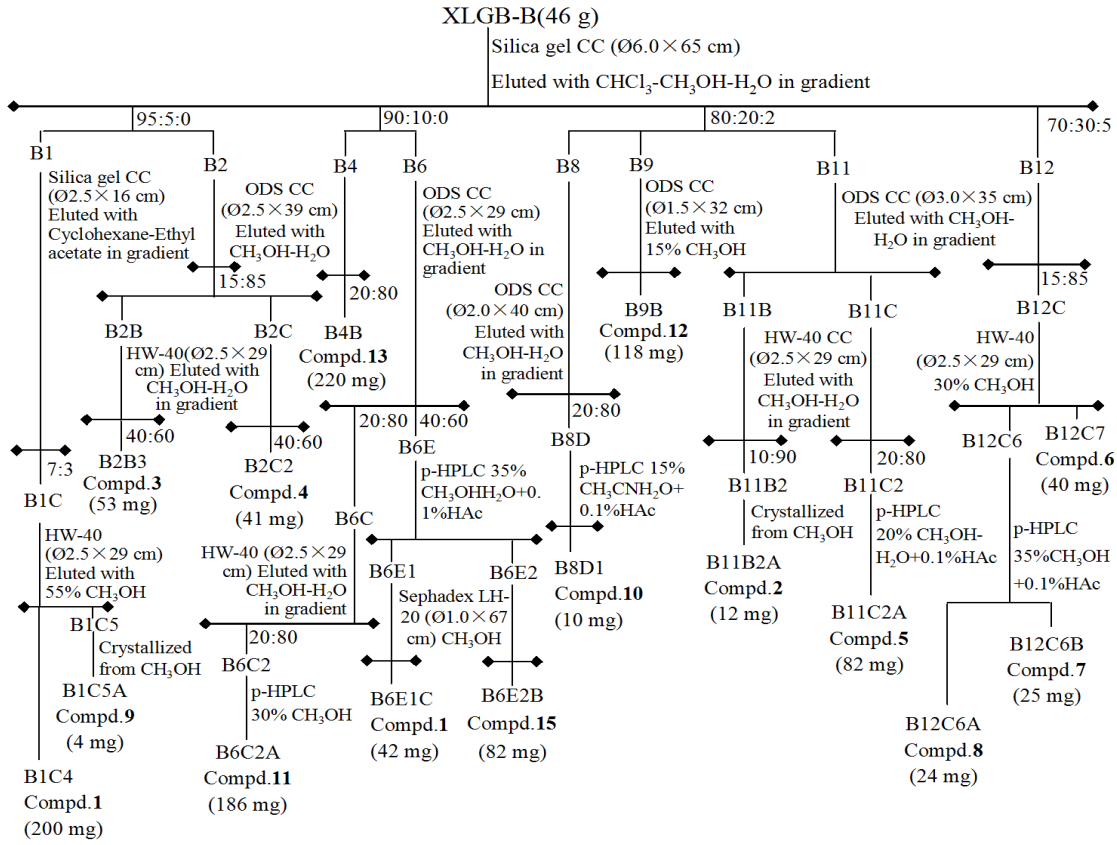

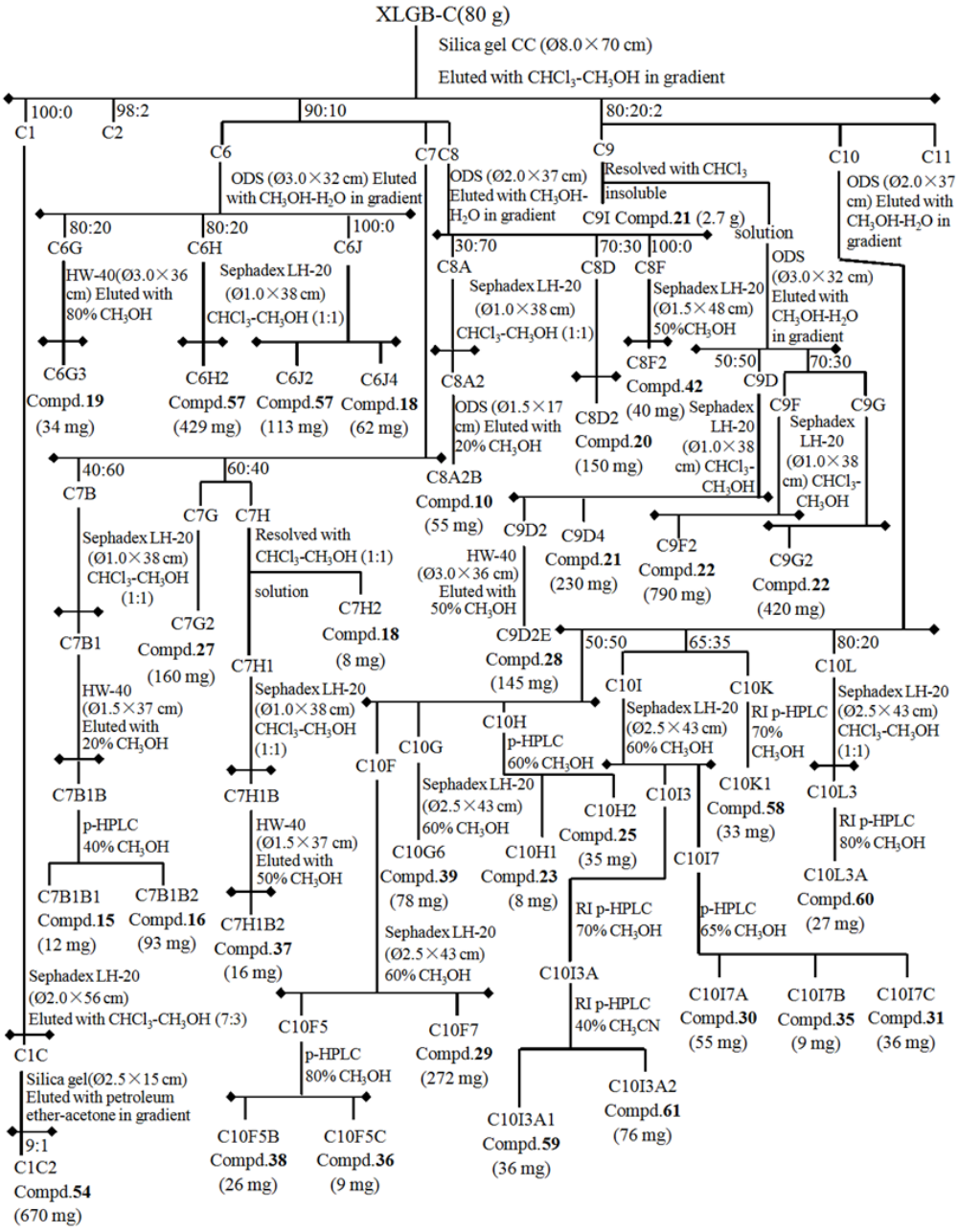

Supplementary Figure 1. Extraction methods of the active compounds from XLGB-B and XLGB-C capsules

6. References

1. Lawrence, R.C.; Felson, D.T.; Helmick, C.G.; Arnold, L.M.; Choi, H.; Deyo, R.A.; Gabriel, S.; Hirsch, R.; Hochberg, M.C.; Hunder, G.G., et al. Estimates of the prevalence of arthritis and other rheumatic conditions in the United States. Part II. *Arthritis Rheum.* **2008**, *58*, 26–35, doi: 10.1002/art.23176.
2. Wallace, I.J.; Worthington, S.; Felson, D.T.; Jurmain, R.D.; Wren, K.T.; Maijanen, H.; Woods, R.J.; Lieberman, D.E. Knee osteoarthritis has doubled in prevalence since the mid-20th century. *Proceedings of the National Academy of Sciences.* **2017**, 114, 9332, doi:10.1073/pnas.1703856114.
3. Mobasheri, A. The future of osteoarthritis therapeutics: Emerging biological therapy. *Curr. Rheumatol. Rep.* **2013**, *15*, 385, doi: 10.1007/s11926-013-0385-4.
4. Shane Anderson, A.; Loeser, R.F. Why is osteoarthritis an age-related disease? *Best Pract. Res. Clin. Rheumatol.* **2010**, *24*, 15–26, doi: 10.1016/j.berh.2009.08.006.
5. Carames, B.; Taniguchi, N.; Otsuki, S.; Blanco, F.J.; Lotz, M. Autophagy is a protective mechanism in normal cartilage, and its aging-related loss is linked with cell death and osteoarthritis. *Arthritis Rheum.* **2010**, *62*, 791–801, doi: 10.1002/art.27305.
6. Loeser, R.F. Age-related changes in the musculoskeletal system and the development of osteoarthritis. *Clin. Geriatr. Med.* **2010**, *26*, 371–386, doi: 10.1016/j.cger.2010.03.002.
7. Krishnan, Y.; Grodzinsky, A.J. Cartilage diseases. *Matrix Biol. J. Int. Soc. Matrix Biol.* **2018**, 51-69, doi: 10.1016/j.matbio.2018.05.005.
8. Clockaerts, S.; Bastiaansen-Jenniskens, Y.M.; Runhaar, J.; Van Osch, G.J.; Van Offel, J.F.; Verhaar, J.A.; De Clerck, L.S.; Somville, J. The infrapatellar fat pad should be considered as an active osteoarthritic joint tissue: A narrative review. *Osteoarthr. Cartil. Osteoarthr. Res. Soc.* **2010**, *18*, 876–882, doi: 10.1016/j.joca.2010.03.014.
9. Williams, A.; Kamper, S.J.; Wiggers, J.H.; O'Brien, K.M.; Lee, H.; Wolfenden, L.; Yoong, S.L.; Robson, E.; McAuley, J.H.; Hartvigsen, J., et al. Musculoskeletal conditions may increase the risk of chronic disease: A systematic review and meta-analysis of cohort studies. *BMC Med.* **2018**, *16*, 167, doi: 10.1186/s12916-018-1151-2.
10. Tellegen, A.R.; Rudnik-Jansen, I.; Pouran, B.; de Visser, H.M.; Weinans, H.H.; Thomas, R.E.; Kik, M.J.L.; Grinwis, G.C.M.; Thies, J.C.; Woike, N., et al. Controlled release of celecoxib inhibits inflammation, bone cysts and osteophyte formation in a preclinical model of osteoarthritis. *Drug Deliv.* **2018**, *25*, 1438–1447, doi: 10.1080/10717544.2018.1482971.
11. Cokelaere, S.M.; Plomp, S.G.M.; de Boef, E.; de Leeuw, M.; Bool, S.; van de Lest, C.H.A.; van Weeren, P.R.; Korthagen, N.M. Sustained intra-articular release of celecoxib in an equine repeated LPS synovitis model. *Eur. J. Pharm. Biopharm.: Off. J. Arb. fur Pharm. Verfahr. e.V* **2018**, *128*, 327–336, doi: 10.1016/j.ejpb.2018.05.001.
12. van den Driest, J.J.; Pijnenburg, P.; Bindels, P.J.E.; Bierma-Zeinstra, S.M.A.; Schiphof, D. Analgesic Use in Dutch Patients with Osteoarthritis: Frequent but Low Doses. *J. Clin. Rheumatol.* **2018**, doi: 10.1097/rhu.0000000000000853.
13. Solomon, D.H.; Husni, M.E.; Libby, P.A.; Yeomans, N.D.; Lincoff, A.M.; Lupsilonscher, T.F.; Menon, V.; Brennan, D.M.; Wisniewski, L.M.; Nissen, S.E., et al. The Risk of Major NSAID Toxicity with Celecoxib, Ibuprofen, or Naproxen: A Secondary Analysis of the PRECISION Trial. *Am. J. Med.* **2017**, *130*, 1415-1422.e1414, doi: 10.1016/j.amjmed.2017.06.028.
14. Pincus, T.; Koch, G.; Lei, H.; Mangal, B.; Sokka, T.; Moskowitz, R.; Wolfe, F.; Gibofsky, A.; Simon, L.; Zlotnick, S., et al. Patient Preference for Placebo, Acetaminophen (paracetamol) or Celecoxib Efficacy Studies (PACES): Two randomised, double blind, placebo controlled, crossover clinical trials in patients with knee or hip osteoarthritis. *Ann. Rheum. Dis.* **2004**, *63*, 931–939, doi: 10.1136/ard.2003.020313.
15. Moskowitz, R.W.; Abramson, S.B.; Berenbaum, F.; Simon, L.S.; Hochberg, M. Coxibs and NSAIDs--is the air any clearer? Perspectives from the OARSI/International COX-2 Study Group Workshop 2007. *Osteoarthr. Cartil. OARS, Osteoarthr. Res. Soc.* **2007**, *15*, 849–856, doi: 10.1016/j.joca.2007.06.012.

16. Marcu, K.B.; Otero, M.; Olivotto, E.; Borzi, R.M.; Goldring, M.B. NF-kappaB signaling: Multiple angles to target OA. *Curr. Drug Targets* **2010**, *11*, 599–613.
17. Urech, D.M.; Feige, U.; Ewert, S.; Schlosser, V.; Ottiger, M.; Polzer, K.; Schett, G.; Lichtlen, P. Anti-inflammatory and cartilage-protecting effects of an intra-articularly injected anti-TNFa single-chain Fv antibody (ESBA105) designed for local therapeutic use. *Ann. Rheum. Dis.* **2010**, *69*, 443–449, doi: 10.1136/ard.2008.105775.
18. Goldring, M.B.; Otero, M. Inflammation in osteoarthritis. *Curr. Opin. Rheumatol.* **2011**, *23*, 471–478, doi: 10.1097/BOR.0b013e328349c2b1.
19. Rovati, L.C.; Girolami, F.; Persiani, S. Crystalline glucosamine sulfate in the management of knee osteoarthritis: Efficacy, safety, and pharmacokinetic properties. *Ther. Adv. Musculoskelet. Dis.* **2012**, *4*, 167–180, doi: 10.1177/1759720x12437753.
20. Jevsevar, D.; Donnelly, P.; Brown, G.A.; Cummins, D.S. Viscosupplementation for Osteoarthritis of the Knee: A Systematic Review of the Evidence. *J. Bone Jt. Surg. Am. Vol.* **2015**, *97*, 2047–2060, doi: 10.2106/jbjs.n.00743.
21. Clough, T.M.; Alvi, F.; Majeed, H. Total ankle arthroplasty: What are the risks? *Bone Jt. J.* **2018**, 1352–1358, doi: 10.1302/0301-620x.100b10.bjj-2018-0180.r1.
22. Ronn, K.; Reischl, N.; Gautier, E.; Jacobi, M. Current surgical treatment of knee osteoarthritis. *Arthritis* **2011**, *2011*, 454873, doi:10.1155/2011/454873.
23. Zhang, W.; Moskowitz, R.W.; Nuki, G.; Abramson, S.; Altman, R.D.; Arden, N.; Bierma-Zeinstra, S.; Brandt, K.D.; Croft, P.; Doherty, M., et al. OARSI recommendations for the management of hip and knee osteoarthritis, Part II: OARSI evidence-based, expert consensus guidelines. *Osteoarthr. Cartil. OARS, Osteoarthr. Res. Soc.* **2008**, *16*, 137–162, doi: 10.1016/j.joca.2007.12.013.
24. Zhu, F.; Ma, X.H.; Qin, C.; Tao, L.; Liu, X.; Shi, Z.; Zhang, C.L.; Tan, C.Y.; Chen, Y.Z.; Jiang, Y.Y. Drug discovery prospect from untapped species: Indications from approved natural product drugs. *PLoS ONE* **2012**, *7*, e39782, doi: 10.1371/journal.pone.0039782.
25. Newman, D.J.; Cragg, G.M.; Snader, K.M. Natural products as sources of new drugs over the period 1981-2002. *J. Nat. Prod.* **2003**, *66*, 1022–1037, doi: 10.1021/np030096l.
26. Toegel, S.; Wu, S.Q.; Otero, M.; Goldring, M.B.; Leelapornpisid, P.; Chiari, C.; Kolb, A.; Unger, F.M.; Windhager, R.; Viernstein, H. Caesalpinia sappan extract inhibits IL1beta-mediated overexpression of matrix metalloproteinases in human chondrocytes. *Genes Nutr.* **2012**, *7*, 307–318, doi: 10.1007/s12263-011-0244-8.
27. Moussaieff, A.; Shohami, E.; Kashman, Y.; Fride, E.; Schmitz, M.L.; Renner, F.; Fiebich, B.L.; Munoz, E.; Ben-Neriah, Y.; Mechoulam, R. Incensole acetate, a novel anti-inflammatory compound isolated from Boswellia resin, inhibits nuclear factor-kappa B activation. *Mol. Pharmacol.* **2007**, *72*, 1657–1664, doi: 10.1124/mol.107.038810.
28. Kim, J.H.; Kismali, G.; Gupta, S.C. Natural products for the prevention and treatment of chronic inflammatory diseases: Integrating traditional medicine into modern chronic diseases care. *Evid.-Based Complementary Altern. Med. : eCAM* **2018**, *2018*, 9837863, doi: 10.1155/2018/9837863.
29. Mobasheri, A.; Henrotin, Y.; Biesalski, H.K.; Shakibaei, M. Scientific evidence and rationale for the development of curcumin and resveratrol as nutraceutricals for joint health. *Int. J. Mol. Sci.* **2012**, *13*, 4202–4232, doi: 10.3390/ijms13044202.
30. Chen, Y.J.; Tsai, K.S.; Chan, D.C.; Lan, K.C.; Chen, C.F.; Yang, R.S.; Liu, S.H. Honokiol, a low molecular weight natural product, prevents inflammatory response and cartilage matrix degradation in human osteoarthritis chondrocytes. *J. Orthop. Res.: Off. Publ. Orthop. Res. Soc.* **2014**, *32*, 573–580, doi: 10.1002/jor.22577.
31. Gui, L.; Shen, H. Application of Xianlinggubao in bone and arthrosis disease. *Chin. J. New Drugs Clin. Rem.* **2007**, *26*, 619–622.
32. Zhu, H.M.; Qin, L.; Garnero, P.; Genant, H.K.; Zhang, G.; Dai, K.; Yao, X.; Gu, G.; Hao, Y.; Li, Z., et al. The first multicenter and randomized clinical trial of herbal Fufang for treatment of postmenopausal

osteoporosis. *Osteoporos. Int.: J. Establ. Result Coop. Eur. Found. Osteoporos. National Osteoporos. Found. USA* **2012**, *23*, 1317–1327, doi: 10.1007/s00198-011-1577-2.

33. Li, Z.R.; Cheng, L.M.; Wang, K.Z.; Yang, N.P.; Yang, S.H.; He, W.; Wang, Y.S.; Wang, Z.M.; Yang, P.; Liu, X.Z., et al. Herbal Fufang Xian Ling Gu Bao prevents corticosteroid-induced osteonecrosis of the femoral head-A first multicentre, randomised, double-blind, placebo-controlled clinical trial. *J. Orthop. Transl.* **2018**, *12*, 36–44, doi: 10.1016/j.jot.2017.11.001.
34. Wang, F.; Shi, L.; Zhang, Y.; Wang, K.; Pei, F.; Zhu, H.; Shi, Z.; Tao, T.; Li, Z.; Zeng, P., et al. A traditional herbal formula xianlinggubao for pain control and function improvement in patients with knee and hand oSteoarthritis: A multicenter, randomized, open-label, controlled trial. *Evid.-Based Complementary alternative Med. : eCAM* **2018**, *2018*, 1827528, doi: 10.1155/2018/1827528.
35. Dai, Y.; Tu, F.J.; Yao, Z.H.; Ding, B.; Xu, W.; Qiu, X.H.; Yao, X.S. Rapid identification of chemical constituents in traditional Chinese medicine fufang preparation xianling gubao capsule by LC-linear ion trap/Orbitrap mass spectrometry. *Am. J. Chin. Med.* **2013**, *41*, 1181–1198, doi: 10.1142/S0192415X13500808.
36. Li, D.; Yuan, T.; Zhang, X.; Xiao, Y.; Wang, R.; Fan, Y.; Zhang, X. Icariin: A potential promoting compound for cartilage tissue engineering. *Osteoarthr. Cartil. OARS, Osteoarthr. Res. Soc.* **2012**, *20*, 1647–1656, doi: 10.1016/j.joca.2012.08.009.
37. Li, C.; Li, Q.; Mei, Q.; Lu, T. Pharmacological effects and pharmacokinetic properties of icariin, the major bioactive component in Herba Epimedii. *Life Sci.* **2015**, *126*, 57–68, doi: 10.1016/j.lfs.2015.01.006.
38. Pietschmann, P.; Mechtcheriakova, D.; Meshcheryakova, A.; Foger-Samwald, U.; Ellinger, I. Immunology of Osteoporosis: A Mini-Review. *Gerontology* **2016**, *62*, 128–137, doi: 10.1159/000431091.
39. Ginaldi, L.; Di Benedetto, M.C.; De Martinis, M. Osteoporosis, inflammation and ageing. *Immun. Ageing* **2005**, *2*, 14, doi: 10.1186/1742-4933-2-14.
40. Faienza, M.F.; Ventura, A.; Marzano, F.; Cavallo, L. Postmenopausal osteoporosis: The role of immune system cells. *Clin. Dev. Immunol.* **2013**, *2013*, 575936, doi: 10.1155/2013/575936.
41. Sapir-Koren, R.; Livshits, G. Postmenopausal osteoporosis in rheumatoid arthritis: The estrogen deficiency-immune mechanisms link. *Bone* **2017**, *103*, 102–115, doi: 10.1016/j.bone.2017.06.020.
42. Mathy-Hartert, M.; Jacquemond-Collet, I.; Priem, F.; Sanchez, C.; Lambert, C.; Henrotin, Y. Curcumin inhibits pro-inflammatory mediators and metalloproteinase-3 production by chondrocytes. *Inflamm. Res.: Off. J. Eur. Histamine Res. Soc.* **2009**, *58*, 899–908, doi: 10.1007/s00011-009-0063-1.
43. Csaki, C.; Mobasheri, A.; Shakibaei, M. Synergistic chondroprotective effects of curcumin and resveratrol in human articular chondrocytes: Inhibition of IL-1beta-induced NF-kappaB-mediated inflammation and apoptosis. *Arthritis Res. Ther.* **2009**, *11*, R165, doi: 10.1186/ar2850.
44. Xu, X.; Shi, D.; Shen, Y.; Xu, Z.; Dai, J.; Chen, D.; Teng, H.; Jiang, Q. Full-thickness cartilage defects are repaired via a microfracture technique and intraarticular injection of the small-molecule compound kartogenin. *Arthritis Res. Ther.* **2015**, *17*, 20, doi: 10.1186/s13075-015-0537-1.
45. Kim, H.K.; Choi, Y.W.; Lee, E.N.; Park, J.K.; Kim, S.G.; Park, D.J.; Kim, B.S.; Lim, Y.T.; Yoon, S. 5-Hydroxymethylfurfural from black garlic extract prevents TNFalpha-induced monocytic cell adhesion to HUVECs by suppression of vascular cell adhesion molecule-1 expression, reactive oxygen species generation and NF-kappaB activation. *Phytother. Res.: PTR* **2011**, *25*, 965–974, doi: 10.1002/ptr.3351.
46. Zeng, L.; Wang, W.; Rong, X.F.; Zhong, Y.; Jia, P.; Zhou, G.Q.; Li, R.H. Chondroprotective effects and multi-target mechanisms of Icariin in IL-1 beta-induced human SW 1353 chondrosarcoma cells and a rat osteoarthritis model. *Int. Immunopharmacol.* **2014**, *18*, 175–181, doi: 10.1016/j.intimp.2013.11.021.
47. Wang, P.; Zhang, F.; He, Q.; Wang, J.; Shiu, H.T.; Shu, Y.; Tsang, W.P.; Liang, S.; Zhao, K.; Wan, C. Flavonoid Compound Icariin Activates Hypoxia Inducible Factor-1alpha in Chondrocytes and Promotes Articular Cartilage Repair. *PLoS ONE* **2016**, *11*, e0148372, doi: 10.1371/journal.pone.0148372.
48. Kankala, R.K.; Lu, F.J.; Liu, C.G.; Zhang, S.S.; Chen, A.Z.; Wang, S.B. Effect of Icariin on Engineered 3D-Printed Porous Scaffolds for Cartilage Repair. *Materials* **2018**, *11*, doi: 10.3390/ma11081390.
49. Calixto-Campos, C.; Carvalho, T.T.; Hohmann, M.S.; Pinho-Ribeiro, F.A.; Fattori, V.; Manchope, M.F.; Zarpelon, A.C.; Baracat, M.M.; Georgetti, S.R.; Casagrande, R., et al. Vanillic Acid Inhibits Inflammatory

Pain by Inhibiting Neutrophil Recruitment, Oxidative Stress, Cytokine Production, and NFkappaB Activation in Mice. *J. Nat. Prod.* **2015**, *78*, 1799–1808, doi: 10.1021/acs.jnatprod.5b00246.

50. Rao, Z.; Wang, S.; Wang, J. Protective effects of psoralidin on IL1betainduced chondrocyte apoptosis. *Mol. Med. Rep.* **2018**, *17*, 3418–3424, doi: 10.3892/mmr.2017.8248.
51. Cao, H.J.; Li, C.R.; Wang, L.Y.; Ziadlou, R.; Grad, S.; Zhang, Y.; Cheng, Y.; Lai, Y.X.; Yao, X.S.; Alini, M., et al. Effect and mechanism of psoralidin on promoting osteogenesis and inhibiting adipogenesis. *Phytomedicine* **2019**, *61*, 152860, doi: 10.1016/j.phymed.2019.152860.
52. Echtermeyer, F.; Bertrand, J.; Dreier, R.; Meinecke, I.; Neugebauer, K.; Fuerst, M.; Lee, Y.J.; Song, Y.W.; Herzog, C.; Theilmeier, G., et al. Syndecan-4 regulates ADAMTS-5 activation and cartilage breakdown in osteoarthritis. *Nature Med.* **2009**, *15*, 1072–1076, doi: 10.1038/nm.1998.
53. Wang, M.; Sampson, E.R.; Jin, H.; Li, J.; Ke, Q.H.; Im, H.J.; Chen, D. MMP13 is a critical target gene during the progression of osteoarthritis. *Arthritis Res. Ther.* **2013**, *15*, R5, doi: 10.1186/ar4133.
54. Li, H.; Wang, D.; Yuan, Y.; Min, J. New insights on the MMP-13 regulatory network in the pathogenesis of early osteoarthritis. *Arthritis Res. Ther.* **2017**, *19*, 248, doi: 10.1186/s13075-017-1454-2.
55. Laine, L.; White, W.B.; Rostom, A.; Hochberg, M. COX-2 selective inhibitors in the treatment of osteoarthritis. *Semin. Arthritis Rheum.* **2008**, *38*, 165–187, doi: 10.1016/j.semarthrit.2007.10.004.
56. Rainsford, K.D. Anti-inflammatory drugs in the 21st century. *Sub-cellular biochemistry* **2007**, *42*, 3–27.
57. Kopp, E.; Ghosh, S. Inhibition of NF-kappa B by sodium salicylate and aspirin. *Science* **1994**, *265*, 956–959.
58. Lee, J.-K.; Lee, S.L.; Shin, T.-Y.S.; Khang, D.K.; Kim, S.-H.K. Anti-inflammatory effect of o-vanillic acid on lipopolysaccharide-stimulated macrophages and inflammation models. *J. Food Nutr. Res.* **2018**, *6*, 227–233.
59. Khan, S.A.; Chatterjee, S.S.; Kumar, V. Low dose aspirin like analgesic and anti-inflammatory activities of mono-hydroxybenzoic acids in stressed rodents. *Life Sci.* **2016**, *148*, 53–62, doi: 10.1016/j.lfs.2016.02.032.
60. Lende, A.B.; Kshirsagar, A.D.; Deshpande, A.D.; Muley, M.M.; Patil, R.R.; Bafna, P.A.; Naik, S.R. Anti-inflammatory and analgesic activity of protocatechuic acid in rats and mice. *Inflammopharmacology* **2011**, *19*, 255–263, doi: 10.1007/s10787-011-0086-4.
61. Ti, H.; Wu, P.; Xu, L.; Wei, X. A novel icariin type flavonoid from Epimedium pseudowushanense. *Nat. Prod. Res.* **2018**, 1–8, doi: 10.1080/14786419.2018.1481840.
62. Oh, Y.C.; Jeong, Y.H.; Cho, W.K.; Ha, J.H.; Lee, S.J.; Ma, J.Y. Inhibitory Effects of Epimedium Herb on the Inflammatory Response In Vitro and In Vivo. *Am. J. Chin. Med.* **2015**, *43*, 953–968, doi: 10.1142/s0192415x1550055x.
63. Liu, M.H.; Sun, J.S.; Tsai, S.W.; Sheu, S.Y.; Chen, M.H. Icariin protects murine chondrocytes from lipopolysaccharide-induced inflammatory responses and extracellular matrix degradation. *Nutr. Res.* **2010**, *30*, 57–65, doi: 10.1016/j.nutres.2009.10.020.
64. Johnstone, B.; Hering, T.M.; Caplan, A.I.; Goldberg, V.M.; Yoo, J.U. In vitro chondrogenesis of bone marrow-derived mesenchymal progenitor cells. *Experimental Cell Res.* **1998**, *238*, 265–272, doi: 10.1006/excr.1997.3858.
65. Zhen, G.; Wen, C.; Jia, X.; Li, Y.; Crane, J.L.; Mears, S.C.; Askin, F.B.; Frassica, F.J.; Chang, W.; Yao, J., et al. Inhibition of TGF-β signaling in mesenchymal stem cells of subchondral bone attenuates osteoarthritis. *Nat. Med.* **2013**, *19*, 704–712, doi :10.1038/nm.3143.
66. Jakob, M.; Demarteau, O.; Schafer, D.; Hintermann, B.; Dick, W.; Heberer, M.; Martin, I. Specific growth factors during the expansion and redifferentiation of adult human articular chondrocytes enhance chondrogenesis and cartilaginous tissue formation in vitro. *J. Cell. Biochem.* **2001**, *81*, 368–377, doi: 10.1002/1097-4644(20010501)81
67. Vainieri, M.L.; Wahl, D.; Alini, M.; van Osch, G.; Grad, S. Mechanically stimulated osteochondral organ culture for evaluation of biomaterials in cartilage repair studies. *Acta Biomater.* **2018**, *81*, 256–266, doi: 10.1016/j.actbio.2018.09.058.
68. Tu, F.; Dai, Y.; Yao, Z.; Wang, X.; Yao, X.; Qin, L. Flavonol glycosides from Epimedium pubescens. *Chem. Pharm. Bull.* **2011**, *59*, 1317–1321, doi: 10.1248/cpb.59.1317.

69. Sebastian Müller, L.A., Xiaomei Wang, M. Zia Karim, Ajay Matta, Arne M.; Stefan Schaeren, S.F., Marcel Jakob, Ivan Martin, Andrea Barbero, W. Mark Erwin. Notochordal cell conditioned medium (NCCM) regenerates end-stage human osteoarthritic articular chondrocytes and promotes a healthy phenotype. *Arthritis Res. Ther.* **2016**, *18*, 125.
70. Liu, S.Q.; Saijo, K.; Todoroki, T.; Ohno, T. Induction of human autologous cytotoxic T lymphocytes on formalin-fixed and paraffin-embedded tumour sections. *Nat. Med.* **1995**, *1*, 267–271.
71. Li, Z.; Lang, G.; Chen, X.; Sacks, H.; Mantzur, C.; Tropp, U.; Mader, K.T.; Smallwood, T.C.; Sammon, C.; Richards, R.G., et al. Polyurethane scaffold with in situ swelling capacity for nucleus pulposus replacement. *Biomaterials* **2016**, *84*, 196–209, doi: 10.1016/j.biomaterials.2016.01.040.
72. de Abreu Costa, L.; Henrique Fernandes Ottoni, M.; Dos Santos, M.G.; Meireles, A.B.; Gomes de Almeida, V.; de Fatima Pereira, W.; Alves de Avelar-Freitas, B.; Eustaquio Alvim Brito-Melo, G. Dimethyl Sulfoxide (DMSO) Decreases Cell Proliferation and TNF-alpha, IFN-gamma, and IL-2 Cytokines Production in Cultures of Peripheral Blood Lymphocytes. *Molecules* **2017**, *22*, doi: 10.3390/molecules22111789.
73. Neumann, A.J.; Gardner, O.F.; Williams, R.; Alini, M.; Archer, C.W.; Stoddart, M.J. Human Articular Cartilage Progenitor Cells Are Responsive to Mechanical Stimulation and Adenoviral-Mediated Overexpression of Bone-Morphogenetic Protein 2. *PLoS ONE* **2015**, *10*, e0136229, doi: 10.1371/journal.pone.0136229.
74. Scotti, C.; Osmokrovic, A.; Wolf, F.; Miot, S.; Peretti, G.M.; Barbero, A.; Martin, I. Response of human engineered cartilage based on articular or nasal chondrocytes to interleukin-1beta and low oxygen. *Tissue Eng. Part A* **2012**, *18*, 362–372, doi: 10.1089/ten.TEA.2011.0234.
75. Whitley, C.B.; Ridnour, M.D.; Draper, K.A.; Dutton, C.M.; Neglia, J.P. Diagnostic test for mucopolysaccharidosis. I. Direct method for quantifying excessive urinary glycosaminoglycan excretion. *Clin. Chem.* **1989**, *35*, 374–379.
76. Livak, K.J.; Schmittgen, T.D. Analysis of relative gene expression data using real-time quantitative PCR and the 2(-Delta Delta C(T)) Method. *Methods* **2001**, *25*, 402–408, doi: 10.1006/meth.2001.1262.
77. Milz, S.; Aktas, T.; Putz, R.; Benjamin, M. Expression of extracellular matrix molecules typical of articular cartilage in the human scapholunate interosseous ligament. *J. Anat.* **2006**, *208*, 671–679, doi: 10.1111/j.1469-7580.2006.00552.x.

Chapter 3

Anti-inflammatory and chondroprotective effects of Vanillic acid and Epimedin C in human osteoarthritic chondrocytes

Reihane Ziadlou [1,2], Andrea Barbero [2], Ivan Martin [2,3], Xin-luan Wang [4], Ling Qin [4,5], Mauro Alini [1] and Sibylle Grad [1,6]

[1] AO Research Institute Davos, Davos Platz, 7270, Switzerland

[2] Department of Biomedical Engineering, University of Basel, Allschwil, 4123, Switzerland

[3] Department of Biomedicine, University Hospital Basel, University of Basel, Basel, 4001, Switzerland

[4] Translational Medicine R&D Center, Shenzhen Institutes of Advanced Technology, Chinese Academy of Sciences, Shenzhen, 518057, China

[5] Department of Orthopaedics & Traumatology, the Chinese University of Hong Kong, Hong Kong SAR, China

[6] Department of Health Sciences and Technology, ETH Zürich, Zürich, 8092, Switzerland

Published in *Biomolecules* **2020***, Jun 19;10(6):932.*

Abstract

In osteoarthritis (OA) inhibition of excessively expressed pro-inflammatory cytokines in the OA joint and increasing the anabolism for cartilage regeneration are necessary. In this ex-vivo study, we used an inflammatory model of *human* OA chondrocytes microtissues, consisting of treatment with cytokines (IL-1β/TNF-α) with or without supplementation of six herbal compounds with previously identified chondroprotective effect. The compounds were assessed for their capacity to modulate the key catabolic and anabolic factors using several molecular analyses. We selectively investigated the mechanism of action of the two most potent compounds Vanillic acid (VA) and Epimedin C (Epi C). After identification of the anti-inflammatory and anabolic properties of VA and Epi C, the Ingenuity Pathway Analysis showed that in both treatment groups, osteoarthritic signaling pathways were inhibited. In the treatment group with VA, NF-κB signaling was inhibited through inhibition of IKK complex and attenuation of phosphorylation. Epi C showed a significant anabolic effect by increasing the expression of collagenous and non-collagenous matrix proteins. In conclusion, VA, through inhibition of phosphorylation in NF-κB signaling pathway and Epi C, by increasing the expression of extracellular matrix components, showed significant anti-inflammatory and anabolic properties and might be potentially used in combination to treat or prevent joint OA.

1. Introduction

Articular cartilage is an avascular tissue with low cell density which is composed of chondrocytes as the unique cellular component existing in the tissue, and extracellular matrix (ECM) molecules including collagens, proteoglycans and non-collagen proteins. The matrix turn-over rate in the tissue is slow, and in the healthy cartilage, there is a balance between synthesis and degradation of ECM components [1]. In osteoarthritis (OA) this equilibrium is disrupted and the rate of degradation of ECM components is higher than the deposition of newly synthesized molecules [2-4]. Previous studies have reported that interleukin 1β (IL1-β) and tumor necrosis factor α (TNF-α) are the main pro-inflammatory cytokines initiating inflammation and causing matrix degradation in OA [5,6]. They activate chondrocytes and synovial cells to produce matrix metalloproteinases (MMPs), aggrecanases, cyclooxygenease-2 (COX-2), prostaglandins (PGEs) and inducible nitric oxide synthase (iNOS) [7]. It is also known that these two cytokines activate or inhibit several different signaling pathways

including the Nuclear factor kappa-light-chain-enhancer of activated B cells (NF-κB), high-mobility group box 1 (HMGB1), mitogen-activated protein kinases (MAPKs), interleukin-1 receptor (IL-1R)/Toll-like receptor (TLR) and phosphoinositide-3-kinase/protein kinase B/ the mammalian target of rapamycin (PI3K/Akt/mTOR) pathways [8-18].

NF-κB controls the expression of genes involved in several physiological responses such as inflammatory response; hence, NF-κB dysregulation can cause inflammatory diseases such as OA and rheumatoid arthritis (RA). The NF-κB proteins are normally forming a complex with nuclear factor of kappa light polypeptide gene enhancer in B-cells inhibitor alpha (IκBα) protein which keeps it in an inactive state in the cytoplasm [19]. In the activated canonical pathway, the IκB kinase (IKK) complex phosphorylates IκB proteins which leads to the activation of NF-κB complex for translocation to the nucleus and the transcription of genes involved in inflammation including immunomodulatory molecules, cytokines, COX-2, MMPs and iNOS [20-22].

Several inhibitors that specifically target signaling pathways by inhibiting key proteins and upstream regulators in the pathway, have shown therapeutic potential for treatment of OA in pre-clinical studies [23-30].

Furthermore, IL-1β and TNF-α suppress the expression of the genes associated with the differentiated chondrocyte phenotype, including type II collagen (COL2A1) and aggrecan (ACAN) [31,32]. Presently available drugs for the treatment of OA including nonsteroidal anti-inflammatory drugs (NSAIDs) and COX2 inhibitors are known to have adverse gastrointestinal and cardiovascular effects [31,33]. Also, some supplements like glucosamine and chondroitin have been used for treatment of OA, though they showed inconsistent and non-significant effects in the treatment of OA [34,35]. In the recent years, several herbal and synthetic small molecules which were more potent than natural supplements (glucosamine) and could circumvent the side effects of NSAIDs, have been attributed a great potential for OA therapy [36-39]. Some of these compounds with herbal origins can act through specific signaling pathways and inhibit inflammation or increase matrix synthesis [40-43]. For instance, compounds including Resveratrol, Curcumin, Honokiol and Anemonin could block IL-1β induced NF-κB signaling and inhibit inflammation [44-48]. Furthermore, Berberine and Geniposide could act through inhibition of p38 signaling pathway [49,50]. Icariin, as a widely-studied herba Epimedii has been proposed as a potential promoting herbal molecule for cartilage repair [51,52]. However, there is limited literature available on the anabolic effect of

herbal compounds in cartilage regeneration. In our previous study, after screening of 34 most abundant compounds in the herbal Fufang Xian Ling Gu Bao formula (XLGB), which has been used for treatment of osteoporosis, aseptic osteonecrosis, osteoarthritis and bone fractures in Traditional Chinese Medicine (TCM) [53-56], we found 6 small molecules with potent anabolic and anti-inflammatory properties [57].

In the current study, RNA sequencing was performed to analyzes the transcriptome of gene expression patterns of IL-1β/TNF-α treated OA chondrocytes in the presence or absence of the six most potent compounds identified in the previous study. These compounds were additionally assayed for their capacity to modulate the transcription and translation of key catabolic and anabolic factors. We then selectively investigated the mechanisms regulating the anti-inflammatory and pro-anabolic effects of the two most effective compounds Vanillic acid (VA) and Epimedin C (Epi C).

2. Materials and Methods

2.1. Isolation of human osteoarthritic chondrocytes and cell expansion

Cartilage tissues were obtained from four patients with end stage OA after the total knee arthroplasty (ages 71, 72, 64 and 82 years; all female) at the University Hospital of Basel under ethical agreement (Ethikkommission beider Basel, Ref.Nr. EK: 78/07). The cells were isolated as described previously elsewhere [58]. In brief, after cutting the tissues with a scalpel into small pieces, they were digested overnight in 0.2 % collagenase II (300 U/mg, Worthington Biochemical Corp, Lakewood, NJ, USA) on an orbital shaker at 37 °C. The isolated chondrocytes were expanded for three passages to 80% confluency in basal medium (BM, Dulbecco's modified Eagle medium, high glucose (DMEM)), 1 mM sodium pyruvate, 10 mM HEPES, 1% penicillin/streptomycin (P/S), and 0.29 mg/mL glutamate (all from Gibco), supplemented with 10% fetal bovine serum (FBS), 1 ng/mL transforming growth factor (TGF)-ß1 and 5 ng/mL fibroblast growth factor-2 (FGF-2) (both from Fitzgerald Acton, MO, USA) in a humidified incubator (37 °C, 5% CO2).

2.2. Inflammatory model of 3D microtissues for small molecules testing

As previously described [57], chondrocytes 3D microtissues (pellets) were generated after centrifugation of the cells at 400 g for 5 min (2.5×10^5 cells per pellet in 250 µL medium) in v-

bottom, non-adherent 96-well plates. 3D microtissue were cultured using standard chondrogenic medium (BM supplemented with 1.25 mg/mL human serum albumin (Gibco, Life Technologies Limited, Paisley, UK), ITS- Premix (Corning, Bedford, MA, USA), 0.1 mM ascorbic acid 2-phosphate (Sigma-Aldrich, St. Louis, MO, USA), 1% P/S, 10 ng/mL TGF-β1 and 10^{-7} M dexamethasone (Sigma Aldrich, St. Louis, MO, USA)). After one week of culture in chondrogenic medium for cartilage matrix generation (phase I), pellets were exposed to interleukin 1 beta (IL-1β) and tumor necrosis factor alpha (TNF-α) (both from Peprotech, London, UK), each at 1 ng/mL, for 72 h (phase II) for induction of inflammation. Simultaneously, pellets were treated with the compounds in their effective dosage from our previous screening study [57], including 1 µM of VA, Psoralidin (PS), Protocatechuicaldehyde (PCA) and 25 µM of Epi C, 4-Hydroxybenzoic acid (4-HBA), 5-Hydroxymethylfurfural (5-HMF), or control vehicle (Ctr vehicle) group containing 0.25 % and 0.01% v/v dimethyl sulfoxide (DMSO). At the end of the phase II, pellets were harvested for RNA extraction, RNA sequencing and transcriptional analysis. The remaining pellets were cultured and treated with the compounds for three more days (Phase III). At the end of each phase (II and III), the supernatants were collected and stored at -20°C for further analysis. In the phase II and phase III, pellets were cultured in chondropermissive medium (chondrogenic medium deprived of TGF-β1 and dexamethasone). 3D microtissues were cultured at 37 °C, 5% CO2, with medium changes twice per week. The chemical structure of the compounds showed previously [57].

2.3. RNA extraction for sequencing and gene expression analysis

We extracted the total RNA with TRI Reagent (Molecular Research Center). Briefly, 1 mL of TRI reagent was added to the pooled replicates of 3 pellets from 4 independent donors. After homogenization by a Tissue Lyser (Qiagen) for 3 minutes and 5 Hz, the phase separation by 1-bromo-3-chloropropane (Sigma) in a volume ratio of 1:10 with the TRI reagent was performed. The quantity and quality of the RNA samples were measured by using Nanodrop (Thermo Scientific, Waltham, MA, USA) and Bioanalyzer (Agilent, Santa Clara, CA, USA). RNA sequencing experiments and further data analysis were conducted at QIAGEN Genomic Services (Hilden, Germany).

2.4. Library preparation for Next Generation Sequencing and Ingenuity Pathway Analysis

The library preparation and Next Generation Sequencing (NGS) was performed through QIAGEN Genomic Services (Hilden, Germany). Microarray data were selectively analyzed for VA and Epi C using QIAGEN's Ingenuity® Pathway Analysis software (IPA®, QIAGEN Redwood City). The significant differently expressed genes were analyzed in different categories including IPA's downstream effect analysis, IPA's upstream effect analysis and the canonical pathways.

2.5. Gene Expression Analysis

For the reverse transcription SuperScript VILO cDNA Synthesis Kit (Life Technologies, Carlsbad, CA) was used. For confirmation of the sequencing results, quantitative real-time PCR was accomplished using the Quant Studio - 6 instrument (Life Technologies). The gene expression assays for C-X-C motif chemokine 12 (*CXCL12*), C-C motif chemokine ligand 11 (*CCL11*), interleukin 23 subunit alpha (*IL23A*), matrix metalloproteinase 12 (*MMP12*), ADAM metallopeptidase with thrombospondin type 1 motif 16 (*ADAMTS16*), interleukin 6 (IL-6), growth differentiation factor 5 (*GDF-5*), cartilage oligomeric matrix protein (*COMP*), cellular communication factor 2 (*CCN2*) and 18S rRNA are listed in Table 1 (all from ThermoFisher Scientific, Waltham, MA, USA). The relative gene expression was calculated using the $2^{-\Delta\Delta CT}$ quantitative method [59], with 18S ribosomal RNA as endogenous control.

RT^2 Profiler PCR Array (Qiagen) in 96-well plates for 84 NF-κB pathway genes and 5 housekeeping genes was performed. The data of the treatment group with VA were normalized to Ctr vehicle group. The relative gene expression was calculated using the $2^{-\Delta\Delta CT}$ quantitative method and normalized with the average of the 4 housekeeping genes beta actin (*ACTB*), beta 2 microglobulin (*B2M*), glyceraldehyde 3-phosphate dehydrogenase (*GAPDH*), and ribosomal protein lateral stalk subunit P0 (*RLPLP0*) as endogenous control.

Table 1. Gene expression assays (*human*) used for Real-Time PCR.

Gene	Probe Type	Assay ID
CXCL12	5′ FAM-3′ NFQ	Hs03676656_mH
CCL11	5′ FAM-3′ NFQ	Hs00237013_m1
IL23A	5′ FAM-3′ NFQ	Hs00372324_m1
MMP12	5′ FAM-3′ NFQ	Hs00159178_m1
ADAMTS16	5′ FAM-3′ NFQ	Hs00373526_m1
IL-6	5′ FAM-3′ NFQ	Hs00174131_m1
COMP	5′ FAM-3′ NFQ	Hs00164359_m1
GDF-5	5′ FAM-3′ NFQ	Hs00167060_m1
CCN2	5′ FAM-3′ NFQ	Hs00170014_m1
18s fast	5′ FAM-3′ NFQ	Hs99999901_s1

CXCL12: C-X-C motif chemokine 12, *CCL11:* C-C motif chemokine ligand 11, *IL23A:* interleukin 23A, *MMP12:* matrix metalloproteinase 12, *ADAMTS16:* A Disintegrin and Metalloproteinase with Thrombospondin motifs 16, *IL-6:* interleukin 6, *GDF-5*: growth differentiation factor 5, *COMP:* cartilage oligomeric matrix protein, *CCN2:* connective tissue growth factor and *18S rRNA* (all from ThermoFisher Scientific). FAM: Carboxyfluorescein; NFQ: nonfluorescent quencher

2.6. Matrix metalloproteinase (MMP) activity in supernatants of treated and control vehicle samples

Using MMP Activity Assay Kit (Abcam, Cambridge, UK), the general activity of MMP enzymes was measured in cell culture supernatants of phase III. In this technique, a fluorescence resonance energy transfer (FRET) peptide as a generic MMP activity indicator is used. After cleavage into two separate fragments by MMPs, the fluorescence is retrieved. Briefly, 25 µL of the samples were mixed with an equal volume of 2 mM 4-aminophenylmercuric acetate (APMA) working solution and incubated for 3 hours at 37 °C to activate the MMPs. Then 50 µL of MMP Green Substrate working solution were added to the sample and control wells of the assay plate. The signal was detected by a fluorescence microplate reader (Victor 3, PerkinElmer, Waltham, MA, US) at Ex/Em = 490/525 nm.

2.7. Immunoassay for pro-inflammatory cytokine quantification

Using the Proinflammatory Panel 1 (*human*) kit (MesoScale Discovery, Rockville, MD), 9 cytokines that are important in inflammation response, immune system regulation as well as other biological processes were measured. For this respect, the supernatants were collected at

day 3 of inflammatory phase III. Concentrations of secreted cytokines in supernatants, including interferon gamma (IFN-γ), IL-1β, IL-2, IL-4, IL-12, IL-13, IL-6, IL-8 and TNF-α were quantified.

2.8. Nuclear and cytoplasmic protein extraction of human OA chondrocytes

To verify the effect of VA (as anti-inflammatory compound) on IL-1β/TNF-α dependent NF-κB pathway activation, levels of key proteins in the NF-κB pathway were assessed by Western blot analysis. For this respect, after 2D expansion of *human* OA chondrocytes in tissue culture flasks (TPP, Trasadingen, Switzerland) to 80% confluency, inflammation was induced using 1 ng/mL IL-1β/TNF-α and the cells were either treated with 1 µM VA simultaneously for 15, 30 and 60 minutes or in the control group with the same concentration of DMSO as control vehicle. Furthermore, a control group without induction of inflammation and treated with DMSO (control positive group) was included. After the treatment, the cells were trypsinized and washed twice in 1 mL ice-cold phosphate buffered saline (PBS). Then, 10 x 10^6 cells were transferred to 1.5 mL microcentrifuge tubes and the cytoplasmic and nuclear cell extracts were prepared based on the manufacture protocol (NE-PER™ Nuclear and Cytoplasmic Extraction Kit, ThermoFisher scientific). Shortly, the cell pellet was resuspended in 200 µL of ice-cold Cytoplasmic Extraction Reagent I (CER I), containing protease inhibitors. After vortexing the tube vigorously for 15 seconds, it was incubated on ice for 10 minutes. Then, 11 µL of CERII was added and the cell suspension was vigorously mixed for 5 seconds. The tube was incubated on ice for 1 minute and centrifuged for 5 minutes at maximum speed in a microcentrifuge (16,000 × g). The supernatant (cytoplasmic extract) was transferred to a pre-chilled tube and stored at -80°C. For nuclear extraction, 100 µL ice-cold Nuclear Extraction Reagent (NER) were added to the pellets and incubated for 40 minutes on ice with continued vortexing for 15 seconds every 10 minutes. Extracts were centrifuged at 16,000 × g for 10 minutes and the supernatant (nuclear extract) fraction immediately transferred to a pre-chilled tube for storage at -80°C.

2.9. Western blotting

The protein concentration of nuclear and cytoplasmic extracts was measured using the bicinchoninic acid assay system (ThermoFisher Scientific) with bovine serum albumin as a standard. Cytoplasmic and nuclear proteins at final amounts of 20 µg and 10 µg, respectively,

per lane were loaded and separated by polyacrylamide gel electrophoresis (7.5%, gels, BioRad). The separated proteins were transferred onto nitrocellulose membranes (BioRad) and incubated in blocking buffer (1X Tris Buffered Saline/Tween (TBST) with 5% w/v nonfat dry milk) for 1 hour. The membranes were incubated overnight at 4°C with primary antibodies against Inhibitor of Nuclear Factor Kappa-B Kinase Subunit Alpha (IKKα), Inhibitor of Nuclear Factor Kappa-B Kinase Subunit beta (IKKβ), NF-κB (p65), Nuclear factor of kappa light polypeptide gene enhancer in B-cells inhibitor alpha (IκBα), Phospho-IκBα (Ser32, P-IκBα), Phospho-NF-κB p65 (Ser536, P-NF-κB), Phospho-IKKα/β (Ser176/180, P-IKKα/β) (all from Cell Signaling) in 1:1000 dilutions and GAPDH (OriGene) in 1:10000 dilution for cytoplasmic protein extracts, and NF-κB (p65), Histon 3 (H3) (Cell Signaling) for nuclear protein extracts. Membranes were washed three times with 1% PBS/Tween and were incubated with secondary antibodies including anti-rabbit IgG, Horse Radish Peroxidase (HRP)-linked antibody or anti-mouse, HRP-linked antibody (Cell Signaling) in 1:2500 final concentration in 5 mL blocking buffer with gentle agitation for 1 hour at room temperature. After 4 times washing with TBST, the blots were prepared for chemiluminescent detection with 1X SignalFire™ ECL Reagent (ThermoFisher Scientific) as HRP chemiluminescent substrate. The quantification of the chemiluminescent signal was carried out with the use of ImageJ software [60].

2.10. Statistical Analysis

Statistical analysis for the gene expression, immunoassay and MMP activity assays were performed using Graphpad Prism 8. One-way analysis of variance (ANOVA) followed by Dunnett's post hoc test (multiple comparison) was utilized as non-parametric test of four independent experiments with three replicates of *human* chondrocytes microtissues. Differences were considered statistically significant at $p < 0.05$. All Graphs are shown as box plots.

For the RNA sequencing dataset, the analysis was based on q-values. q-values are p-values that have been adjusted using the Benjamini-Hochberg False Discovery Rate (FDR) approach to correct for multiple testing. Fold changes with *q*-values below 0.05 were considered significant ($q < 0.05$).

IPA statistical analysis was based on two metrics: p-value and z-score. The *p*-values were provided by Fisher's exact test (right tailed) (*p*-value ≤ 0.05 was considered significant

association). The biological functions that were expected to be increased or decreased according to the gene expression changes in our dataset were identified using the IPA regulation z-score algorithm. The level of the calculated z-score reflects the overall predicted activation state of the regulator (<0: inhibited, >0: activated). A positive or negative z-score value indicates that a function is predicted to be increased or decreased in VA and Epi C treatment groups relative to control vehicle group (values above 2 or below -2 were considered as significant).

For the RT^2 Profiler PCR Array for the NF-κB signaling pathway, the p values were calculated based on a Student's t-test of the replicate $2^{-\Delta CT}$ values for each gene in the treatment groups versus the control group ($p < 0.05$).

For the Western blot bands quantification, two-way analysis of variance (ANOVA) followed by Tukey's post hoc test (multiple comparison) was used as non-parametric test of three independent experiments with different *human* osteoarthritic chondrocytes.

3. Results

3.1. Whole Genome RNA Sequencing and Gene Expression for the Differentially Expressed Genes

After screening of 34 small molecules extracted from XLGB capsule in different concentrations [55], the six most potent compounds including VA (1 μM), 5-HMF (25 μM), 4-HBA (25 μM), Ps (1 μM), PCA (1 μM) and Epi C (25 μM) were selected for next generation sequencing (NGS). To identify the effect of the drugs versus untreated control group, osteoarthritic chondrocytes from four independent human donors were tested for whole genome sequencing. Analysis of the sequencing results showed that about 47 genes in each treatment group were differentially expressed compared with the control group (Supplementary table 1).

3.1.1. Gene Expression Analysis

For the confirmation and validation of RNA sequencing data, real-time PCR analysis was performed for selected genes, including *CXCL12, CCL11, IL23A, MMP12, ADAMTS16, IL-6, COMP, GDF-5*, and *CCN2* (Fig. 1). The data showed that after treatment with all the six compounds, the expression of *CXCL12* and *CCL11* was significantly inhibited in comparison with the Ctr vehicle group. Also, for *IL23A* and *MMP12*, all the compounds except 5-HMF and

PS, could significantly reduce the gene expression respectively. In the treatment group with VA, the gene expression of *ADAMTS16* and *IL-6* was significantly inhibited, while the expression of *COMP* and *GDF-5* was significantly increased. Furthermore, after treatment with Epi C, the expression of *COMP*, *GDF-5* and *CCN2* was significantly up-regulated.

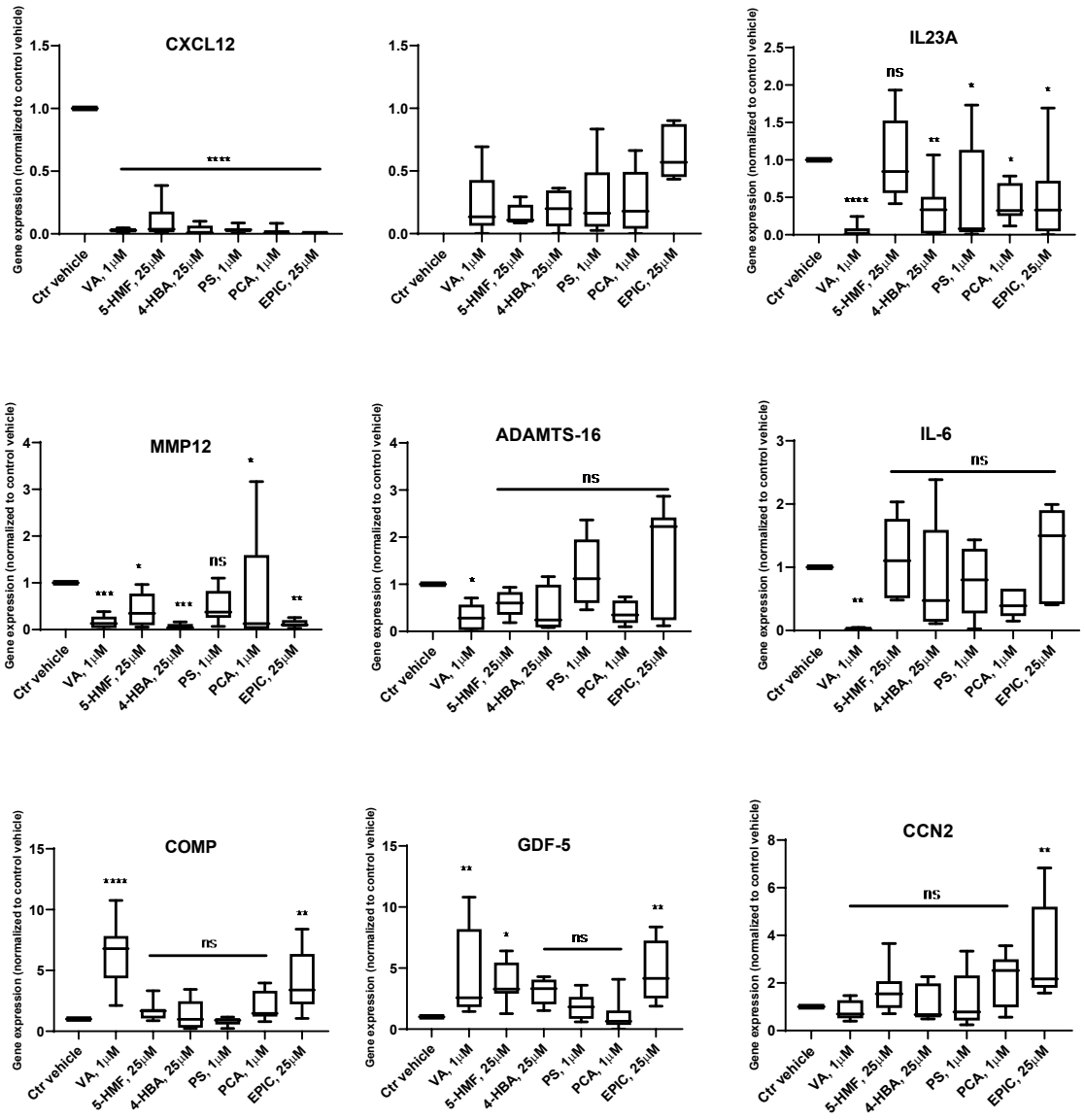

Figure 1. qPCR data showing transcriptional levels of genes differentially expressed in RNA Sequencing dataset in compound treated versus control vehicle (Ctr vehicle) group in *human* OA chondrocytes. $n = 4$; n indicates the number of *human* OA donors; for each donor three experimental replicates were analyzed. Data are normalized to the levels of control groups. For statistical analysis using Graphpad Prism, one-way analysis of variance (ANOVA) followed by Dunnett's *post hoc* test (multiple comparisons) was applied. * $p < 0.01$, ** $p < 0.001$, *** $p < 0.0005$, **** $p < 0.0001$ vs. Ctr vehicle, ns (non-significant).

3.2. Production of Cytokines in the Groups Treated with the Small Molecules versus Control

The concentration of inflammatory cytokines was measured in the conditioned medium of OA chondrocytes microtissues in phase III, which were treated with VA, 5-HMF, 4-HBA, PS, PCA, Epi C and normalized to control vehicle group. The results showed that in the treatment groups with VA, the cytokines including INFγ, IL-1β, IL-2, IL-4, IL-12, IL-13, IL-6, IL-8 and TNF-α were inhibited, and for all of them except for IL-8 and TNF-α the inhibition was significant (Fig. 2).

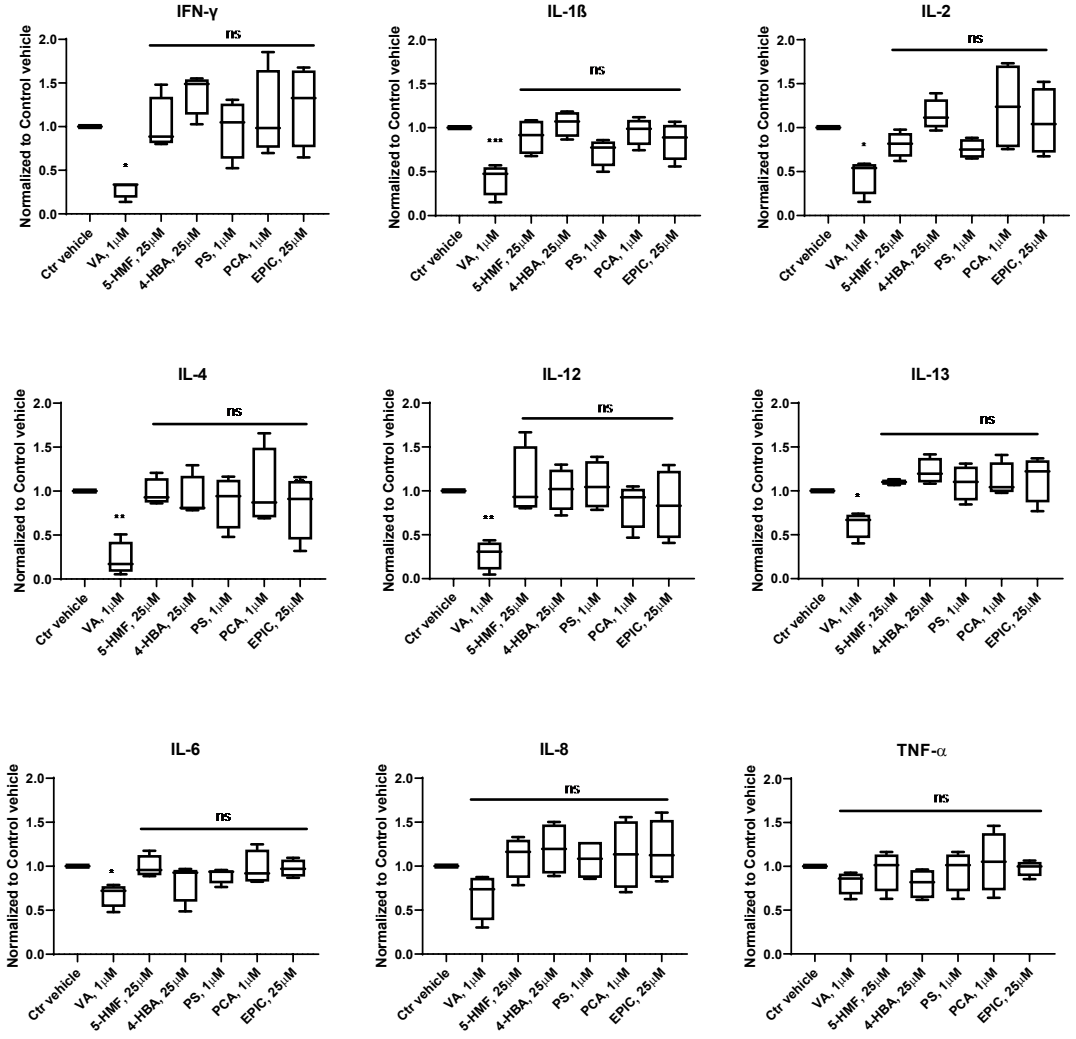

Figure 2. Expression profile of pro-inflammatory cytokines after treatment with VA, 5-HMF, 4-HBA, PS, PCA, and Epi C versus control vehicle (Ctr vehicle) group in the conditioned medium of osteoarthritic chondrocytes microtissues. The cytokines INFγ, IL-1β, IL-2, IL-4, IL-12, IL-13, IL-6, IL-8 and TNF-α in phase III were measured using multiplex immunoassay. n = 4; n indicates the number of human OA chondrocytes donors; for each donor three experimental replicates were analyzed. For the statistical analysis using Graphpad Prism, one-way analysis of variance (ANOVA) followed by Dunnett's post hoc test (multiple comparisons) was applied. * $p < 0.01$, ** $p < 0.001$, *** $p < 0.0005$ vs. Ctr vehicle.

3.3. MMP activity of the groups treated with the small molecules versus Control vehicle

MMPs are the key enzymes for the breakdown of connective tissues and play an important role in the development of OA. MMP activity for the groups treated with VA, 5-HMF, 4-HBA, PS, PCA, and Epi C versus control vehicle group was measured in the conditioned medium of osteoarthritic chondrocytes microtissues in phase III. Total protease activity for the treatment groups with VA and Epi C was significantly decreased compared to the control vehicle group (Fig. 3).

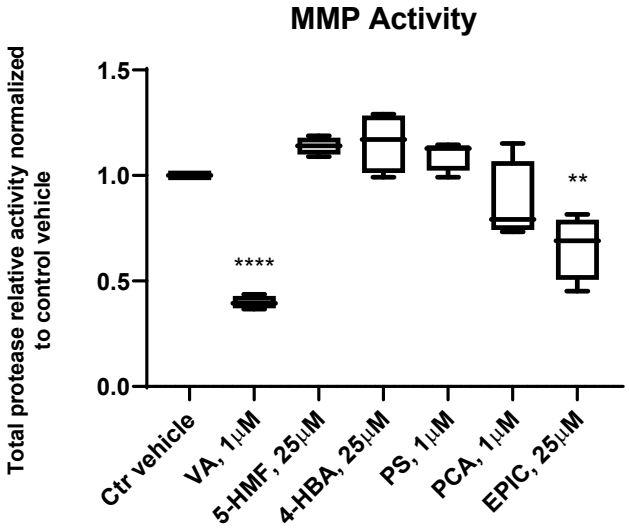

Figure 3. Matrix metalloproteinase (MMP) Activity Assay for the treated groups with VA, 5-HMF, 4-HBA, PS, PCA, and Epi C versus control vehicle (Ctr vehicle) group. MMP activity in the conditioned medium of osteoarthritic chondrocytes microtissues was measured in phase III. For the treatment groups with VA and Epi C MMP activity was significantly decreased compared to Ctr vehicle group. Total protease activity as the average relative fluorescence units (RFU) of 4 independent donors is shown. $n = 4$; n indicates the number of *human* OA chondrocytes donors; for each donor three experimental replicates were analyzed. For statistical analysis using Graphpad Prism, one-way analysis of variance (ANOVA) followed by Dunnett's *post hoc* test (multiple comparisons) was applied. ** $p < 0.001$, *** $p < 0.0005$, **** $p < 0.0001$ vs. Ctr vehicle.

3.4. Ingenuity Pathways Analysis (IPA)

Among all the treatment groups, VA and Epi C showed the most significantly differentially expressed genes and proteins in all tested donors. Therefore, data of whole genome sequencing of these two compounds versus their control negative groups were selected for Ingenuity Pathways Analysis (IPA). In general, the results of the Core analysis of the VA and Epi C data sets were driven by a remarkable down-regulation of different cytokines and chemokines as well as a substantial up-regulation of ribosomal genes and translation elongation/initiation factors.

3.4.1. IPA's downstream effect analysis

The results of IPA's downstream effect analysis for the high-level categories of biological processes demonstrated several relevant categories including Inflammatory Disease, Inflammatory Response, Immune Cell Trafficking, Connective Tissue Disorder, Protein Synthesis and Cellular Growth/Proliferation on top of the list for both VA and Epi C datasets (Supplementary Fig. 1a, b). In the low-level (specific) process or functions that belong to the high-level category "Connective Tissue Disorder" for the VA vs. control (Ctr) group, 4 terms with significant negative activation z-scores, including inflammation of the joint, rheumatic disease, experimentally induced arthritis and chondrodysplasia indicated a significant decrease of all these functions. For the Epi C vs. Ctr group, inflammation of the joint and abnormality of cartilage tissue were top results with negative z-scores (predicted decrease, non-significant) (Supplementary table. 2 a, b). From the table of top connective tissue disorders (Supplementary table 2a), the network of the term "Experimentally-induced arthritis" for VA vs. Ctr group was composed of mostly down-regulated cytokines and chemokines. Some differently expressed components of ECM, collagens, MMPs, ADAMTs, CNN2 up-regulation and NF-κB down-regulation were also observed (Fig. 4a). Also, from the table of top connective tissue disorders, the network of the term "Abnormality of cartilage tissue" for Epi C vs. Ctr group showed up-regulation of collagens, biglycan (BGN), CCN2 and SRY-Box Transcription Factor 9 (SOX9) (Fig. 4b). Furthermore, for VA vs. Ctr group the table of low-level (specific) process or functions that belong to the high-level category "Inflammatory Disease" showed similar results to "Connective Tissue Disorder". Finally, most of the terms for the table of "Immune Cell Trafficking" showed significantly negative activation z-scores that strongly indicated a reduced activation, migration, chemotaxis or movement of different immune cell types. Example network of the term "Activation of Lymphocytes" as the top disorder of "Immune Cell Trafficking" was dominated by down-regulated cytokines, chemokines and down-regulated NF-κB1 (Supplementary Fig. 2a, b). For Epi C vs. Ctr treatment group, the table of low-level (specific) process or functions that belong to the high-level category "Inflammatory Disease" showed negative activation z-scores for the terms Inflammation of the Joints, Rheumatic Disease and Chronic Inflammatory Disorder which suggested a moderate decrease of these functions or processes. The example of network for the term "Inflammation of the Joints" as a decreased function, was supported by the down-regulated chemokines/cytokines as wells as up-regulated ECM components such as COL2A1, BGN, and CCN2 (Supplementary Fig 3a, b). On

the other side, IPA also predicted a mild increase of protein translation and synthesis, which might point to an increase of anabolic activities in the microtissues treated with VA and Epi C. In this regard, several components of the ECM were found to be up-regulated, such as collagen type V alpha1 (COL5A1), collagen type VI alpha3 (COL6A3), collagen type VIII alpha1 (COL8A1), biglycan (BGN), laminin alpha 2 (LAMA2), laminin alpha 3 (LAMA3), laminin beta 1 (LAMB1), laminin gamma 1 (LAMC1) (Supplementary Fig. 4 a, b). Also, IPA upstream regulators were filtered for the proteins that could explain the up-regulation of ECM components in VA and Epi C treatment groups vs. Ctr vehicle. The data revealed that CCN2 and MYC were activated which could explain the up-regulation of ribosomal genes and translation initiation/elongation factors. The example of the upstream regulator network of CCN2 showed the up-regulation of many ECM components (Supplementary Fig. 5a, b).

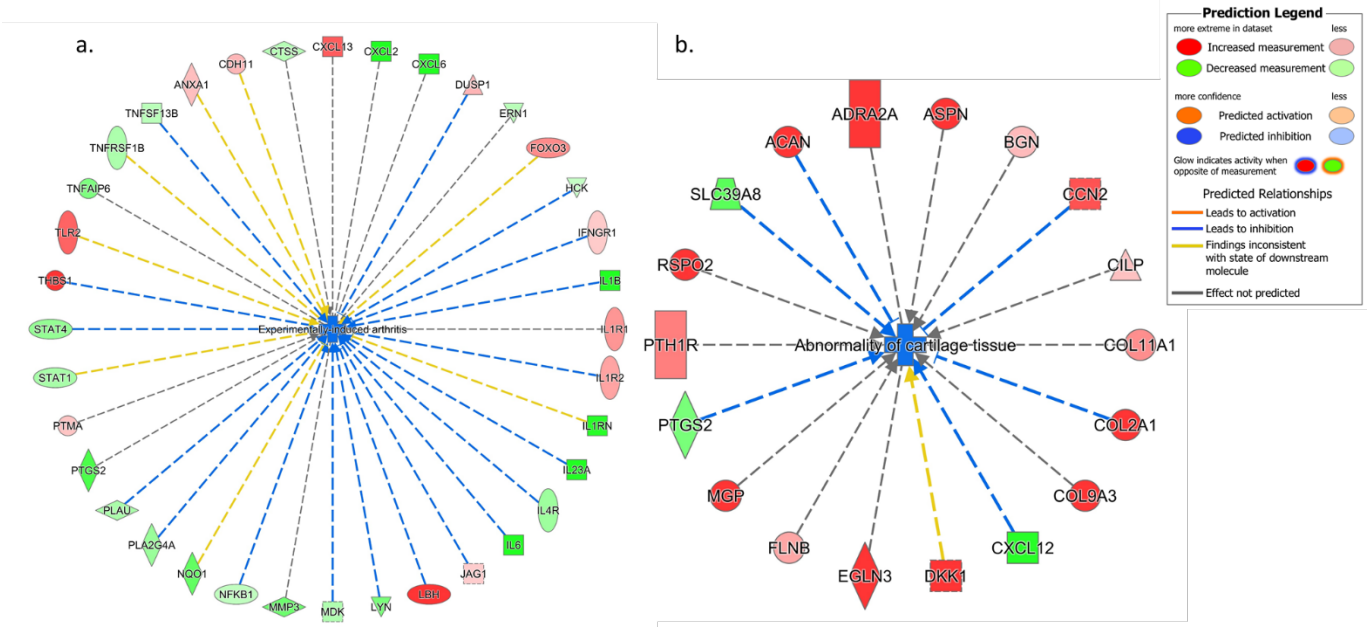

Figure 4. Ingenuity Pathways Analysis (IPA) showing top connective tissue disorders from the table of low-level (specific) process or functions. a) Example network of the term "Experimentally-induced arthritis" for VA vs. Ctr group which was composed of mostly down-regulated cytokines, chemokines and NF-κB down-regulation. b) Example network of the term "Abnormality of cartilage tissue" for Epi C vs. Ctr group which showed up-regulation of collagens, biglycan, CCN2 and SOX9. Red represents up-regulation of genes, while green represents down-regulation of genes. Light red or green represent slight up-regulation or down-regulation.

3.4.2. IPA's upstream regulator analysis

Gene expression changes in the chondrocytes treated with VA and Epi C showed an anti-inflammatory response. This was supported not only by the observed down-regulation of various cytokines, but also by IPA's upstream regulator analysis which suggested that parts of the observed gene expression changes were strongly reminiscent of effects of different anti-inflammatory or immunosuppressive compounds on transcriptomes. More specifically, in the treatment group with VA, different small molecule compounds, known to interfere with the activity of MEK/MAP or PI3 kinases were found in the list of putative upstream regulators (Supplementary table 3). This suggested that the gene expression data showed similar patterns as expected from a treatment with these small molecule kinase inhibitors. This supports the notion that the activities of these MEK/MAP and PI3 kinases were reduced in VA treatment group, which could be a hint at a substantial inhibition or reduced expression of these important kinases. In addition, the down-regulation of NF-κB or ERK1/2 (Fig. 5a, b) and up-regulation of IL-10 as anti-inflammatory cytokine, could account for the observed reduction of cytokine/chemokine expression as well as the anti-inflammatory expression pattern (Supplementary Fig. 6).

For the treatment groups with Epi C, gene expression changes in the treated chondrocytes also suggested an anti-inflammatory response. This was not only supported by the observed down-regulation of various cytokines, but also by IPA's upstream regulator analysis showing that the observed gene expression changes were strongly reminiscent of effects of an anti-inflammatory compound, dexamethasone, on transcriptomes (Supplementary table 4). Also, the upstream regulator table showed that TNF, IFNγ and STAT1 were the top inhibited upstream regulators and the upstream regulator network for the inhibited STAT1 showed several chemokines and cytokines were down-regulated (Supplementary Fig. 7).

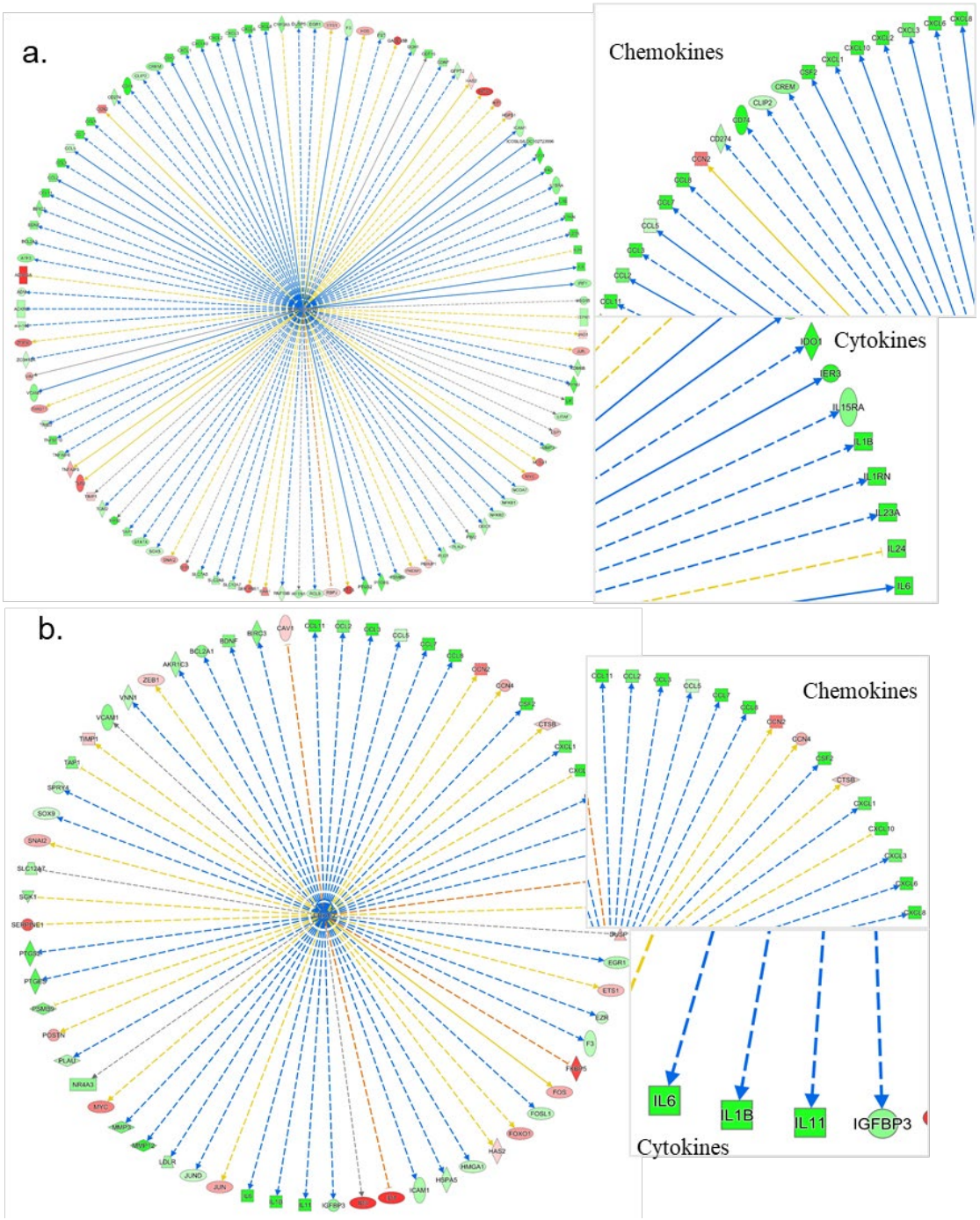

Figure 5. Ingenuity Pathways Analysis (IPA) showing upstream regulators for NF-κB and ERK1/2 for VA vs. Ctr treatment group predicted to be inhibited. The predicted inhibition of these putative upstream regulators largely agrees with the observed down-regulation of numerous chemokines and cytokines. (a) Upstream regulator network for an inhibited NF-κB complex. (b) Upstream regulator network for an inhibited ERK1/2 complex.

3.4.3. The canonical pathways

Moreover, canonical pathways that include NF-κB, such as Osteoarthritis Signaling (this canonical pathway has been described as a critical regulatory element for the onset of osteoarthritis) (Fig. 6 and supplementary Fig. 8), NF-κB signaling or HMGB1 signaling (Supplementary Fig. 9), were predicted to be inhibited. Osteoarthritis Signaling is comprised of several pathways including NF-κB, P38/MAPK, ERK/MAPK, Wnt/β-Catenin and protein kinase A signaling. By the obvious central role of a down-regulated NF-κB complex and negative z-score for the NF-κB pathway, it becomes apparent that this pathway was reduced in its activity after treatment with VA (Fig. 7).

For the treatment groups with Epi C, Osteoarthritis Signaling was significantly affected, and the inhibition of this canonical pathway was more pronounced than in VA treatment group vs. Ctr dataset (Fig. 8 and supplementary Fig. 10). In this instance, the comparison of expected node activities and actual measurements suggested a reduced activity of this canonical pathway. Interestingly, SOX9, COL2A1 and ACAN which are key markers of cartilaginous matrix production were up-regulated while NF-κB was down-regulated (Fig. 8). Additionally, among the canonical pathways that overlap with molecules associated with downstream effect term "protein translation", the mammalian target of rapamycin (mTOR Signaling) was found to be activated. In the canonical pathway “mTOR Signaling” the translational/ribosomal genes were up-regulated and among them, the up-regulation of protein kinase C (PKC) and regulated in development and DNA damage responses 1 (REDD1) was significant (Supplementary Fig. 11). Hence, these activations could indicate the increase in anabolic activities in Epi C vs. Ctr group.

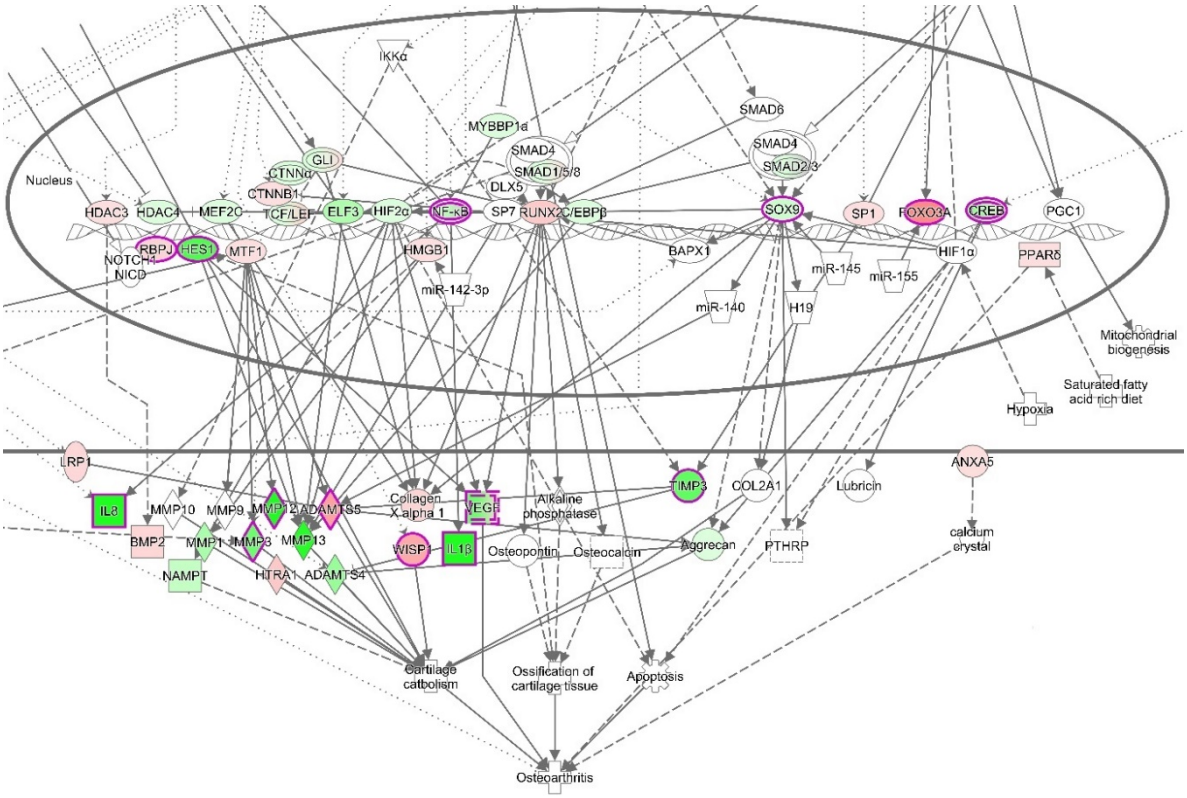

Figure 6. The canonical pathway "Osteoarthritis Signaling" for VA vs. Ctr treatment group. In this instance, the comparison of expected node activities and actual measurements suggest a reduced activity of this canonical pathway (p-value: 5.5E-12 z-score: -0.707). Noteworthy are the down-regulation of NF-κB (expected activation) and inflammatory markers including IL-1β. Red fillings = "activated", green fillings = "inhibited", purple highlights = passed cut-offs, no highlight = didn't pass cut-offs.

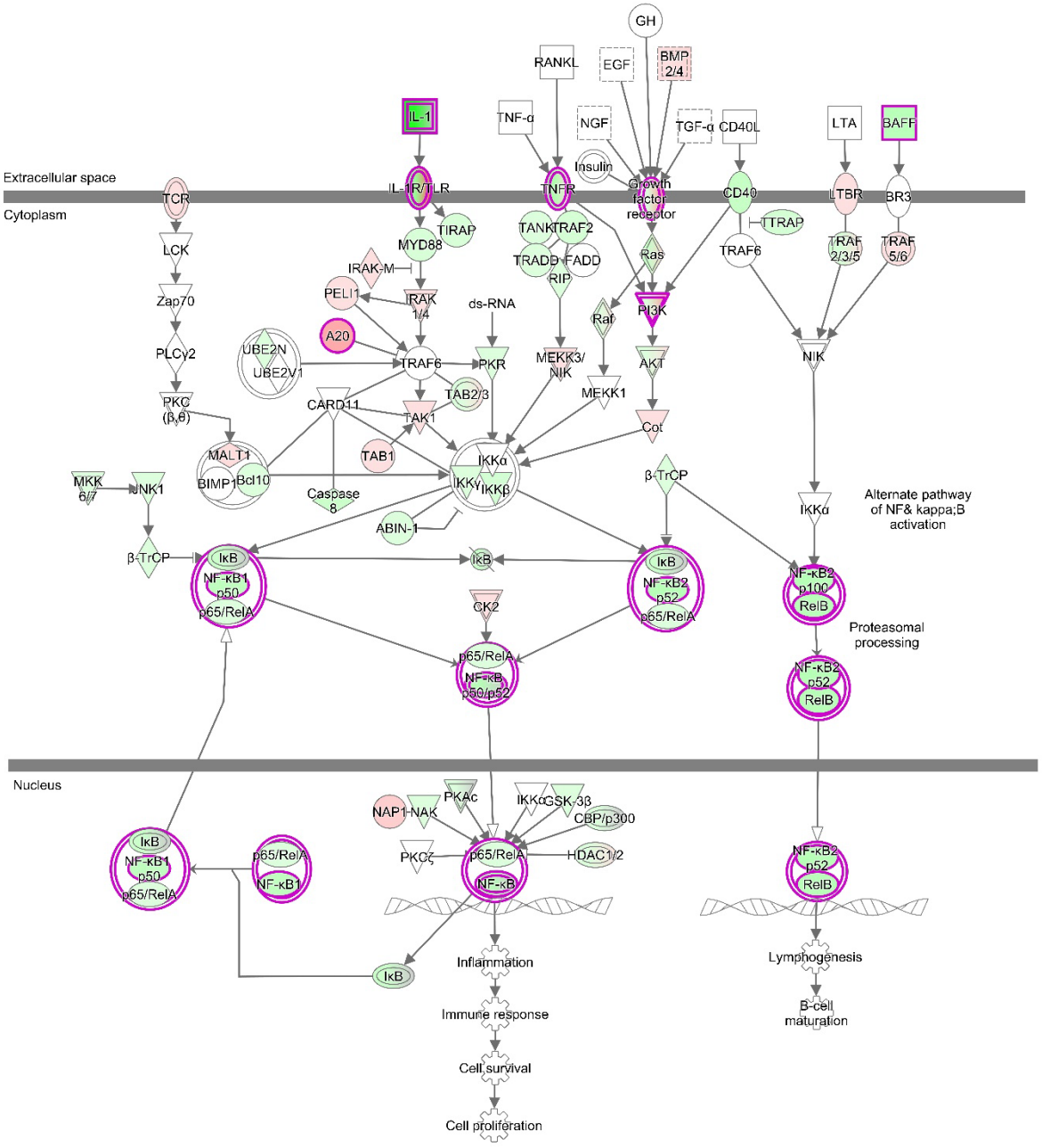

Figure 7. The canonical pathway "NF-kB Signaling" for VA vs. Ctr treatment group. This canonical pathway has a negative activation z-score (*p*-value = 4.25E-4, z-score = -0.5, tendency for inhibition). Red fillings = "activated", green fillings = "inhibited", purple highlights = passed cut-offs, no highlight = didn't pass cut-offs.

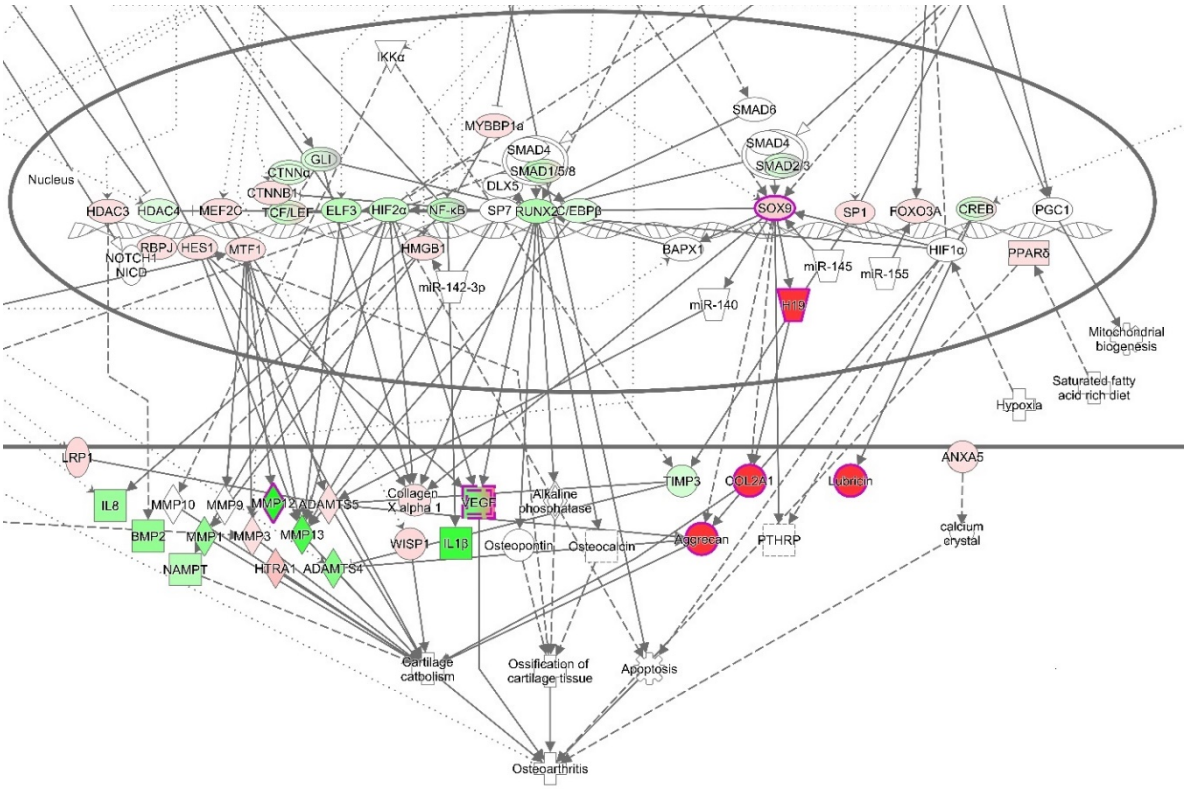

Figure 8. The canonical pathway "Osteoarthritis Signaling" for Epi C vs. Ctr treatment group. This canonical pathway has been described as a critical regulatory element for the onset of osteoarthritis. Based on the activation z-score (*p*-value = 1.45E-3, z-score = -1.213), the normal function of this pathway is reduced. Noteworthy are the down-regulation of NF-κB (expected activation) and the up-regulation of SOX9 (expected inhibition). Red fillings = "activated", green fillings = "inhibited", purple highlights = passed cut-offs, no highlight = didn't pass cut-offs.

3.5. RT² Profiler PCR Array for the NF-κB signaling pathway

The results of the PCR array for the NF-κB signaling pathway for VA vs. Ctr vehicle group showed that many of the genes in the pathway were inhibited after treatment with VA. The data of the treatment group with VA was normalized to the Ctr vehicle group and the fold change of the VA treatment group vs. Ctr vehicle showed significantly differentially expressed genes which are marked by asterisks in the heat map graphs (Fig. 9a, b). Most of the genes with significant p-values were down-regulated. These genes included BCL2 related protein A1 (*BCL2A1*), caspase recruitment domain family 11 (*CARD11*), colony stimulating factor 2 (*CSF2*), interferon gamma (*INFG*), interleukin 1-beta (*IL1β*), interleukin 8 (*CXCL8*), interleukin 1 receptor associated kinase 2 (*IRAK2*), interferon regulatory factor 1 (*IRF1*), lymphotoxin beta receptor superfamily member 3 (*LTBR*), nuclear factor of kappa light polypeptide gene enhancer in B cells inhibitor, alpha (*NFKBIA*), nuclear factor of kappa light polypeptide gene enhancer in B cells 1 (*NF-κB1*), transcription factor RelB (*RELB*), Toll like

receptor 2 (*TLR2*), Toll like receptor 4 (*TLR4*), and tumor necrosis factor (*TNF*). Some other genes, including interleukin 1 receptor 1 (*IL1R1*), Toll like receptor adaptor molecule 2 (*TICAM2*), and tissue inhibitor of metalloproteinase 1 (*TIMP1*) were significantly up-regulated. Also, the volcano plot for VA treatment group vs. Ctr vehicle showed significantly down-regulated genes which passed the -1 threshold for the (log2) fold change difference (Fig. 9c). The genes with significant fold-change values ($p < 0.05$) and fold-regulation values less than -2 are indicated in the Multigroup Plot (Fig. 9d). These genes included *CSF2, INFG, IL1B, CXCL8, TLR4,* and *TNF*.

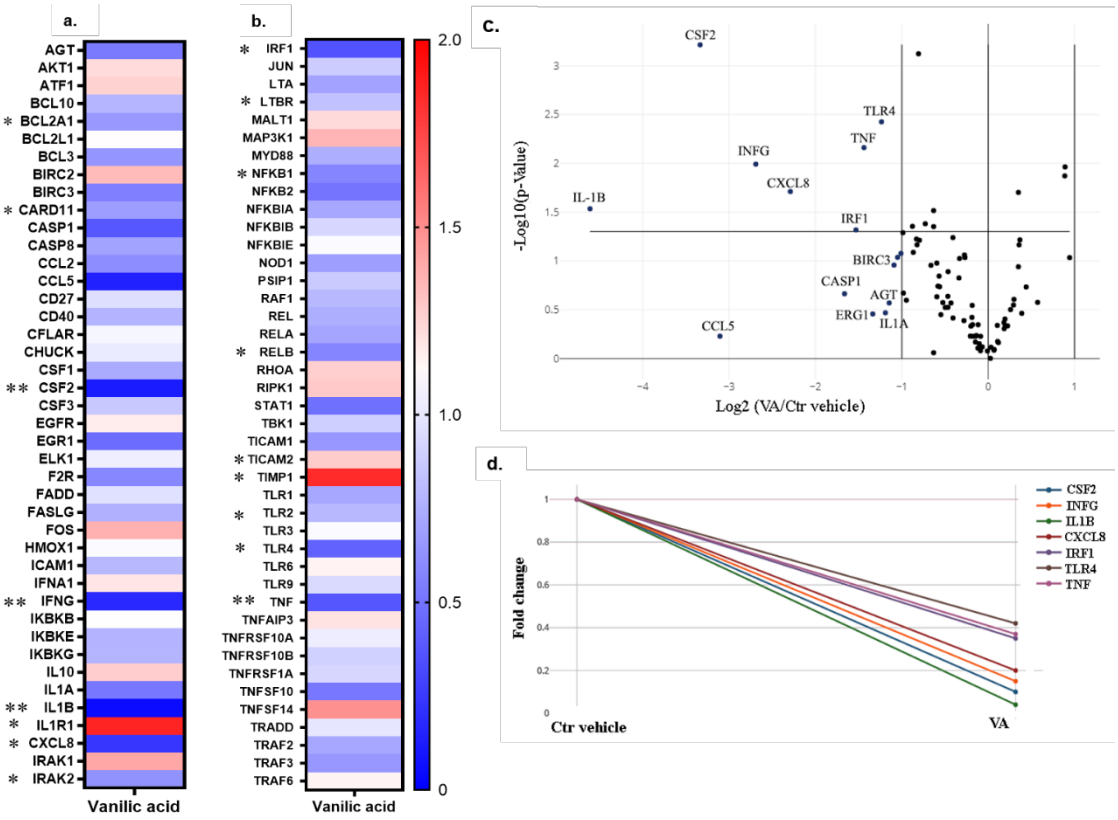

Figure 9. RT^2 Profiler PCR Array for the NF-κB signaling pathway. The data of the treatment group with VA is normalized to the Ctr vehicle group. (a, b) The average of the fold change for 3 donors of *human* OA chondrocytes shown in heat map graphs. The statistically significant genes are highlighted by the asterisk. The p values are calculated based on a Student's t-test of the replicate $2^{-\Delta CT}$ values for each gene in the control group versus treatment group. * $p < 0.05$ ** $p < 0.005$. (c) Volcano plot for VA treatment group versus Ctr vehicle showing significantly down-regulated genes which passed -1 threshold for log2 fold change difference. (d) Multigroup Plot for the genes with significant p-values and log2 fold regulations <-1. These genes include colony stimulating factor 2 (*CSF2*), interferon gamma (*INFG*), interleukin1-beta (*IL1B*), interleukin 8 (*CXCL8*), Toll-like receptor 4 (*TLR4*) and tumor necrosis factor (*TNF*).

3.6. Western blot analysis for the NF-κB signaling pathway

To further investigate the effect of VA on the NF-κB signaling pathway, the expression of the main proteins in the pathway, including IKKα, IKKβ, NF-κB (P65), P-NFκB (P-P65), IκBα, P-IκBα was determined. In the cytoplasmic extracts, the expression of P-P65, P-IκBα, and IKKβ was significantly decreased after 60 min of treatment with VA + IL-1β/TNF-α compared with the 15 min treatment groups; while these three proteins remained constant over time in the IL-1β/TNF-α group. Furthermore, the expression of P-IκBα was significantly decreased after 60 min of treatment with VA compared with the inflammatory untreated control group. On the other hand, the expression of IκBα protein was increasing similarly over time in both the VA + IL-1β/TNF-α and IL-1β/TNF-α groups. After induction of inflammation, the amount of IκBα was reduced due to the phosphorylation leading to its rapid degradation. However, after 60 minutes IκBα was resynthesized and this effeect was reversed. In the control vehicle group, the expression of the proteins at different time points remained intact. Also, the reference protein (GAPDH) was unaffected in all the experimental groups (Fig. 10a, b). In the nuclear extracts, the P65 protein in the treatment group with VA showed slightly decreased expression after 60 min treatment with the drug, while it was not different over time in the inflammatory untreated control group. In the untreated control group, less expression of P65 in the nucleus was observed compared with the inflammatory groups which was not significant. The reference protein histone 3 (H3) was unaffected in the all the experimental groups (Fig. 10 c, d).

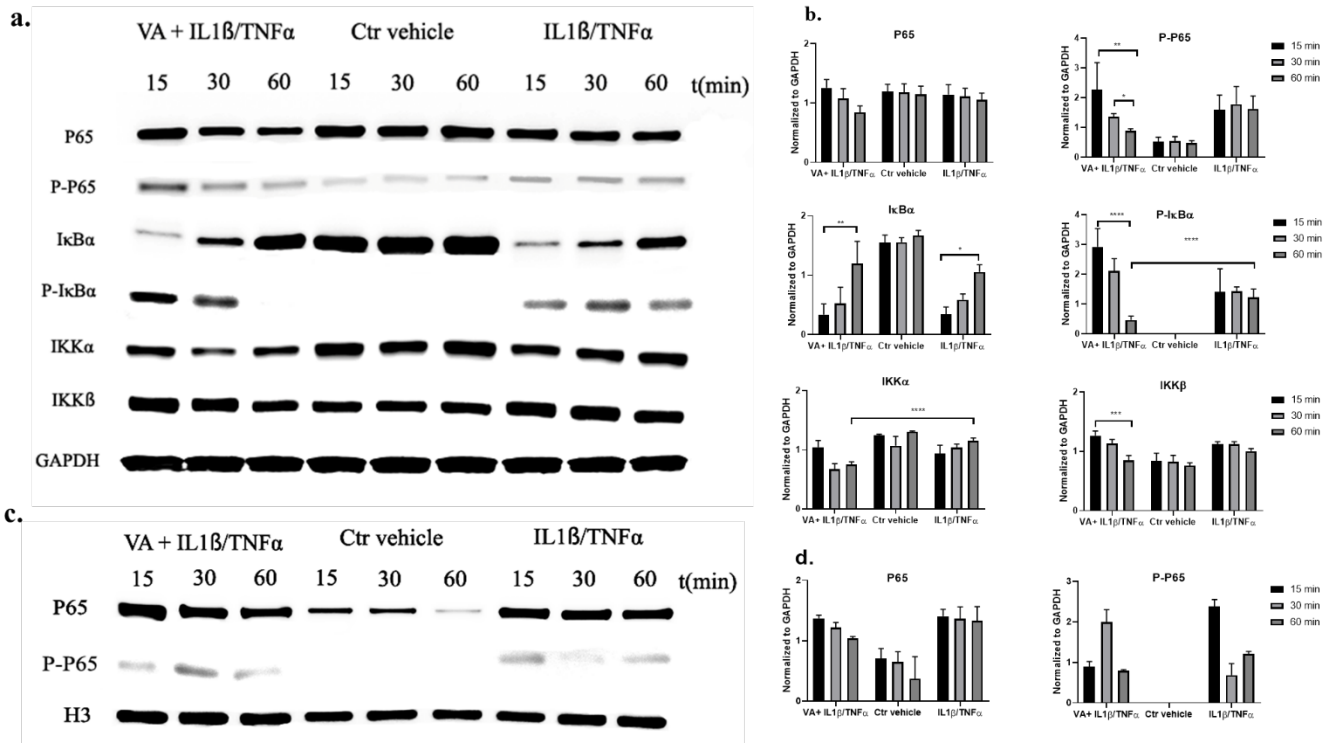

Figure 10. The expression of the main proteins in the NF-κB signaling pathway including IKKα, IKKβ, NF-κB (P65), P-NF-κB (P-P65), IκBα, P-IκBα in treatment groups with VA versus untreated control groups was determined by Western blot analysis. GAPDH was used as endogenous control. After induction of inflammation with 1 ng/mL IL-1β/TNF-α on human OA chondrocytes, the cells either simultaneously were treated with 1 μM VA for 15, 30 and 60 minutes or were treated with 0.01% DMSO as the control vehicle. Furthermore, the Ctr vehicle group without induction of inflammation and treated with 0.01% DMSO (control positive group; Ctr vehicle) was probed. (a) The protein level of cytoplasmic P65, P-P65, IκBα, P-IκBα, IKKα, IKKβ was determined by western blot and GAPDH was used as endogenous control. (b) Quantification of the protein band intensity. The intensity of each protein was determined and normalized to GAPDH. (c) The protein level of nuclear P-65 and P-P65 was determined by western blot and histone 3 (H3) was used as endogenous control. (d) Quantification of nuclear P65 and P-P65 protein band intensity. The intensity of each protein was determined and normalized to H3 endogenous control. For statistical analysis using Graphpad Prism, two-way analysis of variance (ANOVA) followed by Tukey's post hoc test (multiple comparisons) was applied for the treated groups with VA vs. Ctr vehicle and IL-1β/TNF-α groups in three biological replicates (n=3). * $p < 0.01$, ** $p < 0.001$, *** $p < 0.0005$, **** $p < 0.0001$.

4. Discussion

To have an effective treatment against OA, inhibition of pro-inflammatory cytokines that are excessively abundant in osteoarthritic joints is necessary. Furthermore, for regeneration of damaged cartilage, it is essential to increase the chondrocytes anabolism to rebuild cartilage and restore joint function. Inflammatory cytokines including IL-1β and TNF-α initiate the development and progression of OA through activating or inhibiting different signaling pathways such as NF-κB, HMGB1, IL-1R/TLR, MAPKs and PI3K/Akt/mTOR pathways [8-

18]. In our previous study, we used these two inflammatory cytokines on microtissues of *human* primary chondrocytes to develop an inflammatory model of arthritis. After screening of 34 bioactive compounds existing in the over-the-counter XLGB formula in an inflammatory model, we identified six compounds (VA, 5-HMF, 4-HBA, PS, PCA, Epi C) with anti-inflammatory and anabolic properties [57]. In the current study, RNA sequencing, gene expression and ELISA analyses further demonstrated that several pro-inflammatory cytokines which are abundant in arthritic joints, were significantly down-regulated and in the treatment groups with VA and Epi C, the genes for the ECM protein synthesis were significantly up-regulated (Fig. 1, 2). Also, the MMP activity was significantly suppressed in these treatment groups, indicating anti-catabolic effects of VA and Epi C (Fig. 3). The upregulation of TIMP1 as a strong inhibitor of MMPs in the treatment group with VA supported its significant inhibitory effect on MMPs (Fig 9). Therefore, we selected these two most potent compounds (VA, Epi C) for the pathway analysis.

IPA showed that after treatment with VA, osteoarthritic signaling including NF-κB pathway was inhibited (Fig. 6, 7). NF-κB regulates the expression of genes involved in inflammatory response, and several studies have shown that inhibition of NF-κB pathway can decrease the pathogenesis of OA and RA [25,26,61,62]. Recently, several TCM compounds including VA have shown potential in inhibiting inflammatory response through inhibition of different parts of the NF-κB pathway [48,63-70]. An *in vitro* study on lipopolysaccharide (LPS)-stimulated *mouse* peritoneal macrophages showed that VA had anti-inflammatory effects which were mediated by the inhibition of LPS-induced NF-κB activation and IκB-α degradation [71]. Also, an *in vivo* study on a murine model of inflammatory pain showed that VA could inhibit pro-inflammatory cytokine production by suppressing NF-κB activity. Our data suggest that after induction of inflammation in *human* OA chondrocytes and activation of NF-κB pathway, the treatment with VA had inhibitory effects on IKK complex (inhibiting IKK-β subunit), resulting in inhibition of IκBα protein phosphorylation (Fig. 10). In the inactive NF-κB signaling pathway, IκBα protein is bound to the NF-κB dimers which leads to cytoplasmic retention of NF-κB complex. Nevertheless, phosphorylation of IκBα protein initiated by inflammatory cytokines leads to its degradation and the NF-κB dimers would release and translocate to the nucleus, initiating the transcription of genes involved in inflammation. Yin *et al.* also showed that anti-inflammatory small molecules such as Aspirin® or sodium salicylate specifically inhibit IKK-β activity. The mechanism of Aspirin® or sodium salicylate in inhibition of IKK

is due to binding of these compounds to IKK-β and competing with ATP binding [72]. VA, which is the extract of *Radix ET Rhizoma Salviae*, has a molecular structure similar to salicylates; we therefore predict that this compound may be acting by binding to the IKK-α, IKK-β and competing with ATP binding which subsequently result in inhibition of P-IκBα.

Recent studies showed that HMGB1 could promote the pathogenesis of inflammatory diseases including arthritis [73-75]. HMGB1 which is secreted during necrotic cell death and activation of macrophages is very abundant in synovitis and intra-articular fluid of RA patients. The IPA dataset for the treatment group with VA indicated that HMGB1 signaling was inhibited (Supplementary Fig. 8). HMGB1 triggers the signal to the nucleus by activating several mitogen-activated protein kinases leading to a nuclear translocation of NF-κB for initiating an inflammatory response. It can act either alone or in combination with other inflammatory cytokines (INF-γ, IL-1β, TNF-α) which leads to an increased inflammatory signal [76]. IPA dataset for the VA treatment group suggested that INF-γ and TNF receptors were significantly inhibited. Therefore, inhibition of INF-γ, IL-1β and TNF receptors could be a successful approach in inhibition of inflammatory response. Also, upstream regulator analysis for compounds and drugs revealed that VA may act in a similar way like small molecule compounds which are known to interfere with the activity of MEK and PI3 kinases (Supplementary table 3) [77-79]. Most of the established kinase inhibitors are competitive inhibitors of ATP and target the ATP-binding pocket [80-84]. In further studies, it will be important to understand the specific mechanism of action of VA as a competitive inhibitor in development of a drug with less side effects than NSAIDs.

The Toll-like receptors (TLR) /interleukin-1 receptor (IL-1R) or TIR superfamily of receptors are also activated by IL-1β and TNF-α. These receptors including TLR1, TLR2, TLR4, TLR5, and TLR6 which are present in mono or heterodimeric structures are important receptors in cartilage pathologies [85,86]. TLRs are expressed in OA synovial tissues and various endogenous ligands are present within the inflamed joints of OA patients [10,87]. HMGB1 is one of the most known endogenous TLR4 ligands involved in OA pathology. After interaction of the ligands with their receptors, they connect with one or more adaptor proteins. These adaptors, including Myeloid differentiation factor 88 (MyD88), the TIR domain-containing adaptor protein inducing interferon-β (IFNβ) (TRIF; also known as TICAM1), and the TRIF-related adaptor molecule (TRAM; also known as TICAM2) are connected to the cytoplasmic domains of the receptors. MyD88 recruits the members of the interleukin-1 receptor-associated

kinase (IRAK) family (IRAK1, IRAK2 and IRAK4) [88-91]. Phosphorylated IRAK2 possesses kinase activity which react with TNF-receptor-associated factor 6 (TRAF6) and recruits transforming growth factor β-activated kinase 1 (TAK1). Activated TAK1 stimulates the IKK complex, which initiates phosphorylation and following degradation of IκBα leads to the activation of NF-κB for translocation from the cytosol to the nucleus and activation of inflammatory response. Our PCR array dataset showed that several genes associated with this pathway including IRAK2, TLR2 and TLR4 were significantly downregulated. Also, TNF regulates the expression of the transcription factor interferon regulatory factor 1 (IRF1) [92] which was significantly inhibited after treatment with VA (Fig. 9). Therefore, the TIR superfamily of receptors which contributes to IKK phosphorylation and NF-κB activation may be a target for VA and its anti-inflammatory properties (Fig. 11).

All the mentioned signaling pathways are interconnected and act through inhibition of canonical NF-κB pathway which is activated by inflammatory signals, while non-canonical NF-κB pathway which is activated by developmental signals and is necessary for developmental gene expression, is still active [93]. Therefore, after treatment with VA, the expression of inflammatory cytokines including IL1-β, TNF and INF-γ were significantly inhibited. Interestingly, the IL1R1 was significantly up-regulated in the treatment group compared with inflammatory control group. However, previous studies also showed an inverse relation between IL1R1 expression and the amount of IL-1β in OA joints. Wyatt et al. showed that IL1R1 was down-regulated in OA synovium compared to non-arthritic controls [94]. Also, in retinal endothelial cells IL1R1 expression was downregulated during activation by IL1β [95]. Furthermore, clinical trials with OA patients using IL1 receptor antagonist didn't show symptomatic improvements compared with placebo, which could be due to the downregulation of IL1R1 prior to the treatment [96,97].

Furthermore, IL-1β and TNF-α suppress the expression of genes related to the differentiated chondrocyte phenotype, including COL2A1 and ACAN [2,5]. In our previous study, we showed that after treatment with Epi C, not only catabolic marker genes (MMPs) were significantly inhibited, but also anabolic marker genes (COL2A1 and ACAN) were significantly up-regulated [57]. RNA sequencing and gene expression data revealed that besides COL2A1 and ACAN also other anabolic proteins including GDF5, COMP and CCN2 were significantly up-regulated in the treatment group with Epi C (Fig. 1). GDF5 is an important growth factor acting as an extracellular signaling molecule in the formation and repair of joints [98]. COMP is a

crucial structural and functional component of the cartilage ECM which interacts with other ECM proteins and facilitates the interaction of chondrocytes with the ECM [99]. CCN2 plays an important role in promoting growth and differentiation of auricular chondrocytes *in vitro* and *in vivo*. Also, CCN2 can increase the proteoglycan synthesis but does not promote hypertrophy or calcification of articular chondrocytes [100,101]. Furthermore, osteoarthritic signaling pathway and several inflammatory marker genes in the pathway were inhibited in the Epi C group (Fig 8). Therefore, Epi C showed significant anabolic and anti-catabolic effects which play an important role in regeneration of cartilage.

There is very limited literature available on the anabolic effect of Epi C (as *herba Epimedii* extract) which has been used as TCM for the treatment of osteoporosis for many years [102]. Epi C and icariin are the major flavonoid glycosides existing in *herba Epimedii,* and several studies revealed that the flavonoids of *Epimedii* could regulate signaling pathways associated with bone and cartilage repair [52,103-105]. Icariin, as a well-studied small molecule with similar chemical structure as Epi C, showed a great potential in cartilage repair in *in vitro* and *in vivo* studies [52,106]. An *in vitro* and *in vivo* study in murine showed that icariin may act as a hypoxia inducible factor (HIF)-1α activator which could promote chondrocyte proliferation, differentiation, ECM synthesis and articular cartilage repair [106]. Also, the effect of icariin in inhibition of cathepsin K and attenuation of bone and cartilage degradation in a murine model of collagen-induced arthritis and its anti-inflammatory effect in an LPS induced inflammatory murine model were reported [107,108]. In our IPA dataset, mTOR signaling which is responsible for the proliferation and protein translation was predicted to be activated [109] (Supplementary Fig. 11). It was shown that PI3K/AKT/mTOR signaling is necessary for cartilage homeostasis and in the human cartilage with OA, this pathway was down-regulated compared with normal cartilage [18,110]. Previous studies showed that some drugs could attenuate chondrocytes apoptosis and degradation in IL-1β-induced chondrocyte by promoting cell survival and matrix proteins synthesis through activation of PI3K/AKT/mTOR signaling pathway [18,79,111-113]. Therefore, the predicted activation of mTOR signaling could explain the protective and anabolic effects of Epi C on chondrocytes vs Ctr inflammatory group.

Due to the complexity of the different signaling pathways and their interconnections with each other, the exact intervention of the drug with the target often remains undefined. The classical approaches including inhibition at the level of chemokines/cytokines and receptors with small

molecules or antibodies are often insufficient interventions, since they block one ligand or receptor, while the associated intracellular signals remain active through other present ligands or receptors. However, targeting the kinase activity is one of the most novel and effective strategies in inhibition of inflammatory response with promising effects [72,81,83]. Nevertheless, many kinases are involved in several signaling pathways which creates concerns regarding undesired side effects of the inhibition or activation of kinases. So, specificity of the drug in inhibition or activation of kinases in the pathways which are involved in the activation of pro-inflammatory mediators or inhibition of matrix proteins is of great importance. Local drug delivery to the OA joint is another strategy to prevent systemic side effects.

An investigation on the pharmacokinetic and oral bioavailability of Epi C showed that if the drug was administered as a pure compound, its effect was about four-fold higher than that of the complex *herba Epimedii* extracts [114]. The oral bioavailability of Epi C in *herba Epimedii* extract might be affected by the other herbal ingredients suppressing Epi C absorption from the gastrointestinal system. These results highlight the importance of discovering the most potent compounds in the complex herbal extracts towards having a potent drug (or combinations of selected drugs) in which their effects are not masked by other existing compounds in the herbal mixture. Furthermore, formulation of a local drug delivery system can be more easily achieved for a single or combination of the most potent compounds.

In our study, *human* OA chondrocytes as the most clinically relevant source of cells for testing the potent compounds in OA treatments were used. Nevertheless, using this source of cells has some limitations. To have the least amount of heterogeneity in the OA cell population, *human* cells were isolated from macroscopically evident OA areas of the joint; therefore, limited numbers of primary cells were acquired, and passage three chondrocytes were used which might have affected the original OA traits. However, to minimize the cell de-differentiation an established expansion medium supplemented with TGF-β and FGF-2 was used that promotes cell proliferation and maintains cell differentiation capacity [115]. Furthermore, by using IL-1β/TNF-α as inflammatory cytokines, our microtissue model resembled post-traumatic acute inflammation which is not the exact condition in OA characterized by chronic inflammation.

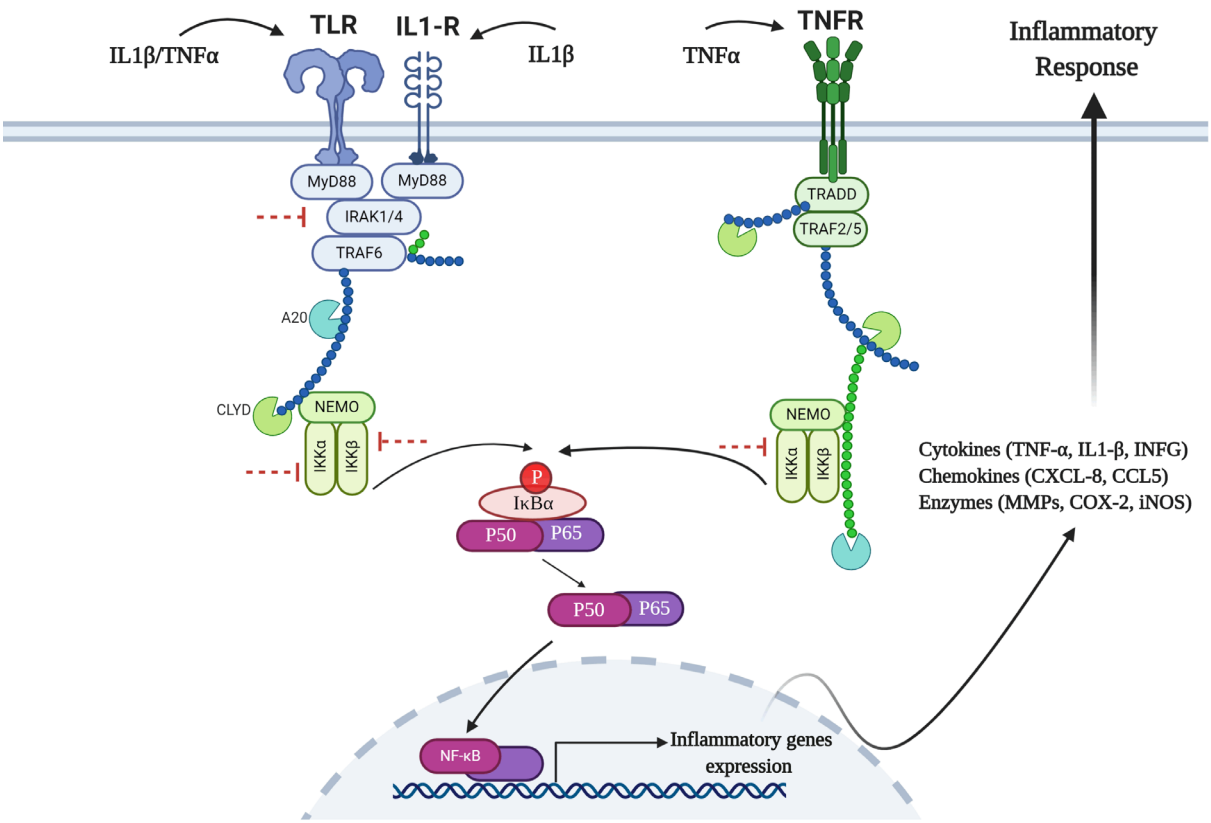

Figure 11. Schematic figure of NF-κB signaling pathway and inhibition of IKK complex after treatment with VA. The red inhibitor arrows showed the inhibitory effect of VA in different parts of the pathway.

5. Conclusions

In conclusion, for the first time the mechanism of action of two potent herbal compounds (VA, Epi C) existing in the XLGB formula were investigated on human osteoarthritic chondrocytes using an ex vivo approach. VA exhibited an important role in attenuation of inflammation by affecting I-κBα phosphorylation in NF-κB signaling pathway and Epi C showed significant anabolic effects with increasing collagenous and non-collagenous matrix proteins for regeneration of cartilage. Therefore, these drugs attenuate cartilage degeneration through regulation of the tissue hemostasis. In further pre-clinical studies, the synergic effects of VA with anti-inflammatory properties and Epi C with anabolic activity warrants to be investigated.

6. Supplementary Information

Supplementary Table 1. Differentially expressed genes after RNA Sequencing

5-HMF

Gene	Control vehicle	5-HMF	log2_fold_change	q_value
TMC5	2.64693	0.0956953	-4.78973	0.0183303
CCL11	21.6693	1.02219	-4.40592	0.0183303
SLAMF7	3.7777	0.440358	-3.10076	0.0183303
LCNL1,PTGDS	32.3785	4.34702	-2.89694	0.0183303
RPLP0P2	13.0693	1.86573	-2.80837	0.0183303
IGFBP3	76.5181	11.124	-2.78213	0.0183303
LGI2	1.67212	0.243663	-2.77872	0.0183303
MEST	1.33042	0.220132	-2.59545	0.0183303
C6orf229,FAM65B	5.5852	0.951031	-2.55405	0.0183303
ADAMTS16	1.72847	0.304215	-2.50634	0.0424614
PLXDC1	9.36292	1.83855	-2.34839	0.0183303
BHLHE22	1.44655	0.313663	-2.20533	0.0424614
SYT7	3.87622	0.858705	-2.17441	0.0183303
MT1G	129.101	578.799	2.16456	0.0183303
GJB2	19.5447	4.45863	-2.13211	0.0183303
RANBP3L	2.02446	0.489476	-2.04823	0.0183303
CXCL12	44.7552	10.8482	-2.0446	0.0183303
COL14A1	5.90115	1.45538	-2.0196	0.0183303
RP11-231C14.6,SNX29P2	3.29369	0.834324	-1.98103	0.0183303
TNFSF18	1.85544	0.481394	-1.94647	0.0319471
CILP	8.55279	2.27515	-1.91043	0.0183303
C2CD4A	1.47128	0.393059	-1.90426	0.0424614
MT1H	43.8177	162.402	1.88999	0.0183303
SEMA3A	1.39115	0.378459	-1.87807	0.0183303
ARHGAP28	5.13577	1.43949	-1.83503	0.0183303
C3AR1	31.9442	9.50822	-1.74831	0.0183303
RP11-274B21.1	5.09561	1.53344	-1.73248	0.0183303
ADAMTS12	2.90448	0.884544	-1.71527	0.0183303
TMEM106A	1.71029	0.527054	-1.69822	0.0183303
CXCL10	44.7117	14.1341	-1.66147	0.0424614
SEMA5A	5.2664	1.70523	-1.62685	0.0183303
IGF1	3.39587	1.10182	-1.62389	0.0183303
ITGB8	6.63335	2.158	-1.62004	0.0183303
CPXM1	4.08831	1.3494	-1.59919	0.0183303
IL7R	10.756	3.59456	-1.58125	0.0183303
TRIM56	13.0652	4.39521	-1.57172	0.0183303
-	2.15229	0.727996	-1.56387	0.0183303
FOXP2	1.57725	0.537849	-1.55214	0.0183303
IGFBP5	81.9929	28.4864	-1.52523	0.0183303
VCAM1	15.7227	5.48587	-1.51906	0.0183303
CH25H	91.9764	32.2598	-1.51153	0.0183303
SEMA4D	5.85942	2.06433	-1.50509	0.0183303
RP11-640M9.2	11.5303	4.09642	-1.49299	0.0183303

4-HBA

Gene	Control vehicle	4-HBA	log2_fold_change	q_value
FOSB	0.263976	37.3909	7.14614	0.0155513
FOS	4.55402	144.096	4.98375	0.0155513
CCL11	21.8856	1.00344	-4.44696	0.0155513
-	0.236927	4.01346	4.08233	0.0351059
C2CD4A	1.482	0.132841	-3.47978	0.0155513
CXCL12	45.0349	4.5926	-3.29366	0.0155513
MMP12	14.236	1.65481	-3.1048	0.0155513
C6orf229,FAM65B	5.60808	0.693199	-3.01617	0.0155513
ADAMTS16	1.7401	0.225879	-2.94555	0.0155513
CXCL13	290.288	40.0756	-2.85669	0.0155513
SFRP2	14.832	2.04785	-2.85653	0.0155513
-	2.65095	0.370007	-2.84088	0.0155513
EGR1	20.5017	142.705	2.79922	0.0155513
RPLP0P2	13.1534	2.08821	-2.6551	0.0155513
COL14A1	5.93573	0.951672	-2.64089	0.0155513
IGFBP3	77.005	12.7427	-2.59528	0.0155513
GJB2	19.6628	3.41116	-2.52714	0.0155513
RP11-367F23.2	1.72502	0.301614	-2.51583	0.0446
CADM3,DARC	5.25611	0.931491	-2.49638	0.0155513
SYT7	3.90202	0.710104	-2.45812	0.0155513
MMP8	24.1625	4.40359	-2.45602	0.0155513
PLXDC1	9.42433	1.91707	-2.29749	0.0155513
AP001434.2, SPATA20P1	3.33822	0.690853	-2.27263	0.0268614
CD248	12.3031	2.87461	-2.09759	0.0155513
QPRT,SPN	2.53519	0.595588	-2.08971	0.0155513
NCALD	1.51106	0.361393	-2.06392	0.0155513
CPXM1	4.1156	1.02489	-2.00563	0.0155513
CH25H	92.5579	23.3474	-1.98709	0.0155513
ADAMTS12	2.92097	0.746958	-1.96735	0.0155513
HAS2	13.1636	3.43491	-1.93821	0.0155513
CILP	8.59468	2.31573	-1.89198	0.0155513
-	1.06049	0.29116	-1.86484	0.0351059
ARHGAP28	5.1644	1.46177	-1.82089	0.0155513
C3AR1	32.056	9.12723	-1.81235	0.0155513
KIAA0226L	6.41788	1.89241	-1.76187	0.0155513
TSPAN11	22.1212	6.53724	-1.75868	0.0155513
SFRP1	1.58589	0.472192	-1.74784	0.0351059
SEMA5A	5.26718	1.57554	-1.74119	0.0155513
IL7R	10.8159	3.26278	-1.72898	0.0155513
CSF2	8.06655	25.8906	1.6824	0.0155513
GALR3	0.488738	1.55064	1.66573	0.0155513
SERPINA1	12.5967	4.05062	-1.63683	0.0268614

Vanillic acid

Gene	Control vehicle	VA	log2_fold_change	q_value
EIF1AY	12.2023	0.0277272	-8.78163	0.0104271
CCL11	20.913	0.203771	-6.6813	0.00330143
MMP12	13.6562	0.169591	-6.33135	0.00330143
CXCL10	43.1215	0.553861	-6.28274	0.00330143
IDO1	6.66431	0.122341	-5.76748	0.00330143
IL23A	182.688	3.8186	-5.58019	0.00330143
MMP7	2.47688	107.857	5.44446	0.00330143
RP11986E7.7,SERPI3, SERPINA4,SERPIN5	10.8106	405.536	5.22931	0.00330143
HIF3A	0.514046	16.8623	5.03576	0.00330143
IL6	6709.62	205.125	-5.03165	0.00330143
LAMA3	0.695779	21.194	4.92888	0.00330143
DKK1	0.913079	26.3309	4.84988	0.00330143
APOD	3.15709	80.1754	4.66649	0.00330143
EREG	58.573	2.53097	-4.53247	0.00330143
SLCO2B1	4.068	0.180563	-4.49374	0.00330143
PTX3	64.4246	1443.97	4.48629	0.00330143
DCLK1	0.0972317	2.08802	4.42457	0.00330143
LINC00473	12.0236	0.64595	-4.2183	0.00330143
CCL8	25.3413	1.41583	-4.16178	0.00330143
PRELP	2.75364	47.4012	4.10551	0.00330143
ZBED3	0.244914	4.19019	4.09667	0.00330143
ITGBL1	10.8984	183.9	4.07674	0.00330143
GBP5	6.94778	0.423924	-4.03467	0.00330143
SLC38A4	0.231164	3.77807	4.03066	0.00330143
PRODH	0.169971	2.54284	3.90308	0.0124428
THBS1	17.9431	259.742	3.85558	0.00330143
TMEM150C	0.840441	11.3287	3.75269	0.00330143
TJP2	1.30083	17.5244	3.75186	0.00330143
FAM46B	0.114869	1.5271	3.73274	0.00330143
CCL3	8.1225	0.623825	-3.70271	0.00330143
ADH1B	0.316882	4.08275	3.68752	0.00330143
IL11	350.332	28.4794	-3.62073	0.00330143
CYP4F22	0.174107	2.13505	3.61622	0.00330143
NCAM1	0.0925037	1.11978	3.59757	0.00330143
CTD-2218G20.1	0.205667	2.37841	3.53161	0.00592391
TNFSF18	1.79154	0.158897	-3.49504	0.00330143
ST6GALNAC5	0.238698	2.5881	3.43863	0.00330143
GPR98,LUCAT1,RP11-213H15.4	2.4874	0.24385	-3.35057	0.0104271
FGFBP2,PROM1	0.431683	4.33999	3.32965	0.00330143
RP11-855A2.5	4.77143	0.496706	-3.26396	0.0416914
COMP	29.7354	272.884	3.19803	0.00330143
SERPINB3,SERPINB4	22.8248	2.52288	-3.17746	0.00330143
ADRA2A	1.29417	11.654	3.17073	0.00330143

Psoralidin

Gene	Control vehicle	PS	log2_fold_change	q_value
TMC5	2.63217	0.0815934	-5.01166	0.0296
GPR171	1.83483	0.10289	-4.15647	0.0471184
CCL11	21.5156	1.50912	-3.8336	0.0296
SLAMF7	3.75147	0.384534	-3.28627	0.0296
MMP12	14.0629	1.64358	-3.09698	0.0296
IGFBP3	75.9714	10.1393	-2.9055	0.0296
C6orf229,FAM65B	5.54657	0.758774	-2.86985	0.0296
CXCL12	44.4236	7.68137	-2.53189	0.0296
ADAMTS16	1.71537	0.306635	-2.48393	0.0296
H19	0.547717	2.84943	2.37917	0.0471184
SFRP2	14.6784	2.89915	-2.33999	0.0296
-	2.61808	0.550791	-2.24893	0.0296
C2CD4A	1.46212	0.307976	-2.24717	0.0471184
COL14A1	5.8572	1.35211	-2.115	0.0296
COL5A3	7.20995	1.78696	-2.01249	0.0296
CD248	12.1363	3.0379	-1.99818	0.0296
OLFML2B	47.6949	12.0031	-1.99043	0.0296
CXCL13	287.107	78.1301	-1.87764	0.0296
GJB2	19.3988	5.29622	-1.87293	0.0296
CXCL10	44.4021	12.2553	-1.85722	0.0296
QPRT,SPN	2.50082	0.707217	-1.82218	0.0296
PLXDC1	9.29195	2.85854	-1.7007	0.0296
SERPING1	21.0017	6.4938	-1.69337	0.0296
SYT7	3.84399	1.20596	-1.67242	0.0296
CILP	8.48368	2.78906	-1.60491	0.0296
RASD1	8.76984	2.92944	-1.58192	0.0296
RPLP0P2	12.9542	4.35935	-1.57123	0.0471184
MAPK10	4.61556	1.57044	-1.55534	0.0296
ARHGAP28	5.09554	1.78527	-1.51309	0.0296
VCAM1	15.6117	5.47361	-1.51206	0.0296
S100A4	517.472	184.818	-1.48537	0.0296
TSPAN11	21.8221	8.40774	-1.376	0.0296
RP11-82L18.4	1.74237	0.711546	-1.29202	0.0471184
MMP8	23.8542	9.78617	-1.28543	0.0296
CH25H	91.3212	39.3359	-1.2151	0.0296
IL7R	10.6755	4.62532	-1.20668	0.0471184
MIR23A,MIR24-2,MIR27A	17.6043	7.74944	-1.18376	0.0471184
ITGB8	6.56586	3.00451	-1.12785	0.0296
ISLR	62.1145	29.6579	-1.06651	0.0296
GAS1	42.5655	20.8757	-1.02786	0.0296
SMOC1	238.548	119.825	-0.993346	0.0471184
HMOX1	197.539	392.255	0.989654	0.0296
IGFBP5	81.4198	43.0461	-0.919498	0.0296

PCA

Gene	Control vehicle	PCA	log2_fold_change	q_value
CCL11	21.6406	0.56146	-5.26841	0.020294
MMP12	14.1281	0.580278	-4.60568	0.020294
IDO1	6.89688	0.348589	-4.30634	0.020294
CXCL10	44.6263	4.00811	-3.4769	0.020294
MIR4477A	0.883464	8.1207	3.20036	0.020294
LGI2	1.66828	0.21936	-2.92699	0.020294
RPLP0P2	13.0234	2.07816	-2.64773	0.020294
SFRP2	14.7299	2.44462	-2.59106	0.020294
CXCL12	44.6469	7.88936	-2.50058	0.020294
PDGFD	1.05835	0.18828	-2.49086	0.020294
-	1.60907	0.301419	-2.41638	0.020294
PLXDC1	9.3396	1.81885	-2.36034	0.020294
SYT7	3.864	0.815163	-2.24493	0.020294
ADAMTS12	2.8952	0.615334	-2.23422	0.020294
CD74	69.8431	15.3655	-2.18443	0.020294
IGFBP3	76.3365	17.9516	-2.08826	0.020294
-	2.63019	0.642128	-2.03423	0.0373667
RP11-81H14.2	5.93571	1.47732	-2.00644	0.0373667
MIR145	1.90096	0.475952	-1.99784	0.020294
SERPING1	21.1015	5.49679	-1.94069	0.020294
CH25H	91.7586	23.9356	-1.93868	0.020294
GJB2	19.4963	5.16469	-1.91645	0.020294
VCAM1	15.6878	4.15746	-1.91586	0.020294
COL14A1	5.88404	1.81486	-1.69695	0.020294
ARHGAP28	5.12052	1.61141	-1.66796	0.020294
EGR1	20.3424	63.7766	1.64854	0.020294
S100A4	519.91	166.012	-1.64697	0.020294
TMEM158	19.1705	6.14241	-1.64201	0.020294
LIPG	4.26873	1.39372	-1.61486	0.020294
TMEM119	64.4319	21.1053	-1.61017	0.020294
DPP4	11.0845	3.65438	-1.60084	0.020294
TSPAN11	21.9278	7.36666	-1.57368	0.020294
CD248	12.195	4.10483	-1.57089	0.020294
C3AR1	31.7871	10.8534	-1.5503	0.020294
CXCL13	288.38	102.208	-1.49646	0.020294
CDCP1	4.40174	1.58396	-1.47454	0.020294
ADAMTS14	3.95449	1.44174	-1.45568	0.020294
IL7R	10.7273	3.93439	-1.44707	0.020294
SEMA5A	5.2209	1.93812	-1.42964	0.020294
C9orf47,S1PR3	16.0296	6.10935	-1.39165	0.020294
HAS2	13.0453	5.02277	-1.37698	0.020294
ITGB8	6.59655	2.5618	-1.36455	0.020294

Epimedin C

Gene	Control vehicle	Epi C	log2_fold_change	q_value
H19	0.537211	65.6371	6.93288	0.0182
MMP7	2.4939	194.161	6.2827	0.0182
HIF3A	0.5177	22.0082	5.40978	0.0182
CA9	2.0508	70.6185	5.10579	0.0383362
RAB11FIP4	0.159334	4.72276	4.88951	0.0182
SPARCL1	0.721847	17.0604	4.56281	0.0182
COL2A1	0.625102	14.7129	4.55684	0.0182
APOD	3.18023	69.3519	4.44673	0.0182
SLC38A4	0.232951	4.7077	4.33692	0.0182
RP11986E7.7,SERPINA3, SERPINA4, SERPINA5	10.8912	195.871	4.16867	0.0182
APLN	0.0956189	1.48885	3.96076	0.0182
COMP	29.9424	463.836	3.95335	0.0182
RSPO2	0.649701	9.99886	3.94392	0.0182
CAPN6	0.25947	3.93384	3.9223	0.0182
HSPB7	0.84741	12.8034	3.91732	0.0182
MATN3	1.41254	20.7226	3.87484	0.0182
DCLK1	0.0979673	1.39937	3.83633	0.0182
PRELP	2.77419	34.6352	3.6421	0.0182
RP11-434D9.1	0.2051	2.5318	3.62576	0.0182
DKK1	0.91998	10.587	3.52455	0.0490286
-	0.716545	7.77418	3.43956	0.0304101
ST6GALNAC5	0.240451	2.43521	3.34023	0.0182
SCRG1	20.5605	207.495	3.33513	0.0182
CTD-2561J22.2	0.255837	2.54356	3.31355	0.0304101
CLEC18A	0.249291	2.20312	3.14365	0.0182
ACAN	10.9287	94.5459	3.11289	0.0182
ZBED3	0.246552	2.06441	3.06577	0.0182
KIAA1456	0.835823	6.91398	3.04825	0.0182
ITGA10	5.30106	42.1127	2.9899	0.0182
FGFBP2,PROM1	0.43552	3.40952	2.96876	0.0182
MMP12	13.7658	1.82289	-2.91679	0.0383362
GPM6B	3.47194	25.5839	2.88142	0.0182
GBP5	7.00352	0.980563	-2.8364	0.0182
CDH23	1.15792	0.16522	-2.80908	0.0304101
ADRA2A	1.30369	9.11261	2.80527	0.0182
WWP2	23.0827	143.939	2.64058	0.0182
S100B	0.781904	4.80197	2.61856	0.0304101
GDF5	1.70156	10.2381	2.58902	0.0182
MFAP5	0.465845	2.73492	2.55358	0.0182
THBS1	18.0735	104.083	2.52579	0.0182
LRMP	1.25509	0.23105	-2.44151	0.0182
CTGF	21.7411	115.549	2.41	0.0182
-	0.349015	1.8206	2.38305	0.0490286
RP11-284F21.8	0.283548	1.47866	2.38262	0.0182
CADPS	0.211655	1.0837	2.35618	0.0182

Supplementary table 2. Low-level (specific) process or functions that belong to the high-level category "Connective Tissue Disorder". a) For the VA vs Ctr group, 4 terms including Inflammation of the joint, Rheumatic disease, experimentally induced arthritis, polyarthritis with significant activation z-scores indicate a significant decrease of all these functions. b) For the Epi C vs Ctr group abnormality of cartilage tissue, Inflammation of joint, are top results with negative z-scores (predicted decrease, non-significant).

a.

The Filter found 10 Functions for Connective Tissue Disorders

Categories	Diseases or Functions Annotation	p-value	Predicted Activation State	Activation z-score	Molecules	# Molecules
Connective Tissue D...	Inflammation of joint	3.31E-37	Decreased	-2.678	↓ABCC1, ↑ABCC2, ↓ABL1, ↑ADA... ...all 181	181
Connective Tissue D...	Rheumatic Disease	4.82E-40	Decreased	-2.501	↓ABCC1, ↑ABCC2, ↓ABL1, ↓ACSL5, ...all 216	216
Connective Tissue D...	Experimentally-induced arthritis	1.19E-13	Decreased	-2.151	↑ANXA1, ↑CDH11, ↓CTSS, ↑CXCL13,...all 36	36
Connective Tissue D...	Polyarthritis	5.11E-17	Decreased	-2.133	↓ADM, ↑ANXA1, ↓CCL3, ↓CCL5, ↓... ...all 43	43
Connective Tissue D...	Systemic lupus erythematosus	1.72E-13		-0.614	↓ACSL5, ↓ADAMTS6, ↑ANXA1, ↓B... ...all 61	61
Connective Tissue D...	Lupus erythematosus	1.00E-13		-0.248	↓ACSL5, ↓ADAMTS6, ↑ANXA1, ↓B... ...all 63	63
Connective Tissue D...	Non-traumatic arthropathy	1.63E-35		-0.021	↓ABCC1, ↑ABCC2, ↑ADAMTS1, ↑... ...all 159	159
Connective Tissue D...	Rheumatoid arthritis	2.44E-29		0.129	↑ADAMTS2, ↑ADGRG6, ↓ADM, ↑... ...all 135	135
Connective Tissue D...	Osteoarthritis	3.38E-16		0.557	↑ADAMTS1, ↑ADAMTS2, ↑ADAMT... ...all 49	49
Connective Tissue D...	Polyarticular juvenile rheumatoid arthritis	1.76E-13			↓ADM, ↓CCL3, ↓CCL5, ↓CD274, ↓C... ...all 26	26

b.

The Filter found 19 Functions for Connective Tissue Disorders

Categories	Diseases or Functions Annotation	p-value	Predicted Activation State	Activation z-score	Molecules	# Molecules
Connective Tissue Disorders,Organis...	Abnormality of cartilage tissue	2.50E-08		-1.915	↑ACAN, ↑ADRA2A, ↑ASPN, ↑BGN, ↑CC... ...all 18	18
Connective Tissue Disorders,Inflam...	Inflammation of joint	3.69E-21		-1.773	↑ACAN, ↑ADAMTS1, ↑ADGRG6, ↑ADRA... ...all 78	78
Connective Tissue Disorders,Organis...	Non-traumatic arthropathy	1.73E-21		-1.446	↑ACAN, ↑ADAMTS1, ↑ADGRG6, ↑ADRA... ...all 71	71
Connective Tissue Disorders,Inflam...	Rheumatic Disease	1.28E-22		-1.134	↑ACAN, ↓ACSL5, ↑ADAMTS1, ↑ADGRG6, ...all 92	92
Connective Tissue Disorders,Heredit...	Hereditary connective tissue disorder	7.02E-07		-1.054	↑ACAN, ↑ADGRG6, ↑ASPN, ↑BGN, ↓CC... ...all 33	33
Connective Tissue Disorders,Develop...	Dysplasia of skeleton	7.97E-10		-1.000	↑ACAN, ↑ADRA2A, ↑BGN, ↑CCN2, ↑CO... ...all 21	21
Connective Tissue Disorders,Inflam...	Polyarthritis	2.02E-06		-0.577	↓CCL20, ↓CD74, ↑COL2A1, ↓CSF3, ↑GA... ...all 15	15
Connective Tissue Disorders,Immun...	Rheumatoid arthritis	1.76E-16			↑ACAN, ↑ADGRG6, ↑ADRA2A, ↓AQP9,↑... ...all 58	58
Connective Tissue Disorders,Inflam...	Osteoarthritis	4.63E-11			↑ACAN, ↑ADAMTS1, ↑ADRA2A, ↑ASPN,'... ...all 24	24
Connective Tissue Disorders,Develop...	Familial skeletal dysplasia	7.78E-09			↑ACAN, ↑BGN, ↑CCN2, ↑COL11A1, ↑CO... ...all 19	19
Connective Tissue Disorders,Develop...	Chondrodysplasia	3.37E-08			↑ACAN, ↑BGN, ↑CCN2, ↑COL11A1, ↑CO... ...all 11	11

Supplementary table 3. The results of the Upstream Regulator Analysis filtered for compounds and drugs and sorted according to their predicted activity and the number of targets. For the VA vs Ctr treatment group, several anti-inflammatory or immunosuppressive chemicals, e.g. dexamethasone or glucocorticoid, were found to be on top of this list. Also, different small molecule compounds, known to interfere with the activity of MEK/MAP or PI3 kinases were also found to be high in that list of putative Upstream Regulators.

MEK/MAP;PI3K Inhibitors

Upstream Regulator	Expr Log Ratio	Molecule Ty...	Predicted Ac...	Activation z...	p-value of o...	Target ...	Mechanistic...
dexamethasone		chemical drug	Activated	8.402	1.33E-85	↓ABCC1,↑...all 298	573 (22)
U0126		chemical - kinase in...	Activated	3.282	1.47E-42	↓ACKR3,↓...all 106	297 (13)
PD98059		chemical - kinase in...	Activated	2.421	9.49E-39	↑ABCC2,↑...all 106	378 (14)
LY294002		chemical - kinase in...	Activated	2.354	3.67E-34	↓ABCC1,↓...all 96	388 (12)
SB203580		chemical - kinase in...	Activated	3.312	1.66E-34	↑ANXA1,↓...all 90	425 (15)
filgrastim		biologic drug	Activated	3.869	2.69E-23	↑ALDH6A1,'...all 73	
cyclosporin A		biologic drug	Activated	2.733	1.44E-16	↑ABCC2,↓...all 63	393 (18)
fluticasone propionate		chemical drug	Activated	4.613	2.53E-40	↑ABLIM3,↓...all 62	454 (18)
genistein		chemical drug	Activated	2.486	8.19E-15	↓ADM,↓A...all 56	364 (15)
diethylstilbestrol		chemical drug	Activated	2.089	6.08E-16	↓AQP9,↑B...all 50	481 (21)
glucocorticoid		chemical drug	Activated	3.721	4.69E-16	↑ANXA1,↓...all 49	313 (14)
epigallocatechin-gallate		chemical drug	Activated	2.940	7.68E-15	↓CCL2,↓C...all 41	314 (16)
15-deoxy-delta-12,14 -PGJ 2		chemical - endogen...	Activated	2.166	1.69E-14	↓BIRC3,↓...all 36	292 (15)
simvastatin		chemical drug	Activated	2.109	1.07E-11	↑ADAMTS1,...all 35	344 (15)
methotrexate		chemical drug	Activated	2.772	1.72E-09	↓CCL11,↓...all 34	377 (17)
prednisolone		chemical drug	Activated	3.044	4.46E-10	↓BAG1,↓B...all 34	419 (19)
bexarotene		chemical drug	Activated	2.753	2.59E-10	↓AKR1C3,↑...all 31	487 (22)
caffeic acid phenethyl ester		chemical drug	Activated	2.652	3.26E-15	↓ABL1,↓B...all 28	280 (12)
hydrocortisone		chemical - endogen...	Activated	3.050	3.32E-10	↓ADM,↓C...all 26	463 (21)
Sb202190		chemical - kinase in...	Activated	2.657	7.96E-10	↓CCL2,↓C...all 24	364 (15)
GW3965		chemical reagent	Activated	2.006	3.16E-08	↑ADRA2A,↑...all 21	445 (24)
Bay 11-7082		chemical - kinase in...	Activated	3.522	4.82E-12	↓BCL2A1,↓...all 20	257 (11)
aspirin		chemical drug	Activated	2.296	4.03E-08	↓CCL2,↓C...all 19	302 (16)
Sn50 peptide		chemical toxicant	Activated	2.542	9.63E-11	↓BCL2A1,↓...all 18	409 (15)
glutamine		chemical - endogen...	Activated	2.079	1.08E-06	↓ATF4,↓A...all 17	341 (19)
fingolimod		chemical drug	Activated	2.605	2.60E-07	↓BDNF,↓C...all 16	321 (17)
Go 6976		chemical - kinase in...	Activated	2.552	9.00E-09	↓ABCA7,↓...all 16	279 (14)
carbon monoxide		chemical - endogen...	Activated	2.188	3.34E-08	↓ATF4,↓B...all 15	339 (15)
BAPTA-AM		chemical reagent	Activated	2.189	1.21E-09	↓ATF3,↓B...all 15	360 (20)
diphenyleneiodonium		chemical reagent	Activated	2.064	1.07E-06	↓CCL2,↓C...all 13	337 (17)
etanercept		biologic drug	Activated	3.420	1.66E-09	↓CCL2,↓C...all 12	375 (15)
apigenin		chemical - endogen...	Activated	2.964	1.40E-04	↓CCL2,↓C...all 12	290 (19)
2,4,5,2',4',5'-hexachlorobiphenyl		chemical toxicant	Activated	2.309	3.06E-03	↓AGPAT4,↑...all 12	
phenylbutazone		chemical drug	Activated	2.229	8.11E-06	↑ABCC2,↑...all 12	241 (7)
infliximab		biologic drug	Activated	2.137	1.12E-04	↓CXCL1,↓...all 11	405 (19)
resolvin D1		chemical - endogen...	Activated	2.043	1.06E-07	↓CCL2,↓C...all 11	362 (15)
PS-1145		chemical - kinase in...	Activated	2.262	5.08E-11	↓CCL2,↓C...all 11	296 (16)
sorafenib		chemical drug	Activated	2.720	2.81E-07	↓ATF5,↓C...all 11	415 (23)

Supplementary table 4. The results of the Upstream Regulator Analysis filtered for compounds and drugs and sorted according to their predicted activity and the number of targets. For the Epi C vs Ctr treatment group, several anti-inflammatory or immunosuppressive chemicals, e.g. dexamethasone or glucocorticoid, were found to be on top of this list. All z scores are above 2 which showed they are significantly activated.

Upstream Regula...	Expr Log Ratio	Molecule Type	Predicted Activati...	Activation z-score	Flags	p-value of overlap	Target molec...	Mechanistic Net...
dexamethasone		chemical drug	Activated	5.030		9.16E-37	↑ACTG2,↑ADA....all 117	198 (21)
beta-estradiol		chemical - endogenous ...	Activated	2.144		2.48E-13	↑ADAMTS1,↑AL....all 75	187 (20)
dihydrotestosterone		chemical - endogenous ...	Activated	2.274	bias	1.52E-15	↑ADAMTS1, ↑A.... ...all 40	214 (24)
filgrastim		biologic drug	Activated	2.990		6.56E-07	↓CD74, ↑CST3,↓....all 23	
cyclosporin A		biologic drug	Activated	2.925		3.19E-06	↓AKR1B1,↑APOD, ...all 22	139 (20)
diethylstilbestrol		chemical drug	Activated	2.302		2.30E-06	↓AQP9, ↑CCNA2, ...all 18	109 (7)
metribolone		chemical reagent	Activated	2.221	bias	1.07E-04	↑ADAMTS1, ↑A.... ...all 15	223 (23)
bexarotene		chemical drug	Activated	2.699		2.52E-06	↓AKR1C1/AKR1C2 ...all 14	85 (13)
deferoxamine		chemical drug	Activated	2.280	bias	7.72E-05	↑ADGRG1, ↑CA9, ...all 12	114 (15)
cyclic AMP		chemical - endogenous ...	Activated	2.113	bias	3.12E-03	↑ADRA2A,↓CCL2, ...all 11	168 (21)
R5020		chemical reagent	Activated	2.588	bias	5.19E-07	↑CCN2,↑DKK1,↑....all 10	102 (14)
allopurinol		chemical drug	Activated	2.530	bias	9.21E-07	↑ADAMTS1, ↓C.... ...all 10	134 (16)
quercetin		chemical drug	Activated	2.138		3.91E-04	↓CCL2, ↓CXCL10,↑....all 9	123 (19)
17-alpha-ethinylestradiol		chemical drug	Activated	2.157		8.17E-04	↓AQP9, ↓CD74, ↑.... ...all 9	183 (19)
methapyrilene		chemical drug	Activated	2.236		1.67E-03	↑CBS/CBSL,↑CST3, ...all 8	
GnRH-A		chemical reagent	Activated	2.425		9.62E-04	↓FST, ↑GADD45B,↑....all 6	134 (12)
corticosterone		chemical - endogenous ...	Activated	2.200		1.25E-02	↑CCN2,↑DDIT4,↑....all 6	
phenylbutazone		chemical drug	Activated	2.433	bias	3.61E-04	↑ADAMTS1, ↑LA.... ...all 6	
2-bromoethylamine		chemical reagent	Activated	2.425	bias	1.17E-04	↑ADAMTS1, ↑LA.... ...all 6	
gentamicin C		chemical drug	Activated	2.449	bias	5.13E-04	↑ADAMTS1, ↑LA.... ...all 6	
fenamic acid		chemical reagent	Activated	2.425	bias	7.68E-04	↑ADAMTS1, ↑LA.... ...all 6	
triamterene		chemical drug	Activated	2.433	bias	6.05E-04	↑ADAMTS1, ↑LA.... ...all 6	
vancomycin		biologic drug	Activated	2.401	bias	2.55E-03	↑ADAMTS1, ↑LA.... ...all 6	
hexachlorobenzene		chemical toxicant	Activated	2.236	bias	2.03E-03	↑LAMC2,↑MYC,↑....all 5	77 (6)
lomustine		chemical drug	Activated	2.236	bias	3.38E-03	↑LAMC2,↑MYC,↑....all 5	
phenacetin		chemical drug	Activated	2.236	bias	5.01E-04	↑LAMC2,↑MYC,↑....all 5	
eicosapentenoic acid		chemical drug	Activated	2.235		1.53E-02	↓CCL2, ↓MMP8,↓....all 5	
etanercept		biologic drug	Activated	2.236	bias	9.79E-05	↓CCL2, ↓CCL20,↓....all 5	129 (16)
ethionine		chemical toxicant	Activated	2.000	bias	3.24E-03	↑LAMC2,↑MYC,↑....all 4	
2,4,5,2',4',5'-hexachlorobip		chemical toxicant	Activated	2.000		9.90E-02	↑AOX1, ↑EBF1, ↑.... ...all 4	

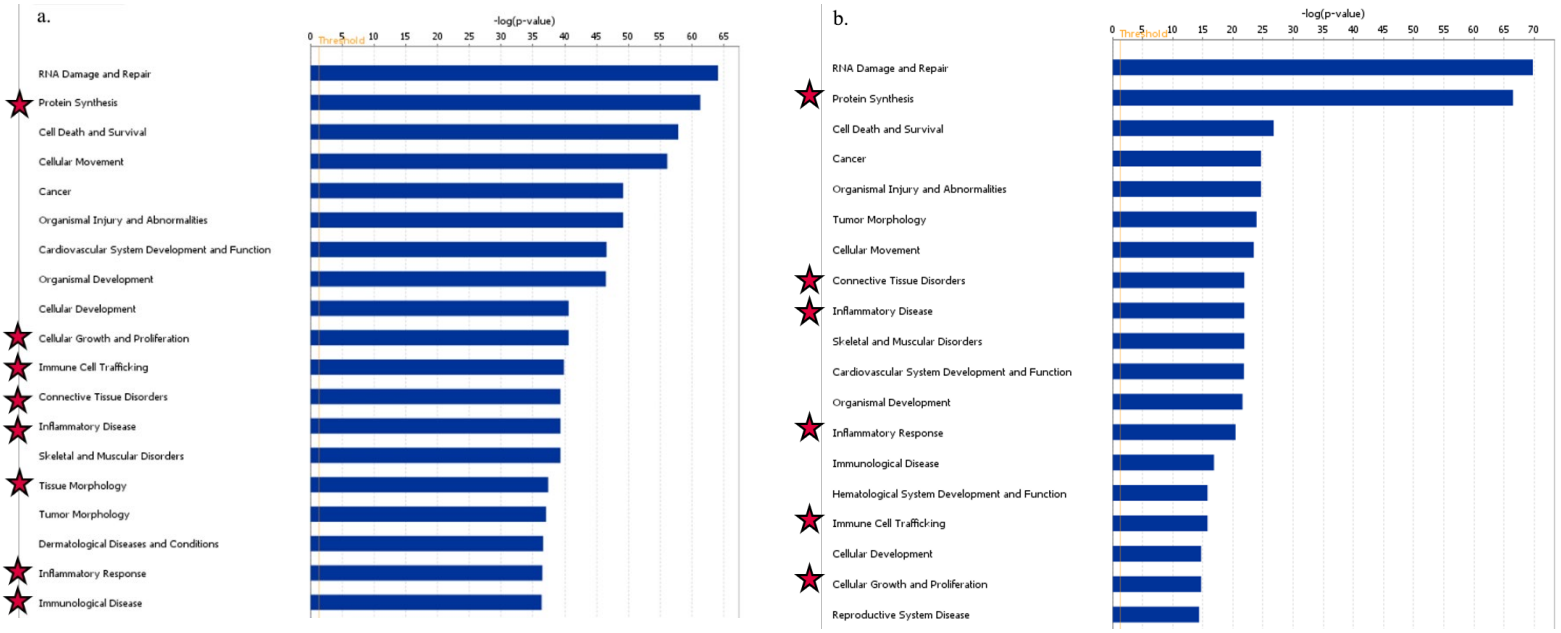

Supplementary Figure 1. Top Diseases and Biological Functions from the Core analysis. a) Top results from the downstream effect analysis that was run as part of the Core analysis to identify functional endpoints, biological and cellular processes that overlap with the VA vs. Ctr negative dataset. b) Downstream effect analysis related to the biological and cellular processes that overlap with the Epi C vs. Ctr negative group dataset. The marked terms are high-level categories of biological and clinical processes or functions that fit to the expected biological context. The p-values are provided by Fisher's exact test (right tailed) to assess whether a given overlap is due to chance alone (low p-value rejects the null hypothesis = significant association).

a.

The Filter found 36 Functions for Immune Cell Trafficking

Categories	Diseases or Functions Annotation	p-value	Predicted Activation State	Activation z-score	Molecules	# Molecules
Cell-To-Cell Signali...	Activation of leukocytes	1.90E-18	Decreased	-3.828	↓AGRN, ↑AHNAK, ↑ANXA1, ↑AN... ...all 105	105
Cell-To-Cell Signali...	Activation of lymphocytes	5.46E-13	Decreased	-3.689	↓AGRN, ↑AHNAK, ↑ANXA1, ↓BTN... ...all 69	69
Cellular Movement,...	Migration of phagocytes	6.23E-18	Decreased	-3.447	↓ABCC1, ↓ABL1, ↑ALCAM, ↑ANXA1, ...all 59	59
Cellular Movement,...	Chemotaxis of leukocytes	9.23E-16	Decreased	-3.378	↓ACKR3, ↑ANXA1, ↓AQP9, ↓C3AR1, ...all 64	64
Cellular Movement,...	Chemotaxis of phagocytes	2.36E-15	Decreased	-3.335	↑ANXA1, ↓AQP9, ↓C3AR1, ↑C5AR2, ...all 56	56
Hematological Syst...	Accumulation of phagocytes	1.43E-18	Decreased	-3.313	↓ACKR3, ↑ANXA1, ↓CCL11, ↓CCL2, ...all 41	41
Cell-To-Cell Signali...	Activation of phagocytes	3.64E-13	Decreased	-3.100	↑ANXA1, ↑ANXA2, ↓ATF3, ↓BDNF, ...all 60	60
Hematological Syst...	Accumulation of leukocytes	1.15E-23	Decreased	-3.092	↓ACKR3, ↑ANXA1, ↓BCL2A1, ↑BGN, ...all 65	65
Cellular Movement,...	Cell movement of phagocytes	2.98E-26	Decreased	-2.970	↓ABCC1, ↓ABL1, ↓ADM, ↑ALCAM, ...all 110	110
Cellular Movement,...	Cell movement of macrophages	2.57E-19	Decreased	-2.850	↓ABL1, ↑ANXA1, ↓C3AR1, ↑CAV1, ...all 62	62
Cell-To-Cell Signali...	Activation of antigen presenting cells	5.27E-13	Decreased	-2.732	↑ANXA2, ↓ATF3, ↓BDNF, ↓CCL11, ...all 54	54
Cellular Movement,...	Homing of leukocytes	2.52E-18	Decreased	-2.716	↓ACKR3, ↑ANXA1, ↓AQP9, ↓C3AR1, ...all 71	71
Cellular Movement,...	Cell movement of neutrophils	5.02E-21	Decreased	-2.670	↓ADM, ↑ANXA1, ↑ANXA2, ↓AQP9, ...all 68	68
Cellular Movement,...	Cell movement of antigen presenting cells	4.69E-20	Decreased	-2.585	↓ABCC1, ↓ABL1, ↑ALCAM, ↑ANXA1, ...all 74	74
Cellular Movement,...	Migration of mononuclear leukocytes	2.21E-20	Decreased	-2.444	↓ABCC1, ↓ACKR3, ↑ANXA1, ↑ANX... ...all 76	76
Cell-To-Cell Signali...	Recruitment of leukocytes	4.27E-25	Decreased	-2.415	↑ADGRG6, ↑ANXA1, ↓C3AR1, ↑C... ...all 75	75
Cell-To-Cell Signali...	Recruitment of phagocytes	8.33E-19	Decreased	-2.368	↑ADGRG6, ↑ANXA1, ↓C3AR1, ↑C... ...all 56	56
Hematological Syst...	Accumulation of granulocytes	1.88E-14	Decreased	-2.301	↑ANXA1, ↓BCL2A1, ↓CCL11, ↓CCL2, ...all 30	30
Cellular Movement,...	Cell movement of granulocytes	1.42E-23	Decreased	-2.297	↓ADM, ↑ANXA1, ↑ANXA2, ↓AQP9, ...all 81	81
Cell-To-Cell Signali...	Adhesion of immune cells	3.59E-17	Decreased	-2.263	↓ABL1, ↑ALCAM, ↑ANXA1, ↓BMPE... ...all 66	66
Cellular Movement,...	Lymphocyte migration	5.11E-17	Decreased	-2.252	↓ABCC1, ↓ACKR3, ↑ANXA1, ↑CAV1, ...all 67	67
Cellular Movement,...	Cell movement of leukocytes	1.42E-34	Decreased	-2.240	↓ABCC1, ↓ABL1, ↓ACKR3, ↓ADM, ...all 152	152
Cellular Movement,...	Leukocyte migration	1.36E-40	Decreased	-2.008	↓ABCC1, ↓ABL1, ↓ACKR3, ↑ADG... ...all 182	182

b.

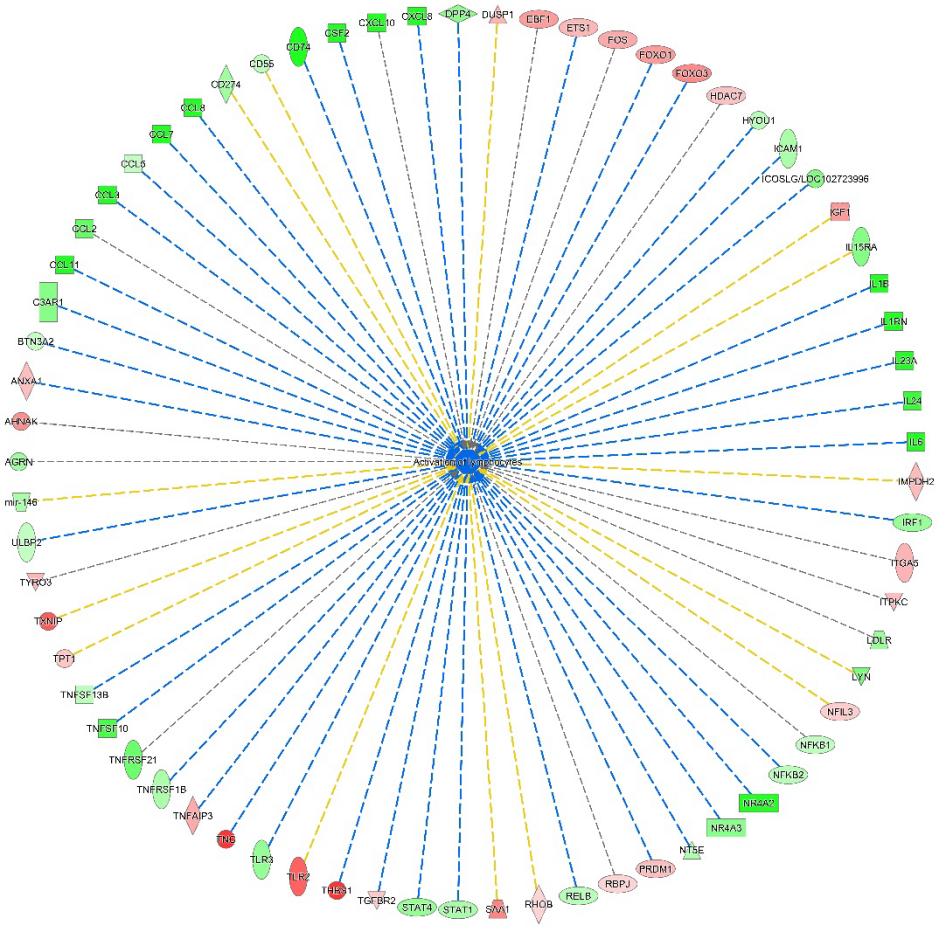

Supplementary Figure 2. a) Low-level (specific) process or functions that belong to the high-level category "Immune cell trafficking". For the VA vs. Ctr group; most terms in this table have significantly negative activation z-scores. b) The network of the term "Activation of lymphocytes" in the list of top disorder in the high-level category "Immune cell trafficking". The central term "Activation of lymphocytes" is filled with blue. A blue filling marks a predicted "decrease" of the function or process. The nodes in the periphery are filled with either green (down-regulation in the experiment) or red (up-regulation in the experiment).

a.

The Filter found 11 Functions for Inflammatory Disease

Categories	Diseases or Functions Annotation	p-value	Predicted Activation State	Activation z-score	Molecules	# Molecules
Connective Tissue Disorders,Inflamm...	Inflammation of joint	3.69E-21		-1.773	↑ACAN, ↑ADAMTS1,↑ADGRG6, ↑ADRA... ...all 78	78
Connective Tissue Disorders,Inflamm...	Rheumatic Disease	1.28E-22		-1.134	↑ACAN, ↓ACSL5, ↑ADAMTS1,↑ADGRG6, ...all 92	92
Inflammatory Disease	Chronic inflammatory disorder	4.03E-12		-0.651	↑ACAN, ↑ADGRG6, ↑ADRA2A, ↓AQP9,↑.....all 66	66
Connective Tissue Disorders,Inflamm...	Polyarthritis	2.02E-06		-0.577	↓CCL20, ↓CD74, ↑COL2A1, ↓CSF3, ↑GA... ...all 15	15
Connective Tissue Disorders,Immun...	Rheumatoid arthritis	1.76E-16			↑ACAN, ↑ADGRG6, ↑ADRA2A, ↓AQP9,↑.....all 58	58
Connective Tissue Disorders,Inflamm...	Osteoarthritis	4.63E-11			↑ACAN, ↑ADAMTS1,↑ADRA2A, ↑ASPN,`.....all 24	24
Inflammatory Disease,Neurological D...	Inflammatory demyelinating disease	4.45E-08			↑ADRA2A, ↑ALCAM, ↓BST2, ↓CCL2,↑CR.....all 21	21
Connective Tissue Disorders,Immun...	Systemic lupus erythematosus	8.59E-08			↓ACSL5, ↓BST2, ↓CCL2, ↓CXCL10, ↓EPS... ...all 26	26
Inflammatory Disease,Neurological D...	Multiple Sclerosis	1.53E-07			↑ADRA2A, ↑ALCAM, ↓BST2, ↓CCL2,↑CR.....all 20	20
Connective Tissue Disorders,Immun...	Polyarticular juvenile rheumatoid arth	6.51E-07			↓CCL20, ↓CD74, ↑GADD45B, ↑IL6R, ↓N... ...all 11	11
Connective Tissue Disorders,Inflamm...	Intervertebral disc disorder	4.10E-06			↑ADRA2A, ↑ASPN, ↑CCN2, ↑CILP, ↑COL1... ...all 8	8

b.

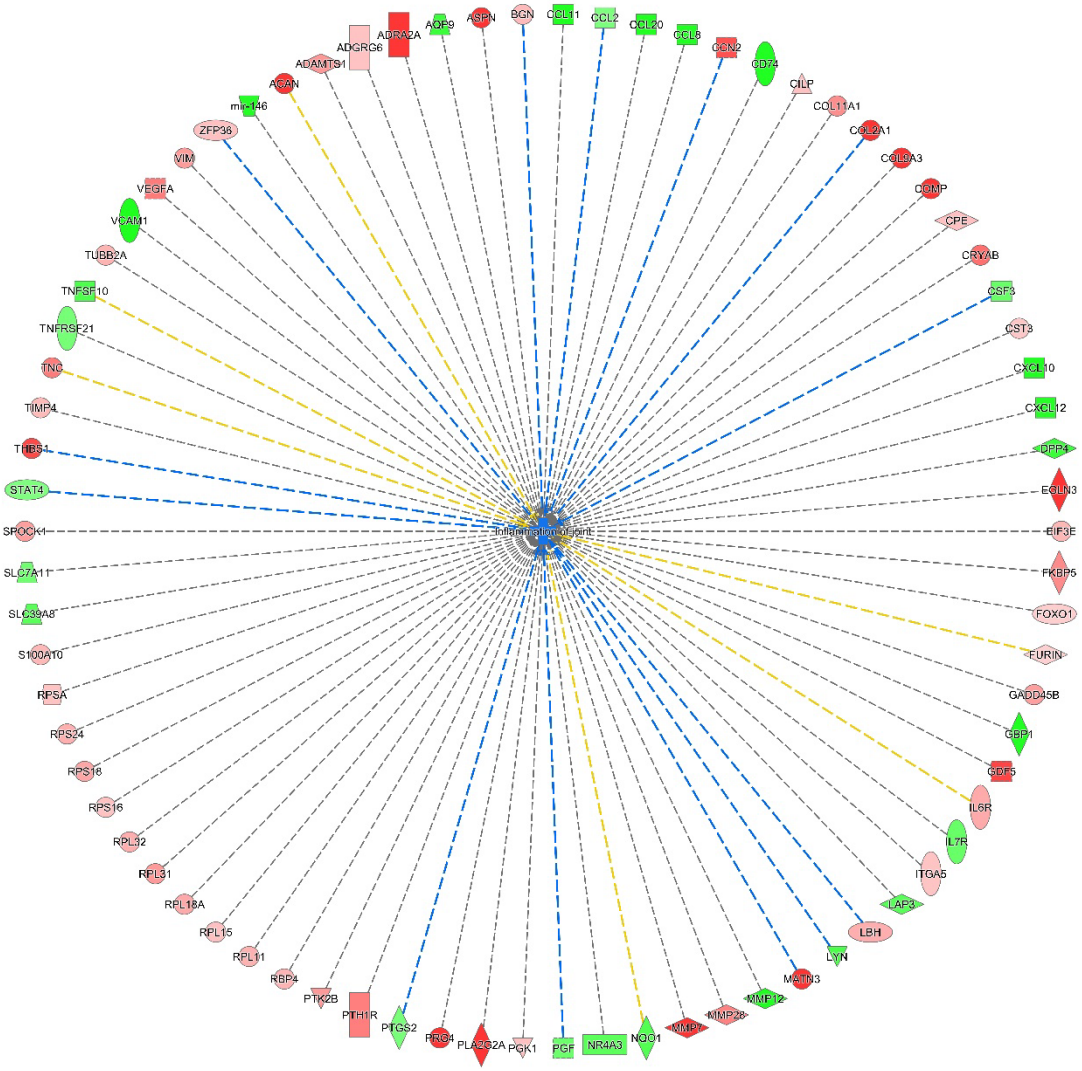

Supplementary Figure 3. a) Table of low-level (specific) process or functions that belong to the high-level category “Inflammatory disease” for Epi C vs. Ctr vehicle group. b) Example network of the term “Inflammation of the joints”. The term "Inflammation of the joints" was decreased and this is supported by down-regulated chemokines and cytokines as well as up-regulated ECM components, such as COL2A1, BGN, and CCN2. The central term “Inflammation of the joints” is filled with blue. A blue filling marks a predicted “decrease” of the function or process. The nodes in the periphery are filled with either green (down-regulation in the experiment) or red (up-regulation in the experiment).

a.

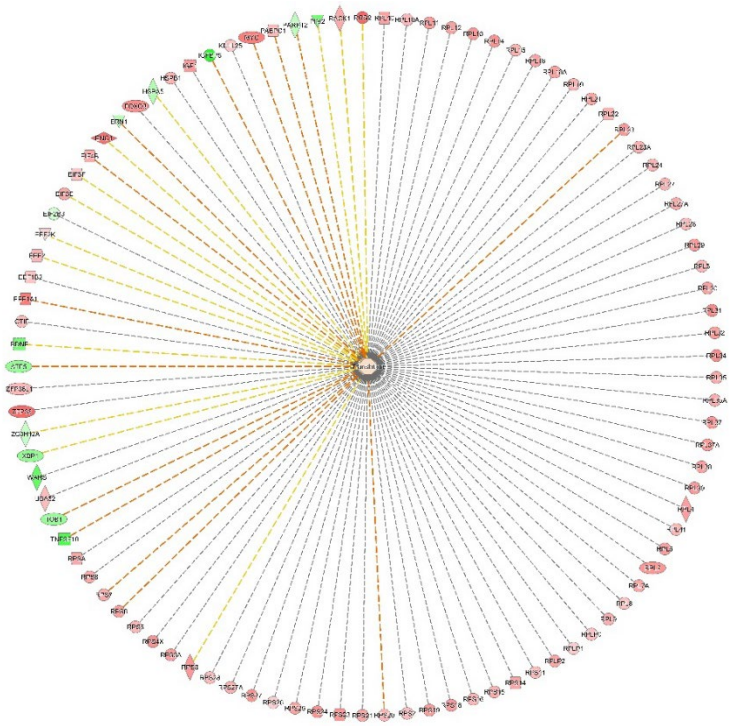

b.

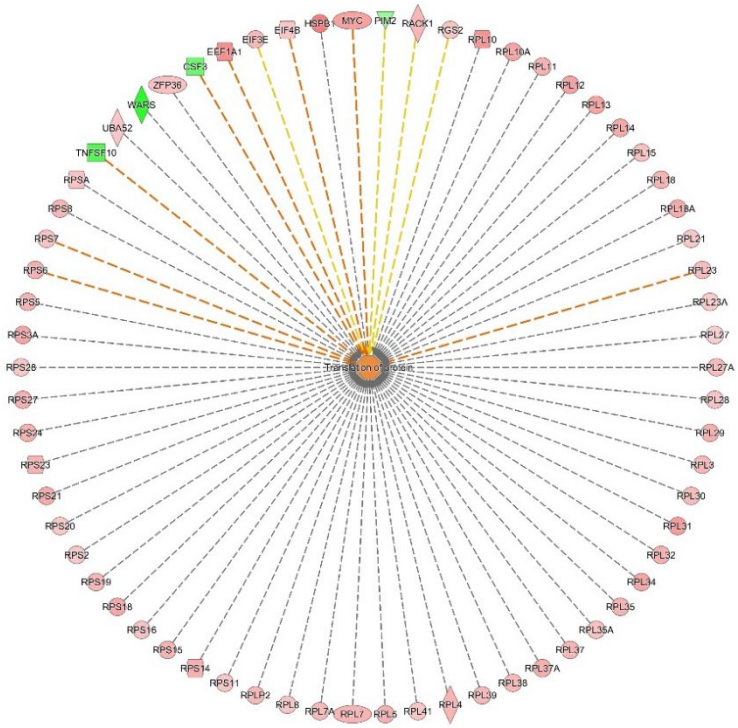

Supplementary Figure 4. Example network of the term “Translation” that belongs to the high-level category “Protein synthesis”. Most of these data set nodes represent ribosomal genes or translation initiation/elongation factors. a) The network for the VA vs. Ctr vehicle group and b) The network for the Epi C vs. Ctr vehicle group are shown. The central node represents the term and the nodes in the periphery, associated with this term are shown. The central term “Translation” is filled with orange, which indicates the predicted tendency for “increase” (non-significant). The nodes in the periphery are filled with either green (down-regulation in the experiment) or red (up-regulation in the experiment). Some of the proteins with increased expression are COL5A1, COL6A3, COL8A1, BGN, LAMA2, LAMA3, LAMB1, LAMC1.

a.

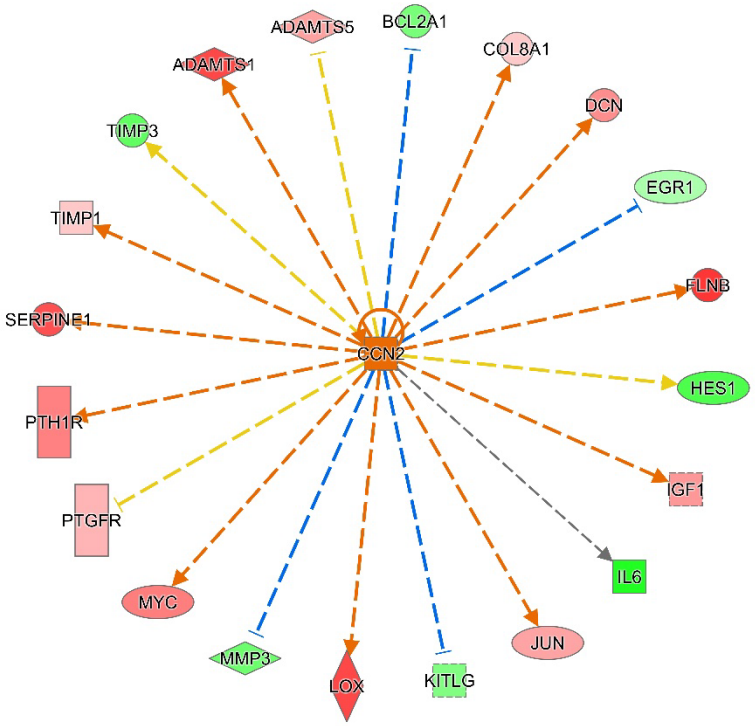

b.

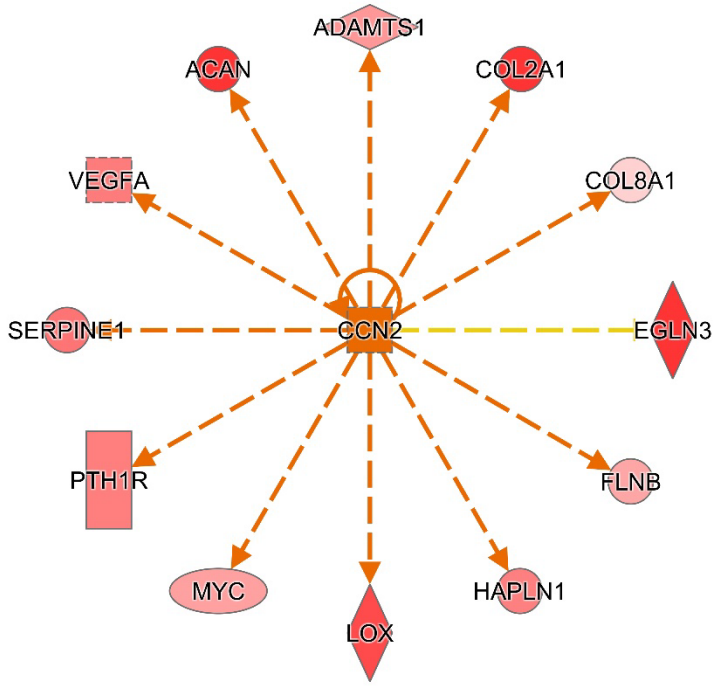

Supplementary Figure 5. The example of the upstream regulator network of CCN2. a) The network for the VA vs. Ctr vehicle group and b) The network for the Epi C vs. Ctr vehicle group are shown. The central node represents the upstream regulator and the nodes in the periphery data set represent molecules regulated by the upstream regulator. The central term "CCN2" is filled with orange, which indicates the predicted increase. The nodes in the periphery are filled with either green (down-regulation in the experiment) or red (up-regulation in the experiment). This network provides one explanation for the up-regulation of many ECM components.

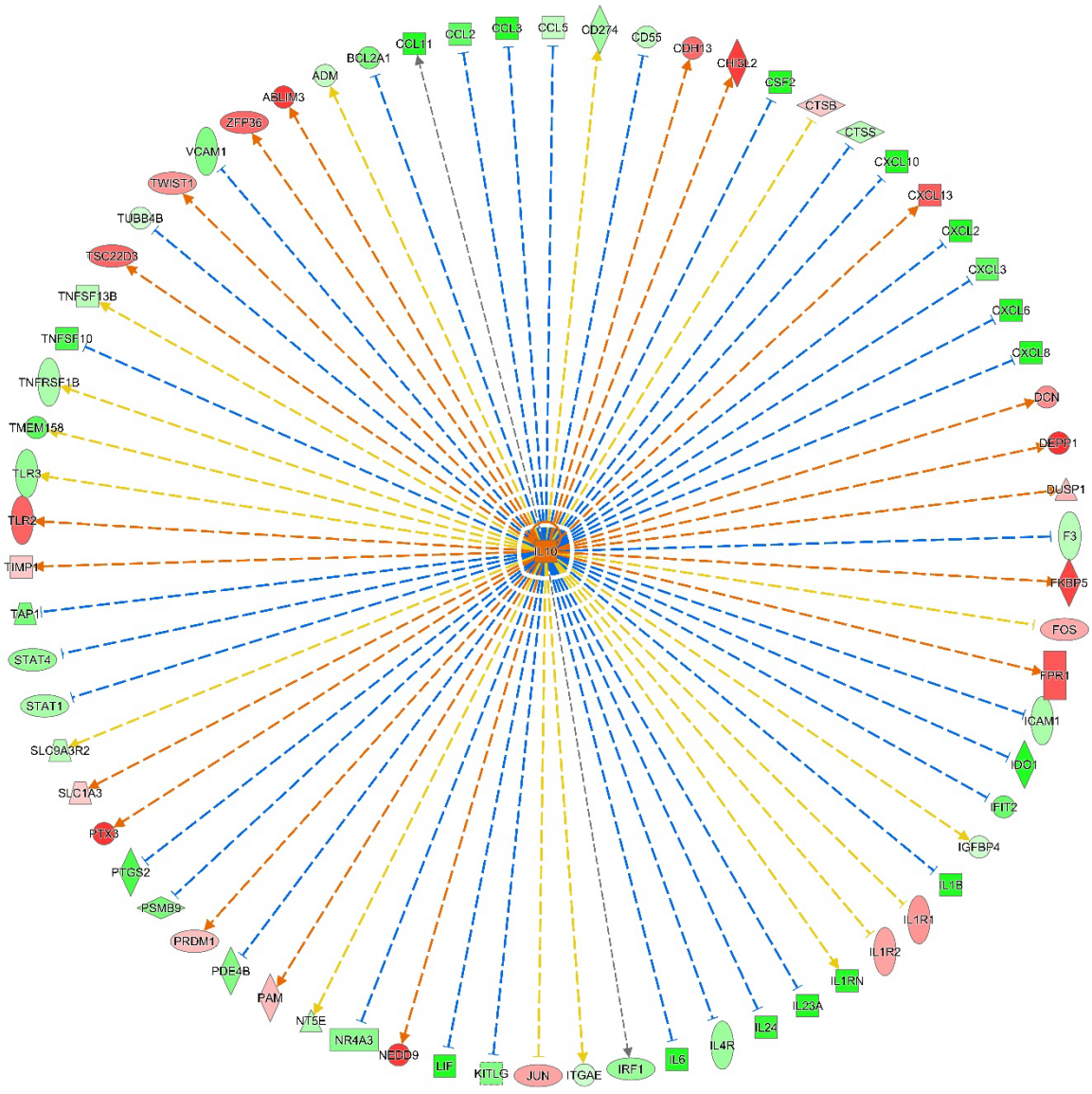

Supplementary Figure 6. The example of the upstream regulator network of IL-10. The central node represents the upstream regulator and the nodes in the periphery data set represent molecules regulated by the upstream regulator. The central term "IL10" is filled with orange, which indicates the up-regulation of the IL-10. This network provides one explanation for the down-regulation of many different chemokines and cytokines in the experiment.

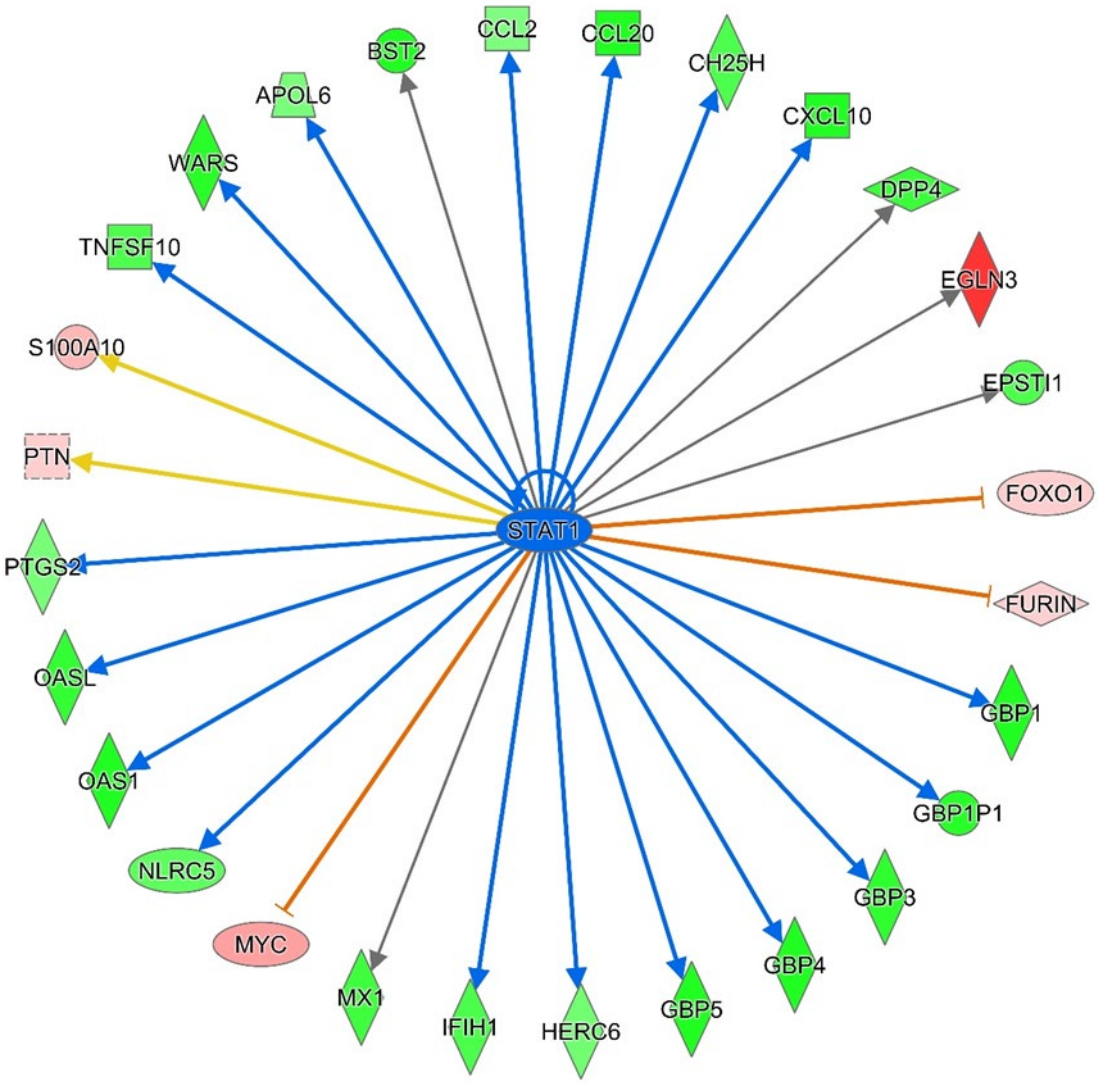

Supplementary Figure 7. The example of the upstream regulator network for the inhibited STAT1 in Epi C vs. Ctr group. The predicted inhibition of this putative upstream regulator relates to down-regulation of selected chemokines and cytokines. The central term "STAT1" is filled with blue. A blue filling marks a predicted "decrease" of the function or process. The nodes in the periphery are filled with either green (down-regulation in the experiment) or red (up-regulation in the experiment).

a.

b.

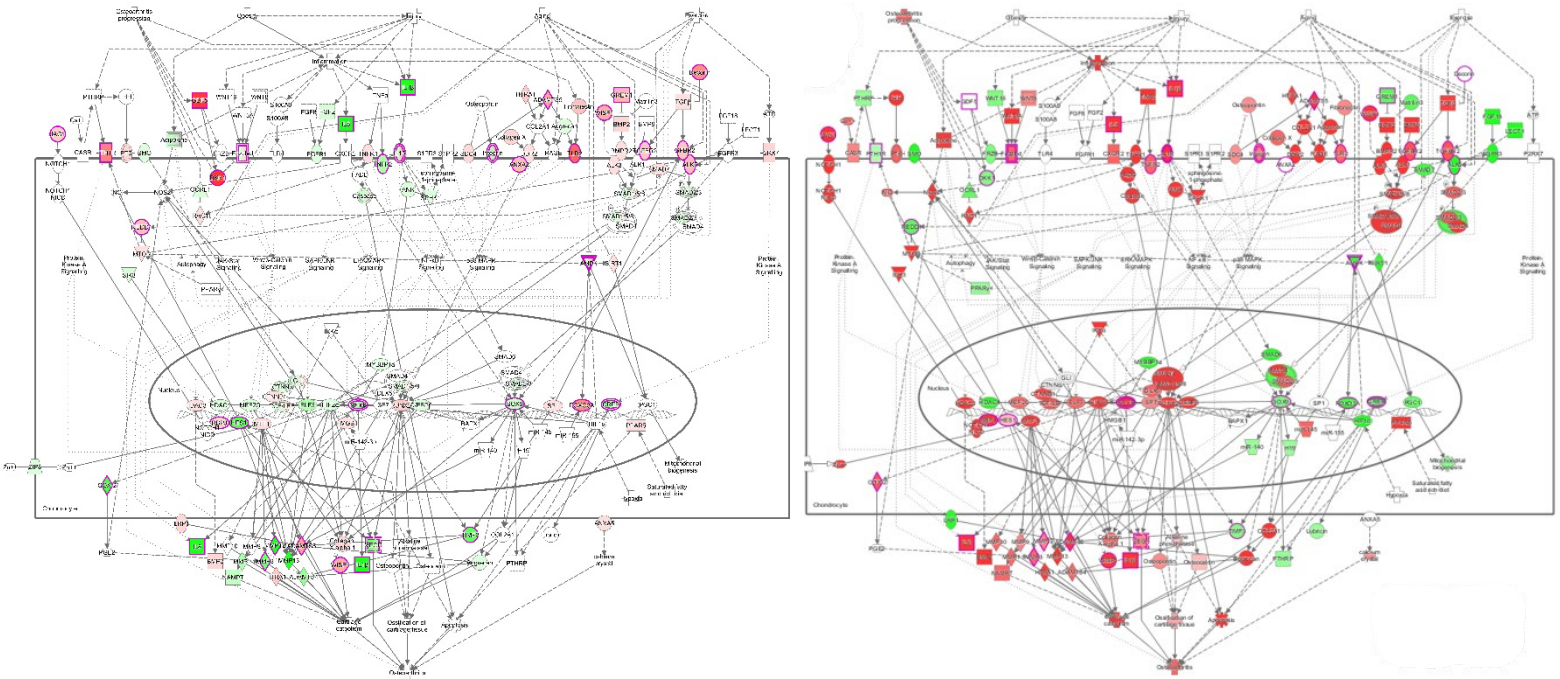

Supplementary Figure 8. The first relevant and significant canonical pathway for VA vs. Ctr treatment group is the “Osteoarthritis signaling”. a) The activation z-score suggests a tendency for inhibition. Based on the activation z-score, the normal function of this pathway is reduced. Elements of this canonical pathway are shown as different shapes (nodes). These shapes are filled with red (up-regulation in the experiment) or green (down-regulation in the experiment). b) Shows the canonical pathway “Osteoarthritis signaling” overlaid with expected node activities considering this pathway as being fully activated (The expected activities are a result of curations of relevant papers, reviews and textbooks and can be compared to overlays of actual experimental measurements). Red fillings represent “activated”, green fillings “inhibited”. Nodes with purple highlights (borders) have passed the cut-offs.

a.

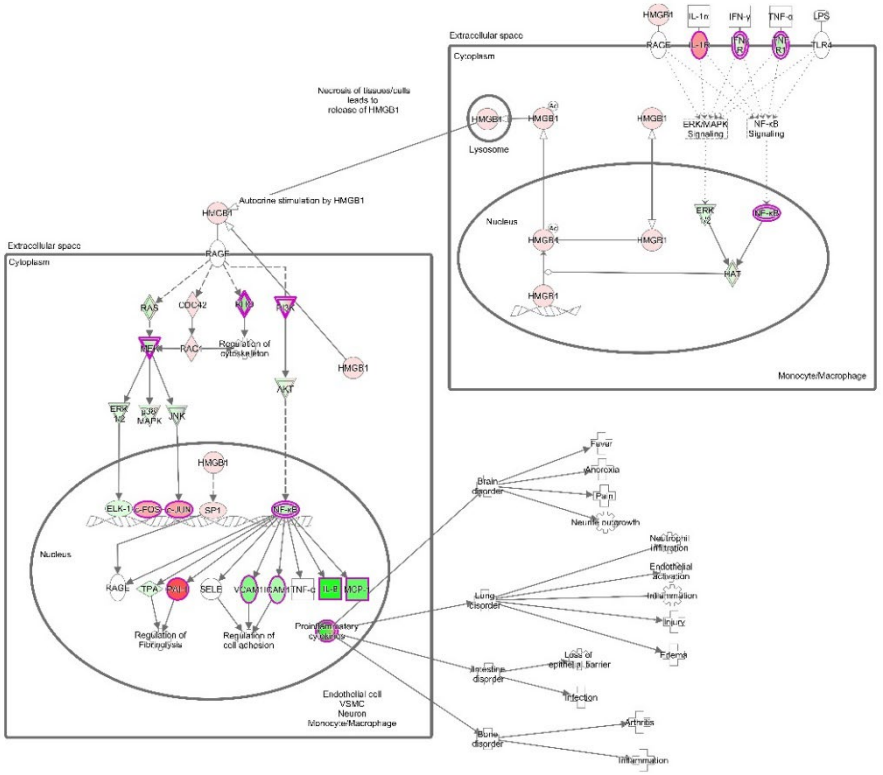

b.

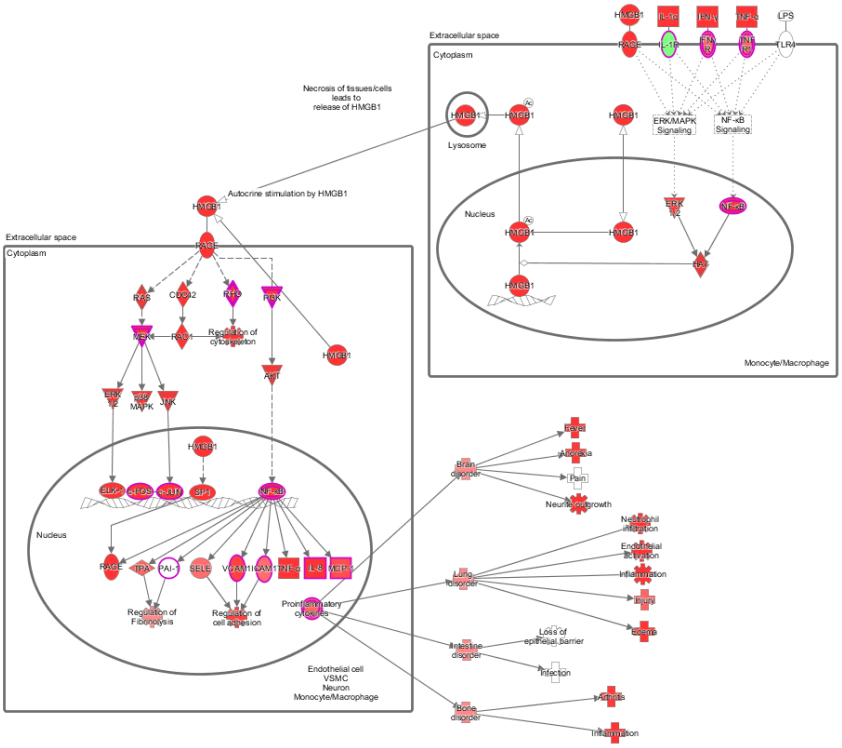

Supplementary Figure 9. The canonical pathway "HMGB1 signaling" overlaid with experimental data from VA vs. Ctr group. a) The activation z-score is negative and is very close to the significance threshold. Therefore, we would assume that this pathway has a strong tendency to be inhibited. Central to this pathway is the down-regulation of NF-κB. b) "HMGB1 signaling" overlaid with expected activities. The comparison of the expected activities and actual measurements confirms the inhibition of this pathway. Red fillings represent "activated", green fillings "inhibited" purple highlights = passed cut-offs, no highlight = didn't pass cut-offs.

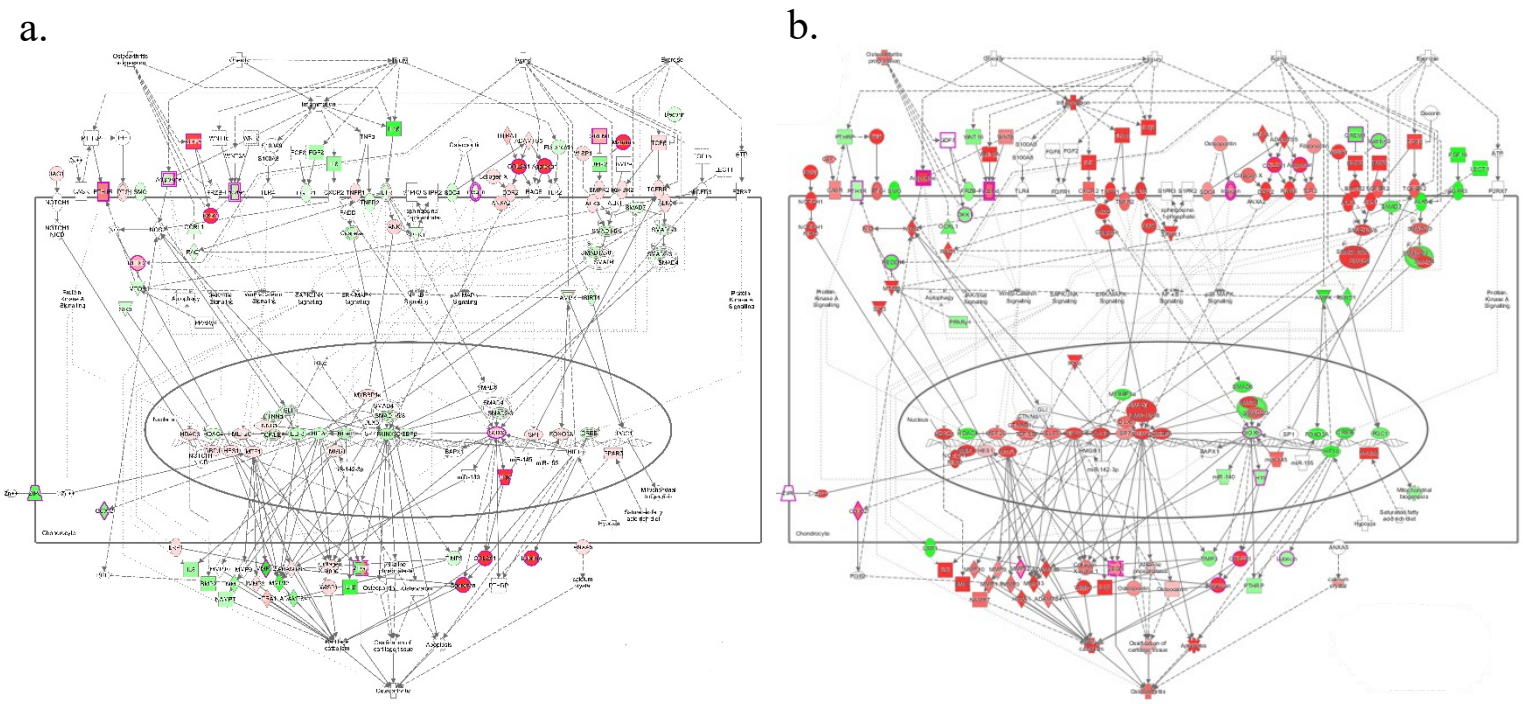

Supplementary Figure 10. The first relevant and significant canonical pathway for Epi C vs. Ctr treatment group is the "Osteoarthritis signaling". a) The activation z-score suggests a tendency for inhibition. Based on the activation z-score (p-value = 1.45E-3, z-score = -1.213), the normal function of this pathway is reduced. Elements of this canonical pathway are shown as different shapes (nodes). These shapes are filled with red (up-regulation in the experiment) or green (down-regulation in the experiment). b) Shows the canonical pathway "Osteoarthritis signaling" overlaid with expected node activities considering this pathway as being fully activated (The expected activities are a result of curations of relevant papers, reviews and textbooks and can be compared to overlays of actual experimental measurements). Red fillings represent "activated", green fillings "inhibited". Nodes with purple highlights (borders) have passed the cut-offs.

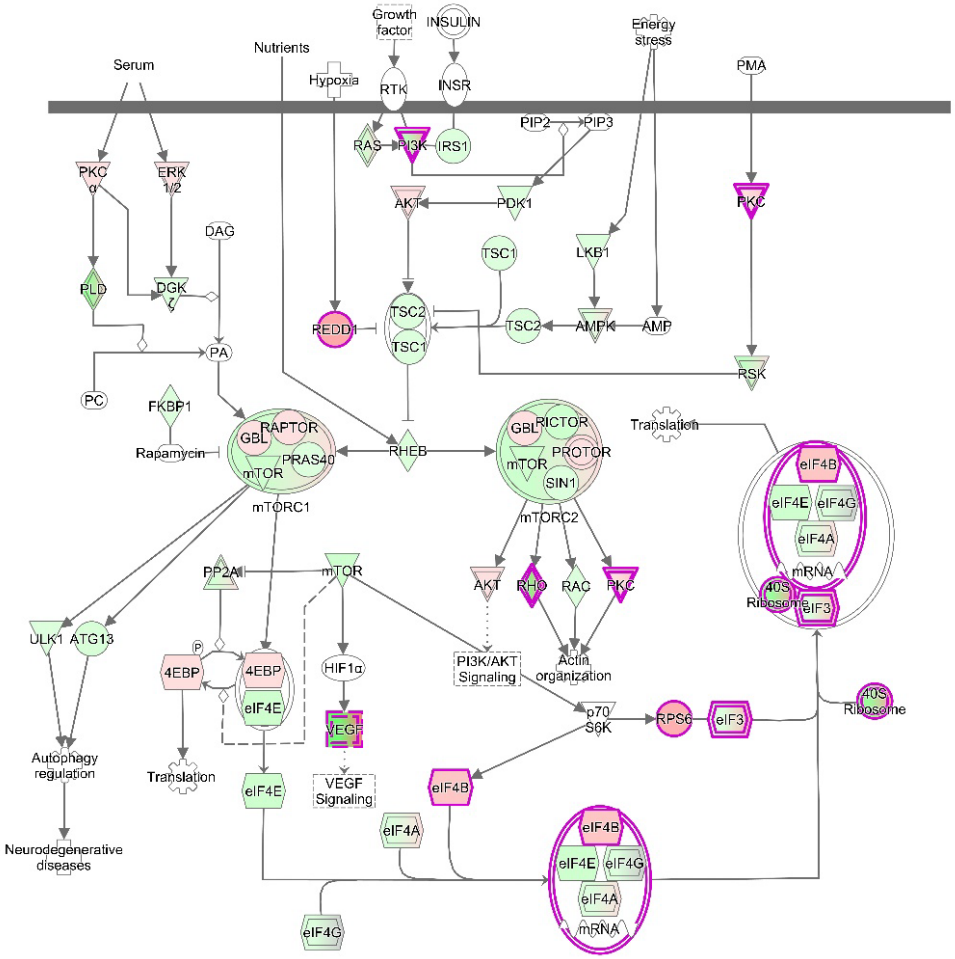

Supplementary Figure 11. The canonical pathway "mTOR signaling". This pathway was found to be moderately activated (insignificant). A visual inspection of the pathway reveals up-regulated translation initiation/elongation factors and ribosomal genes. PKC and REDD1 are up-regulated. Red fillings represent "activated", green fillings "inhibited". Nodes with purple highlights (borders) have passed the cut-offs.

7. References

1. Poole, A.R.; Kojima, T.; Yasuda, T.; Mwale, F.; Kobayashi, M.; Laverty, S. Composition and structure of articular cartilage: a template for tissue repair. *Clin Orthop Relat Res* **2001**, 10.1097/00003086-200110001-00004, S26-33, doi:10.1097/00003086-200110001-00004.

2. Goldring, M.B.; Marcu, K.B. Cartilage homeostasis in health and rheumatic diseases. *Arthritis research & therapy* **2009**, *11*, 224-224, doi:10.1186/ar2592.

3. Wang, M.; Shen, J.; Jin, H.; Im, H.J.; Sandy, J.; Chen, D. Recent progress in understanding molecular mechanisms of cartilage degeneration during osteoarthritis. *Ann N Y Acad Sci* **2011**, *1240*, 61-69, doi:10.1111/j.1749-6632.2011.06258.x.

4. Glyn-Jones, S.; Palmer, A.J.; Agricola, R.; Price, A.J.; Vincent, T.L.; Weinans, H.; Carr, A.J. Osteoarthritis. *Lancet (London, England)* **2015**, *386*, 376-387, doi:10.1016/s0140-6736(14)60802-3.

5. Goldring, M.B.; Otero, M. Inflammation in osteoarthritis. *Curr Opin Rheumatol* **2011**, *23*, 471-478, doi:10.1097/BOR.0b013e328349c2b1.

6. Kapoor, M.; Martel-Pelletier, J.; Lajeunesse, D.; Pelletier, J.P.; Fahmi, H. Role of proinflammatory cytokines in the pathophysiology of osteoarthritis. *Nature reviews. Rheumatology* **2011**, *7*, 33-42, doi:10.1038/nrrheum.2010.196.

7. Melchiorri, C.; Meliconi, R.; Frizziero, L.; Silvestri, T.; Pulsatelli, L.; Mazzetti, I.; Borzi, R.M.; Uguccioni, M.; Facchini, A. Enhanced and coordinated in vivo expression of inflammatory cytokines and nitric oxide synthase by chondrocytes from patients with osteoarthritis. *Arthritis and rheumatism* **1998**, *41*, 2165-2174, doi:10.1002/1529-0131(199812)41:12<2165::aid-art11>3.0.co;2-o.

8. Loeser, R.F.; Erickson, E.A.; Long, D.L. Mitogen-activated protein kinases as therapeutic targets in osteoarthritis. *Current opinion in rheumatology* **2008**, *20*, 581-586, doi:10.1097/BOR.0b013e3283090463.

9. Mariani, E.; Pulsatelli, L.; Facchini, A. Signaling pathways in cartilage repair. *International journal of molecular sciences* **2014**, *15*, 8667-8698, doi:10.3390/ijms15058667.

10. Kim, H.A.; Cho, M.L.; Choi, H.Y.; Yoon, C.S.; Jhun, J.Y.; Oh, H.J.; Kim, H.Y. The catabolic pathway mediated by Toll-like receptors in human osteoarthritic chondrocytes. *Arthritis and rheumatism* **2006**, *54*, 2152-2163, doi:10.1002/art.21951.

11. Liu-Bryan, R.; Terkeltaub, R. Chondrocyte innate immune myeloid differentiation factor 88-dependent signaling drives procatabolic effects of the endogenous Toll-like receptor 2/Toll-like receptor 4 ligands low molecular weight hyaluronan and high mobility group box chromosomal protein 1 in mice. *Arthritis and rheumatism* **2010**, *62*, 2004-2012, doi:10.1002/art.27475.

12. Choi, M.-C.; Jo, J.; Park, J.; Kang, H.K.; Park, Y. NF-κB Signaling Pathways in Osteoarthritic Cartilage Destruction. In *Cells*, 2019; Vol. 8.

13. Marcu, K.B.; Otero, M.; Olivotto, E.; Borzi, R.M.; Goldring, M.B. NF-kappaB signaling: multiple angles to target OA. *Curr Drug Targets* **2010**, *11*, 599-613.

14. Olivotto, E.; Otero, M.; Marcu, K.B.; Goldring, M.B. Pathophysiology of osteoarthritis: canonical NF-κB/IKKβ-dependent and kinase-independent effects of IKKα in cartilage degradation and chondrocyte differentiation. *RMD Open* **2015**, *1*, e000061, doi:10.1136/rmdopen-2015-000061.

15. García-Arnandis, I.; Guillén, M.I.; Gomar, F.; Pelletier, J.-P.; Martel-Pelletier, J.; Alcaraz, M.J. High mobility group box 1 potentiates the pro-inflammatory effects of interleukin-1β in osteoarthritic synoviocytes. *Arthritis research & therapy* **2010**, *12*, R165, doi:10.1186/ar3124.

16. Nefla, M.; Holzinger, D.; Berenbaum, F.; Jacques, C. The danger from within: alarmins in arthritis. *Nature Reviews Rheumatology* **2016**, *12*, 669-683, doi:10.1038/nrrheum.2016.162.

17. Aulin, C.; Lassacher, T.; Palmblad, K.; Erlandsson Harris, H. Early stage blockade of the alarmin HMGB1 reduces cartilage destruction in experimental OA. *Osteoarthritis and cartilage* **2020**, https://doi.org/10.1016/j.joca.2020.01.003, doi:https://doi.org/10.1016/j.joca.2020.01.003.

18. Sun, K.; Luo, J.; Guo, J.; Yao, X.; Jing, X.; Guo, F. The PI3K/AKT/mTOR signaling pathway in osteoarthritis: a narrative review. *Osteoarthritis and cartilage* **2020**, *28*, 400-409, doi:10.1016/j.joca.2020.02.027.

19. Ghosh, S.; May, M.J.; Kopp, E.B. NF-kappa B and Rel proteins: evolutionarily conserved mediators of immune responses. *Annu Rev Immunol* **1998**, *16*, 225-260, doi:10.1146/annurev.immunol.16.1.225.

20. Hayden, M.S.; Ghosh, S. NF-kappaB, the first quarter-century: remarkable progress and outstanding questions. *Genes Dev* **2012**, *26*, 203-234, doi:10.1101/gad.183434.111.

21. Tak, P.P.; Firestein, G.S. NF-kappaB: a key role in inflammatory diseases. *The Journal of clinical investigation* **2001**, *107*, 7-11, doi:10.1172/jci11830.

22. Lawrence, T. The nuclear factor NF-kappaB pathway in inflammation. *Cold Spring Harb Perspect Biol* **2009**, *1*, a001651, doi:10.1101/cshperspect.a001651.

23. Favata, M.F.; Horiuchi, K.Y.; Manos, E.J.; Daulerio, A.J.; Stradley, D.A.; Feeser, W.S.; Van Dyk, D.E.; Pitts, W.J.; Earl, R.A.; Hobbs, F., et al. Identification of a novel inhibitor of mitogen-activated protein kinase kinase. *The Journal of biological chemistry* **1998**, *273*, 18623-18632, doi:10.1074/jbc.273.29.18623.

24. Dinarello, C.A.; Simon, A.; van der Meer, J.W. Treating inflammation by blocking interleukin-1 in a broad spectrum of diseases. *Nat Rev Drug Discov* **2012**, *11*, 633-652, doi:10.1038/nrd3800.

25. Pande, V.; Ramos, M.J. NF-kappaB in human disease: current inhibitors and prospects for de novo structure based design of inhibitors. *Curr Med Chem* **2005**, *12*, 357-374, doi:10.2174/0929867053363180.

26. Burke, J.R.; Pattoli, M.A.; Gregor, K.R.; Brassil, P.J.; MacMaster, J.F.; McIntyre, K.W.; Yang, X.; Iotzova, V.S.; Clarke, W.; Strnad, J., et al. BMS-345541 is a highly selective inhibitor of I kappa B kinase that binds at an allosteric site of the enzyme and blocks NF-kappa B-dependent transcription in mice. *The Journal of biological chemistry* **2003**, *278*, 1450-1456, doi:10.1074/jbc.M209677200.

27. Liu, S.; Cao, C.; Zhang, Y.; Liu, G.; Ren, W.; Ye, Y.; Sun, T. PI3K/Akt inhibitor partly decreases TNF-alpha-induced activation of fibroblast-like synoviocytes in osteoarthritis. *J Orthop Surg Res* **2019**, *14*, 425, doi:10.1186/s13018-019-1394-4.

28. Erasalo, H.; Laavola, M.; Hamalainen, M.; Leppanen, T.; Nieminen, R.; Moilanen, E. PI3K inhibitors LY294002 and IC87114 reduce inflammation in carrageenan-induced paw oedema and down-regulate inflammatory gene expression in activated macrophages. *Basic Clin Pharmacol Toxicol* **2015**, *116*, 53-61, doi:10.1111/bcpt.12284.

29. Gupta, S.C.; Sundaram, C.; Reuter, S.; Aggarwal, B.B. Inhibiting NF-kappaB activation by small molecules as a therapeutic strategy. *Biochim Biophys Acta* **2010**, *1799*, 775-787, doi:10.1016/j.bbagrm.2010.05.004.

30. Kumar, S.; Boehm, J.; Lee, J.C. p38 MAP kinases: key signalling molecules as therapeutic targets for inflammatory diseases. *Nat Rev Drug Discov* **2003**, *2*, 717-726, doi:10.1038/nrd1177.

31. Wieland, H.A.; Michaelis, M.; Kirschbaum, B.J.; Rudolphi, K.A. Osteoarthritis - an untreatable disease? *Nat Rev Drug Discov* **2005**, *4*, 331-344, doi:10.1038/nrd1693.

32. Saklatvala, J. Tumour necrosis factor alpha stimulates resorption and inhibits synthesis of proteoglycan in cartilage. *Nature* **1986**, *322*, 547-549, doi:10.1038/322547a0.

33. Williams, A.; Kamper, S.J.; Wiggers, J.H.; O'Brien, K.M.; Lee, H.; Wolfenden, L.; Yoong, S.L.; Robson, E.; McAuley, J.H.; Hartvigsen, J., et al. Musculoskeletal conditions may increase the risk of chronic disease: a systematic review and meta-analysis of cohort studies. *BMC Med* **2018**, *16*, 167, doi:10.1186/s12916-018-1151-2.

34. Clegg, D.O.; Reda, D.J.; Harris, C.L.; Klein, M.A.; O'Dell, J.R.; Hooper, M.M.; Bradley, J.D.; Bingham, C.O., 3rd; Weisman, M.H.; Jackson, C.G., et al. Glucosamine, chondroitin sulfate, and the two in combination for painful knee osteoarthritis. *N Engl J Med* **2006**, *354*, 795-808, doi:10.1056/NEJMoa052771.

35. Henrotin, Y.; Mobasheri, A. Natural Products for Promoting Joint Health and Managing Osteoarthritis. *Curr Rheumatol Rep* **2018**, *20*, 72, doi:10.1007/s11926-018-0782-9.

36. Shi, Y.; Hu, X.; Cheng, J.; Zhang, X.; Zhao, F.; Shi, W.; Ren, B.; Yu, H.; Yang, P.; Li, Z., et al. A small molecule promotes cartilage extracellular matrix generation and inhibits osteoarthritis development. *Nat Commun* **2019**, *10*, 1914, doi:10.1038/s41467-019-09839-x.

37. Johnson, K.; Zhu, S.; Tremblay, M.S.; Payette, J.N.; Wang, J.; Bouchez, L.C.; Meeusen, S.; Althage, A.; Cho, C.Y.; Wu, X., et al. A stem cell-based approach to cartilage repair. *Science (New York, N.Y.)* **2012**, *336*, 717-721, doi:10.1126/science.1215157.

38. Yano, F.; Hojo, H.; Ohba, S.; Fukai, A.; Hosaka, Y.; Ikeda, T.; Saito, T.; Hirata, M.; Chikuda, H.; Takato, T., et al. A novel disease-modifying osteoarthritis drug candidate targeting Runx1. *Annals of the rheumatic diseases* **2013**, *72*, 748-753, doi:10.1136/annrheumdis-2012-201745.

39. Cai, G.; Liu, W.; He, Y.; Huang, J.; Duan, L.; Xiong, J.; Liu, L.; Wang, D. Recent advances in kartogenin for cartilage regeneration. *J Drug Target* **2019**, *27*, 28-32, doi:10.1080/1061186x.2018.1464011.

40. Zhu, F.; Ma, X.H.; Qin, C.; Tao, L.; Liu, X.; Shi, Z.; Zhang, C.L.; Tan, C.Y.; Chen, Y.Z.; Jiang, Y.Y. Drug discovery prospect from untapped species: indications from approved natural product drugs. *PLoS One* **2012**, *7*, e39782, doi:10.1371/journal.pone.0039782.

41. Newman, D.J.; Cragg, G.M.; Snader, K.M. Natural products as sources of new drugs over the period 1981-2002. *J Nat Prod* **2003**, *66*, 1022-1037, doi:10.1021/np030096l.

42. Mobasheri, A. The future of osteoarthritis therapeutics: emerging biological therapy. *Curr Rheumatol Rep* **2013**, *15*, 385, doi:10.1007/s11926-013-0385-4.

43. Kim, J.H.; Kismali, G.; Gupta, S.C. Natural Products for the Prevention and Treatment of Chronic Inflammatory Diseases: Integrating Traditional Medicine into Modern Chronic Diseases Care. *Evid Based Complement Alternat Med* **2018**, *2018*, 9837863, doi:10.1155/2018/9837863.

44. Shakibaei, M.; Csaki, C.; Nebrich, S.; Mobasheri, A. Resveratrol suppresses interleukin-1beta-induced inflammatory signaling and apoptosis in human articular chondrocytes: potential for use as a novel nutraceutical for the treatment of osteoarthritis. *Biochem Pharmacol* **2008**, *76*, 1426-1439, doi:10.1016/j.bcp.2008.05.029.

45. Csaki, C.; Mobasheri, A.; Shakibaei, M. Synergistic chondroprotective effects of curcumin and resveratrol in human articular chondrocytes: inhibition of IL-1beta-induced NF-kappaB-mediated inflammation and apoptosis. *Arthritis research & therapy* **2009**, *11*, R165, doi:10.1186/ar2850.

46. Moussaieff, A.; Shohami, E.; Kashman, Y.; Fride, E.; Schmitz, M.L.; Renner, F.; Fiebich, B.L.; Munoz, E.; Ben-Neriah, Y.; Mechoulam, R. Incensole acetate, a novel anti-inflammatory compound isolated from Boswellia resin, inhibits nuclear factor-kappa B activation. *Mol Pharmacol* **2007**, *72*, 1657-1664, doi:10.1124/mol.107.038810.

47. Chen, Y.J.; Tsai, K.S.; Chan, D.C.; Lan, K.C.; Chen, C.F.; Yang, R.S.; Liu, S.H. Honokiol, a low molecular weight natural product, prevents inflammatory response and cartilage matrix degradation in human osteoarthritis chondrocytes. *Journal of orthopaedic research : official publication of the Orthopaedic Research Society* **2014**, *32*, 573-580, doi:10.1002/jor.22577.

48. Wang, Z.; Huang, J.; Zhou, S.; Luo, F.; Xu, W.; Wang, Q.; Tan, Q.; Chen, L.; Wang, J.; Chen, H., et al. Anemonin attenuates osteoarthritis progression through inhibiting the activation of IL-1beta/NF-kappaB pathway. *Journal of cellular and molecular medicine* **2017**, *21*, 3231-3243, doi:10.1111/jcmm.13227.

49. Yu, S.M.; Cho, H.; Kim, G.H.; Chung, K.W.; Seo, S.Y.; Kim, S.J. Berberine induces dedifferentiation by actin cytoskeleton reorganization via phosphoinositide 3-kinase/Akt and p38 kinase pathways in rabbit articular chondrocytes. *Exp Biol Med (Maywood)* **2016**, *241*, 800-807, doi:10.1177/1535370216631028.

50. Chen, Y.; Shou, K.; Gong, C.; Yang, H.; Yang, Y.; Bao, T. Anti-Inflammatory Effect of Geniposide on Osteoarthritis by Suppressing the Activation of p38 MAPK Signaling Pathway. *BioMed research international* **2018**, *2018*, 8384576, doi:10.1155/2018/8384576.

51. Li, C.; Li, Q.; Mei, Q.; Lu, T. Pharmacological effects and pharmacokinetic properties of icariin, the major bioactive component in Herba Epimedii. *Life Sci* **2015**, *126*, 57-68, doi:10.1016/j.lfs.2015.01.006.

52. Li, D.; Yuan, T.; Zhang, X.; Xiao, Y.; Wang, R.; Fan, Y.; Zhang, X. Icariin: a potential promoting compound for cartilage tissue engineering. *Osteoarthritis and cartilage* **2012**, *20*, 1647-1656, doi:10.1016/j.joca.2012.08.009.

53. Zhu, H.M.; Qin, L.; Garnero, P.; Genant, H.K.; Zhang, G.; Dai, K.; Yao, X.; Gu, G.; Hao, Y.; Li, Z., et al. The first multicenter and randomized clinical trial of herbal Fufang for treatment of postmenopausal osteoporosis. *Osteoporos Int* **2012**, *23*, 1317-1327, doi:10.1007/s00198-011-1577-2.

54. Li, Z.R.; Cheng, L.M.; Wang, K.Z.; Yang, N.P.; Yang, S.H.; He, W.; Wang, Y.S.; Wang, Z.M.; Yang, P.; Liu, X.Z., et al. Herbal Fufang Xian Ling Gu Bao prevents corticosteroid-induced osteonecrosis of the femoral head-A first multicentre, randomised, double-blind, placebo-controlled clinical trial. *J Orthop Translat* **2018**, *12*, 36-44, doi:10.1016/j.jot.2017.11.001.

55. Wang, F.; Shi, L.; Zhang, Y.; Wang, K.; Pei, F.; Zhu, H.; Shi, Z.; Tao, T.; Li, Z.; Zeng, P., et al. A Traditional Herbal Formula Xianlinggubao for Pain Control and Function Improvement in Patients with Knee and Hand Osteoarthritis: A Multicenter, Randomized, Open-Label, Controlled Trial. *Evid Based Complement Alternat Med* **2018**, *2018*, 1827528, doi:10.1155/2018/1827528.

56. Yao, Z.H.; Qin, Z.F.; Cheng, H.; Wu, X.M.; Dai, Y.; Wang, X.L.; Qin, L.; Ye, W.C.; Yao, X.S. Simultaneous Quantification of Multiple Representative Components in the Xian-Ling-Gu-Bao Capsule by Ultra-Performance Liquid Chromatography Coupled with Quadrupole Time-of-Flight Tandem Mass Spectrometry. *Molecules* **2017**, *22*, doi:10.3390/molecules22060927.

57. Ziadlou, R.; Barbero, A.; Stoddart, M.J.; Wirth, M.; Li, Z.; Martin, I.; Wang, X.L.; Qin, L.; Alini, M.; Grad, S. Regulation of Inflammatory Response in Human Osteoarthritic Chondrocytes by Novel Herbal Small Molecules. *Int J Mol Sci* **2019**, *20*, doi:10.3390/ijms20225745.

58. Sebastian Müller, L.A., Xiaomei Wang, M. Zia Karim, Ajay Matta, Arne Mehrkens,; Stefan Schaeren, S.F., Marcel Jakob, Ivan Martin, Andrea Barbero, W. Mark Erwin. Notochordal cell conditioned medium (NCCM) regenerates end-stage human osteoarthritic articular chondrocytes and promotes a healthy phenotype. *Arthritis research & therapy* **2016**, *18*.

59. Livak, K.J.; Schmittgen, T.D. Analysis of relative gene expression data using real-time quantitative PCR and the 2(-Delta Delta C(T)) Method. *Methods* **2001**, *25*, 402-408, doi:10.1006/meth.2001.1262.

60. Schneider, C.A.; Rasband, W.S.; Eliceiri, K.W. NIH Image to ImageJ: 25 years of image analysis. *Nature methods* **2012**, *9*, 671-675, doi:10.1038/nmeth.2089.

61. Yamamoto, Y.; Gaynor, R.B. Therapeutic potential of inhibition of the NF-kappaB pathway in the treatment of inflammation and cancer. *The Journal of clinical investigation* **2001**, *107*, 135-142, doi:10.1172/jci11914.

62. Roman-Blas, J.A.; Jimenez, S.A. NF-κB as a potential therapeutic target in osteoarthritis and rheumatoid arthritis. *Osteoarthritis and cartilage* **2006**, *14*, 839-848, doi:https://doi.org/10.1016/j.joca.2006.04.008.

63. Zhou, Y.; Ming, J.; Deng, M.; Li, Y.; Li, B.; Li, J.; Ma, Y.; Chen, Z.; Liu, S. Berberine-mediated up-regulation of surfactant protein D facilitates cartilage repair by modulating immune responses via the inhibition of TLR4/NF-kB signaling. *Pharmacol Res* **2020**, *155*, 104690, doi:10.1016/j.phrs.2020.104690.

64. Zhang, Y.; Zeng, Y. Curcumin reduces inflammation in knee osteoarthritis rats through blocking TLR4 /MyD88/NF-kappaB signal pathway. *Drug Dev Res* **2019**, *80*, 353-359, doi:10.1002/ddr.21509.

65. Lou, Y.; Wang, C.; Tang, Q.; Zheng, W.; Feng, Z.; Yu, X.; Guo, X.; Wang, J. Paeonol Inhibits IL-1beta-Induced Inflammation via PI3K/Akt/NF-kappaB Pathways: In Vivo and Vitro Studies. *Inflammation* **2017**, *40*, 1698-1706, doi:10.1007/s10753-017-0611-8.

66. Xie, L.; Xie, H.; Chen, C.; Tao, Z.; Zhang, C.; Cai, L. Inhibiting the PI3K/AKT/NF-kappaB signal pathway with nobiletin for attenuating the development of osteoarthritis: in vitro and in vivo studies. *Food Funct* **2019**, *10*, 2161-2175, doi:10.1039/c8fo01786g.

67. Jiang, Y.; Sang, W.; Wang, C.; Lu, H.; Zhang, T.; Wang, Z.; Liu, Y.; Xue, B.; Xue, S.; Cai, Z., et al. Oxymatrine exerts protective effects on osteoarthritis via modulating chondrocyte homoeostasis and suppressing osteoclastogenesis. *Journal of cellular and molecular medicine* **2018**, 10.1111/jcmm.13674, doi:10.1111/jcmm.13674.

68. Ying, X.; Chen, X.; Cheng, S.; Shen, Y.; Peng, L.; Xu, H.Z. Piperine inhibits IL-beta induced expression of inflammatory mediators in human osteoarthritis chondrocyte. *Int Immunopharmacol* **2013**, *17*, 293-299, doi:10.1016/j.intimp.2013.06.025.

69. Luo, Z.; Hu, Z.; Bian, Y.; Su, W.; Li, X.; Li, S.; Wu, J.; Shi, L.; Song, Y.; Zheng, G., et al. Scutellarin Attenuates the IL-1beta-Induced Inflammation in Mouse Chondrocytes and Prevents Osteoarthritic Progression. *Front Pharmacol* **2020**, *11*, 107, doi:10.3389/fphar.2020.00107.

70. Huang, X.; Xi, Y.; Mao, Z.; Chu, X.; Zhang, R.; Ma, X.; Ni, B.; Cheng, H.; You, H. Vanillic acid attenuates cartilage degeneration by regulating the MAPK and PI3K/AKT/NF-κB pathways. *European Journal of Pharmacology* **2019**, *859*, 172481, doi:https://doi.org/10.1016/j.ejphar.2019.172481.

71. Kim, M.C.; Kim, S.J.; Kim, D.S.; Jeon, Y.D.; Park, S.J.; Lee, H.S.; Um, J.Y.; Hong, S.H. Vanillic acid inhibits inflammatory mediators by suppressing NF-kappaB in lipopolysaccharide-stimulated mouse peritoneal macrophages. *Immunopharmacol Immunotoxicol* **2011**, *33*, 525-532, doi:10.3109/08923973.2010.547500.

72. Yin, M.J.; Yamamoto, Y.; Gaynor, R.B. The anti-inflammatory agents aspirin and salicylate inhibit the activity of I(kappa)B kinase-beta. *Nature* **1998**, *396*, 77-80, doi:10.1038/23948.

73. Kokkola, R.; Li, J.; Sundberg, E.; Aveberger, A.C.; Palmblad, K.; Yang, H.; Tracey, K.J.; Andersson, U.; Harris, H.E. Successful treatment of collagen-induced arthritis in mice and rats by targeting extracellular high mobility group box chromosomal protein 1 activity. *Arthritis and rheumatism* **2003**, *48*, 2052-2058, doi:10.1002/art.11161.

74. Taniguchi, N.; Kawahara, K.; Yone, K.; Hashiguchi, T.; Yamakuchi, M.; Goto, M.; Inoue, K.; Yamada, S.; Ijiri, K.; Matsunaga, S., et al. High mobility group box chromosomal protein 1 plays a role in the pathogenesis of rheumatoid arthritis as a novel cytokine. *Arthritis and rheumatism* **2003**, *48*, 971-981, doi:10.1002/art.10859.

75. Kokkola, R.; Sundberg, E.; Ulfgren, A.K.; Palmblad, K.; Li, J.; Wang, H.; Ulloa, L.; Yang, H.; Yan, X.J.; Furie, R., et al. High mobility group box chromosomal protein 1: a novel proinflammatory mediator in synovitis. *Arthritis and rheumatism* **2002**, *46*, 2598-2603, doi:10.1002/art.10540.

76. Andersson, U.; Erlandsson-Harris, H. HMGB1 is a potent trigger of arthritis. *J Intern Med* **2004**, *255*, 344-350, doi:10.1111/j.1365-2796.2003.01303.x.

77. Manning, G.; Whyte, D.B.; Martinez, R.; Hunter, T.; Sudarsanam, S. The protein kinase complement of the human genome. *Science (New York, N.Y.)* **2002**, *298*, 1912-1934, doi:10.1126/science.1075762.

78. Karaman, M.W.; Herrgard, S.; Treiber, D.K.; Gallant, P.; Atteridge, C.E.; Campbell, B.T.; Chan, K.W.; Ciceri, P.; Davis, M.I.; Edeen, P.T., et al. A quantitative analysis of kinase inhibitor selectivity. *Nat Biotechnol* **2008**, *26*, 127-132, doi:10.1038/nbt1358.

79. Greene, M.A.; Loeser, R.F. Function of the chondrocyte PI-3 kinase-Akt signaling pathway is stimulus dependent. *Osteoarthritis and cartilage* **2015**, *23*, 949-956, doi:10.1016/j.joca.2015.01.014.

80. Vlahos, C.J.; Matter, W.F.; Hui, K.Y.; Brown, R.F. A specific inhibitor of phosphatidylinositol 3-kinase, 2-(4-morpholinyl)-8-phenyl-4H-1-benzopyran-4-one (LY294002). *The Journal of biological chemistry* **1994**, *269*, 5241-5248.

81. Kong, D.; Yamori, T. ZSTK474 is an ATP-competitive inhibitor of class I phosphatidylinositol 3 kinase isoforms. *Cancer Sci* **2007**, *98*, 1638-1642, doi:10.1111/j.1349-7006.2007.00580.x.

82. Ghoreschi, K.; Laurence, A.; O'Shea, J.J. Selectivity and therapeutic inhibition of kinases: to be or not to be? *Nat Immunol* **2009**, *10*, 356-360, doi:10.1038/ni.1701.

83. Rokosz, L.L.; Beasley, J.R.; Carroll, C.D.; Lin, T.; Zhao, J.; Appell, K.C.; Webb, M.L. Kinase inhibitors as drugs for chronic inflammatory and immunological diseases: progress and challenges. *Expert Opin Ther Targets* **2008**, *12*, 883-903, doi:10.1517/14728222.12.7.883.

84. Barouch-Bentov, R.; Sauer, K. Mechanisms of drug resistance in kinases. *Expert Opin Investig Drugs* **2011**, *20*, 153-208, doi:10.1517/13543784.2011.546344.

85. O'Neill, L.A.; Bowie, A.G. The family of five: TIR-domain-containing adaptors in Toll-like receptor signalling. *Nat Rev Immunol* **2007**, *7*, 353-364, doi:10.1038/nri2079.

86. Barreto, G.; Sandelin, J.; Salem, A.; Nordstrom, D.C.; Waris, E. Toll-like receptors and their soluble forms differ in the knee and thumb basal osteoarthritic joints. *Acta Orthop* **2017**, *88*, 326-333, doi:10.1080/17453674.2017.1281058.

87. Carmody, R.J.; Chen, Y.H. Nuclear factor-kappaB: activation and regulation during toll-like receptor signaling. *Cell Mol Immunol* **2007**, *4*, 31-41.

88. Oshiumi, H.; Matsumoto, M.; Funami, K.; Akazawa, T.; Seya, T. TICAM-1, an adaptor molecule that participates in Toll-like receptor 3-mediated interferon-beta induction. *Nat Immunol* **2003**, *4*, 161-167, doi:10.1038/ni886.

89. Yamamoto, M.; Sato, S.; Mori, K.; Hoshino, K.; Takeuchi, O.; Takeda, K.; Akira, S. Cutting edge: a novel Toll/IL-1 receptor domain-containing adapter that preferentially activates the IFN-beta promoter in the Toll-like receptor signaling. *J Immunol* **2002**, *169*, 6668-6672, doi:10.4049/jimmunol.169.12.6668.

90. Loiarro, M.; Ruggiero, V.; Sette, C. Targeting TLR/IL-1R signalling in human diseases. *Mediators of inflammation* **2010**, *2010*, 674363, doi:10.1155/2010/674363.

91. Fitzgerald, K.A.; Palsson-McDermott, E.M.; Bowie, A.G.; Jefferies, C.A.; Mansell, A.S.; Brady, G.; Brint, E.; Dunne, A.; Gray, P.; Harte, M.T., et al. Mal (MyD88-adapter-like) is required for Toll-like receptor-4 signal transduction. *Nature* **2001**, *413*, 78-83, doi:10.1038/35092578.

92. Bonelli, M.; Dalwigk, K.; Platzer, A.; Olmos Calvo, I.; Hayer, S.; Niederreiter, B.; Holinka, J.; Sevelda, F.; Pap, T.; Steiner, G., et al. IRF1 is critical for the TNF-driven interferon response in rheumatoid fibroblast-like synoviocytes. *Experimental & Molecular Medicine* **2019**, *51*, 75, doi:10.1038/s12276-019-0267-6.

93. Shih, V.F.; Tsui, R.; Caldwell, A.; Hoffmann, A. A single NFkappaB system for both canonical and non-canonical signaling. *Cell Res* **2011**, *21*, 86-102, doi:10.1038/cr.2010.161.

94. Wyatt, L.A.; Nwosu, L.N.; Wilson, D.; Hill, R.; Spendlove, I.; Bennett, A.J.; Scammell, B.E.; Walsh, D.A. Molecular expression patterns in the synovium and their association with advanced symptomatic knee osteoarthritis. *Osteoarthritis and cartilage* **2019**, *27*, 667-675, doi:10.1016/j.joca.2018.12.012.

95. Aveleira, C.; Castilho, Á.; Baptista, F.; Simões, N.; Fernandes, C.; Leal, E.; Ambrósio, A.F. High glucose and interleukin-1β downregulate interleukin-1 type I receptor (IL-1RI) in retinal endothelial cells by enhancing its degradation by a lysosome-dependent mechanism. *Cytokine* **2010**, *49*, 279-286, doi:https://doi.org/10.1016/j.cyto.2009.11.014.

96. Chevalier, X.; Goupille, P.; Beaulieu, A.D.; Burch, F.X.; Bensen, W.G.; Conrozier, T.; Loeuille, D.; Kivitz, A.J.; Silver, D.; Appleton, B.E. Intraarticular injection of anakinra in osteoarthritis of the knee: a multicenter, randomized, double-blind, placebo-controlled study. *Arthritis and rheumatism* **2009**, *61*, 344-352, doi:10.1002/art.24096.

97. Sellam, J.; Berenbaum, F. The role of synovitis in pathophysiology and clinical symptoms of osteoarthritis. *Nature reviews. Rheumatology* **2010**, *6*, 625-635, doi:10.1038/nrrheum.2010.159.

98. Syddall, C.M.; Reynard, L.N.; Young, D.A.; Loughlin, J. The Identification of Trans-acting Factors That Regulate the Expression of GDF5 via the Osteoarthritis Susceptibility SNP rs143383. *PLOS Genetics* **2013**, *9*, e1003557, doi:10.1371/journal.pgen.1003557.

99. Hedbom, E.; Antonsson, P.; Hjerpe, A.; Aeschlimann, D.; Paulsson, M.; Rosa-Pimentel, E.; Sommarin, Y.; Wendel, M.; Oldberg, A.; Heinegard, D. Cartilage matrix proteins. An acidic oligomeric protein (COMP) detected only in cartilage. *The Journal of biological chemistry* **1992**, *267*, 6132-6136.

100. Xing, X.; Li, Z.; Yu, Z.; Cheng, G.; Li, D.; Li, Z. Effects of connective tissue growth factor (CTGF/CCN2) on condylar chondrocyte proliferation, migration, maturation, differentiation and signalling pathway. *Biochem Biophys Res Commun* **2018**, *495*, 1447-1453, doi:10.1016/j.bbrc.2017.11.190.

101. Fujisawa, T.; Hattori, T.; Ono, M.; Uehara, J.; Kubota, S.; Kuboki, T.; Takigawa, M. CCN family 2/connective tissue growth factor (CCN2/CTGF) stimulates proliferation and differentiation of auricular chondrocytes. *Osteoarthritis and cartilage* **2008**, *16*, 787-795, doi:10.1016/j.joca.2007.11.001.

102. Wang, L.; Li, Y.; Guo, Y.; Ma, R.; Fu, M.; Niu, J.; Gao, S.; Zhang, D. Herba Epimedii: An Ancient Chinese Herbal Medicine in the Prevention and Treatment of Osteoporosis. *Curr Pharm Des* **2016**, *22*, 328-349, doi:10.2174/1381612822666151112145907.

103. Li, X.-F.; Xu, H.; Zhao, Y.-J.; Tang, D.-Z.; Xu, G.-H.; Holz, J.; Wang, J.; Cheng, S.-D.; Shi, Q.; Wang, Y.-J. Icariin augments bone formation and reverses the phenotypes of osteoprotegerin-deficient mice through the activation of Wnt/β-catenin-BMP signaling. *Evidence-Based Complementary and Alternative Medicine* **2013**, *2013*.

104. Shou, D.; Zhang, Y.; Shen, L.; Zheng, R.; Huang, X.; Mao, Z.; Yu, Z.; Wang, N.; Zhu, Y. Flavonoids of Herba Epimedii Enhances Bone Repair in a Rabbit Model of Chronic Osteomyelitis During Post-infection Treatment and Stimulates Osteoblast Proliferation in Vitro. *Phytother Res* **2017**, *31*, 330-339, doi:10.1002/ptr.5755.

105. Huang, X.; Wang, X.; Zhang, Y.; Shen, L.; Wang, N.; Xiong, X.; Zhang, L.; Cai, X.; Shou, D. Absorption and utilisation of epimedin C and icariin from Epimedii herba, and the regulatory mechanism via the BMP2/ Runx2 signalling pathway. *Biomedicine & Pharmacotherapy* **2019**, *118*, 109345, doi:https://doi.org/10.1016/j.biopha.2019.109345.

106. Wang, P.; Zhang, F.; He, Q.; Wang, J.; Shiu, H.T.; Shu, Y.; Tsang, W.P.; Liang, S.; Zhao, K.; Wan, C. Flavonoid Compound Icariin Activates Hypoxia Inducible Factor-1alpha in Chondrocytes and Promotes Articular Cartilage Repair. *PLoS One* **2016**, *11*, e0148372, doi:10.1371/journal.pone.0148372.

107. Sun, P.; Liu, Y.; Deng, X.; Yu, C.; Dai, N.; Yuan, X.; Chen, L.; Yu, S.; Si, W.; Wang, X., et al. An inhibitor of cathepsin K, icariin suppresses cartilage and bone degradation in mice of collagen-induced arthritis. *Phytomedicine* **2013**, *20*, 975-979, doi:10.1016/j.phymed.2013.04.019.

108. Liu, M.H.; Sun, J.S.; Tsai, S.W.; Sheu, S.Y.; Chen, M.H. Icariin protects murine chondrocytes from lipopolysaccharide-induced inflammatory responses and extracellular matrix degradation. *Nutr Res* **2010**, *30*, 57-65, doi:10.1016/j.nutres.2009.10.020.

109. Chen, J.; Long, F. mTOR signaling in skeletal development and disease. *Bone research* **2018**, *6*, 1, doi:10.1038/s41413-017-0004-5.

110. Rosa, S.C.; Rufino, A.T.; Judas, F.; Tenreiro, C.; Lopes, M.C.; Mendes, A.F. Expression and function of the insulin receptor in normal and osteoarthritic human chondrocytes: modulation of anabolic gene expression, glucose transport and GLUT-1 content by insulin. *Osteoarthritis and cartilage* **2011**, *19*, 719-727, doi:10.1016/j.joca.2011.02.004.

111. Yang, Y.; Wang, Y.; Zhao, M.; Jia, H.; Li, B.; Xing, D. Tormentic acid inhibits IL-1β-induced chondrocyte apoptosis by activating the PI3K/Akt signaling pathway. *Molecular medicine reports* **2018**, *17*, 4753-4758, doi:10.3892/mmr.2018.8425.

112. Zhao, H.; Zhang, T.; Xia, C.; Shi, L.; Wang, S.; Zheng, X.; Hu, T.; Zhang, B. Berberine ameliorates cartilage degeneration in interleukin-1β-stimulated rat chondrocytes and in a rat model of osteoarthritis via Akt signalling. *Journal of cellular and molecular medicine* **2014**, *18*, 283-292, doi:10.1111/jcmm.12186.

113. Iwasa, K.; Hayashi, S.; Fujishiro, T.; Kanzaki, N.; Hashimoto, S.; Sakata, S.; Chinzei, N.; Nishiyama, T.; Kuroda, R.; Kurosaka, M. PTEN regulates matrix synthesis in adult human chondrocytes under oxidative stress. *Journal of orthopaedic research : official publication of the Orthopaedic Research Society* **2014**, *32*, 231-237, doi:10.1002/jor.22506.

114. Lee, C.J.; Wu, Y.T.; Hsueh, T.Y.; Lin, L.C.; Tsai, T.H. Pharmacokinetics and oral bioavailability of epimedin C after oral administration of epimedin C and Herba Epimedii extract in rats. *Biomed Chromatogr* **2014**, *28*, 630-636, doi:10.1002/bmc.3081.

115. Jakob, M.; Demarteau, O.; Schafer, D.; Hintermann, B.; Dick, W.; Heberer, M.; Martin, I. Specific growth factors during the expansion and redifferentiation of adult human articular chondrocytes enhance chondrogenesis and cartilaginous tissue formation in vitro. *J Cell Biochem* **2001**, *81*, 368-377, doi:10.1002/1097-4644(20010501)81:2<368::aid-jcb1051>3.0.co;2-j.

Chapter 4

Optimization of hyaluronic acid-tyramine/silk-fibroin composite hydrogels for cartilage tissue engineering and delivery of anti-inflammatory and anabolic drugs

Reihane Ziadlou[1,2], Stijn Rotman[1], Andreas Teuschl[4], Elias Salzer[4], Andrea Barbero[2], Ivan Martin[2,3], Mauro Alini[1], David Eglin[1] and Sibylle Grad[1,5]

[1] AO Research Institute Davos, Davos Platz, 7270, Switzerland

[2] Department of Biomedical Engineering, University of Basel, Allschwil, 4123, Switzerland

[3] Department of Biomedicine, University Hospital Basel, University of Basel, Basel, 4001, Switzerland

[4] Department of Biochemical Engineering, University of Applied Sciences Technikum Wien, 1200 Vienna, Austria

[5] Department of Health Sciences and Technology, ETH Zürich, Zürich, 8092, Switzerland

Published in *Materials Science and Engineering. C* **2021** *Jan;120:111701.*

Abstract

Injury of articular cartilage leads to an imbalance in tissue homeostasis and due to the poor self-healing capacity of cartilage the affected tissue often exhibits osteoarthritic changes. In recent years, injectable and highly tunable composite hydrogels for cartilage tissue engineering and drug delivery have been introduced as a desirable alternative to invasive treatments. In this study, we aimed to formulate injectable hydrogels for drug delivery and cartilage tissue engineering by combining different concentrations of Hyaluronic Acid-Tyramine (HA-Tyr) with regenerated silk-fibroin (SF) solutions. Upon enzymatic crosslinking, the gelation and mechanical properties were characterized over time. To evaluate the effect of the hydrogel's compositions and properties on extracellular matrix (ECM) deposition, bovine chondrocytes were embedded in enzymatically crosslinked HA-Tyr/SF composites (in further work abbreviated as HA/SF) or HA-Tyr hydrogels. We demonstrated that all hydrogel formulations were cytocompatible and could promote the expression of cartilage matrix proteins allowing chondrocytes to produce ECM, while the most prominent chondrogenic effects were observed in hydrogels with HA20/SF80 polymeric ratios. Unconfined mechanical testing showed that the compressive modulus for HA20/SF80 chondrocyte-laden constructs was increased almost 10-fold over 28 days of culture in chondrogenic medium which confirmed the superior production of ECM in this hydrogel compared to other hydrogels in this study. Furthermore, in hydrogels loaded with anabolic and anti-inflammatory drugs, HA20/SF80 hydrogel showed the longest and the most sustained release profile over time which is desirable for the long treatment duration typically necessary for osteoarthritic joints. In conclusion, HA20/SF80 hydrogels were successfully established as a suitable injectable biomaterial for cartilage tissue engineering and drug delivery applications.

Keywords: hydrogel, hyaluronic acid-tyramine, silk-fibroin, enzymatic cross-linking, cell encapsulation, tissue engineering, drug delivery, mechanical testing

1. Introduction

Articular cartilage (AC) is a highly structured and hydrated functional tissue with remarkable load-bearing properties that facilitate smooth and painless movement of joints. Chondrocytes in AC are surrounded by a self-produced tissue specific extracellular matrix (ECM) that is mainly composed of collagen type II, aggrecan and other proteoglycans. Because of the avascular nature of cartilage, slow matrix turn-over rate and low cell density, the intrinsic

healing capacity of articular cartilage is minimal [1,2]. Injury of articular cartilage leads to an imbalance in tissue homeostasis which is associated with a high risk of progressing towards osteoarthritis (OA). OA, or degenerative joint disease, is the major cause of disability in the elderly population [3-5]. Conventional treatment approaches for cartilage repair including autologous chondrocyte implantation (ACI), microfracture treatments, total joint arthroplasty and allografts, all have several short and long term limitations [6-9]. A different approach for prevention or treatment of OA could involve locally injectable hydrogels that can be utilized in two distinct strategies. First, hydrogels can be used for local delivery of drugs with anti-catabolic and anabolic effects in order to create a beneficial environment for cartilage regeneration. Secondly, hydrogels can serve as scaffold material for cartilage tissue engineering (TE) approaches in which chondrocytes are being embedded within the hydrogel and then injected at the site of damage. Hydrogels are materials of high-water content, similar to articular cartilage ECM and are widely used for cartilage TE and drug delivery purposes [10-12]. Due to the hydrophilic nature of hydrogels, they are permeable for oxygen and nutrients which are necessary factors for cell proliferation and phenotypic behaviour in 3D microenvironments [13].

Several hydrogels from natural polymers such as, hyaluronic acid (HA), agarose, alginate and collagen have been used for 3D culture of chondrocytes [14-19]. HA is a major component of articular cartilage ECM and is present in the synovial fluid, interacting biologically and mechanically within the water rich environment. HA has been introduced as a biodegradable, non-immunogenic and non-inflammatory polysaccharide which can promote maintenance of the chondrogenic phenotype and ECM synthesis of embedded cells [20-24]. In order to establish a HA hydrogel, HA polymers need to be functionalized with crosslinking groups. In several studies Tyramine (Tyr) modified HA (HA-Tyr) has been introduced as an enzymatically crosslinked hydrogel for drug delivery and TE applications [25-28]. It is known that cells can bind to, proliferate and spread in HA-Tyr via HA-binding cell-surface proteins which makes it a suitable material for cell encapsulation and TE applications [29,30]. Nevertheless, HA-Tyr based hydrogels are relatively fast degradable in presence of physiological levels of hyaluronidase, depending on Tyr degree of substitution and H_2O_2 concentrations during crosslinking [26,30]. It was shown that with increasing concentrations of H_2O_2 and HRP, stiffer hydrogels which are less degradable could be achieved [30,31]. However, high concentrations of HRP and H_2O_2 will increase cytotoxicity and potentially induce immune responses [32,33].

Also, with encapsulating high numbers of cells in HA-Tyr hydrogels their mechanical properties were significantly decreased (storage modulus <1 kPa) which is not sufficient for maintaining the chondrogenic phenotype and matrix production [31,34-38]. Thus, HA-Tyr hydrogels can benefit from a composite system that improves mechanical properties and reduces the degradation rate.

Silk-fibroin (SF) protein derived from Bombyx mori (B. mori) cocoons can form biocompatible hydrogels with adequate mechanical strength and slow rate of degradation which makes it a suitable biomatrix for long-term cell culture [39-41]. However, due to the slow gelation of SF upon enzymatic crosslinking and lack of cell specific epitopes for cell adhesion, clinical cell-laden applications are impractical [42,43]. In addition, crystallization and self-assembly of the SF polymers leading to significant changes in mechanical properties were reported [44]. A composite hydrogel comprising of HA-Tyr and SF (HA/SF) has the potential to preserve the superior properties of both hydrogels, but also to diminish their previously described weaknesses. Due to the presence of Tyr in HA-Tyr and tyrosine in the heavy chain of SF, enzymatic crosslinking of the composite hydrogels leads to the formation of covalently crosslinked gels with di-tyramine, di-tyrosine and tyramine-tyrosine bonds [45]. Raia et al. showed that the enzymatic crosslinking of composite HA/SF hydrogels can provide a controllable gelation and degradation with a possibility to tune stiffness and viscoelasticity by changing the HA-Tyr concentration and thus the polymeric HA/SF ratio [45], providing a platform for TE and drug delivery applications. It was previously reported that injection of the enzymatically crosslinkable HA-Tyr encapsulated with anti-inflammatory drug (dexamethasone), could successfully reduce inflammation in animal models of arthritis [25,28]. Also, SF has previously been used as an injectable material for sustained drug delivery applications [39]. Therefore, with the clinical application in mind, the injectability and the anti-inflammatory properties credited to HA and SF materials make them advantageous to serve as a delivery system for either cells and/or small molecules for cartilage regeneration [20,46].

In this study, we hypothesize that with combining different concentrations of HA-Tyr with regenerated aqueous SF solutions we could formulate a tunable and injectable hydrogel for cartilage TE and drug delivery purposes. For the first time, chondrocyte embedded in HA/SF composite hydrogels were assessed in terms of cell viability, phenotypic behaviour and ECM production. Upon enzymatic crosslinking with HRP and H_2O_2, the gelation and mechanical

properties were characterized over time. We also showed that HA/SF hydrogel composition affects the release of small hydrophobic anti-inflammatory and anabolic drugs. Our findings highlight the potential of HA/SF hydrogels for applications in cartilage regeneration.

2. Materials and Methods

2.1 HA-Tyr Synthesis

To synthesize HA-Tyr, the carboxyl groups of HA were substituted with Tyr through an amidation procedure, using a previously established protocol [47]. Briefly, sodium hyaluronate from Streptococcus equi (Contipro Biotechs.r.o., Czech Republic) with average molecular weight of 290 kDa was dissolved in deionized H_2O (10 mg/mL). For HA modification a ligation reaction was catalyzed by adding 5 mmol 4-(4,6-dimethoxy-1,3,5-triazin-2-yl)-4-methylmorpholinium chloride (DMTMM) (TCI Europe N.V.) coupling agent and subsequently 5 mmol Tyr (Sigma-Aldrich, St. Louis, MO) was added dropwise to the solution. The reaction occurred at 37 °C under continuous stirring for 24 hours. The HA-Tyr product was precipitated by adding 8% v/v saturated sodium chloride solution and a three-fold volume of 96% ethanol. After several washing steps with aqueous solutions containing increasing ethanol concentrations (up to 100% ethanol), the product was filtered and dried under vacuum for 48 hours. The amidation reaction was repeated to increase the degree of substitution (DS) to a final value of 14% (DSmol in percent). The degree of tyramine hydrochloride substitution of HA-Tyr was determined with proton nuclear magnetic resonance spectroscopy (1H-NMR) and ultraviolet−visible spectroscopy (UV−vis) measurements. HA-Tyr products were stored at room temperature and obscured from light until further use.

2.2 Preparation of Silk-fibroin solution

Using silk cocoons from B. mori silkworm, 8% aqueous silk solutions were prepared by the protocol described elsewhere [41]. Briefly, sericin protein was removed from B. mori silkworm cocoons to prevent potential immunogenic host reactions. To achieve this, cocoons were degummed by placing 5 g of cleaned and cut cocoons in 2 L of a boiling 0.02 M sodium carbonate (Na_2CO_3) solution (Sigma-Aldrich, St. Louis, MO) for 30 min, with manual stirring every 10 minutes. Degummed SF was washed several times in distilled H_2O and dried overnight at room temperature. After weighing the dried degummed SF, 35-40% of the weight was lost which is expected due to the sericin protein removal. The SF was dissolved in 9.3 M LiBr

solution at 60 °C for 4 hours, yielding a 20 w/v% solution. Throughout this process, the solution was stirred every 30 minutes. Subsequently, the solution was dialyzed against demineralized H_2O using a Slide-a-Lyzer dialysis cassette (MWCO 3500; Thermo Fisher Scientific, Inc., Rockford, IL) for 48 hours exchanging the water several times. After centrifugation, the final concentration of SF aqueous solution was determined by weighing airdried samples and adjusted to 8% v/v.

2.3 Preparation of HA/SF hydrogels

HA-Tyr (DS = 14%) was dissolved at a final concentration of 28 mg/mL in ultrapure distilled water overnight at 4 °C under agitation. SF solution (80 mg/mL) and HA-Tyr (28 mg/mL) were mixed with ultrapure water through gentle pipetting to acquire a final SF concentration of 20 mg/mL and final HA concentrations of 1.05, 2.22, and 5 mg/mL. HA-Tyr hydrogels consisted of 5 mg/mL of HA and SF hydrogels comprised 20 mg/mL of SF. The final concentrations of HA-Tyr are listed in Table 1. Crosslinking was initiated at 37 °C by adding 10 U/mL of aqueous horseradish peroxidase (HRP) solution to the solubilized polymer mixtures which was followed by addition of 0.01% H_2O_2 (final molarity of 3.2 mM) (both from Sigma-Aldrich, St. Louis, MO). Henceforth, samples are named according to the ratio of HA-Tyr and SF non-crosslinked hydrogels (also defined as precursor hydrogels) in the final sample as can be seen in Table 1.

Table 1. Sample precursor compositions. Samples are reported by the mass percent of HA-Tyramine (HA-Tyr), while the silk-fibroin (SF) concentration in all samples containing SF is constant (20 mg/mL). All samples were crosslinked at 37 °C with 10 U/mL of HRP, followed by 0.01% H_2O_2 (3.2 mM).

Sample name	Final HA-Tyr concentration (mg/mL)	Final SF concentration (mg/mL)
HA100/SF0	5	0
HA20/SF80	5	20
HA10 /SF90	2.22	20
HA5/SF95	1.05	20
HA0/SF100	0	20

2.4 Rheological measurements and gelation time

Rheological measurements were performed to investigate the viscoelastic properties of the hydrogels, using an Anton Paar MCR-302 rheometer equipped with a Peltier temperature control unit. The experiments were performed at 37 °C on the rheometer using a 25 mm stainless steel upper cone and Peltier bottom plate to perform oscillatory and rotational tests (time sweep and strain sweep). The hydrogel precursors were mixed with HRP as described, loaded onto the plate, and subsequently, after lowering the cone, H_2O_2

was added into the gap. To prevent evaporation during analysis, an oil layer was deployed around the system. The storage modulus (G') and loss modulus (G") of the hydrogels were measured at 1 Hz with a strain of 1%, until a plateau value was reached. After allowing for complete gelation with time sweep test, strain sweeps between 0.1%-500%, at 1 Hz were applied (amplitude sweep). Furthermore, the gelation time was evaluated by vial inversion test. For this respect, the enzymatic crosslinking of the hydrogels was initiated by adding H_2O_2 into the vials while they were kept and monitored at 37 °C. The time at which the solution was gelled and was not flowing after the vial inversion was considered as the gelation time.

2.5 Cell-laden constructs

For preparation of the cell-laden hydrogels, chondrocytes were harvested from articular cartilage of fetlock joints of young calves as previously described [48]. Briefly, after cutting the tissues with a scalpel into small pieces in a sterile environment, they were pre-digested with 0.1% Pronase (Roche, Switzerland) and subsequently digested with 600 U/ml Collagenase II (BioConcept, Switzerland) in Dulbecco's modified Eagle medium (DMEM) by overnight stirring in a spinner flask at 37°C, 5% CO2. The isolated chondrocytes were expanded for one passage to reach 80% confluency in basal medium (BM) containing high glucose DMEM supplemented with 1 mM sodium pyruvate, 10 mM HEPES, 1% penicillin/streptomycin (P/S), 10% fetal bovine serum (FBS) (all from Gibco, UK), 1 ng/mL transforming growth factor (TGF)-ß1 and 5 ng/mL fibroblast growth factor-2 (FGF-2) (both from Fitzgerald) in a humidified incubator (37 °C, 5% CO2). For cell encapsulation, passage 1 harvested chondrocytes were suspended in culture medium and a final concentration of 20 x 10^6 cells/mL was embedded in the non-crosslinked precursor hydrogel formulations mentioned in Table 1. After dispersion of the cells in the precursor hydrogel (as explained in section 2.3), enzymatic crosslinking was initiated by adding 0.01% of H_2O_2 in a humidified incubator (37 °C, 5% CO2). The 3D cell scaffolds were cultured for up to 28 days in standard chondrogenic medium containing BM supplemented with 1.25 mg/mL human serum albumin (Gibco, UK), ITS-Premix (Corning, USA), 0.1 mM ascorbic acid 2-phosphate (Sigma-Aldrich, St. Louis, MO, USA), 1% P/S, 10 ng/mL TGF-β1 and 10^{-7} M dexamethasone (Sigma-Aldrich, USA) or in chondro-permissive medium which is comprised of chondrogenic medium without TGF- β1. The experiments were performed on three replicates of two independent bovine donors.

2.6 Cell viability after encapsulation in the hydrogels

The viability of the hydrogel encapsulated cells was assessed at 24h, 72h and 7 days using a live/dead (L/D) assay, where living cells are stained with calcein-AM (Ca-AM), and dead cells with ethidium homodimer-1 (EthD-1) (both from Sigma-Aldrich, St. Louis, MO). Hydrogel discs (2mm height) were prepared with a biopsy punch of 4 mm in diameter. After three washes with phosphate buffer saline (PBS), the discs were protected from light and incubated in a staining solution containing 10 μM Ca-AM and 1 μM EthD-1 in serum-free high glucose DMEM for 90 minutes in a humidified incubator (37°C, 5% CO2). The hydrogels were imaged with a confocal laser scanning microscope (LSM510, Zeiss) in which both single plane and Z-stack images were acquired. For quantification of the cell viability, three different fields of view were imaged which were counted and quantified with ImageJ/Fiji.

2.7 Mechanical testing

Unconfined compression tests were performed on an Instron 5866 electromechanical test instrument equipped with a 10-N load cell. Cell encapsulated hydrogels were tested after 3, 7, 14, 21 and 28 days of cell culture in chondrogenic medium. The hydrogels (4 mm diameter and ~2 mm height) were placed between stainless steel parallel plates through which after a pre-load, three cycles of load-unload to 20% strain were applied. A strain rate of 0.667% per second was implemented and the compressive modulus and hysteresis were calculated between 5 and 10% strain in the second cycle of load-unload for each sample to ensure there are no measurement artefacts. Subsequently, strain was held constant at 20% and stress relaxation tests were performed for duration of 600 seconds. Using python software, compressive modulus and the percentage of the relaxation were determined in four replicates.

2.8 RNA extraction and gene expression analysis

For total RNA extraction from cell-seeded hydrogels at days 0 (monolayer culture at passage 1), 3, 7 and 21 of chondrogenic culture, 1 mL of TRI reagent (Molecular Research Center) was added to the scaffolds and the constructs were homogenized by a Tissue Lyser (Qiagen, Hilden, Germany) for 5 min at 5 Hz. Subsequently, the RNA was extracted using phase separation by 1-bromo-3-chloropropane (Sigma-Aldrich, St. Louse, MO, USA) in a volume ratio of 1:10 with the TRI reagent. By using a nano-photometer (Nanodrop, Thermo Scientific), the quantity and quality of the RNA samples was measured. Reverse RNA transcription was performed using 1

μg of total RNA sample, random hexamer primers and TaqMan reverse transcription reagents (Applied Biosystems, Carlsbad, CA, United States). Quantitative real-time PCR (qPCR) was carried out using TaqMan Universal Master Mix (Applied biosystems, Foster City, CA, USA) and the Quant Studio 6 Flex Instrument and software (Applied biosystems) were used for detection. The gene expression assays and sequences for bovine ribosomal protein lateral stalk subunit P0 (RPLP0), aggrecan (ACAN), collagen type II alpha 1 chain (COL2A1), collagen type I alpha 2 chains (COL1A2), SRY-Box Transcription Factor 9 (SOX-9), cartilage oligomeric matrix protein (COMP), matrix metalloproteinase 1 (MMP1) and interleukin 6 (IL-6) are shown in Table 2. The relative gene expression was calculated using the 2-ΔΔCT quantification method [49], with RPLP0 as endogenous control. The level of gene expression was normalized relative to the day 0 monolayer culture to quantify the effects of 3D cell culture in HA/SF hydrogels.

Table 2. Oligonucleotide primers and probes and assays (*bovine*) used for Quantitative Real-Time PCR.

Gene	Primer/Probe Type	Sequence
ACAN	Primer forward (5′-3′) Primer reverse (5′-3′) Probe (5′ FAM/3′ TAMRA)	CCA ACG AAA CCT ATG ACG TGT ACT GCA CTC GTT GGC TGC CTC ATG TTG CAT AGA AGA CCT CGC CCT CCA
COL2A1	Primer forward (5′-3′) Primer reverse (5′-3′) Probe (5′ FAM/3′ TAMRA)	AAG AAA CAC ATC TGG TTT GGA GAA A TGTTTGGAGTGGGTTTCAGAAATA CAA CGG TGG CTT CCA CTT CAG CTA TGG
COL1A2	Primer forward (5′-3′) Primer reverse (5′-3′) Probe (5′ FAM/3′ TAMRA)	TGC AGT AAC TTC GTG CCT AGC A CGC GTG GTC CTC TAT CTC CA CAT GCC AAT CCT TAC AAG AGG CAA CTG C
COMP	Primer forward (5′-3′) Primer reverse (5′-3′) Probe (5′ FAM/3′ TAMRA)	CCA GAA GAA CGA CGA CCA GAA TCT GAT CTG AGT TGG GCA CCT T ACG GCG ACC GGA TCC GCA A
MMP1	Primer forward (5′-3′) Primer reverse (5′-3′) Probe (5′ FAM/3′ TAMRA)	TTC AGC TTT CTC AGG ACG ACA TT CGA CTG GCT GAG TGG GAT TT TCC AGG CCA TCT ACG GAC CTT CCC
IL-6	Primer forward (5′-3′) Primer reverse (5′-3′) Probe (5′ FAM/3′ TAMRA)	TTC CAA AAA TGG AGG AAA AGG A TCC AGA AGA CCA GCA GTG GTT TCC AGA AGA CCA GCA GTG GTT
RPLP0	5′ FAM-3′ NFQ	Bt03218086_m1

ACAN: aggrecan; *COL2A1*: collagen type II; *COL2A1*: collagen type I*; COMP:* cartilage oligomeric matrix protein; *MMP1*: matrix metalloproteinase 1; *IL-6*: interleukin 6; FAM: Carboxyfluorescein; TAMRA: Tetramethylrhodamine.

2.9 Histology and immunohistochemistry

Hydrogel discs were prepared with a biopsy punch of 4 mm in diameter at days 1, 14, 21 and 28. The discs were washed with PBS and fixed in 4% formaldehyde overnight at 4 °C. Subsequently, the discs were washed 3 times in PBS and incubated overnight in 5% sucrose solution at 4 °C. Then, the samples were embedded in cryo-compound and were sectioned with a cryostat at 8 µm thickness. To visualize cells, collagen and proteoglycan deposition, Hematoxylin-eosin (HE), nuclear fast red stain, Safranin-O/Fast green and Alcian blue staining were performed. For Safranin-O/Fast green staining, the slides were first incubated with Weigert's Haematoxylin for 10 minutes; then, the sections were stained with 0.02% Fast green in ultrapure (ddH_2O) water for 5 min to reveal collagen deposition. Subsequently, the sections were stained with 0.1% Safranin-O for 12 min, to reveal proteoglycan deposition, followed by sequential differentiation in 70%, 96% and 100% ethanol. For Alcian blue staining, the proteoglycans were stained with Alcian blue in acidic pH for 30 minutes. Afterwards, the slides were counterstained with nuclear fast red stain (Sigma) for nuclear staining.

The presence of collagen type II (COL-II) was identified immunohistochemically using an antibody against COL-II (CIIC1; 2 µg/mL IgG, Developmental Studies Hybridoma Bank, University of Iowa). Briefly, after enzyme treatment with 25 mg/mL hyaluronidase and 0.25 U/mL chondroitinase ABC at 37 °C for 30 minutes (Sigma-Aldrich, St. Louse, MO, USA), non-specific binding sites were blocked with horse serum (Vector Laboratories, Burlingame, CA, USA) for 1h at RT. After incubation with the primary antibody, the protein was detected using secondary biotinylated anti-mouse antibody (Vector Laboratories) followed by incubation with avidin-biotin-peroxidase complex (Vectastain ABC Kit, Mouse IgG, Vector Laboratories). Peroxidase activity was visualized using diaminobenzidine (DAB) as a substrate (ImmPACT DAB, Substrate for Peroxidase, Vector Laboratories).

2.10 Drug encapsulation and release study

HA100/SF0, HA20/SF80 and HA10/SF90 hydrogels were loaded with 1 mM of Vanillic acid (VA) or Epimedin C (Epi C), which both showed anti-catabolic and anabolic effects on human chondrocytes in a previous screening study performed by the authors [50]. The drug loaded constructs were prepared by mixing 1 mM of small molecules with hydrogel precursors as

explained in section 2.3. Enzymatical crosslinking was initiated following addition of 3.2 mM H_2O_2 to 1 mL precursor hydrogel and the gelation was proceeded at 37 °C in a microtube. Then, 500 µL of PBS was added to each hydrogel after gelation for the drug release. In order to quantify the drug release, 10 µL of the aspirated release media was injected into a high-pressure liquid chromatography (HPLC) device (Agilent 1200) with a C18 column. For VA release media the mobile phase consisted of acetonitrile/0.5% acetic acid (12:88 v/v), and for Epi C release media the mobile phase was acetonitrile/water (30:70 v/v). VA was detected by UV absorption at 260 nm and Epi C at 270 nm. The flowrate of the mobile phase was consistent at 1 mL/min. With the described protocol, peaks for VA and Epi C were detected approximately 6 minutes and 5 minutes after sample injection. Standard curves of VA and Epi C in PBS were used to correlate HPLC detection peaks with drug concentration of the release media. After 60 days, the hydrogels were digested in 1 mL of an enzyme cocktail consisting of hyaluronidase (Sigma-Aldrich, St. Louis, MO), and protease (Pronase, Sigma-Aldrich, St. Louis, MO) dissolved at 1 U/mL and 0.001 U/mL in PBS, respectively.

2.11 Statistical analysis

Statistical comparisons were performed using Graphpad Prism 8. One-way analysis of variance (ANOVA) followed by Tukey's post hoc test (multiple comparison) was applied as non-parametric test of two independent experiments with different *bovine* chondrocytes donors. To evaluate statistical significance among the groups, differences were considered statistically significant at $p < 0.05$.

3. Results

3.1 Hydrogel gelation

Different concentrations of HA-Tyr were mixed with SF to characterize gelation and mechanical properties over time. Possible crosslinking sites in the composite hydrogel systems comprise di-tyramine between hyaluronan macromolecules, di-tyrosine between fibroin proteins and tyramine-tyrosine bonds between hyaluronan and fibroin (Fig. 1A). Vial inversion test showed that increasing HA-Tyr concentration at a constant fibroin concentration, decreased the gelation time. The sol-gel transition duration for the pure HA-Tyr hydrogel was the shortest and occurred a few seconds after initiation of enzymatic crosslinking with H_2O_2, as assessed by

vial-inversion test. The slowest sol-gel transition happened for the pure SF hydrogel with a gelation time of approximately 33 minutes. Conversely, by increasing HA-Tyr concentration, the gelation time in composite hydrogels was gradually decreasing, with 13, 6 and 3 minutes for complete gelation of HA5/SF95, HA10/SF90 and HA20/SF80 composite hydrogels, respectively (Fig. 1B).

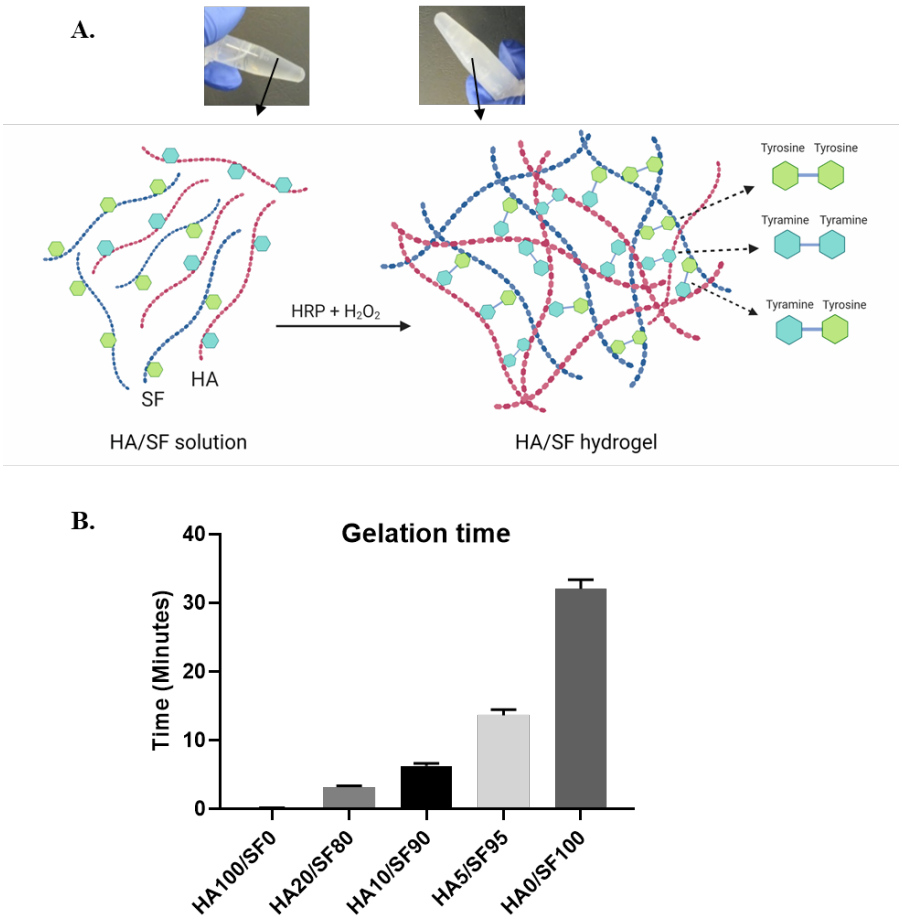

Figure 1. Hydrogel gelation for the HA100/SF0, HA20/SF80, HA10/SF90, HA5/SF95 and HA0/SF100 precursors (n = 3). (A) The schematic illustration representing the potential covalent crosslinking in HA-SF composite hydrogels which can occur between tyramine residues of HA and tyrosine in the silk after enzymatic crosslinking. (B) Timing of transition from sol to gel via vial inversion test showed that with increasing HA concentration, the gelation time for the hydrogels was decreased.

3.2 Rheological measurements

The rheological measurements indicated that the storage modulus and shear mechanical properties of the hydrogels could be tuned based on the HA-Tyr and SF ratio. The time needed for the hydrogels to reach the maximum mechanical stability due to completed gelation was dependent on the hydrogel precursors ratio. The HA100/SF0 hydrogel reached a final storage

modulus in a few minutes, which was much faster than HA/SF composite gels. The higher the HA-Tyr proportion in the hydrogel composition was, the faster the maximum mechanical stability was achieved. For HA0/SF100 and HA5/SF95 the time to reach the completed crosslinking was between 60-75 minutes, while for HA10/SF90 and HA20/SF80 the time for reaching the complete crosslinking was reduced to 50 and 20 minutes, respectively (Fig. 2A). Furthermore, the strain sweep showed that HA0/SF100 and HA5/SF95 composite hydrogels could withstand over 100% strain before mechanical failure. By increasing the HA-Tyr concentration in the composite hydrogels the strain at failure was gradually reduced, but significantly higher compared to HA100/SF0 hydrogels that started to fail at less than 10% strain (Fig. 2B). Furthermore, the storage modulus for HA100/SF0 hydrogel was the lowest, reaching around 0.32 ± 0.003 kPa, and with increasing the HA-Tyr concentration in the composite HA/SF hydrogels, the stiffness increased and reached 3.97 ± 0.02 kPa for HA20/SF80 hydrogels (approx. 10 fold increase) (Fig 2C).

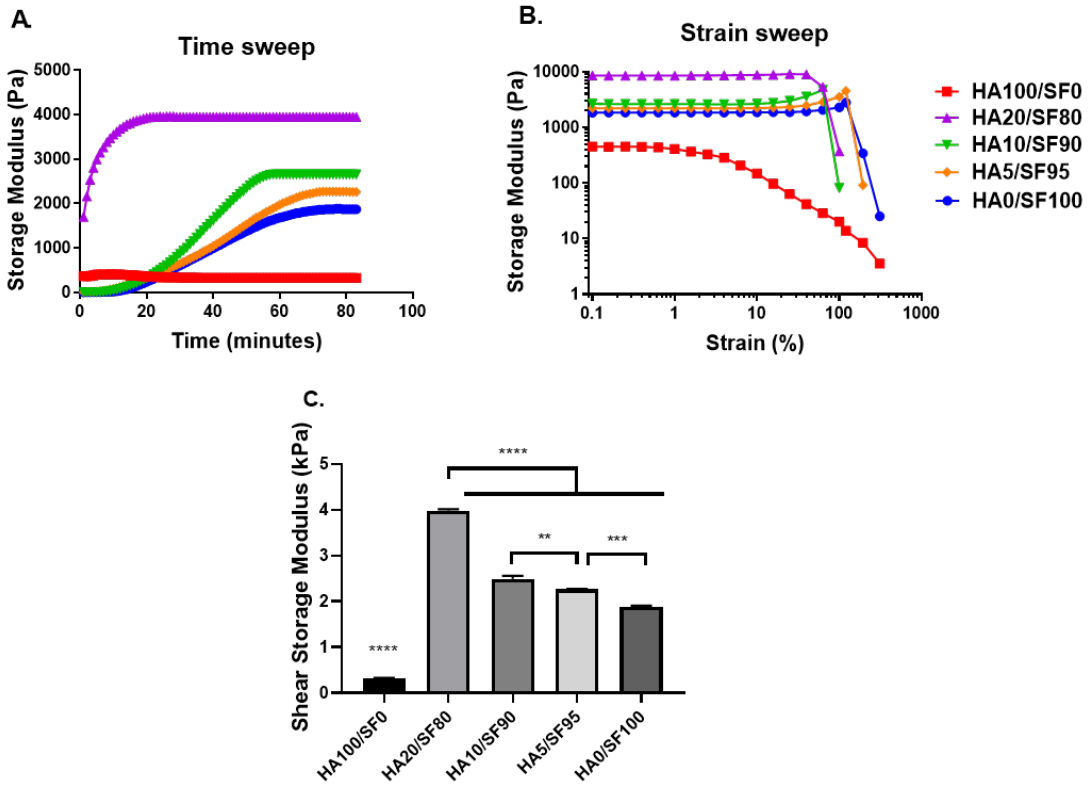

Figure 2. Rheological measurements for the HA100/SF0, HA20/SF80 and HA10/SF90, HA5/SF95 and HA0/SF100 hydrogels. (A) Time sweeps showed that HA100/SF0 hydrogels reached the maximum storage faster than other hydrogels and with decreasing HA concentration, the time to reach the final plateau was increased. (B) Strain sweeps determined that the hydrogels with SF in their formulation, withstood strains above 100%. Increased HA-Tyr concentration gradually lowered strain at failure and HA100/SF0 hydrogels failed at strains above 10%. (C) Final shear storage moduli showed that HA100/SF0 had a lower storage modulus than the hydrogels with SF

in their formulation. HA20/SF80 showed the highest storage modulus of all groups. Values are presented as mean ± SD. For statistical analysis one-way analysis of variance (ANOVA) followed by Tukey's post hoc test (multiple comparisons) was applied. (n = 3) ** $p < 0.001$ *** $p < 0.0005$, **** $p < 0.0001$.

3.3 Chondrocytes viability after encapsulation in hydrogels

To determine the effect of enzymatic crosslinking, hydrogel composition and high density cell encapsulation (20 x 10^6 cells/mL) on cell viability, live-dead assay was performed for the cells encapsulated in HA100/SF0, HA20/SF80 and HA10/SF90 hydrogels, at days 1, 3 and 7. Due to the slow gelation of the HA0/SF100 and HA5/SF95 hydrogels, the cells were sedimented on the bottom of the plate and the crosslinking didn't take place in these hydrogels in presence of the cells. Therefore, these groups were removed from our cell-laden experiments. Furthermore, the effect of culture media composition (chondrogenic or chondro-permissive medium) on cytocompatibility of hydrogels was assessed. We observed are that for the HA20/SF80 cell-laden hydrogels, more than 95% of the chondrocytes cultured in either chondrogenic or chondro-permissive medium were viable at all time points. Therefore, enzymatic crosslinking did not have a negative effect on cell viability. In HA100/SF0 cell-laden hydrogel, the chondrocytes in the chondrogenic medium was slightly decreased from 95% at day 1 to 91% at day 7. Interestingly, for the HA10/SF90 cell-laden hydrogel, the number of viable cells in the chondrogenic medium was increased from 93% at day 1 to 98% at day 7, while in the chondro-permissive medium the viable cells were slightly decreased from 90% at day 1, to 86% at day 7. These results showed the effect of TGF-β1 on the chondrocytes viability in HA10/SF90 hydrogels, while for the HA20/SF80 the percentage of viable cells was not affected by the cell culture media composition and during the culture period (Fig 3. A-D). Also, we observed that in the HA10/SF90 hydrogel, the chondrocytes appeared elongated, resembling fibroblast-like morphology which may indicate onset of chondrocyte de-differentiation; while, HA100/SF0 and HA20/SF80 hydrogels could maintain the rounded chondrogenic morphology of chondrocytes (Fig. 3 E).

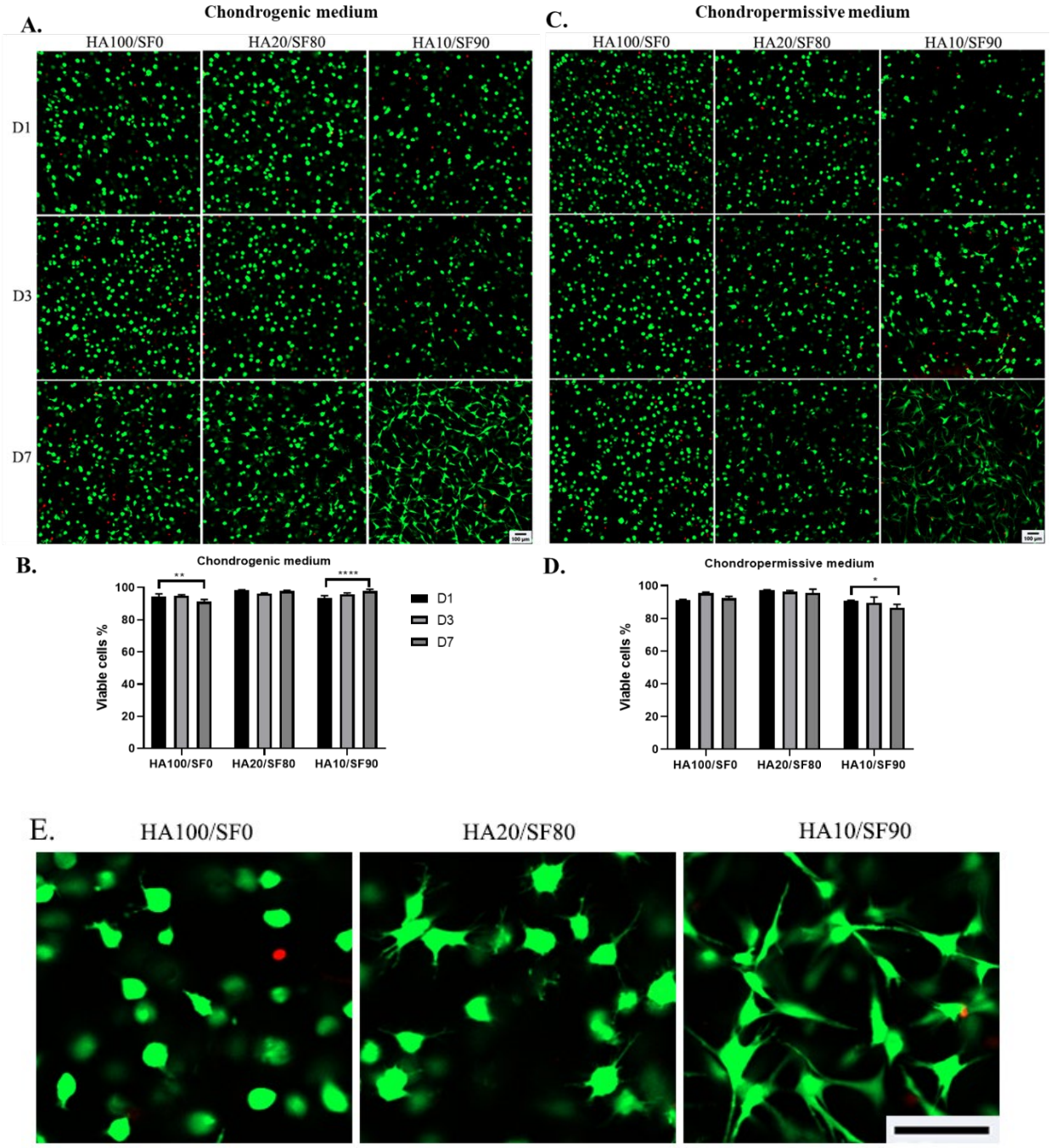

Figure 3. Cell viability for the cell-laden hydrogels (HA100/SF0, HA20/SF80 and HA10/SF90) with live-dead assay at days 1, 3 and 7. (A) Representative confocal images of live/dead stained encapsulated cells within the hydrogels with seeding density of 20 x 10^6 cells/mL cultured in chondrogenic medium. Scale bar: 100 µm. (B) Quantification of the cell viability as the percentage of Ca-AM positive cells at days 1, 3 and 7, cultured in chondrogenic medium. (C) Representative confocal images of live/dead stained encapsulated cells within the hydrogels with seeding density of 20 x 10^6 cells/mL cultured in chondro-permissive medium. Scale bar: 100 µm (D) Quantification of the cell viability as the percentage of total cells at days 1, 3 and 7, cultured in chondro-permissive medium. Values are presented as mean ± SD from 3 replicates of 2 independent donors and 5 images per group. * $p < 0.01$, ** $p < 0.001$, *** $p < 0.0005$. (E) Representative high magnification image showing the morphology of the cells in the hydrogels at day 7 of culture in chondrogenic medium. Scale bar: 100 µm

3.4 Gene expression analysis

To evaluate the effect of the hydrogel's 3D environment and the presence of TGF-β1 on the chondrogenic and pro-inflammatory marker genes, real-time PCR analysis was performed for genes including *COL2A1, COL1A2, ACAN, COMP*, *MMP1* and *IL-6* (Fig. 4). The results showed that for all the cell-laden constructs cultured in chondrogenic medium, the expression of *COL2A1* was up-regulated compared with day 0 control (monolayer culture at passage 1) and *COL2A1* expression in HA20/SF80 hydrogels was significantly increased from day 3 to day 7. Additionally, the expression of *COL1A2* was significantly down-regulated at day 21 and was lower than day 0 control (below 1) in all hydrogels. The expression of *ACAN* and *COMP* showed a peak at day 7 in HA20/SF80 and was higher than day 0 control in all hydrogels at all time points. Furthermore, the expression of the catabolic marker gene *MMP1* in HA10/SF90 and HA20/SF80 was significantly down-regulated at day 21 in comparison with day 3. The expression of the pro-inflammatory marker gene *IL-6* was down-regulated compared with day 0 monolayer culture in all cell-laden hydrogels and showed the lowest levels in HA100/SF0 and HA20/SF80 hydrogels at day 21 (Fig. 4).

For the cell-laden constructs cultured in chondro-permissive medium, the expression of *COL2A1* in HA10/SF90 and HA20/SF80 hydrogels was significantly increased during culture time and reached 10-fold up-regulation at day 21 compared to day 0. While for HA100/SF0 hydrogel the expression of *COL2A1* did not change over culture time and was significantly lower than HA10/SF90 and HA20/SF80 hydrogels at day 21. Also, the expression of *COL1A2* was significantly down-regulated at day 21 compared with day 3 in all hydrogels. The expression of *ACAN* in HA20/SF80 hydrogels at day 3 was the highest between all groups and timepoints and was reduced gradually till day 21. Furthermore, the expression of *COMP* was significantly increased in HA100/SF0 and HA20/SF80 hydrogels at day 21 compared to earlier time points and compared to *COMP* expression in HA10/SF80 hydrogels. The expression of catabolic and pro-inflammatory marker genes *MMP1* and *IL-6*, normalized with day 0 monolayer culture, was down-regulated (below 1) in all cell-laden hydrogels and this down-regulation was progressing until day 21 for all cell-laden hydrogels (Fig. 4).

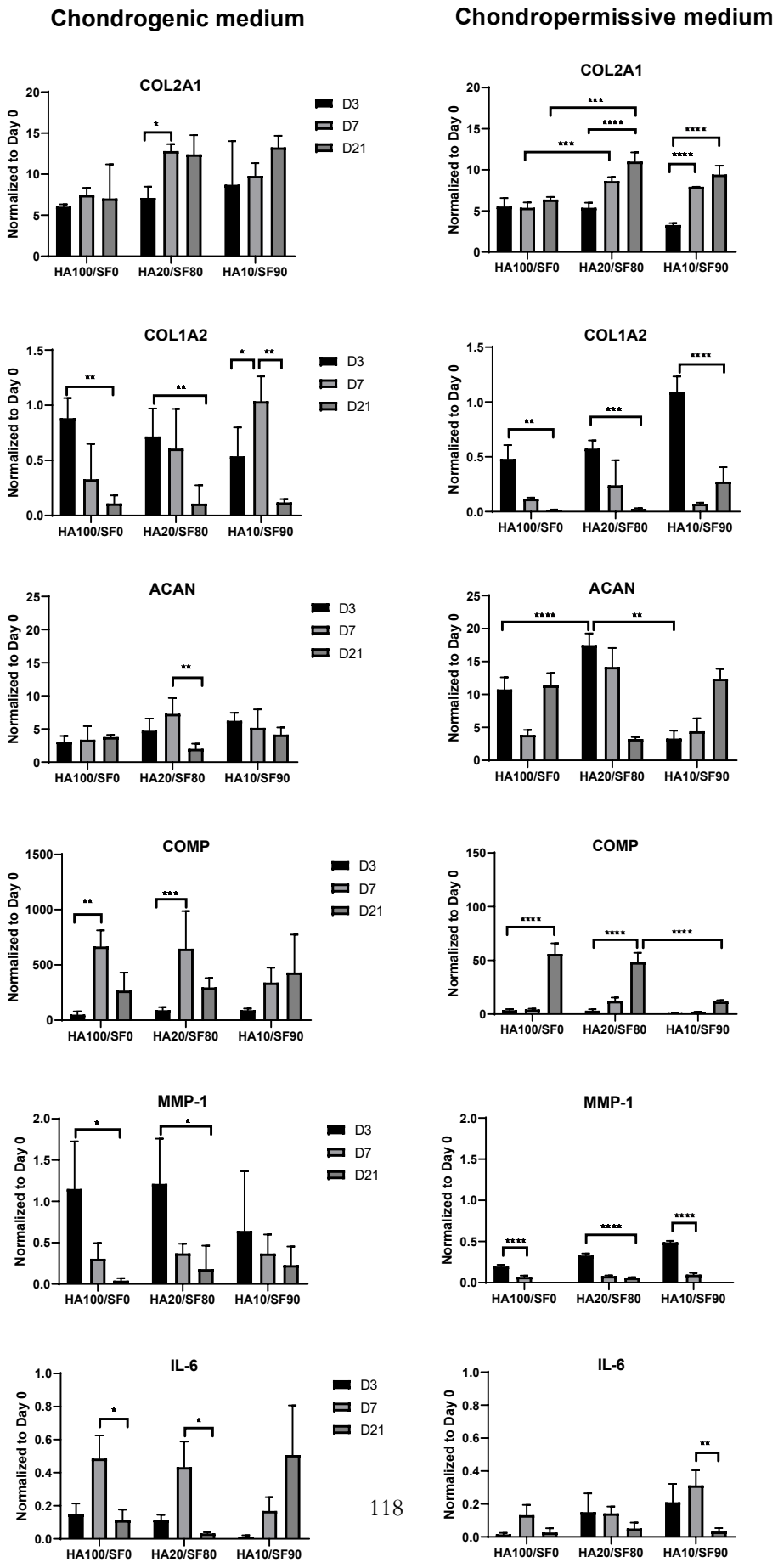
Chondrogenic medium
Chondropermissive medium
COL2A1
COL1A2
ACAN
COMP
MMP-1
IL-6
Normalized to Day 0
D3
D7
D21
HA100/SF0
HA20/SF80
HA10/SF90

Figure 4. Gene expression profile showing transcriptional level of chondrogenic and pro-inflammatory marker genes including *COL2A1, COL1A1, ACAN, COMP, MMP1* and *IL-6* for the cells encapsulated in HA100/SF0, HA20/SF80 and HA10/SF90 at days 3, 7 and 21 cultured in chondrogenic medium and chondropermissive medium in 2 independent donors of bovine chondrocytes; for each donor three experimental replicates were analyzed. Data was normalized to the levels of Day 0 control group. Data are presented as mean ± SD. For statistical analysis using Graphpad Prism 8, one-way analysis of variance (ANOVA) followed by Tukey's post hoc test (multiple comparisons) was applied. * $p < 0.01$, ** $p < 0.001$, *** $p < 0.0005$, **** $p < 0.0001$.

3.5 Mechanical testing analysis

Unconfined compressive properties of the cell-free and cell-laden constructs including HA100/SF0, HA20/SF80 and HA10/SF90, were determined at days 1, 7, 14, 21 and 28. Initially at day 1, all hydrogels had compressive modulus ranging between ~1 and 4 kPa with the highest value measured for HA20/SF80 hydrogels. In cell-free constructs, the compressive modulus of all hydrogel remained almost constant until day 21. However, for HA20/SF80 and HA10/SF90 hydrogels at day 28, the compressive modulus was significantly increased and reached a final modulus of 19.2 ± 1.8 kPa and 16.9 ± 0.2 kPa, respectively, while for HA100/SF0 this value remained unchanged. Therefore, in the cell-free constructs the significant increase in the compressive modulus of HA20/SF80 and HA10/SF90 was due to the formation of β-sheet secondary structures in SF. After culture of the cell-laden constructs in chondrogenic medium, the compressive modulus for HA20/SF80 hydrogels was significantly higher than the other groups (both cell-laden and cell-free) and reached a final compressive modulus of 29.06 ± 3.1 kPa at day 28 which confirmed the significant matrix deposition in this hydrogel. Also, for HA100/SF0 and HA10/SF90 hydrogels, the compressive modulus was increased over time and reached the final moduli of 15.9 ± 1.1 kPa and 11.49 ± 0.1 kPa at day 28, respectively (Fig. 5 A, B). The results showed that the percentage of the relaxation was significantly increased in all cell-laden hydrogels from day 1 to day 7 of culture in chondrogenic medium. The percentage of the stress-relaxation was initially the highest for HA10/SF90 hydrogels at day 1 and this value was increased over the period of culture in all hydrogels (Supplementary Fig. 1).

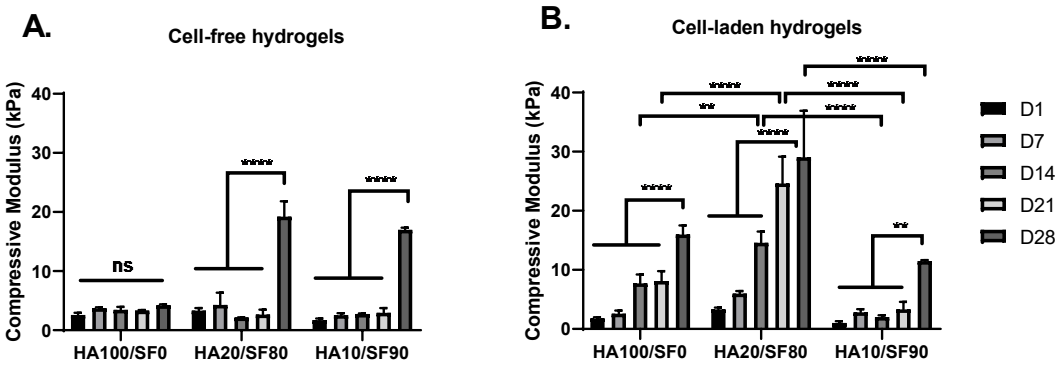

Figure 5. Mechanical testing for HA100/SF0, HA20/SF80, HA10/SF90 cell-laden hydrogel constructs at days 1, 7, 14, 21 and 28. (A) The compressive moduli of the cell-free hydrogels over the period of 28 days. (B) The compressive moduli of the cell-laden hydrogels cultured in chondrogenic medium showed most pronounced increase in compressive modulus for HA20/SF80 hydrogels. Values are presented as mean ± SD from 3 replicates of 2 independent donors per group. For statistical analysis using Graphpad Prism 8, one-way analysis of variance (ANOVA) followed by Tukey's post hoc test (multiple comparisons) was applied. ** $p < 0.001$, *** $p < 0.0005$, **** $p < 0.0001$ and ns (non-significant).

3.6 Histological analysis

To observe matrix deposition in the hydrogels, Safranin-O (Saf-O) and Alcian blue staining were performed for the hydrogel constructs cultured in chondrogenic medium at days 1, 14, 21 and 28. The results showed that sulphated glycosaminoglycans (sGAG) were produced and deposited in all the hydrogels, in the period of 28 days of the culture in chondrogenic medium indicating that the hydrogels supported chondrogenesis. However, the intensity of staining for sGAG and matrix deposition was the strongest for HA20/SF80 composite hydrogels at days 14, 21 and 28 (Fig. 6A and supplementary Fig. 2). The immunostaining for COL2 at day 21 showed that the specific cartilaginous ECM proteins were also expressed in the hydrogels. We also observed that in HA100/SF0 and HA20/SF80 hydrogels, the chondrogenic morphology was maintained, as indicated by the rounded cells residing within the lacuna.While, in HA10/SF90 hydrogels the chondrocytes were not embedded in lacuna and the cells showed a fibroblast-like morphology (Fig. 6B and supplementary Fig. 2).

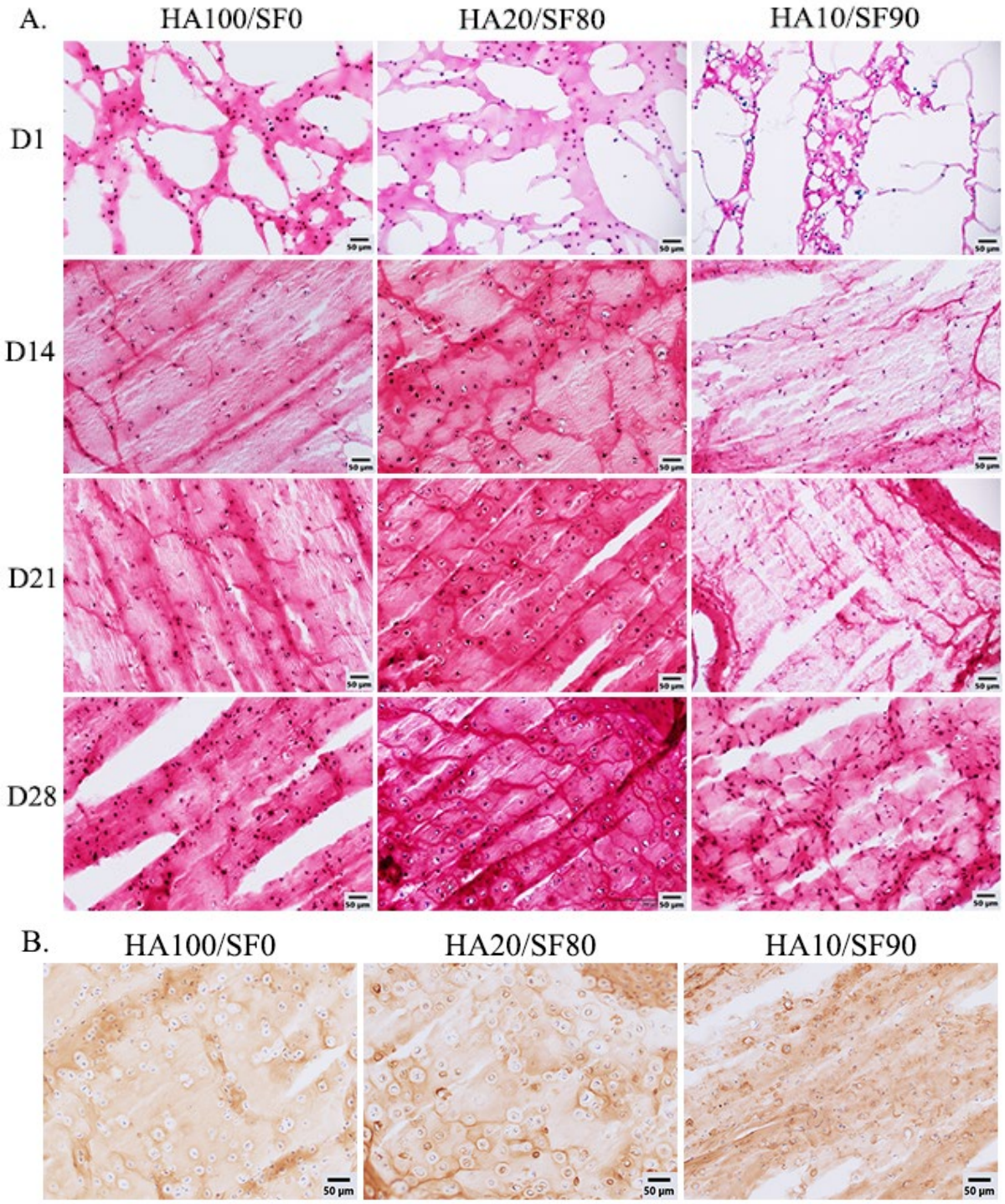

Figure 6. Histological and immunohistochemical characterization of the cell-encapsulated hydrogel constructs including HA100/SF0, HA20/SF80 and HA10/SF90. (A) Safranin-O staining for the hydrogels at days 1, 14, 21 and 28 representing the highest amount of matrix deposition in HA20/SF80 over all time points. (B) Immunostaining for type II collagen at day 21 revealed that the COL2 was accumulated in all hydrogels and the chondrogenic cell morphology was maintained in HA100/SF0 and HA20/SF80 hydrogels. Scale bars = 50 µm.

3.7 Compounds release study

The molecular structures, standard curves and cumulative release of VA and Epi C from various HA/SF hydrogel compositions at a drug load of 1 mM can be seen in Figure 8. Pure HA-Tyr gels (HA100/SF0) showed very low release of VA (3.0%) and Epi C (7.1%) over the experimental period of 60 days. Composite HA/SF hydrogels showed a substantial increase in drug release that could be observed for both VA and Epi C. When comparing HA20/SF80 and HA10/SF90 hydrogels, a profound difference was seen in VA release while Epi C release was minimally affected by the higher SF ratio in the hydrogel. Epi C showed strong burst release during the first week of the release experiment (54.0% for both composite hydrogels), followed by a plateau phase over the rest of the experiment in which less than 1% of the initial drug load was released to the surrounding PBS. The highest cumulative VA release (70.1%) was seen when the compound was embedded in HA20/SF80. Negligible quantities of VA and Epi C were recovered upon overnight enzymatic degradation of the hydrogels at day 60, indicating that possible degradation products of VA and Epi C could have remained unidentified during the HPLC measurements.

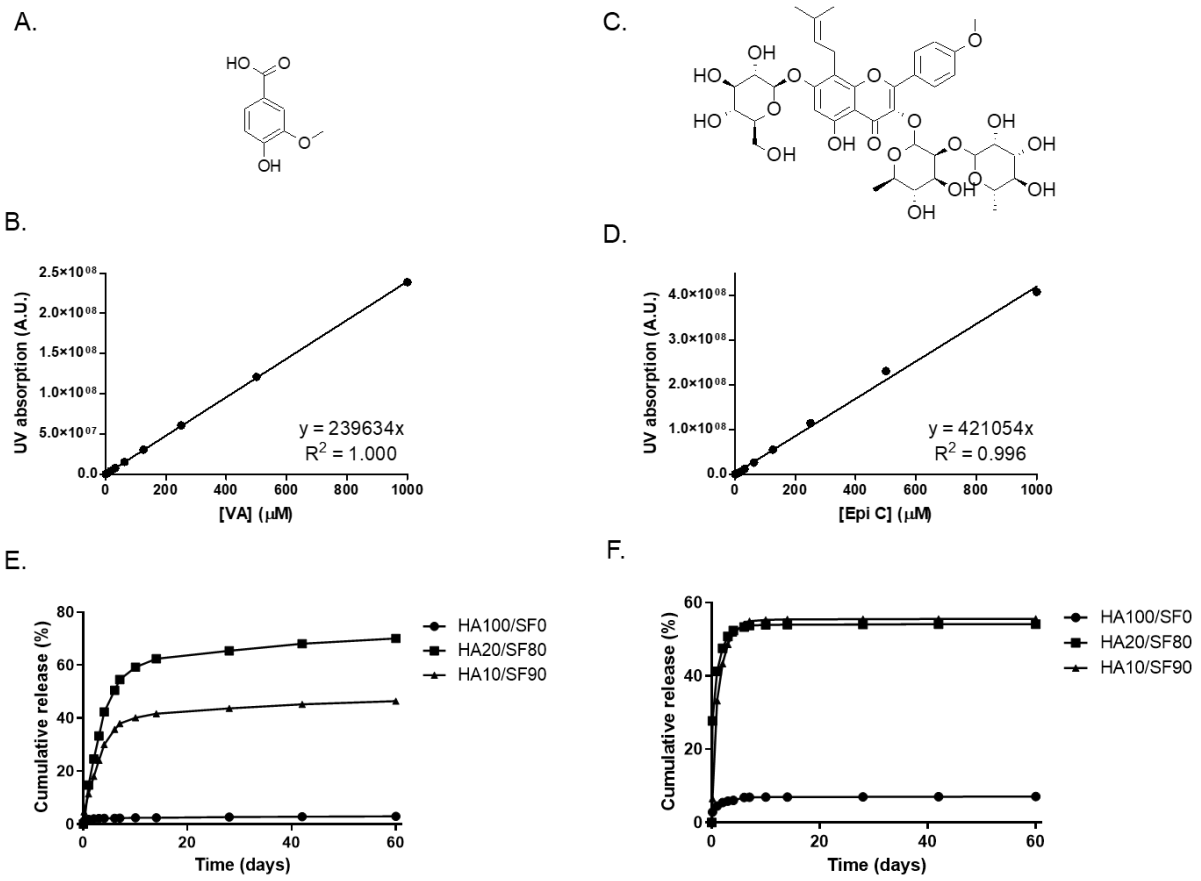

Figure 7. Release study for the compounds loaded in HA100/SF0, HA20/SF80 and HA10/SF90 hydrogels. Molecular structure of (A) VA and (C) Epi C. Standard curves of (B) VA and (D) Epi C in PBS. Cumulative release profiles of (E) VA and (F) Epi C from HA and HA/SF composite hydrogels.

4. Discussion

Tunable composite hydrogels for cartilage TE and drug delivery therapies have been introduced in recent years as a desirable alternative to invasive treatments [51,52]. Previous publication regarding HA/SF composite hydrogels showed that HA5/SF95, HA10/SF90 and HA20/SF80 hydrogels formed an interconnected hydrogel network with di-tyramine, di-tyrosine and tyramine-tyrosine bonds [45]. In this work, these composite HA/SF hydrogels were further assessed for their ability to provide an encapsulating matrix for chondrocytes and as carrier material for anti-inflammatory drugs. Initially, the hydrogels mechanical properties and gelation time were characterized over time. The rheological time sweep showed that due to higher polymer amount in HA20/SF80 hydrogels, more available crosslinking sites were present and the higher crosslink density (di-tyramine, di-tyrosine and tyramine-tyrosine) resulted in higher storage modulus (4 kPa) compared with other hydrogels in this study (Fig. 2A). Also, the strain sweep showed that HA0/SF100 and HA5/SF95 composite hydrogels could resist over 100% strain before mechanical failure and by increasing HA-Tyr concentration in the composite hydrogels the strain at failure was gradually reduced. However, a significant improvement was observed for the composite hydrogels compared to HA100/SF0 hydrogels that started to fail at less than 10% strain (Fig. 2B). These mechanical properties could make the composite hydrogels suitable for the TE of joint cartilage which is normally affected by physiological loads of approximately 20% strain [53,54]. The duration of gelation of composite HA/SF hydrogels was directly related to the HA-Tyr and SF ratio, corroborating the findings from Raia *et al.* [45]. The extremely fast gelation of HA100/SF0 and the slow gelation of HA0/SF100 indicate that the crosslinking kinetics of HA and SF materials were different. HA20/SF80 and HA10/90 optimized ratio had a gelation time of 3 and 6 minutes allowing easy handling for clinical applications including drugs or cells loading, prior to injection and setting [55] (Fig. 1 A, B). While to our knowledge there is no evidence that, from a chemical standpoint, the formation of di-tyramine bonds is favorable over that of di-tyrosine bonds, there might be a difference in the number of available phenol groups in both polymers. With our synthesized HA showing a tyramine DS of 14% and SF having approximately 5% tyrosine in their heavy chain amino acids [56], an abundance of phenols should be present in all hydrogel

groups to facilitate fast enzymatic crosslinking. Another reason for the slower gelation of SF might be the formation of β-sheet structures that reduce the polymer chain mobility.

When assessing the encapsulated drug release from the composite hydrogels, VA was generally released slower compared to Epi C (Fig. 7). This was surprising and perhaps counter intuitive due to the much lower molecular weight of VA (Fig. 7A, B) and thus increased diffusion kinetics. However, with the gels being formed by crosslinking between phenol groups of tyramine and tyrosine, it is possible that crosslinking of the VA phenol group with the hydrogel occurs as well. This hypothesis is supported by the fact that hydrogels with a 10 mM VA load were not able to gel (data not shown). Epi C also has ring structures, but their 3D conformation would result in more steric hinderance, mostly preventing such drug-hydrogel interactions. The covalent C-C bond that can form between VA and tyramine or tyrosine groups is considered stable and is unlikely to provide a sustained release of VA through crosslink degradation. However, ring structures associated with the crosslinked VA could provide physical interactions with encapsulated VA through π-π stacking of their planar aromatic rings. Enzymatic hydrogel degradation at the end of the drug release study with hyaluronidase to provide HA cleavage might not have broken up phenol complexes between Tyramine groups and VA, explaining why negligible VA quantities were observed in the endpoint degraded gels. Therefore, to prevent the covalent reaction between VA and tyramine or tyrosine, one could consider encapsulating VA in microparticles that can be added to SF/HA hydrogels. This approach could minimize VA-hydrogel interaction during crosslinking and potentially allow for a slower VA release.

To evaluate the effect of hydrogel composition and stiffness on the ECM deposition, bovine chondrocytes were embedded at high density (20 x 10^6 cells/mL) in enzymatically crosslinked HA/SF composites or HA-Tyr hydrogels. Previous studies with high density cell-laden SF hydrogels showed that such hydrogels are favorable for the redifferentiation of culture-expanded chondrocytes and ECM deposition [57]. However, due to the slow gelation, crosslinking did not occur in HA0/SF100 and HA5/SF95 hydrogels in the presence of high numbers of cells, while composites with the higher percentage of HA (HA20/SF80, HA10/SF90) due to faster gelation were crosslinked successfully. Another reason for this lack of crosslinking in the presence of cells, could be due to the absence of cell specific epitopes in SF hydrogels which can be compensated by crosslinking with HA-Tyr [30,45]. For HA100/SF0

hydrogels the crosslinking in the presence of the cells was possible due to the ability of the cell's CD44 receptors to interact with the HA and interaction of tyramine residuals with extracellular matrix components [29,58]. It was previously shown that with encapsulating high numbers of cells in HA-Tyr hydrogels their mechanical properties were significantly decreased (storage modulus <1 kPa) which is not optimal for promoting ECM production by the cells [31,38]. Also, it was shown that by increasing the H_2O_2 concertation stiffer materials could be formed [30,31]. Nevertheless, the small mech size of highly crosslinked HA-Tyr gels was previously resulting in insufficient transport of nutrients, restriction of cell growth and prevention of cellular remodeling [30]. We observed that in HA100/SF0 hydrogels in chondrogenic medium, the proportion of viable cells was decreased over-time which could be due to the limited transfer of nutrients to the cells encapsulated in the hydrogels. Also, high concentrations of HRP and H_2O_2 could increase cytotoxicity and will potentially induce immune responses [32,33]. We showed that in the presence of 0.01% H_2O_2 and with a high chondrocyte density, more than 90% of the chondrocytes cultured in chondrogenic medium were viable in all hydrogel formulations. In HA20/SF80 hydrogels more than 95% of the chondrocytes were viable in both chondrogenic and chondro-permissive media over the culture period. This high cell viability verified a proper stiffness of the hydrogels in diffusion of nutrition, providing a favorable environment for the metabolism of the chondrocytes (Fig. 3 A, B). Additionally, HA100/SF0 and HA20/SF80 composite hydrogels could promote re-differentiation of the chondrocytes by preserving the chondrogenic phenotype. The expression of chondrogenic marker genes (*COL2a1, ACAN* and *COMP*) in all chondrocyte-laden constructs was up-regulated compared with day 0 control, with up-regulation being most pronounced in HA20/SF80 hydrogels in both chondrogenic and chondro-permissive conditioned media. The expression of pro-inflammatory marker genes (*MMP1 and IL-6*) was down-regulated compared with day 0 control, which supports the anti-inflammatory properties of SF and HA based hydrogels that were reported previously [20,46]. Furthermore, the ECM deposition was increased in all hydrogels over 28 days of culture with the most noticeable increase for HA20/SF80 hydrogels as was characterized by Safranin-O and Alcian blue staining (Fig. 6 and supplementary Fig 2).

The unconfined compressive properties showed that compressive modulus for the HA20/SF80 chondrocyte-laden constructs was significantly increased over 28 days of culture in chondrogenic medium reaching the same value as explanted cartilage tissues in previous studies

[59,60]. This higher level of compressive modulus was not only due to the superior matrix deposition in HA20/SF80 hydrogels, but also due to intrinsic features of the HA/SF hydrogels which were getting stiffer over-time, most probably due to the formation of β-sheets secondary structures in SF [42,45,61]. The hydrogel stiffening was significant in cell-free HA/SF composite hydrogels from day 21 to day 28. In HA100/SF0 and HA20/SF80 cell-laden constructs, there was a gradual increase in compressive modulus from day 1 to day 28 due to the matrix deposition, whereby this increase was significantly higher in HA20/SF80 hydrogels. However, in HA10/SF90 hydrogels, we didn't observe an increasing trend in matrix deposition from day 1 to day 21, while there was a peak at day 28 similar to cell-free hydrogels. This may indicate that the matrix deposition was not considerable in these hydrogels and the observed peak at day 28 was due to the formation of β-sheet structures. Also, it is known that adherent cells like chondrocytes, sense viscoelasticity of their surrounding environment and the stiffness of the matrix can influence contractility and spreading of the cells [62]. Therefore, there is a feedback loop of physical and biochemical signals in response to the elasticity of the extracellular microenvironment which influences cell fate and morphology [63]. In this study we showed for the first time that HA20/SF80 could provide the most adequate environment for the chondrocytes to re-differentiate and deposit ECM to reach mechanical and biological properties similar to native cartilage [59].

Furthermore, Lee et al. showed that in fast relaxing hydrogels which dissipate elastic stresses more quickly, chondrocytes tend to form interconnected regions of ECM, while in slow relaxing hydrogels, elastic stresses restrict cell movement and growth which limits chondrocyte matrix production [64]. In this study, we observed that in the cell-laden HA100/SF0 and HA20/SF80 hydrogels, the percentage of the stress relaxation was significantly increased from day 1 to day 7, which was due to the matrix deposition in the hydrogels. These results highlight the impact of controlled change of hydrogel mechanical properties over the culture period on cell differentiation and fate. In this regard, HA100/SF0 and HA20/SF80 showed suitable moderate elastic properties in the initial phase of the cell culture that diminish over time.

Furthermore, HA100/SF0 hydrogels were very fast degradable and these hydrogels were degraded over the period of culture, while composite hydrogels remained intact till the end of the culture period of 28 days (data not shown). It has been shown that scaffolds more resistant to degradation support the matrix production by chondrocytes for a longer period, making them

suitable for *ex vivo* and *in vivo* applications [65]. Therefore, the degradation rate of hydrogels and their potential in supporting cell maturation and matrix deposition should be evaluated in further *ex vivo* and *in vivo* applications.

Due to the very limited number of human chondrocytes, several monolayer passages are usually necessary before utilization for TE studies [50]. Therefore, in this study to prevent the use of de-differentiated cells due to the expansion, minimally expanded bovine chondrocytes were used. However, this source of cells has limited relevance for further pre-clinical and clinical applications and the utilization of other sources of cells including human articular chondrocytes, mesenchymal stem cells (MSCs) and nasal chondrocytes are envisioned [31,66] .

Several previous studies showed that mechanical stimulation is necessary for promoting ECM production in chondrocytes and MSCs [31,67]. Since our hydrogels showed proper mechanical properties in withstanding mechanical loads, the mechanobiology of the chondrocytes encapsulated in the HA20/SF80 hydrogels in response to mechanical compression and shear should be evaluated in future experiments using a cartilage bioreactor system as has been established by our group [68].

In conclusion, with the enzymatic crosslinking of SF and HA-Tyr solutions, we developed an injectable and tunable composite hydrogel for cartilage tissue engineering and drug delivery purposes. We demonstrated that all hydrogels were cytocompatible and that HA100/SF0 and HA20/SF80 composite hydrogels could preserve the chondrogenic phenotype through increased expression of chondrogenic marker genes and ECM production. Also, the unconfined compressive modulus for the HA20/SF80 chondrocyte-laden constructs was significantly increased over 28 days of culture in chondrogenic medium confirming the superior ECM deposition in this composite hydrogel. Furthermore, in the drug loaded hydrogels, HA20/SF80 hydrogel showed the longest and the most sustained release profile for VA and Epi C over time, which is necessary for the long treatment duration for OA joints. Future *in vivo* experiments in an OA joint model should assess whether the release of VA and/or Epi C is effective in counteracting inflammation and promoting chondrocyte ECM production.

5. Supplementary Information

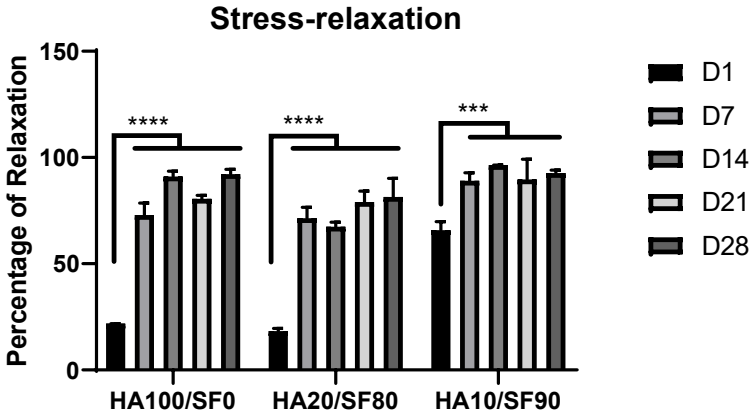

Supplementary Figure 1. The percentage of the stress-relaxation in cell-laden hydrogels cultured in chondrogenic medium for 28 days. Values are presented as mean ± SD from 3 replicates of 2 independent donors per group. For statistical analysis using Graphpad Prism 8, one-way analysis of variance (ANOVA) followed by Tukey's post hoc test (multiple comparisons) was applied. *** $p < 0.0005$, **** $p < 0.0001$.

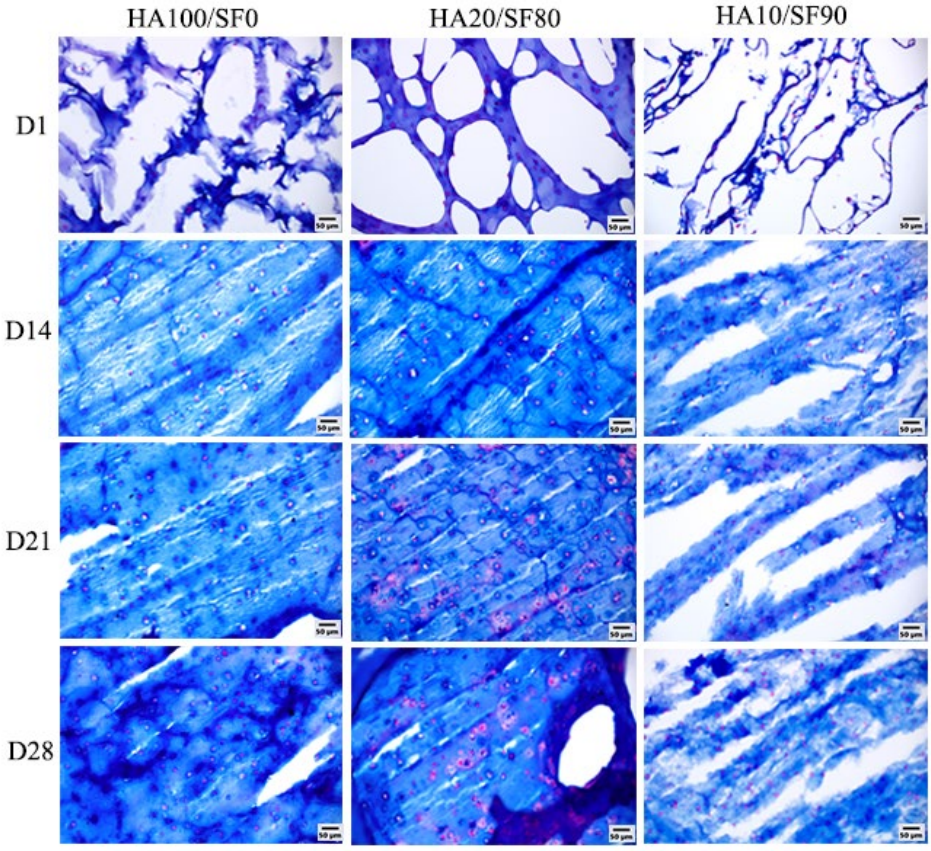

Supplementary Figure 2. Histological characterization of the cell-encapsulated hydrogel constructs including HA100/SF0, HA20/SF80 and HA10/SF90. (A) Alcian blue staining for the hydrogels at days 1, 14, 21 and 28 representing the highest amount of matrix deposition in HA20/SF80 over all time points.

6. References

1. Krishnan, Y.; Grodzinsky, A.J. Cartilage diseases. *Matrix Biol* **2018**, *71-72*, 51-69, doi:10.1016/j.matbio.2018.05.005.

2. Poole, A.R.; Kojima, T.; Yasuda, T.; Mwale, F.; Kobayashi, M.; Laverty, S. Composition and structure of articular cartilage: a template for tissue repair. *Clin Orthop Relat Res* **2001**, 10.1097/00003086-200110001-00004, S26-33, doi:10.1097/00003086-200110001-00004.

3. Loeser, R.F. Age-related changes in the musculoskeletal system and the development of osteoarthritis. *Clin Geriatr Med* **2010**, *26*, 371-386, doi:10.1016/j.cger.2010.03.002.

4. Heidari, B. Knee osteoarthritis prevalence, risk factors, pathogenesis and features: Part I. *Caspian J Intern Med* **2011**, *2*, 205-212.

5. Sandell, L.J.; Aigner, T. Articular cartilage and changes in Arthritis: Cell biology of osteoarthritis. *Arthritis research & therapy* **2001**, *3*, 107, doi:10.1186/ar148.

6. Minas, T.; Ogura, T.; Bryant, T. Autologous Chondrocyte Implantation. *JBJS Essent Surg Tech* **2016**, *6*, e24, doi:10.2106/jbjs.st.16.00018.

7. Gortz, S.; Bugbee, W.D. Allografts in articular cartilage repair. *Instr Course Lect* **2007**, *56*, 469-480.

8. Wylde, V.; Beswick, A.; Bruce, J.; Blom, A.; Howells, N.; Gooberman-Hill, R. Chronic pain after total knee arthroplasty. *EFORT Open Rev* **2018**, *3*, 461-470, doi:10.1302/2058-5241.3.180004.

9. Roberts, S.; Menage, J.; Sandell, L.J.; Evans, E.H.; Richardson, J.B. Immunohistochemical study of collagen types I and II and procollagen IIA in human cartilage repair tissue following autologous chondrocyte implantation. *Knee* **2009**, *16*, 398-404, doi:10.1016/j.knee.2009.02.004.

10. Liu, M.; Zeng, X.; Ma, C.; Yi, H.; Ali, Z.; Mou, X.; Li, S.; Deng, Y.; He, N. Injectable hydrogels for cartilage and bone tissue engineering. *Bone Research* **2017**, *5*, 17014, doi:10.1038/boneres.2017.14.

11. Vega, S.L.; Kwon, M.Y.; Burdick, J.A. Recent advances in hydrogels for cartilage tissue engineering. *Eur Cell Mater* **2017**, *33*, 59-75, doi:10.22203/eCM.v033a05.

12. Toh, W.S.; Spector, M.; Lee, E.H.; Cao, T. Biomaterial-Mediated Delivery of Microenvironmental Cues for Repair and Regeneration of Articular Cartilage. *Molecular Pharmaceutics* **2011**, *8*, 994-1001, doi:10.1021/mp100437a.

13. Hoffman, A.S. Hydrogels for biomedical applications. *Advanced drug delivery reviews* **2012**, *64*, 18-23, doi:https://doi.org/10.1016/j.addr.2012.09.010.

14. Pauly, H.M.; Place, L.W.; Haut Donahue, T.L.; Kipper, M.J. Mechanical Properties and Cell Compatibility of Agarose Hydrogels Containing Proteoglycan Mimetic Graft Copolymers. *Biomacromolecules* **2017**, *18*, 2220-2229, doi:10.1021/acs.biomac.7b00643.

15. Augst, A.D.; Kong, H.J.; Mooney, D.J. Alginate hydrogels as biomaterials. *Macromolecular bioscience* **2006**, *6*, 623-633, doi:10.1002/mabi.200600069.

16. Lee, K.Y.; Mooney, D.J. Alginate: properties and biomedical applications. *Progress in polymer science* **2012**, *37*, 106-126, doi:10.1016/j.progpolymsci.2011.06.003.

17. Antoine, E.E.; Vlachos, P.P.; Rylander, M.N. Review of collagen I hydrogels for bioengineered tissue microenvironments: characterization of mechanics, structure, and transport. *Tissue engineering. Part B, Reviews* **2014**, *20*, 683-696, doi:10.1089/ten.TEB.2014.0086.

18. Jin, G.Z.; Kim, H.W. Efficacy of collagen and alginate hydrogels for the prevention of rat chondrocyte dedifferentiation. *Journal of tissue engineering* **2018**, *9*, 2041731418802438, doi:10.1177/2041731418802438.

19. Li, L.; Yu, F.; Zheng, L.; Wang, R.; Yan, W.; Wang, Z.; Xu, J.; Wu, J.; Shi, D.; Zhu, L., et al. Natural hydrogels for cartilage regeneration: Modification, preparation and application. *Journal of orthopaedic translation* **2019**, *17*, 26-41, doi:https://doi.org/10.1016/j.jot.2018.09.003.

20. Masuko, K.; Murata, M.; Yudoh, K.; Kato, T.; Nakamura, H. Anti-inflammatory effects of hyaluronan in arthritis therapy: Not just for viscosity. *International journal of general medicine* **2009**, *2*, 77-81.

21. Akmal, M.; Singh, A.; Anand, A.; Kesani, A.; Aslam, N.; Goodship, A.; Bentley, G. The effects of hyaluronic acid on articular chondrocytes. *The Journal of bone and joint surgery. British volume* **2005**, *87*, 1143-1149, doi:10.1302/0301-620x.87b8.15083.

22. Jansen, E.J.; Emans, P.J.; Douw, C.M.; Guldemond, N.A.; Van Rhijn, L.W.; Bulstra, S.K.; Kuijer, R. One intra-articular injection of hyaluronan prevents cell death and improves cell metabolism in a model of injured articular cartilage in the rabbit. *Journal of orthopaedic research : official publication of the Orthopaedic Research Society* **2008**, *26*, 624-630, doi:10.1002/jor.20569.

23. Yasuda, T. Hyaluronan inhibits prostaglandin E2 production via CD44 in U937 human macrophages. *The Tohoku journal of experimental medicine* **2010**, *220*, 229-235, doi:10.1620/tjem.220.229.

24. Roth, A.; Mollenhauer, J.; Wagner, A.; Fuhrmann, R.; Straub, A.; Venbrocks, R.A.; Petrow, P.; Brauer, R.; Schubert, H.; Ozegowski, J., et al. Intra-articular injections of high-molecular-weight hyaluronic acid have biphasic effects on joint inflammation and destruction in rat antigen-induced arthritis. *Arthritis research & therapy* **2005**, *7*, R677-686, doi:10.1186/ar1725.

25. Lee, F.; Chung, J.E.; Kurisawa, M. An injectable hyaluronic acid-tyramine hydrogel system for protein delivery. *Journal of controlled release : official journal of the Controlled Release Society* **2009**, *134*, 186-193, doi:10.1016/j.jconrel.2008.11.028.

26. Kurisawa, M.; Chung, J.E.; Yang, Y.Y.; Gao, S.J.; Uyama, H. Injectable biodegradable hydrogels composed of hyaluronic acid-tyramine conjugates for drug delivery and tissue engineering. *Chemical communications (Cambridge, England)* **2005**, 10.1039/b506989k, 4312-4314, doi:10.1039/b506989k.

27. Toh, W.S.; Lim, T.C.; Kurisawa, M.; Spector, M. Modulation of mesenchymal stem cell chondrogenesis in a tunable hyaluronic acid hydrogel microenvironment. *Biomaterials* **2012**, *33*, 3835-3845, doi:https://doi.org/10.1016/j.biomaterials.2012.01.065.

28. Kim, K.S.; Park, S.J.; Yang, J.A.; Jeon, J.H.; Bhang, S.H.; Kim, B.S.; Hahn, S.K. Injectable hyaluronic acid–tyramine hydrogels for the treatment of rheumatoid arthritis. *Acta Biomaterialia* **2011**, *7*, 666-674, doi:https://doi.org/10.1016/j.actbio.2010.09.030.

29. Sherman, L.; Sleeman, J.; Herrlich, P.; Ponta, H. Hyaluronate receptors: key players in growth, differentiation, migration and tumor progression. *Current opinion in cell biology* **1994**, *6*, 726-733, doi:10.1016/0955-0674(94)90100-7.

30. Loebel, C.; Stauber, T.; D'Este, M.; Alini, M.; Zenobi-Wong, M.; Eglin, D. Fabrication of cell-compatible hyaluronan hydrogels with a wide range of biophysical properties through high tyramine functionalization. *Journal of Materials Chemistry B* **2017**, *5*, 2355-2363, doi:10.1039/C6TB03161G.

31. Behrendt, P.; Ladner, Y.; Stoddart, M.J.; Lippross, S.; Alini, M.; Eglin, D.; Armiento, A.R. Articular Joint-Simulating Mechanical Load Activates Endogenous TGF-β in a Highly Cellularized Bioadhesive

Hydrogel for Cartilage Repair. *The American journal of sports medicine* **2020**, *48*, 210-221, doi:10.1177/0363546519887909.

32. Sminia, T.; Delemarre, F.; Janse, E.M. Histological observations on the intestinal immune response towards horseradish peroxidase in rats. *Immunology* **1983**, *50*, 53-56.

33. Gardner, A.M.; Xu, F.H.; Fady, C.; Jacoby, F.J.; Duffey, D.C.; Tu, Y.; Lichtenstein, A. Apoptotic vs. nonapoptotic cytotoxicity induced by hydrogen peroxide. *Free radical biology & medicine* **1997**, *22*, 73-83, doi:10.1016/s0891-5849(96)00235-3.

34. Spiller, K.L.; Maher, S.A.; Lowman, A.M. Hydrogels for the repair of articular cartilage defects. *Tissue engineering. Part B, Reviews* **2011**, *17*, 281-299, doi:10.1089/ten.TEB.2011.0077.

35. Bhumiratana, S.; Eton, R.E.; Oungoulian, S.R.; Wan, L.Q.; Ateshian, G.A.; Vunjak-Novakovic, G. Large, stratified, and mechanically functional human cartilage grown in vitro by mesenchymal condensation. *Proceedings of the National Academy of Sciences of the United States of America* **2014**, *111*, 6940-6945, doi:10.1073/pnas.1324050111.

36. Stern, R.; Kogan, G.; Jedrzejas, M.J.; Soltes, L. The many ways to cleave hyaluronan. *Biotechnology advances* **2007**, *25*, 537-557, doi:10.1016/j.biotechadv.2007.07.001.

37. Hunziker, E.B. Articular cartilage repair: basic science and clinical progress. A review of the current status and prospects. *Osteoarthritis and cartilage* **2002**, *10*, 432-463, doi:10.1053/joca.2002.0801.

38. Wang, L.S.; Du, C.; Toh, W.S.; Wan, A.C.; Gao, S.J.; Kurisawa, M. Modulation of chondrocyte functions and stiffness-dependent cartilage repair using an injectable enzymatically crosslinked hydrogel with tunable mechanical properties. *Biomaterials* **2014**, *35*, 2207-2217, doi:10.1016/j.biomaterials.2013.11.070.

39. Yucel, T.; Lovett, M.L.; Kaplan, D.L. Silk-based biomaterials for sustained drug delivery. *Journal of controlled release : official journal of the Controlled Release Society* **2014**, *190*, 381-397, doi:10.1016/j.jconrel.2014.05.059.

40. Partlow, B.P.; Hanna, C.W.; Rnjak-Kovacina, J.; Moreau, J.E.; Applegate, M.B.; Burke, K.A.; Marelli, B.; Mitropoulos, A.N.; Omenetto, F.G.; Kaplan, D.L. Highly tunable elastomeric silk biomaterials. *Adv Funct Mater* **2014**, *24*, 4615-4624, doi:10.1002/adfm.201400526.

41. Rockwood, D.N.; Preda, R.C.; Yucel, T.; Wang, X.; Lovett, M.L.; Kaplan, D.L. Materials fabrication from Bombyx mori silk fibroin. *Nature protocols* **2011**, *6*, 1612-1631, doi:10.1038/nprot.2011.379.

42. Hasturk, O.; Jordan, K.E.; Choi, J.; Kaplan, D.L. Enzymatically crosslinked silk and silk-gelatin hydrogels with tunable gelation kinetics, mechanical properties and bioactivity for cell culture and encapsulation. *Biomaterials* **2020**, *232*, 119720, doi:https://doi.org/10.1016/j.biomaterials.2019.119720.

43. Vepari, C.; Kaplan, D.L. Silk as a Biomaterial. *Progress in polymer science* **2007**, *32*, 991-1007, doi:10.1016/j.progpolymsci.2007.05.013.

44. Partlow, B.P.; Bagheri, M.; Harden, J.L.; Kaplan, D.L. Tyrosine Templating in the Self-Assembly and Crystallization of Silk Fibroin. *Biomacromolecules* **2016**, *17*, 3570-3579, doi:10.1021/acs.biomac.6b01086.

45. Nicole R. Raia, B.P.P., Meghan McGill, Erica Palma Kimmerling,; Chiara E. Ghezzi, D.L.K. Enzymatically crosslinked silk-hyaluronic acid hydrogels. *Biomaterials* **2017**, *131*, 58-67.

46. Crivelli, B.; Perteghella, S.; Bari, E.; Sorrenti, M.; Tripodo, G.; Chlapanidas, T.; Torre, M.L. Silk nanoparticles: from inert supports to bioactive natural carriers for drug delivery. *Soft Matter* **2018**, *14*, 546-557, doi:10.1039/c7sm01631j.

47. Loebel, C.; D'Este, M.; Alini, M.; Zenobi-Wong, M.; Eglin, D. Precise tailoring of tyramine-based hyaluronan hydrogel properties using DMTMM conjugation. *Carbohydr Polym* **2015**, *115*, 325-333, doi:10.1016/j.carbpol.2014.08.097.

48. Grad, S.; Gogolewski, S.; Alini, M.; Wimmer, M.A. Effects of simple and complex motion patterns on gene expression of chondrocytes seeded in 3D scaffolds. *Tissue engineering* **2006**, *12*, 3171-3179, doi:10.1089/ten.2006.12.3171.

49. Livak, K.J.; Schmittgen, T.D. Analysis of relative gene expression data using real-time quantitative PCR and the 2(-Delta Delta C(T)) Method. *Methods* **2001**, *25*, 402-408, doi:10.1006/meth.2001.1262.

50. Ziadlou, R.; Barbero, A.; Stoddart, M.J.; Wirth, M.; Li, Z.; Martin, I.; Wang, X.L.; Qin, L.; Alini, M.; Grad, S. Regulation of Inflammatory Response in Human Osteoarthritic Chondrocytes by Novel Herbal Small Molecules. *Int J Mol Sci* **2019**, *20*, doi:10.3390/ijms20225745.

51. Elisseeff, J. Injectable cartilage tissue engineering. *Expert opinion on biological therapy* **2004**, *4*, 1849-1859, doi:10.1517/14712598.4.12.1849.

52. Kretlow, J.D.; Klouda, L.; Mikos, A.G. Injectable matrices and scaffolds for drug delivery in tissue engineering. *Advanced drug delivery reviews* **2007**, *59*, 263-273, doi:10.1016/j.addr.2007.03.013.

53. Armstrong, C.G.; Bahrani, A.S.; Gardner, D.L. In vitro measurement of articular cartilage deformations in the intact human hip joint under load. *The Journal of bone and joint surgery. American volume* **1979**, *61*, 744-755.

54. Park, S.; Hung, C.T.; Ateshian, G.A. Mechanical response of bovine articular cartilage under dynamic unconfined compression loading at physiological stress levels. *Osteoarthritis and cartilage* **2004**, *12*, 65-73, doi:10.1016/j.joca.2003.08.005.

55. Moreira Teixeira, L.S.; Feijen, J.; van Blitterswijk, C.A.; Dijkstra, P.J.; Karperien, M. Enzyme-catalyzed crosslinkable hydrogels: Emerging strategies for tissue engineering. *Biomaterials* **2012**, *33*, 1281-1290, doi:https://doi.org/10.1016/j.biomaterials.2011.10.067.

56. McGill, M.; Grant, J.M.; Kaplan, D.L. Enzyme-Mediated Conjugation of Peptides to Silk Fibroin for Facile Hydrogel Functionalization. *Annals of biomedical engineering* **2020**, 10.1007/s10439-020-02503-2, doi:10.1007/s10439-020-02503-2.

57. Wang, Y.; Blasioli, D.J.; Kim, H.J.; Kim, H.S.; Kaplan, D.L. Cartilage tissue engineering with silk scaffolds and human articular chondrocytes. *Biomaterials* **2006**, *27*, 4434-4442, doi:10.1016/j.biomaterials.2006.03.050.

58. Aruffo, A.; Stamenkovic, I.; Melnick, M.; Underhill, C.B.; Seed, B. CD44 is the principal cell surface receptor for hyaluronate. *Cell* **1990**, *61*, 1303-1313, doi:10.1016/0092-8674(90)90694-a.

59. Patel, J.M.; Wise, B.C.; Bonnevie, E.D.; Mauck, R.L. A Systematic Review and Guide to Mechanical Testing for Articular Cartilage Tissue Engineering. *Tissue engineering. Part C, Methods* **2019**, *25*, 593-608, doi:10.1089/ten.TEC.2019.0116.

60. Park, S.; Krishnan, R.; Nicoll, S.B.; Ateshian, G.A. Cartilage interstitial fluid load support in unconfined compression. *Journal of biomechanics* **2003**, *36*, 1785-1796, doi:10.1016/s0021-9290(03)00231-8.

61. Stoppel, W.L.; Gao, A.E.; Greaney, A.M.; Partlow, B.P.; Bretherton, R.C.; Kaplan, D.L.; Black Iii, L.D. Elastic, silk-cardiac extracellular matrix hydrogels exhibit time-dependent stiffening that modulates cardiac fibroblast response. *Journal of Biomedical Materials Research Part A* **2016**, *104*, 3058-3072, doi:10.1002/jbm.a.35850.

62. Discher, D.E.; Janmey, P.; Wang, Y.L. Tissue cells feel and respond to the stiffness of their substrate. *Science (New York, N.Y.)* **2005**, *310*, 1139-1143, doi:10.1126/science.1116995.

63. Vogel, V.; Sheetz, M. Local force and geometry sensing regulate cell functions. *Nature Reviews Molecular Cell Biology* **2006**, *7*, 265-275, doi:10.1038/nrm1890.

64. Lee, H.P.; Gu, L.; Mooney, D.J.; Levenston, M.E.; Chaudhuri, O. Mechanical confinement regulates cartilage matrix formation by chondrocytes. *Nature materials* **2017**, *16*, 1243-1251, doi:10.1038/nmat4993.

65. Sarem, M.; Arya, N.; Heizmann, M.; Neffe, A.T.; Barbero, A.; Gebauer, T.P.; Martin, I.; Lendlein, A.; Shastri, V.P. Interplay between stiffness and degradation of architectured gelatin hydrogels leads to differential modulation of chondrogenesis in vitro and in vivo. *Acta Biomater* **2018**, *69*, 83-94, doi:10.1016/j.actbio.2018.01.025.

66. Mumme, M.; Barbero, A.; Miot, S.; Wixmerten, A.; Feliciano, S.; Wolf, F.; Asnaghi, A.M.; Baumhoer, D.; Bieri, O.; Kretzschmar, M., et al. Nasal chondrocyte-based engineered autologous cartilage tissue for repair of articular cartilage defects: an observational first-in-human trial. *Lancet (London, England)* **2016**, *388*, 1985-1994, doi:10.1016/s0140-6736(16)31658-0.

67. Li, Z.; Yao, S.; Alini, M.; Grad, S. Different response of articular chondrocyte subpopulations to surface motion. *Osteoarthritis and cartilage* **2007**, *15*, 1034-1041, doi:10.1016/j.joca.2007.03.001.

68. Grad, S.; Lee, C.R.; Wimmer, M.A.; Alini, M. Chondrocyte gene expression under applied surface motion. *Biorheology* **2006**, *43*, 259-269.

Chapter 5

Animal Models of Osteochondral Defect for Testing Biomaterials

Xiangbo Meng[1,2], **Reihane Ziadlou[3]**, Sibylle Grad[3], Mauro Alini[3], Chunyi Wen[4], Yuxiao Lai[2], Ling Qin[2,5], Yanyan Zhao[1] and Xinluan Wang[2,5]

[1] College of Pharmaceutical Sciences, Hebei University, Baoding, China

[2] Translational Medicine R&D Center, Institute of Biomedical and Health Engineering, Shenzhen Institutes of Advanced Technology, Chinese Academy of Sciences, Shenzhen, China

[3] AO Research Institute Davos, Clavadelerstrasse 8, 7270 Davos Platz, Switzerland

[4] Department of Biomedical Engineering, Faculty of Engineering, The Hong Kong Polytechnic University, Hung Hom, Kowloon, Hong Kong SAR, China

[5] Musculoskeletal Research Laboratory, Department of Orthopaedics & Traumatology, The Chinese University of Hong Kong, Hong Kong SAR, China

Published in *Biochemistry Research International* **2020** *Jan 28;2020:9659412.*

Abstract

The treatment of osteochondral defects (OCD) remains a great challenge in orthopaedics. Tissue engineering holds a good promise for regeneration of OCD. In the light of tissue engineering, it is critical to establish an appropriate animal model to evaluate the degradability, biocompatibility, and interaction of implanted biomaterials with host bone/cartilage tissues for OCD repair *in vivo*. Currently, model animals that are commonly deployed to create osteochondral lesions range from rats, rabbits, dogs, pigs, goats, and sheep and horses to non-human primates. It is essential to understand the advantages and disadvantages of each animal model in terms of the accuracy and effectiveness of the experiment. Therefore, this review aims to introduce the common animal models of OCD for testing biomaterials and to discuss their applications in translational research. In addition, we have reviewed surgical protocols for establishing OCD models and biomaterials that promote osteochondral regeneration. For small animals, the non-load-bearing region such as the groove of femoral condyle is commonly chosen for testing degradation, biocompatibility, and interaction of implanted biomaterials with host tissues. For large animals, closer to clinical application, the load-bearing region (medial femoral-condyle) is chosen for testing the durability and healing outcome of biomaterials. This review provides an important reference for selecting a suitable animal model for the development of new strategies for osteochondral regeneration.

1.Introduction

Osteochondral defects (OCD) are a common condition caused by severe trauma, sports injuries, or physical diseases, leading to joint pain, deformity, and dysfunction [1]. Joint injuries caused by trauma and sports accidents often progress into osteoarthritis (OA). So, OCD are also a significant cause of OA [2]. OA has been reported to be the third most common musculoskeletal disease in the world [3]. The global prevalence of OA for persons older than 60 years is estimated at 33.6% for women and 24.3% for men [4]. As cartilage has no vasculature and lymphatic vessels and mature chondrocytes have limited proliferation and migration capabilities, cartilage regeneration remains a major challenge. OCD including lesions or degeneration of cartilage, subchondral bone, and bone-cartilage interfaces are notorious for being unable to heal. In order to repair OCD, the tissue complex of bone, cartilage, and bone-cartilage interfaces must be taken into account for repair and regeneration [5, 6]. Yet, those OCDs are difficult to treat because the cartilage and the subchondral bone are tissues with

different intrinsic healing capacities. The current clinical treatments for repair of OCD are only palliative rather than curative [7]. The common goal of successful treatments is to relieve pain, repair damaged tissue, and improve joint function [8]. Current methods for treatment of cartilage lesions mainly include medical treatments (nonsteroid anti-inflammatory drugs (NSAIDs), pain killers, and hormones, etc.) and surgical treatment (arthroscopic lavage and debridement, cell-based therapy, and tissue-based therapy) [9]. Unfortunately, the medical treatments only relieve pain, rather than restoring the structural integrity of the articular cartilage [10], and the surgical treatments cannot restore neo-tissue close to normal cartilage [9].Therefore, the treatment effect is not ideal, and the development of new treatment strategies is an urgent need. However, any new treatment strategy must be tested in animals to ensure its safety, feasibility, and effectiveness before clinical testing. It is very important to simulate human symptoms using appropriate animal models before clinical trials. At the same time, animal models are effective for developing OCD repair methods. Therefore, it is crucial to establish a suitable animal model for evaluating the effectiveness and safety of new treatment strategies. In this review, we summarize the benefits and limitations of each species for reproducing specific defects, analyze and compare the similarities between animal models and human clinical conditions, and emphasize the factors that need to be considered when selecting animals.

2. Selection Criteria and Critical Size

2.1. General Selection Criteria

The ideal animal model should be as close to the clinical setting as possible, have biological similarity, and be a suitable model for cartilage physiology [11, 12]. A range of factors must be considered to select an applicable animal model for OCD regeneration. Before selecting an ideal animal model, it is crucial to decide whether a small or large animal model would be suitable for a particular OCD regeneration. The small animal models for OCD regeneration include rats and rabbits [13], while large animal models for OCD repair include dogs, pigs, sheep, goats, and horses [14]. Every animal has its advantages and limitations. When assessing the clinical potential of new strategies, the animal model that most closely represents human anatomy and physiology should be selected [15]. In addition, when investigating articular osteochondral repair in vivo, the factors to be considered include joint size, cartilage thickness,

defect depth and diameter, skeletal maturity age, joint load distribution, and affordability and convenience of animal handling (Table 1) [16–18].

2.2. Critical Size of OCD

The critical size defect is defined as the smallest defect size (in diameter) the animal cannot self- repair without intervention [19]. In animal experiments, the understanding of critical-sized defects is crucial for reducing costs and animal suffering, at the same time still providing reliable data on the research results. So, the critical size of the defect should be considered to select the appropriate animal model for OCD repair. Katagiri et al. found that, in the rat knee, OCD with a diameter of 1.4 mm and a depth of 1.0 mm could not spontaneously recover the osteochondral unit, thus defining the critical size of rat knee osteochondral injury [20], whereby the mean animal weight is about 0.3 kg. The critical-sized defect of the rabbit knee has been defined as 3 mm, which can prevent spontaneous healing [21]. This dimension has, however, been questioned due to reported spontaneous healing [11]. Larger defects with diameters of 4 mm to 5 mm may be more appropriate [22, 23]. For the canine model with a mean weight of about 30 kg, the critical size of the OCD has been considered to be 4 mm [19, 24]. Gotterbarm et al. considered that OCD of 6.3 mm should be defined as the critical-sized defect in the porcine model with a mean weight of about 38 kg [25]. The critical-sized defect in sheep models has been considered to be 7 mm, while its average weight is about 70 kg [11]. In the goat model, 6 mm OCD proved to be unable to heal spontaneously and has been defined as a critical dimension defect, while the average weight is about 48 kg [26, 27]. The critical-sized defects in the equine femoral trochlear and condyle models are considered to be around 9 mm [28, 29]. In addition, Salonius et al. [30] reported 4 mm in diameter as critical osteochondral lesion size in the equine carpal joint model. The horse is the largest animal model for articular cartilage regeneration with an average weight of 400 kg.

3. Small Animal Models

Small animal models are crucial in “proof-of-concept” studies, especially for testing biosafety. In these studies, concepts are validated, and *in vitro* results are first translated *in vivo*. Small animals are inexpensive, easy to handle and feed, and often used to investigate the pathophysiology and pathogenesis of the disease [31]. However, the limitations of small animal models for OCD regeneration consist in the small size of the knee joint and the thin cartilage

thickness [32, 33]. It is therefore difficult to design surgical OCD models suitable for comparison with human conditions.

3.1. Rats

The rat models used for OCD regeneration have several advantages, as rats are inexpensive, easy to handle and house, and clinically more relevant than mice. The skeletal maturity of rats is approximately 7 months [34]. Rats aged between 9 and 12 weeks have been used to evaluate the degradation rate and safety profile of biomaterials, whereby the experimental period of implants generally lasts 8–12 weeks (Table 2). The critical size of rat OCD was defined as 1.4 mm [20]. The cartilage thickness of the medial femoral condyle in rat is around 0.1 mm [11]. Most commonly, OCD of 2.0 mm diameter and 2.0 mm depth on the trochlear groove of the femur have been used for the assessment of biomaterial strategies. However, their small joint size and thin cartilage remain the main limitations for testing of biomaterials in the rat OCD model [20]. Therefore, the rat model seems to be applicable for preliminary *in vivo* evaluation but not for preclinical studies.

3.1.1. Experimental Protocol of Animal Surgeries.

In typical procedures, animals were anaesthetized and shaved, and the knee was disinfected. A medial temporal medial longitudinal incision was made to expose the synovium of the knee joint, and then the trochlear groove was further exposed after the lateral patellar luxation. The defect (1.5–2 mm diameter and 2 mm depth) was drilled in the center of the trochlear groove. The biomaterials were implanted, after irrigating the joint with sterile isotonic saline. Lastly, the patella was relocated, and the wound sutured in layers [40].

3.1.2. Applications of Rat OCD Model for Testing of Osteochondral Repair Materials.

Using a 12-week-old rat model, Lee and Im [35] found that SOX trio-co-transduced adipose tissue derived stem cells (ASCs) in fibrin gel promoted the OCD (2mm diameter and 2mm depth) regeneration and attenuated the progression of OA caused by surgery. Muttigi et al. [36] created an OCD of 2mm diameter and 2mm depth in the patellar groove of the femur. The model was created to assess the effect of matrilin-3 codelivery with ASCs. They found that matrilin-3 codelivery with ASCs enhanced the formation of cartilage tissue and concluded that matrilin-3 may be an attractive biochemical factor that promotes stem cell repair of articular cartilage. Mahmoud et al. [37] used 10-week-old rat to create an OCD model in the femur

patellar groove (2 mm diameter and 2 mm depth) to test the efficacy of multilineage-differentiating stress enduring (Muse) cell transplantation for OCD repair. They found that injection of Muse cells was a promising method to repair an OCD, especially when subchondral bone is covered by fibrous tissue. Dahlin et al. [38] cultured bovine articular chondrocytes with rat mesenchymal stem cells (MSCs) onto electrospun poly(3-caprolactone) (PCL) scaffolds and implanted them into OCD (2mm diameter and 2 mm depth) in the rat trochlear groove. The results showed cocultures of articular chondrocytes and MSCs have the potential to repair cartilage defects *in vivo*. Li et al. [39] combined poly(lactide-coglycolide)/hydroxyapatite (PLGA/ HA) composite scaffolds with MSCs to successfully repair cartilage defects, while these implants may also be valuable for other clinical applications.

Table 1: Comparison of age, cartilage, and defect size in different species.

Species	Age of skeletal maturity	Cartilage thickness	Cartilage volume	Critical-sized defect	Common defect depth
Rat	7 months	0.1 mm	2.17 mm^3	1.4 mm	1.0–2.0 mm
Rabbit	9 months	0.3 mm	53 mm^3	3.0 mm	3.0–5.0 mm
Dog	12-24 months	0.95 mm	82.39 mm^3	4.0 mm	10–12 mm
Pig	18 months	1.5 mm	107.47 mm^3	6.3 mm	8–10 mm
Sheep	2-3 years	0.45 mm	359.54 mm^3	7.0 mm	6–13 mm
Goat	2-3 years	1.1 mm	251.65 mm^3	6.0 mm	6–12 mm
Horse	2-4 years	1.75 mm	334.73 mm^3	4.0 mm/9.0 mm	10 mm
Monkey	10 years [16]	0.5–0.7 mm [17]	—	—	2–4 mm
Human	18–22 years	2.35 mm	552.25 mm^3	—	—

Table 2: Examples of studies using rat osteochondral defect models.

Authors	Age	Defect size (diameter × depth)	Location	Endpoint	Material tested
Lee and Im [35]	12 weeks	2 mm × 2 mm	The trochlear groove of the femur	8 weeks	SOX trio-co-transduced ASCs
Muttigi et al. [36]	12 weeks	2 mm × 2 mm	The center of the groove	12 weeks	Matrilin-3/mesenchymal stem cell
Mahmoud et al. [37]	10 weeks	2 mm × 2 mm	The patellar groove of the femur	4, 12 weeks	Muse cells
Dahlin et al. [38]	10–12 weeks	2 mm × 2 mm	The center of the trochlear groove	4, 8 weeks	PCL scaffold/MSC
Li et al. [39]	12 weeks	1.5 mm × 2 mm	The trochlear groove	6, 12 weeks	PLGA/HA-MSC

3.2. Rabbit.

The rabbit model provides a suitable small animal model for assessing the repair of OCD, as rabbits have larger joints for surgical procedures [41]. The age of skeletal maturity in rabbits is 9 months. Rabbits aged between 3 and 8 months have been used to evaluate the degradation rate and safety of biomaterials, and the experimental period of implants generally lasted 8–24 weeks (Table3).The cartilage of rabbit is relatively thin, showing an average cartilage thickness

of 0.44±0.08 mm for the trochlear groove and 0.3±0.07 mm for the medial femoral condyle [47]. In addition, the subchondral bone of the rabbit trochlea (386±160 μm) is similar to the human medial femoral condyle (213±116μm), and both have a relatively thin bone plate and a more porous and lower density subchondral bone [48]. The relative length of the trochlear groove is greater compared with the human knee joint, which is probably related to the mainly squatting posture of the animal. Besides, the rabbit has faster skeletal change and bone turnover in comparison with other species [49]. Defects have been created in the femoral trochlea [50, 51], the medial femoral condyle [52, 53], and the lateral femoral condyle[54].OCD of 3.0–5.0 mm diameter and 2.0–5.0 mm depth are often used to evaluate biomaterials in rabbit models.

Table 3: Examples of studies using rabbit osteochondral defect models.

Authors	Age/ weight	Defect size (diameter × depth)	Location	Endpoint	Material tested
Liao et al. [42]	2–2.5 kg	4 mm × 3 mm	The trochlear groove	6, 12, and 18 weeks	CSMA/PECA/GO hybrid scaffold
Bauer et al. [43]	8 months	4 mm × 5 mm	The medial trochlear groove	4 and 12 weeks	Hyaluronic acid thioester
Ruan et al. [44]	6 months	4 mm × 3 mm	The medial trochlear groove	4, 8, and 12 weeks	SF/CS/nHA phase scaffold
Meng et al. [45]	4–6 months	4 mm × 2 mm	The trochlear groove	6, 12, and 24 weeks	AMP-E7/BM-MSC
Zhang et al. [46]	2.5–3 kg	4 mm × 4 mm	The patellar groove	6 and 12 weeks	COL-nanofiber and COL scaffolds

3.2.1. Experimental Protocol of Animal Surgeries.

In most studies, the creation of an OCD was based on the following protocol. The rabbits were anaesthetized; then, a medial peripatellar incision was made to expose the knee joint. The patella was dislocated laterally, and the articular surface of the distal femur was exposed. A cylindrical OCD was made using an electrical trephine in the trochlear groove (Fig- ure 1). After irrigating the joint with sterile isotonic saline, the biomaterials were implanted. Lastly, the patella was relocated and the wound sutured in layers [50, 51].

3.2.2. Applications of Rabbit OCD Models for Testing of Osteochondral Repair Materials.

Liao et al. [42] prepared a novel hybrid scaffold composed of methacrylated chondroitin sulfate (CSMA), poly(ethylene glycol) methyl ether-ε-caprolactone-acryloyl chloride (MPEG-PCL-AC, PECA was used as abbreviation for MPEG-PCL-AC), and graphene oxide (GO) and evaluated its application for cartilage regeneration using the rabbit OCD model. Micro- CT and

histological observations showed that the CSMA/ PECA/GO scaffold group had better chondrocyte morphology, integration, and continuous subchondral bone and thicker newly formed cartilage. Bauer et al. [43] used a 4 mm diameter and 5 mm depth rabbit OCD model to test hyaluronic acid thioester to promote articular cartilage regeneration. Ruan et al. [44] synthesized a novel biphasic scaffold, which contained a silk-fibroin/chitosan (SF/CS) and an osteoblastic phase (SF/CS/nHA). Bone marrow derived mesenchymal stem cells (BMSCs) showed high cell viability on this scaffold. This scaffold may be an attractive implant that has potential applications in the treatment of OCD. Meng et al. [45] established a functional scaffold named APM-E7 by conjugating a BMSCs affinity peptide (E7) onto the acellular peritoneum matrix (APM). Then, they established a full-thickness OCD model, 4 mm in diameter and 2 mm in height, in 6-month-old rabbits to test the APM-E7 scaffold. The results showed APM-E7 scaffold could support cell attachment. Zhang et al. [46] fabricated a bilayer microporous scaffold with collagen and electrospun poly-L-lactic acid nanofibers (COL-nanofiber) and applied it in a rabbit OCD model. The results showed that implantation of COL-nanofiber scaffold with cells induced cartilage and subchondral bone formation.

4. Large Animal Models

The large animals, such as goats, sheep, pigs, dogs, and horses, have the advantages of joint size and cartilage thickness and also have the most similar clinical lesions to humans [55]. Although large animals may be closer to human clinical conditions, they require greater logistic, fi- nancial, and ethical considerations. When planning in vivo studies, a multivariate analysis should be performed for each animal model. Ultimately, the scientific goals are crucial for determining the appropriate animal model [31]. According to available reports, the mean volume of human cartilage defects is around 552.25 mm3, and the diameter of human cartilage defects requiring treatment is usually 10 mm or more [56, 57]. However, in common animal models, the cartilage volume and cartilage thickness are smaller than in humans (Table 2) [11, 58].

4.1. Dog.

The dog is considered to be a very friendly and loving partner over the world. The social and ethical issues associated with the use of dogs as preclinical and translational animal models are main reasons for their limited use [14]. Dogs are susceptible to cartilage diseases such as exfoliative osteochondritis and osteoarthritis, and dogs lack the ability to repair cartilage

defects intrinsically [31]. Therefore, using this model to study osteoarthritis may be closer to humans. Dogs are also suitable for studies that require specific sports and rehabilitation protocols. Dog's skeleton mature age is about 12 to 24 months. The thickness of the cartilage on the medial condyle of the dog has been reported to be 0.95 mm [11]. Defects have been located in the femoral trochlea [59], the medial femoral condyle [60], and both condyles concurrently and medial tibial plateau [61]. Defect diameters have ranged from 2 to 10 mm, and 4 mm is the most common one (Table 4).

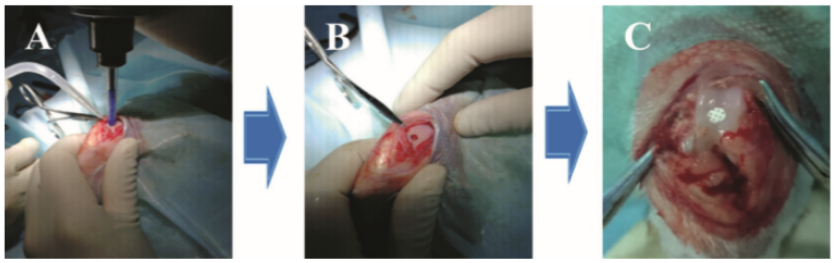

FIGURE 1: The process of the OCD regeneration in rabbits. A: the OCD were generated by electric drill in the femoral patellar groove; B: a 3.2 mm in diameter and 3.0 mm deep OCD was obtained; C: the biomaterial was implanted into the OCD.

TABLE 4: Examples of studies using dog osteochondral defect models.

Authors	Age	Defect size (diameter × depth)	Location	Endpoint	Material tested
Lv and Yu [59]	12 months	6 mm × 12 mm	The right knee joint	12 and 24 weeks	Nano-β-TCP/Col I/Col II/ BMSCs
McCarty et al. [60]	—	4.5 mm × 10 mm	The medial femoral condyle	12 months	Osteochondral allograft
Salkeld et al. [61]	1.6 years	6 mm × 11 mm	The medial femoral condyle and medial tibial plateau surfaces	12, 24, and 52 weeks	Pyrolytic carbon scaffold and Co-Cr alloy scaffold
Yamazoe et al. [62]	1–3 years	5 mm × 4.5 mm	The femoral condyles	2, 4, and 10 weeks	Atelocollagen gel/MSCs

4.1.1. Experimental Protocol of Animal Surgeries.

Dogs were anaesthetized intravenously. The dog was fixed on the operating table in a supine position and the hair was shaved over the knee joint. The operating field was disinfected, and an incision was created in the skin of the knee joint. The knee flexion was approximately 70°; a defect was created in the femoral trochlea, the medial femoral condyle, or condyles concurrently and medial tibial plateau. Scaffolds were implanted, and the wound layer was sutured [59].

4.1.2. Applications of Dog OCD Models for Testing of Osteochondral Repair Materials.

Lv and Yu [59] investigated the articular OCD (6 mm diameter and 12 mm depth) repair using a composite lamellar scaffold of nano-β-tri- calcium phosphate (β-TCP)/collagen (col) I and II with BMSCs in the canine knee joint. The composite lamellar scaffold was gradually degraded

and absorbed, while new cartilage tissue was formed. Salkeld et al. [61] used a 6 mm diameter and 11 mm deep OCD in the medial femoral condyle of the canine knee to test a pyrolytic carbon implant. They found that the pyrolytic carbon as a hemiarthroplasty implant material was superior to cobalt-chromium (Co-Cr) alloy. In addition, pyrolytic carbon implants reduced wear, degradation, and cellular changes at the surface of the tibial cartilage. Yamazoe et al. [62] proposed that autologous transplantation of an atelocollagen gel containing canine-derived mesenchymal stem cells could not promote the repair of canine knee joint but rather the subchondral bone regeneration.

4.2. Pig.

Pigs are considered to be a suitable animal model for mimicking human diseases and have widely been used in biomedical research [63, 64]. The pig joint size, weight requirements, and cartilage thickness are closer to humans than dogs and smaller animal models. In addition, the bone apposition rate and trabecular thickness of the mini-pig are similar to human bones. However, purchase and maintenance of pigs are very expensive. Pigs generally reach skeletal maturity in around 18 months [14]. Fisher et al. [65] reported a cartilage thickness of 1.5 mm at the medial femoral condyle level in mini-pig. Gotterbarm et al. [25] showed that 6.3 mm diameter OCD did not spontaneously heal in mini-pig, confirming the applicability of this pig breed to articular cartilage research. The large majority of the cartilage regeneration studies in the mini-pig are performed on the joint knee, involving the medial [66] or femoral condyles [67, 68], or femoral trochlea. Generally, 6 mm to 8 mm diameter or larger dimensions OCD are created, and the postoperative follow-up period is usually between 3 and 24 months (Table 5).

Table 5: Examples of studies using pig osteochondral defect models.

Authors	Age	Defect size (diameter × depth)	Location	Endpoint	Material tested
Christensen et al. [68]	19.8 months	6 mm × 8 mm	The medial trochlear and the lateral trochlear	6, 24 months	Autologous dual-tissue transplantation/autologous cartilage chips
Betsch et al. [66]	18–30 months	6 mm × 10 mm	The medial femoral condyle	26 weeks	EPO/BMAC/scaffold
Jagodzinski et al. [69]	14 months	7 mm × 10 mm	The medial or lateral femoral condyles	3 months	Bone marrow derived cell concentrates

4.2.1. Experimental Protocol of Animal Surgeries.

After animals were anaesthetized, a 5 cm incision was created in the skin to expose the medial condyle. A cylindrical OCD was created in the knee joint. The implant was placed into the

defect and taken care of to ensure that the scaffold was flushed with the surface of the surrounding articular cartilage. Lastly, the wound was sutured in layers [66].

4.2.2. Applications of Pig OCD Models for Testing of Osteochondral Repair Materials.

Several studies on cartilage and cartilage defects have been reported using min-pig. Christensen and coauthors [68] created OCD of 6 mm diameter and 8 mm depth in the medial trochlear to investigate the role of cartilage chips. They found that the cartilage chips promoted the formation of fibrocartilage rather than fibrous tissue. Betsch et al. [66] found that the combination of erythropoietin (EPO) and bone marrow aspirate concentrate (BMAC) could promote osteochondral healing in mini-pig OCD. Jagodzinski et al. [69] found that stem cell concentrates enhanced the attachment of new bone but did not enhance the mechanical properties and histological appearance of cartilage regenerates in mini-pig OCD models.

4.3. Sheep.

Sheep is one of the commonly used animal models in orthopaedic research. The anatomy of the knee is similar to humans. However, due to the thinness of the cartilage, most of the defects are located in the subchondral bone, and the skeletal maturation is later, representing certain limitations [11]. Sheep aged between 2 and 3 years have been used to evaluate the degradation rate and safety profile of biomaterials, and the experimental period of implants generally lasted for 16–52 weeks. The critical-sized defect has been reported as 7 mm. The cartilage thickness of the medial femoral condyle is approximately 0.45 mm. The location of the cartilage defects in the sheep model has involved the medial femoral condyle [67, 70, 71], both femoral condyles [72, 73], and the femoral trochlea [70]. OCD with a diameter of 6–8 mm and a depth of 5–13 mm were used for the assessment of biomaterial strategies (Table 6).

4.3.1. Experimental Protocol of Animal Surgeries.

The sheep were anaesthetized; then, sheep were placed in dorsal recumbency. The skin on the right knee was sterilized and was ready for sterile surgery. The lateral para-aortic joint was incised to expose the medial and lateral femoral condyles. An ideal OCD was created in the medial and lateral femoral condyles using a suitable drill bit. After irrigating the joint with sterile isotonic saline, the biomaterials were implanted. Lastly, the wound was sutured in layers [72].

Table 6: Examples of studies using sheep osteochondral defect models.

Authors	Age	Defect size (diameter × depth)	Location	Endpoint	Material tested
Schlichting et al. [70]	2 and 3 years	7.3 mm × 10 mm	The femoral condyles	3, 6 months	Stiff scaffold
Bernstein et al. [71]	2–4 year	7 mm × 25 mm	The femoral condyles	6, 12, 26, and 52 weeks	β-TCP/chondrocytes
Mohan et al. [72]	>3.5 years	6 mm × 6 mm	MFCs and LFCs	1 year	PLGA/β-TCP
Yucekul et al. [74]	—	8 mm × 10 mm	The lateral condyles	3, 6 and 12 months	PLLA/PCL/β-TCP
Mrosek et al. [75]	—	8 mm × 13 mm	The medial femoral condyle	16 weeks	Trabecular metal with an autologous periosteum graft

Table 7: Examples of studies using goat osteochondral defect models.

Authors	Age/ weight	Defect size (diameter × depth)	Location	Endpoint	Material tested
Zhang et al. [76]	12 months	6 mm × 8 mm	Knee joint	12, 24 weeks	BMSC-integrated osteochondral scaffolds
van Bergen et al. [77]	4-year-old	6 mm × 6 mm	Knee joint	24 weeks	Demineralized bone matrix
Kon et al. [78]	2-year-old	6 mm × 10 mm	The load-bearing medial femoral condyle	24 weeks	Aragonite-hyaluronate
Sun et al. [79]	22.5 kg	9 mm × 3 mm	The weight bearing area of the medial femoral condyle	24 weeks	Gene enhanced tissue engineering followed mosaicplasty
Pei et al. [80]	—	6 mm × 12 mm	The femoral medial condyle weight-bearing area	12 and 24 weeks	Tissue-engineered osteochondral graft

4.3.2. Applications of Sheep OCD Models for Testing of Osteochondral Repair Materials.

Schlichting et al. [70] created an 8 mm in diameter and 15 mm deep OCD in the femoral condyles of 24 sheep to prove that stiff scaffolds could improve bone and cartilage regeneration. Bernstein et al. [71] indicated that microporous β-TCP scaffolds with chondrocytes were favorable for the treatment of OCD using the sheep model. Mohan et al. [72] compared microfracture and osteochondral methods using microsphere-based gradient plugs in sheep models. They found that gradient scaffolds had better cartilage repair capacity for OCD. Yucekul et al. [74] investigated a biodegradable, tri-layered poly(glycolic acid) mesh/poly(l-lactic acid)-colorant tide- mark layer/collagen type I and ceramic microparticle coated poly(l-lactic acid)-poly(ε-caprolactone) monolith) osteochondral plug indicated for the repair of cartilage defects (8 mm 10 mm) in sheep. The scaffold proved to have a significant positive effect on the healing of osteo- chondral lesions. Mrosek et al. [75] demonstrated that trabecular metal (TM) was a very suitable material for reconstructing bone defects. TM enabled excellent bone ingrowth and rapid integration.

4.4. Goat.

Goats are similar to sheep and are easy to raise and manage. The skeletal maturity of goats is similar to that of sheep, namely, about 2 to 3 years [11]. Goats aged between 2 and 4 years have

been used to evaluate the degradation rate and safety profile of biomaterials, and the experimental period of implants generally lasted for 6–12 months (Table 7). The thickness of cartilage in goat is greater than that in sheep, and the subchondral bone is softer than that in sheep, which renders goats prone to osteochondral bone defects. Goat joints are usually larger than canine joints, and the most common defect size is 6 mm in diameter; this size has been proven to be unable to heal spontaneously. Defects have been created in the femoral trochlea, the medial femoral condyle, the lateral femoral condyle, and the talus [76, 77, 81]. If the limitations of large animal models can be overcome, including higher costs and adequate facility requirements, the goat model is a viable large animal model for cartilage and osteochondral lesions. However, the size of the lesions is still smaller than the human-related clinical diagnosis (Table 7).

4.4.1. Experimental Protocol of Animal Surgeries.

Surgery was performed under general anesthesia via joint surgery. Using retractors with the limb placed at maximal flexion, the implantation site was exposed. Defect was created and an implant was inserted via a surgical tool. The implant reached its final position in a press-fit manner, slightly below the articular surface. The knee capsule and skin were then sutured.

4.4.2. Applications of Goat OCD Models for Testing of Osteochondral Repair Materials.

Goat has been successfully used as a model for OCD to evaluate new implants. Zhang et al. [76] fabricated BMSC-integrated osteochondral scaf- folds that could promote the repair of OCD in goats. van Bergen et al. [77] used a 6 mm OCD in the talus goat model to evaluate the effectiveness of demineralized bone matrix (DBM) with and without platelet-rich plasma (PRP). They found that PRP would further enhance the regenerative capacity of DBM. Kon et al. [78] created critical-sized defects of 6 mm diameter and 10 mm depth in the medial femoral condyle of the knee joint. The defect model was created to test the in vivo effect of aragonite-hyaluronate (Ar-HA) scaffolds. They found that the Ar-HA scaffold might induce cartilage and subchondral bone regeneration. Sun et al. [79] evaluated the efficacy of gene enhanced tissue engineering following mosaicplasty in a goat model. They found that gene enhancement could effectively restore a 9 mm diameter OCD in a goat model. Pei et al. [80] used the goat OCD model and implanted a tissue-engineered osteochondral (TEO) graft to investigate its reparative efficacy. Their results showed that this TEO was a promising substitute biomaterial for osteochondral regeneration.

4.5. Horse.

As horses are robust and long-lived animals, they are suitable models for assessing the repair of superficial cartilage and subchondral bone in chronic injuries in weight-bearing conditions. Similar to humans, the horses suffer from cartilage diseases and have very weak cartilage self-repairing ability [82]. It is reported that the thickness of articular cartilage is 1.75 mm, which is closest to human cartilage thickness (2.35 mm). Cartilage and OCD of 15 to 20 mm can be assessed in horses. In addition, the upright knee joint with large joint size, thick joint cartilage, and fully straightened gait process is closer to the human knee anatomy than the other animal models. The age of skeletal maturity in the horse is 2–4 years. The age of horses used ranges from 2 to 6 years. Defects have been created in the femoral trochlea [83], the medial femoral condyle [84], the lateral trochlear ridge [85], and the medial surface of lateral trochlea of the talus [86]. A 10 mm in diameter and 5 mm–10 mm deep defect has often been created to simulate osteochondral defects. The major disadvantages of equine models include high cost, inconvenient management, and long-term care during and after surgery. High joint load conditions, high prices, and the need for highly specialized facilities limit the use of horse models for researchers (Table 8).

Table 8: Examples of studies using horse osteochondral defect models.

Authors	Age	Defect size (diameter × depth)	Location	Endpoint	Material tested
Seo et al. [83]	3.6 ± 2.3 years	10 mm × 5 mm	The medial condyle	6 months	GT/MSCs/BMP-2/PRP implantation
Bolanos et al. [84]	6 years	11 mm × 10 mm	The middle aspect of medial femoral trochlear ridge	6 months	CDM/CaP
McCarrel et al. [85]	2–5 years	10 mm × 10 mm	The lateral trochlear ridge	4, 12, and 24 months	Biphasic cartilage repair device
Maninchedda et al. [86]	3 years	10 mm × 5 mm	The medial surface of lateral trochlea of talus	6 months	Type II collagen

Table 9: Examples of studies using monkey cartilage or osteochondral defect models.

Authors	Age	Defect size (diameter × depth)	Location	Endpoint	Treatment
Buckwalter et al. [90]	—	3.2 mm × 4 mm	The patella and the medial femoral condyle	8 weeks	Intermittent passive motion (IPM) or cast-immobilization (CI)
Ma et al. [91]	3–5 years old	3.2 mm × 2 mm	Knee joints	24 weeks	MSC-loaded ADM scaffold
Jiang et al. [92]	3–5 years old	3 mm × 2 mm	The surface of distal femurs	24 weeks	Autologous selected chondrogenic clonal MSCs

4.5.1. Experimental Protocol of Animal Surgeries.

Horse was positioned in dorsal recumbence. General anesthesia was maintained and a 5 cm incision made between the middle and medial patellar ligaments. OCD were created using a

power-driven drill. Defect site and joints were flushed with saline solution before implantation. Scaffolds were press-fit implanted into each defect. Wounds were sutured in four layers (joint capsule, deep fascia, superficial fascia, and skin) and a stent bandage was applied over the incision [84].

4.5.2. Applications of Horse OCD Models for Testing of Osteochondral Repair Materials. Bolanos et al. [84] used a horse model to investigate the effect of decellularized cartilage-derived matrix (CDM) scaffolds with a calcium phosphate (CaP) base for the repair of OCD. Seo et al. [83] evaluated the efficacy of a synovial flap and gelatin/β-tri- calcium phosphate (GT) sponge loaded with mesenchymal stem cells (MSCs), bone morphogenetic protein-2 (BMP-2), and platelet-rich plasma (PRP) for repairing of OCD in horses. The results showed that the GT/MSCs/BMP-2/PRP implantation promoted osteochondral regeneration in the equine model. McCarrel et al. [85] used a 10 mm in diameter and 10 mm deep equine model to test a biphasic cartilage repair device (CRD) for feasibility of arthroscopic implantation and long-term repair of OCD. Maninchedda et al. [86] established a 10 mm in diameter and 5 mm deep OCD model in 3-year-old horses, and the defect was filled with chitosan- GP. After 180 days, they found that the implanted chitosan- GP did not cause any important inflammatory reaction and allowed cell growth.

5. Non-human Primate Model

Most animal models differ in biomechanical functions and/ or physiological responses from human, limiting the ability to extrapolate data to clinical practice. The nonhuman primate (NHP) models overcomes many of these limitations, as they have similar genetic, physiological, and behavioral characteristics to humans and can highly mimic human health issues [87, 88]. Some reports have used NHP to study cartilage regeneration. Kagimoto et al. used a monkey model to assess the safety and efficacy of the xenotransplantation of human cartilage progenitor cells. They found that autologous transplantation of cartilage progenitor cells may be effective in repairing elastic cartilage [89]. Buckwalter et al. used skeletally mature cynomolgus monkeys to create 3.2 mm in diameter and 4.0 mm deep osteochondral defects of the articular surfaces of the patella (PA) and the medial femoral condyle (FC) in both knees and then treated them with intermittent passive motion (IPM) or cast-immobilization (CI). However, they found that repair of acute osteochondral damage in primates failed to restore normal articular surfaces within eight weeks [90]. Ma et al. suggested that the chondrogenic

clonal MSC-loaded mon- key acellular dermal matrix (MSC-ADM) scaffold can improve cartilage damage in cynomolgus monkey models and can be used to repair similar human cartilage defects [91]. Jiang et al. made 3 mm in diameter and 2 mm deep cartilage defects on the distal femurs surface of cynomolgus monkeys and treated them with autologous selected chondrogenic clonal MSCs (sC-MSCs). They found that sC-MSCs can effectively improve the healing of cartilage damage in monkey OA induced by collagenase [92] (Table 9). Despite having big similarity to humans, NHP have been seldom utilized in cartilage regeneration research, due to scarcity, high costs, ethical consideration, and high profile in animal welfare and also because these are often unable to provide additional information beyond the aforementioned large animal models.

6. Selecting an Appropriate Animal Model Based on Multiple Factors

The selection of animal models is critical to promote translational research to the clinical application of biomaterials. Generally, small animal models including rats and rabbits are beneficial for early-phase testing, such as testing degradation, biocompatibility, and interaction of implanted biomaterials with host tissues. Because they are economical and easy to handle and have short time for healing (usually 12 weeks for rabbits) [19], large animals are more suitable for late-phase translational research because their articular cartilage structure is much similar to the mechanical load on humans [93, 94]. However, large animal study is often limited by high costs, long duration (at least 24 weeks), or even ethics. For example, it is difficult to obtain ethical permission to use dogs in some countries or districts pertaining to their companion animal status. Multiple factors should be considered for selecting the appropriate animal models to achieve specific study objectives, such as the size and location of the defect, age, study duration, and surgical considerations. Besides scientific evaluation, the choice is also influenced by practical aspects such as ethics, costs, and housing.

7. Conclusion

In this review, we summarize the benefits and limitations of each species for reproducing specific defects, analyze and compare the similarities between animal models and human clinical situations, and emphasize the factors we need to consider when choosing animals. This review provides an important reference for selecting a suitable animal model(s) for the development of new strategies for osteochondral regeneration.

References

[1] C. Deng, J. Chang, and C. Wu, “Bioactive scaffolds for osteochondral regeneration,” Journal of Orthopaedic Trans- lation, vol. 17, pp. 15–25, 2019.

[2] W. Yuk-wai Lee and B. Wang, “Cartilage repair by mesen- chymal stem cells: clinical trial update and perspectives,” Journal of Orthopaedic Translation, vol. 9, pp. 76–88, 2017.

[3] T. Vos, A. D. Flaxman, M. Naghavi, and R. Lozano, “Years lived with disability (YLDs) for 1160 sequelae of 289 diseases and injuries 1990–2010: a systematic analysis for the global burden of disease study 2010,” Lancet, vol. 380, no. 9859, pp. 2163–2196, 2012.

[4] D. Pereira, B. Peleteiro, J. Arau´jo, J. Branco, R. A. Santos, and

E. Ramos, “The effect of osteoarthritis definition on preva- lence and incidence estimates: a systematic review,” Osteo- arthritis and Cartilage, vol. 19, no. 11, pp. 1270–1285, 2011.

[5] C. Deng, H. Zhu, J. Li et al., “Bioactive scaffolds for regen- eration of cartilage and subchondral bone interface,” Thera- nostics, vol. 8, no. 7, pp. 1940–1955, 2018.

[6] D. J. Huey, J. C. Hu, and K. A. Athanasiou, “Unlike bone, cartilage regeneration remains elusive,” Science, vol. 338, no. 6109, pp. 917–921, 2012.

[7] S. P. Nukavarapu and D. L. Dorcemus, “Osteochondral tissue engineering: current strategies and challenges,” Biotechnology Advances, vol. 31, no. 5, pp. 706–721, 2013.

[8] R. A. Magnussen, W. R. Dunn, J. L. Carey, and K. P. Spindler, “Treatment of focal articular cartilage defects in the knee: a systematic review,” Clinical Orthopaedics and Related Re- search, vol. 466, no. 4, pp. 952–962, 2008.

[9] S.-S. Seo, C.-W. Kim, and D.-W. Jung, “Management of focal chondral lesion in the knee joint,” Knee Surgery & Related Research, vol. 23, no. 4, pp. 185–196, 2011.

[10] J. H. Guettler, C. K. Demetropoulos, K. H. Yang, and K. A. Jurist, “Osteochondral defects in the human knee—influence of defect size on cartilage rim stress and load redistribution to surrounding cartilage,” The American Journal of Sports Medicine, vol. 32, no. 6, pp. 1451–1458, 2004.

[11] B. J. Ahern, J. Parvizi, R. Boston, and T. P. Schaer, “Preclinical animal models in single site cartilage defect testing: a sys- tematic review,” Osteoarthritis and Cartilage, vol. 17, no. 6, pp. 705–713, 2009.

[12] Y. Li, S.-K. Chen, L. Li, L. Qin, X.-L. Wang, and Y.-X. Lai, “Bone defect animal models for testing efficacy of bone substitute biomaterials,” Journal of Orthopaedic Translation, vol. 3, no. 3, pp. 95–104, 2015.

[13] A. da Silva Morais, J. M. Oliveira, and R. L. Reis, “Small animal models,” Osteochondral Tissue Engineering, vol. 1059, pp. 423–439, 2018.

[14] I. R. Dias, C. A. Viegas, and P. P. Carvalho, “Large animal models for osteochondral regeneration,” Osteochondral Tissue Engineering, vol. 1059, pp. 441–501, 2018.

[15] M. Rudert, “Histological evaluation of osteochondral defects: consideration of animal models with emphasis on the rabbit, experimental setup, follow-up and applied methods,” Cells Tissues Organs, vol. 171, no. 4, pp. 229–240, 2002.

[16] R. J. Colman, M. A. Lane, N. Binkley, F. H. Wegner, and J. W. Kemnitz, “Skeletal effects of aging in male rhesus monkeys,” Bone, vol. 24, no. 1, pp. 17–23, 1999.

[17] J. Malda, J. C. de Grauw, K. E. M. Benders et al., “Of mice, men and elephants: the relation between articular cartilage thickness and body mass,” PLoS One, vol. 8, no. 2, 2013.

[18] C. J. Moran, A. Ramesh, P. A. Brama, J. M. O’Byrne, F. J. O’Brien, and T. J. Levingstone, “The benefits and limitations of animal models for translational research in cartilage repair,” Journal of Experimental Orthopaedics, vol. 3, no. 1, p. 1, 2016.

[19] J. L. Cook, C. T. Hung, K. Kuroki et al., “Animal models of cartilage repair,” Bone & Joint Research, vol. 3, no. 4, pp. 89–94, 2014.

[20] H. Katagiri, L. F. Mendes, and F. P. Luyten, “Definition of a critical size osteochondral knee defect and its negative effect on the surrounding articular cartilage in the rat,” Osteoarthritis and Cartilage, vol. 25, no. 9, pp. 1531–1540, 2017.

[21] Y.-B. Park, C.-W. Ha, J.-A. Kim et al., “Effect of transplanting various concentrations of a composite of human umbilical cord blood-derived mesenchymal stem cells and hyaluronic acid hydrogel on articular cartilage repair in a rabbit model,” PLoS One, vol. 11, no. 11, Article ID e0165446, 2016.

[22] Y. Du, H. Liu, Q. Yang et al., “Selective laser sintering scaffold with hierarchical architecture and gradient composition for osteochondral repair in rabbits,” Biomaterials, vol. 137, pp. 37–48, 2017.

[23] T. Chen, J. Bai, J. Tian, P. Huang, H. Zheng, and J. Wang, “A single integrated osteochondral in situ composite scaffold with a multi-layered functional structure,” Colloids and Surfaces B: Biointerfaces, vol. 167, pp. 354–363, 2018.

[24] D. Kazemi, K. Shams Asenjan, N. Dehdilani, and H. Parsa, “Canine articular cartilage regeneration using mesenchymal stem cells seeded on platelet rich fibrin,” Bone & Joint Re- search, vol. 6, no. 2, pp. 98–107, 2017.

[25] T. Gotterbarm, S. J. Breusch, U. Schneider, and M. Jung, “The minipig model for experimental chondral and osteochondral defect repair in tissue engineering: retrospective analysis of 180 defects,” Laboratory Animals, vol. 42, no. 1, pp. 71–82, 2008.

[26] T. J. Levingstone, A. Ramesh, R. T. Brady et al., “Cell-free multi-layered collagen-based scaffolds demonstrate layer specific regeneration of functional osteochondral tissue in caprine joints,” Biomaterials, vol. 87, pp. 69–81, 2016.

[27] D. W. Jackson, P. A. Lalor, H. M. Aberman, and T. M. Simon, “Spontaneous repair of full-thickness defects of articular cartilage in a goat model—a preliminary study,” The Journal of Bone and Joint Surgery-American Volume, vol. 83, no. 1, pp. 53–64, 2001.

[28] A. J. Nixon, E. Rickey, T. J. Butler, M. S. Scimeca, N. Moran, and G. L. Matthews, “A chondrocyte infiltrated collagen type I/III membrane (MACI implant) improves cartilage healing in the equine patellofemoral joint model,” Osteoarthritis and Cartilage, vol. 23, no. 4, pp. 648–660, 2015.

[29] C. W. McIlwraith, L. A. Fortier, D. D. Frisbie, and A. J. Nixon, “Equine models of articular cartilage repair,” Cartilage, vol. 2, no. 4, pp. 317–326, 2011.

[30] E. Salonius, L. Rieppo, M. J. Nissi et al., “Critical-sized cartilage defects in the equine carpus,” Connective Tissue Re- search, vol. 60, no. 2, pp. 95–106, 2019.

[31] C. R. Chu, M. Szczodry, and S. Bruno, “Animal models for cartilage regeneration and repair,” Tissue Engineering Part B Reviews, vol. 16, no. 1, pp. 105–115, 2010.

[32] C. A. Vilela, C. Correia, J. M. Oliveira, R. A. Sousa, J. Espregueira-Mendes, and R. L. Reis, “Cartilage repair using hydrogels: a critical review of in vivo experimental designs,” ACS Biomaterials Science & Engineering, vol. 1, no. 9, pp. 726–739, 2015.

[33] A. M. McCoy, “Animal models of osteoarthritis: comparisons and key considerations,” Veterinary Pathology, vol. 52, no. 5, pp. 803–818, 2015.

[34] R. X. Fan, H. Gong, R. Zhang, J. Z. Gao, Z. B. Jia, and Y. J. Hu, “Quantification of age-related tissue-level failure strains of rat femoral cortical bones using an approach combining macrocompressive test and microfinite element analysis,” Journal of Biomechanical Engineering-Transactions of the Asme, vol. 138, no. 4, 2016.

[35] J.-M. Lee and G.-I. Im, “SOX trio-co-transduced adipose stem cells in fibrin gel to enhance cartilage repair and delay the progression of osteoarthritis in the rat,” Biomaterials, vol. 33, no. 7, pp. 2016–2024, 2012.

[36] M. S. Muttigi, B. J. Kim, B. Choi et al., “Matrilin-3 codelivery with adipose-derived mesenchymal stem cells promotes articular cartilage regeneration in a rat osteochondral defect model,” Journal of Tissue Engineering and Regenerative Medicine, vol. 12, no. 3, pp. 667–675, 2018.

[37] E. E. Mahmoud, N. Kamei, R. Shimizu et al., “Therapeutic potential of multilineage-differentiating stress-enduring cells for osteochondral repair in a rat model,” Stem Cells Inter- national, vol. 2017,

Article ID 8154569, 8 pages, 2017.

[38] R. L. Dahlin, L. A. Kinard, J. Lam et al., "Articular chondrocytes and mesenchymal stem cells seeded on biodegradable scaffolds for the repair of cartilage in a rat osteochondral defect model," Biomaterials, vol. 35, no. 26, pp. 7460–7469, 2014.

[39] H. Li, Q. Zheng, Y. Xiao, J. Feng, Z. Shi, and Z. Pan, "Rat cartilage repair using nanophase PLGA/HA composite and mesenchymal stem cells," Journal of Bioactive and Compatible Polymers, vol. 24, no. 1, pp. 83–99, 2009.

[40] K.-S. Park, B.-J. Kim, E. Lih et al., "Versatile effects of magnesium hydroxide nanoparticles in PLGA scaffold-mediated chondrogenesis," Acta Biomaterialia, vol. 73, pp. 204–216, 2018.

[41] X. Wang, J. D. Mabrey, and C. M. Agrawal, "An interspecies comparison of bone fracture properties," Bio-Medical Materials and Engineering, vol. 8, no. 1, pp. 1–9, 1998.

[42] J. Liao, Y. Qu, B. Chu, X. Zhang, and Z. Qian, "Biodegradable CSMA/PECA/graphene porous hybrid scaffold for cartilage tissue engineering," Scientific Reports, vol. 5, no. 1, p. 9879, 2015.

[43] C. Bauer, V. Jeyakumar, E. Niculescu-Morzsa, D. Kern, and S. Nehrer, "Hyaluronan thiomer gel/matrix mediated healing of articular cartilage defects in New Zealand white rabbits—a pilot study," Journal of Experimental Orthopaedics, vol. 4, no. 1, p. 14, 2017.

[44] S.-Q. Ruan, L. Yan, J. Deng, W.-L. Huang, and D.-M. Jiang, "Preparation of a biphase composite scaffold and its appli- cation in tissue engineering for femoral osteochondral defects in rabbits," International Orthopaedics, vol. 41, no. 9, pp. 1899–1908, 2017.

[45] Q. Meng, X. Hu, H. Huang et al., "Microfracture combined with functional pig peritoneum-derived acellular matrix for cartilage repair in rabbit models," Acta Biomaterialia, vol. 53, pp. 279–292, 2017.

[46] S. Zhang, L. Chen, Y. Jiang et al., "Bi-layer collagen/micro- porous electrospun nanofiber scaffold improves the osteo- chondral regeneration," Acta Biomaterialia, vol. 9, no. 7, pp. 7236–7247, 2013.

[47] T. Rasanen and K. Messner, "Regional variations of indentation stiffness and thickness of normal rabbit knee articular cartilage," Journal of Biomedical Materials Research, vol. 31, no. 4, pp. 519–524, 1996.

[48] A. Chevrier, A. S. M. Kouao, G. Picard, M. B. Hurtig, and M. D. Buschmann, "Interspecies comparison of subchondral bone properties important for cartilage repair," Journal of Orthopaedic Research, vol. 33, no. 1, pp. 63–70, 2015.

[49] S. Castañeda, R. Largo, E. Calvo et al., "Bone mineral mea- surements of subchondral and trabecular bone in healthy and osteoporotic rabbits," Skeletal Radiology, vol. 35, no. 1, pp. 34–41, 2006.

[50] J. Radhakrishnan, A. Manigandan, P. Chinnaswamy, A. Subramanian, and S. Sethuraman, "Gradient nano-engineered in situ forming composite hydrogel for osteochondral regeneration," Biomaterials, vol. 162, pp. 82–98, 2018.

[51] X. Liu, X. Jin, and P. X. Ma, "Nanofibrous hollow micro- spheres self-assembled from star-shaped polymers as inject- able cell carriers for knee repair," Nature Materials, vol. 10, no. 5, pp. 398–406, 2011.

[52] H. Schmal, J. M. Kowal, M. Kassem et al., "Comparison of regenerative tissue quality following matrix-associated cell implantation using amplified chondrocytes compared to synovium-derived stem cells in a rabbit model for cartilage lesions," Stem Cells International, vol. 2018, Article ID 4142031, 12 pages, 2018.

[53] T. J. Levingstone, E. Thompson, A. Matsiko, A. Schepens, J. P. Gleeson, and F. J. O'Brien, "Multi-layered collagen-based scaffolds for osteochondral defect repair in rabbits," Acta Biomaterialia, vol. 32, pp. 149–160, 2016.

[54] M. Ramallal, E. Maneiro, E. Lopez et al., "Xeno-implantation of pig chondrocytes into rabbit to treat localized articular cartilage defects: an animal model," Wound Repair and Re- generation, vol. 12, no. 3, pp. 337–345, 2004.

[55] B. Schneider-Wald, A. K. von Thaden, and M. L. R. Schwarz, "Defect models for the regeneration of articular cartilage in large animals," Der Orthopaede, vol. 42, no. 4, pp. 242–253, 2013.

[56] E. B. Hunziker, "Articular cartilage repair: basic science and clinical progress. A review of the current

status and prospects," Osteoarthritis and Cartilage, vol. 10, no. 6, pp. 432–463, 2002.

[57] P. S. J. M. Bouwmeester, R. Kuijer, G. N. Homminga, S. K. Bulstra, and R. G. T. Geesink, "A retrospective analysis of two independent prospective cartilage repair studies: autogenous perichondrial grafting versus subchondral drilling 10 years post-surgery," Journal of Orthopaedic Research, vol. 20, no. 2, pp. 267–273, 2002.

[58] D. D. Frisbie, M. W. Cross, and C. W. McIlwraith, "A comparative study of articular cartilage thickness in the stifle of animal species used in human pre-clinical studies com- pared to articular cartilage thickness in the human knee," Veterinary and Comparative Orthopaedics and Traumatology, vol. 19, no. 3, pp. 142–146, 2006.

[59] Y. M. Lv and Q. S. Yu, "Repair of articular osteochondral defects of the knee joint using a composite lamellar scaffold," Bone & Joint Research, vol. 4, no. 4, pp. 56–64, 2015.

[60] E. C. McCarty, R. R. Fader, J. J. Mitchell, R. E. Glenn, H. G. Potter, and K. P. Spindler, "Fresh osteochondral allo- graft versus autograft: twelve-month results in isolated canine knee defects," The American Journal of Sports Medicine, vol. 44, no. 9, pp. 2354–2365, 2016.

[61] S. L. Salkeld, L. P. Patron, J. C. Lien, S. D. Cook, and D. G. Jones, "Biological and functional evaluation of a novel pyrolytic carbon implant for the treatment of focal osteo- chondral defects in the medial femoral condyle: assessment in a canine model," Journal of Orthopaedic Surgery and Research, vol. 11, no. 1, p. 155, 2016.

[62] K. Yamazoe, H. Mishima, K. Torigoe et al., "Effects of ate- locollagen gel containing bone marrow-derived stromal cells on repair of osteochondral defect in a dog," Journal of Vet- erinary Medical Science, vol. 69, no. 8, pp. 835–839, 2007.

[63] L. V. Sondergaard, F. Dagnaes-Hansen, and M. S. Herskin, "Welfare assessment in porcine biomedical research—suggestion for an operational tool," Research in Veterinary Science, vol. 91, no. 3, pp. e1–e9, 2011.

[64] F. J. van der Staay, B. Pouzet, M. Mahieu, R. E. Nordquist, and T. Schuurman, "The d-amphetamine-treated Gottingen miniature pig: an animal model for assessing behavioral effects of antipsychotics," Psychopharmacology, vol. 206, no. 4, pp. 715–729, 2009.

[65] M. B. Fisher, N. S. Belkin, A. H. Milby et al., "Cartilage repair and subchondral bone remodeling in response to focal lesions in a mini-pig model: implications for tissue engineering," Tissue Engineering Part A, vol. 21, no. 3-4, pp. 850–860, 2015.

[66] M. Betsch, S. Thelen, L. Santak et al., "The role of erythropoietin and bone marrow concentrate in the treatment of osteochondral defects in mini-pigs," PLoS One, vol. 9, no. 3, Article ID e92766, 2014.

[67] S. Pilichi, S. Rocca, R. R. Pool et al., "Treatment with embryonic stem-like cells into osteochondral defects in sheep femoral condyles," BMC Veterinary Research, vol. 10, no. 1, p. 301, 2014.

[68] B. B. Christensen, C. B. Foldager, M. L. Olesen, K. C. Hede, and M. Lind, "Implantation of autologous cartilage chips improves cartilage repair tissue quality in osteochondral defects: a study in gottingen minipigs," The American Journal of Sports Medicine, vol. 44, no. 6, pp. 1597–1604, 2016.

[69] M. Jagodzinski, C. Liu, D. Guenther et al., "Bone marrow- derived cell concentrates have limited effects on osteochondral reconstructions in the mini pig," Tissue Engineering Part C: Methods, vol. 20, no. 3, pp. 215–226, 2014.

[70] K. Schlichting, H. Schell, R. U. Kleemann et al., "Influence of scaffold stiffness on subchondral bone and subsequent cartilage regeneration in an ovine model of osteochondral defect healing," The American Journal of Sports Medicine, vol. 36, no. 12, pp. 2379–2391, 2008.

[71] A. Bernstein, P. Niemeyer, G. Salzmann et al., "Microporous calcium phosphate ceramics as tissue engineering scaffolds for the repair of osteochondral defects: histological results," Acta Biomaterialia, vol. 9, no. 7, pp. 7490–7505, 2013.

[72] N. Mohan, V. Gupta, B. P. Sridharan et al., "Microsphere- based gradient implants for osteochondral regeneration: a long-term study in sheep," Regenerative Medicine, vol. 10, no. 6, pp. 709–728, 2015.

[73] M. Caminal, D. Peris, C. Fonseca et al., "Cartilage resurfacing potential of PLGA scaffolds loaded with

autologous cells from cartilage, fat, and bone marrow in an ovine model of osteochondral focal defect," Cytotechnology, vol. 68, no. 4, pp. 907–919, 2016.

[74] A. Yucekul, D. Ozdil, N. H. Kutlu, E. Erdemli, H. M. Aydin, and M. N. Doral, "Tri-layered composite plug for the repair of osteochondral defects: in vivo study in sheep," Journal of Tissue Engineering, vol. 8, 2017.

[75] E. H. Mrosek, H.-W. Chung, J. S. Fitzsimmons, S. W. O'Driscoll, G. G. Reinholz, and J. C. Schagemann, "Porous tantalum biocomposites for osteochondral defect repair: a follow-up study in a sheep model," Bone & Joint Research, vol. 5, no. 9, pp. 403–411, 2016.

[76] T. Zhang, H. Zhang, L. Zhang et al., "Biomimetic design and fabrication of multilayered osteochondral scaffolds by low- temperature deposition manufacturing and thermal-induced phase-separation techniques," Biofabrication, vol. 9, no. 2, Article ID 025021, 2017.

[77] C. J. A. van Bergen, G. M. M. J. Kerkhoffs, M. Özdemir et al., "Demineralized bone matrix and platelet-rich plasma do not improve healing of osteochondral defects of the talus: an experimental goat study," Osteoarthritis and Cartilage, vol. 21, no. 11, pp. 1746–1754, 2013.

[78] E. Kon, G. Filardo, J. Shani et al., "Osteochondral regeneration with a novel aragonite-hyaluronate biphasic scaffold: up to 12- month follow-up study in a goat model," Journal of Orthopaedic Surgery and Research, vol. 10, no. 1, p. 81, 2015.

[79] J. Sun, X.-K. Hou, and Y.-X. Zheng, "Restore a 9 mm diameter osteochondral defect with gene enhanced tissue engineering followed mosaicplasty in a goat model," Acta Orthopaedica et Traumatologica Turcica, vol. 50, no. 4, pp. 464–469, 2016.

[80] Y. Pei, J.-J. Fan, X.-Q. Zhang, Z.-Y. Zhang, and M. Yu, "Repairing the osteochondral defect in goat with the tissue- engineered osteochondral graft preconstructed in a double- chamber stirring bioreactor," BioMed Research International, vol. 2014, Article ID 219203, 11 pages, 2014.

[81] A. He, L. Liu, X. Luo et al., "Repair of osteochondral defects with in vitro engineered cartilage based on autologous bone marrow stromal cells in a swine model," Scientific Reports, vol. 7, no. 1, p. 40489, 2017.

[82] T. G. Koch and D. H. Betts, "Stem cell therapy for joint problems using the horse as a clinically relevant animal model," Expert Opinion on Biological Therapy, vol. 7, no. 11, pp. 1621–1626, 2007.

[83] J.-P. Seo, Y. Kambayashi, M. Itho et al., "Effects of a synovial flap and gelatin/beta-tricalcium phosphate sponges loaded with mesenchymal stem cells, bone morphogenetic protein-2, and platelet rich plasma on equine osteochondral defects," Research in Veterinary Science, vol. 101, pp. 140–143, 2015.

[84] R. A. V. Bolanos, S. M. Cokelaere, J. M. E. McDermott et al., "The use of a cartilage decellularized matrix scaffold for the repair of osteochondral defects: the importance of long-term studies in a large animal model," Osteoarthritis and Cartilage, vol. 25, no. 3, pp. 413–420, 2017.

[85] T. M. McCarrel, S. L. Pownder, S. Gilbert et al., "Two-year evaluation of osteochondral repair with a novel biphasic graft saturated in bone marrow in an equine model," Cartilage, vol. 8, no. 4, pp. 406–416, 2017.

[86] U. Maninchedda, O. M. Lepage, M. Gangl et al., "Development of an equine groove model to induce metacarpophalangeal osteoarthritis: a pilot study on 6 horses," PLoS One, vol. 10, no. 2, Article ID e0115089, 2015.

[87] I. Messaoudi and D. K. Ingram, "Overview of aging research using nonhuman primate models," Age, vol. 34, no. 5, pp. 1047–1049, 2012.

[88] R. M. Anderson and R. J. Colman, "Prospects and perspectives in primate aging research," Antioxidants & Redox Signaling, vol. 14, no. 2, pp. 203–205, 2011.

[89] S. Kagimoto, T. Takebe, S. Kobayashi et al., "Auto- transplantation of monkey ear perichondrium-derived pro- genitor cells for cartilage reconstruction," Cell Transplantation, vol. 25, no. 5, pp. 951–962, 2016.

[90] J. A. Buckwalter, J. A. Martin, M. Olmstead, K. A. Athanasiou, M. P. Rosenwasser, and V. C. Mow, "Osteochondral repair of primate knee femoral and patellar articular surfaces: implications for preventing

post-traumatic osteoarthritis," Iowa Orthopedic Journal, vol. 23, pp. 66–74, 2003.

[91] A. Ma, L. Jiang, L. Song et al., "Reconstruction of cartilage with clonal mesenchymal stem cell-acellular dermal matrix in cartilage defect model in nonhuman primates," International Immunopharmacology, vol. 16, no. 3, pp. 399–408, 2013.

[92] L. Jiang, A. L. Ma, L. J. Song et al., "Cartilage regeneration by selected chondrogenic clonal mesenchymal stem cells in the collagenase-induced monkey osteoarthritis model," Journal of Tissue Engineering and Regenerative Medicine, vol. 8, no. 11, pp. 896–905, 2014.

[93] L. Cong, F. A. Ran, D. Cox et al., "Multiplex genome engineering using CRISPR/Cas systems," Science, vol. 339, no. 6121, pp. 819–823, 2013.

[94] I. Tessaro, V. T. Nguyen, A. Di Giancamillo et al., "Animal models for cartilage repair," Journal of Biological Regulators and Homeostatic Agents, vol. 32, no. 6 Suppl. 1, pp. 105–116, 2018.

Chapter 6

General discussion and future prospective

Discussion and perspectives

In this thesis, we aimed to find an effective biological therapy to treat or impede OA and to regenerate damaged articular cartilage. To achieve this goal, inhibition of pro-inflammatory cytokines that are excessively abundant in osteoarthritic joints is necessary [1]. Furthermore, for regeneration of damaged cartilage, it is essential to increase the chondrocytes anabolism for cartilage tissue to recover. Pharmacological therapy and tissue engineering approaches are the two most promising strategies towards cartilage regeneration. Currently, there is no effective pharmacotherapy featuring both anti-inflammatory and anabolic effects to restore the degenerated cartilage in OA or other degenerative joint diseases. Therefore, towards the first aim of this thesis, we used an inflammatory model of human OA chondrocytes microtissues, in which after screening of 34 herbal compounds with potential anti-inflammatory and anabolic effects, VA, Epi C, PS, PCA, 4-HBA and 5-HMF were selected for further studies (Chapter 2). We selectively identified the mechanism of action of VA and Epi C, as they appeared the most potent in terms of promoting ECM deposition and up regulating chondrogenic marker genes. Our results indicated that VA had significant anti-inflammatory effects through inhibition of IKK complex in NF-κB signaling and Epi C showed a significant anabolic effect by increasing the expression of collagenous and non-collagenous matrix proteins (Chapter 3). Additionally, we developed a tunable and injectable hydrogel for drug delivery and cartilage tissue engineering by crosslinking different concentrations of HA-Tyramine (HA-Tyr) with aqueous Silk-fibroin (SF) solutions (Chapter 4).

The small molecules used in this thesis were extracted from the over-the-counter XLGB formula which is used for the treatment of osteoporosis and osteoarthritis and a recent clinical study showed both efficacy and safety of XLGB herbal formula for treatment of OA [2-4]. XLGB is composed of six species of herbs containing various molecular compounds. We showed that VA, Epi C, PS, PCA, 4-HBA and 5-HMF were the most potent compounds existing in this formula in terms of anti-inflammatory and anabolic effects on human OA chondrocytes (Chapter 2). In the past years, the interest in herbal medicines and nutraceuticals has grown. However, an investigation on the pharmacokinetic and oral bioavailability of complex *herba Epimedii* extracts (the origin of the small molecule Epi C) in comparison with the single compound (Epi C) showed that if the drug was administered as a pure compound, its effect was about four-fold higher than that of the complex *herba Epimedii* extracts [5]. So, the oral

bioavailability of Epi C in *herba Epimedii* extract might be affected by the other herbal ingredients suppressing Epi C absorption from the gastrointestinal system or through competitive binding to the related receptors by compounds that are less efficient than Epi C. These results highlight the importance of discovering the most potent compounds in the complex herbal extracts towards having a potent drug whose effects are not masked by other compounds in the herbal mixture. Furthermore, optimization of a local drug delivery system can be more easily achieved for a single or combination of the most potent compounds. Since most of the tested compounds in our study are novel in the orthopedic field, their dose in our study was selected based on reported concentrations of similar herbal compounds that showed an optimal dose between 1 μM and 50 μM [6-10]. Nevertheless, these concentrations are too high to be effective for systemic pharmacotherapy applications and additional studies will be required to identify the optimal dose for each single drug.

To develop an *ex vivo* inflammatory model, we used inflammatory cytokines (IL-1β and TNF-α) on microtissues of human primary chondrocytes. IL-1β and TNF-α are the two most critical inflammatory cytokines for initiation and progression of OA and RA. They act by suppressing the expression of genes related to the differentiated chondrocyte phenotype, including COL2A1 and ACAN and by activating different signaling pathways such as NF-κB, HMGB1, IL-1R/TLR, MAPKs and PI3K/Akt [11-15]. Therefore, our model was suitable for testing the potential of small molecules to modulate the activation of these pathways and targeting these signaling pathways with small molecules, could provide a successful therapy for OA. However, by using IL-1β/TNF-α as inflammatory cytokines, our microtissue model resembled post-traumatic acute inflammation which is not the exact representative condition in OA characterized by chronic inflammation. Furthermore, in early and end stage OA, mild to moderate inflammation of synovial membrane is existing which was not implemented in our *in vitro* inflammatory model [16,17]. Therefore, towards development of a more clinically relevant model, the effect of the compounds in presence of osteoarthritic synovial cells or macrophages, which are infiltrated in inflammatory conditions into the synovial membrane, should be evaluated [18]. Moreover, there is an inter-donor variability in response to the inflammation and the treatment with drugs which could be due to the different types and stages of OA in primary chondrocytes. Also, in our screening study (Chapter 2), we used the compounds after induction of acute inflammation in phase III which is not the most relevant model for investigating the

anti-inflammatory effects of the drugs. Therefore, in further studies (Chapter 3), the selected compounds were added simultaneously with the inflammatory cytokines to evaluate the inhibitory effects of the compounds in our *in vitro* inflammatory model. To investigate the mechanism of action of VA, Epi C, PS, PCA, 4-HBA and 5-HMF in inhibition of inflammation and regeneration of the cartilage, RNA sequencing, gene expression and ELISA analyses confirmed that several pro-inflammatory cytokines, which are naturally abundant in arthritic joints, were significantly down-regulated. Additionally, in the treatment groups with VA and Epi C, the genes responsible for the ECM protein synthesis were significantly up-regulated, while the MMP activity was significantly suppressed, indicating anabolic and anti-catabolic effects of VA and Epi C. The upregulation of TIMP1 as a strong inhibitor of MMPs in the treatment group with VA supported its significant inhibitory effect on MMPs. Therefore, we selected these two most potent compounds (VA, Epi C) for the pathway analysis (Chapter 3). RNA-sequencing and IPA showed that besides COL2A1 and ACAN, GDF5, COMP and CCN2 were significantly up-regulated in the treatment group with Epi C. All the mentioned collagenous and non-collagenous proteins are crucial components of the cartilage ECM that provide structural and functional properties [19-21]. Furthermore, after treatment with VA, signaling pathways involved in initiation of OA which were correlated with canonical NF-κB pathway were inhibited. NF-κB regulates the expression of genes involved in inflammatory response, and several studies have shown that inhibition of the canonical NF-κB pathway can decrease the pathogenesis of OA [22,23]. Therefore, after treatment with VA, the expression of inflammatory cytokines including IL1-β, TNF and INF-γ were significantly inhibited. With immunoblotting assay, we demonstrated that after induction of inflammation in human OA chondrocytes and activation of NF-κB pathway, the simultaneous treatment with VA had inhibitory effects on IKK complex (inhibiting IKK-β subunit) resulting in inhibition of IκB protein phosphorylation. Yin *et al.* also showed that anti-inflammatory small molecules such as Aspirin® or sodium salicylate specifically inhibit IKK-β activity. The mechanism of Aspirin® or sodium salicylate in inhibition of IKK is due to binding of these compounds to IKK-β and competition with ATP binding [24]. VA, which is the extract of *Radix et Rhizoma Salviae*, has a molecular structure similar to salicylates; we therefore predict that this compound may be acting by binding to the IKK-α, IKK-β and competing with ATP binding which subsequently result in inhibition of P-IκBα (Chapter 3).

However, due to the complexity of the different signaling pathways and their interconnections with each other, the exact intervention of the drug with the target often remains undefined. The classical approaches including inhibition at the level of chemokines/cytokines and receptors with small molecules or antibodies are often insufficient interventions, since they block one ligand or receptor, while the associated intracellular signals remain active due to other present ligands or receptors. Therefore, targeting the kinase activity is one of the most novel and effective strategies in inhibition of inflammatory response with promising effects [25,26]. Nevertheless, many kinases are involved in several signaling pathways which creates concerns regarding undesired side effects of the inhibition of kinases [27]. So, specificity of the drug in terms of inhibition of kinases in pathways involved in the activation and release of pro-inflammatory mediators is of great importance. Furthermore, local drug delivery to the OA joint is another strategy to prevent systemic side effects.

To achieve this, we developed tunable and injectable hydrogels for drug delivery and cartilage tissue engineering through crosslinking of different concentrations of HA-Tyramine (HA-Tyr) with aqueous Silk-fibroin (SF) solutions (Chapter 4). Anti-inflammatory properties accredited to HA and SF materials make them advantageous to serve as a delivery system for either small molecules or cells for cartilage regeneration [28,29]. Furthermore, these materials are biodegradable and biocompatible, whereby SF shows a much lower degradation rate compared with HA, which makes it suitable for the long-term drug release in OA joints [30]. However, due to the slow gelation of SF upon the enzymatic crosslinking, clinical drug delivery and cell-laden applications are considered impractical. Therefore, by combining SF and HA-Tyr, we can preserve the superior properties of both hydrogels, while diminishing the limitations of both components. When VA and Epi C were separately encapsulated in SF/HA composite hydrogels, we observed that the release of VA was generally slower compared with Epi C. But, due to the much lower molecular weight of VA and thus increased diffusion kinetics, the slower release of VA compared with Epi C was controversial. However, with the gels being formed by crosslinking between phenol groups of tyramine and tyrosine, it is possible that crosslinking of the VA phenol group with the hydrogel occurs as well. Epi C also has ring structures, but their 3D conformation would result in more steric hinderance, mostly preventing such drug-hydrogel interactions. Therefore, to prevent the covalent reaction between VA and tyramine or tyrosine, encapsulating VA in microparticles that can be added to SF/HA precursor hydrogels could be

considered for further studies. This approach could minimize VA-hydrogel interaction during crosslinking and potentially allow for a sustained VA release. Also, the enzymatic crosslinking and the mechanical properties of the hydrogels after addition of microparticles to the hydrogels should be investigated, as the presence of microparticles most likely affects both parameters. Furthermore, due to the presence of hyaluronidase and proteinase in native tissue, the degradation rate and therefore the release profile of the hydrogels can be different from *in vitro* studies. Therefore, for evaluation of the degradation rate and the drug release with an optimal concentration, further *in vivo* studies are essential. We also showed that the duration of gelation was very tunable and related to the HA and SF ratio, whereby with increasing the concentrations of HA, faster gelation could be achieved. Therefore, the crosslinking kinetics of HA and SF materials was different and HA20/SF80 showed the most relevant gelation time after mixing precursors with HRP and H_2O_2 (3 minutes), making it suitable for clinical applications [31].

Additionally, for regeneration of damaged cartilage, a hydrogel which can support the ECM matrix production is of great interest. To evaluate the effect of hydrogel composition and stiffness on the ECM deposition, a high density (20 x 10^6 cells/mL) of bovine chondrocytes were embedded in enzymatically crosslinked HA/SF composites or HA-Tyr hydrogels. Previous studies with high density cell-laden SF hydrogels showed that such hydrogels were favorable for the redifferentiation of culture-expanded chondrocytes and ECM deposition [32]. We showed that in the presence of 0.01% H_2O_2 and with a high chondrocyte density, more than 90% of the chondrocytes cultured in chondrogenic medium were viable in all hydrogels. This high cell viability verified a proper diffusion of nutrition, providing a favorable environment for the metabolism of the chondrocytes. Additionally, HA100/SF0 and HA20/SF80 composite hydrogels could promote re-differentiation of the chondrocytes by preserving the chondrogenic phenotype. The expression of chondrogenic marker genes (COL2a1, ACAN and COMP) in all chondrocyte-laden constructs was up-regulated compared with day 0 control, with up-regulation being significantly higher in HA20/SF80 hydrogels in both chondrogenic and chondro-permissive media. The expression of pro-inflammatory marker genes (MMP1 and IL-6) was down-regulated compared with day 0 control, which supports the anti-inflammatory properties of SF and HA based hydrogels as was reported previously. Furthermore, the ECM matrix deposition was increased in all hydrogels over 28 days of culture with the most significant increase for HA20/SF80 hydrogels as characterized by Safranin-O staining. The

unconfined compressive properties showed that compressive modulus for the HA20/SF80 chondrocyte-laden constructs was significantly increased over 28 days of culture in chondrogenic medium reaching the same value as explanted cartilage tissues in previous studies [33]. This higher amount of compressive modulus was not only due to the superior matrix deposition in HA20/SF80 hydrogels, but also due to the intrinsic features of the HA/SF hydrogels which were getting stiffer over-time due to the formation of β-sheets in SF [34,35].

Also, it is known that adherent cells like chondrocytes, sense viscoelasticity of their surrounding environment and the stiffness of the matrix can influence contractility and spreading of the cells [36]. Therefore, there is a feedback loop of physical and biochemical signals in response to the elasticity of the extracellular microenvironment which influences cell fate and morphology [37]. In this study we showed for the first time that HA20/SF80, could provide the most adequate environment for the chondrocytes to re-differentiate and deposit ECM to reach mechanical and biological properties similar to native cartilage. Furthermore, Lee *et al.* showed that in fast relaxing hydrogels that dissipate elastic stresses more quickly, chondrocytes tend to form interconnected regions of ECM, while in slow relaxing hydrogels, elastic stresses restrict cell movement and growth which limits chondrocyte matrix production [38]. In this study, we observed that in the cell-laden hydrogels from day 1 to day 7 in HA100/SF0 and HA20/SF80 hydrogels, the percentage of the stress relaxation was significantly increased which was due to the matrix deposition in the hydrogels. On the other hand, in HA10/SF90 hydrogels, the percentage of stress relaxation from day 1 was high, allowing the cells to spread and to de-differentiate towards fibroblastic morphology and the matrix deposition was subsequently diminished in these hydrogels. These results highlight the impact of controlled change of hydrogel mechanical properties over the culture period on cell proliferation and fate. In this regard, HA100/SF0 and HA20/SF80 show suitable moderate elastic properties in the initial phase of the cell culture that diminish over time. However, HA100/SF0 hydrogels were very fast degradable and these hydrogels were degraded over the period of culture, while composite hydrogels remained intact till the end of culture period at 28 days. It has been shown that scaffolds more resistant to degradation support the matrix production by chondrocytes for a longer period, making them suitable for *ex vivo* and *in vivo* applications [39] (Chapter 4).

Several previous studies showed that mechanical stimulation is necessary for promoting the ECM production in articular chondrocytes, nasal chondrocytes or mesenchymal stem cells (MSCs) [40-44]. Since our hydrogels showed proper mechanical properties in withstanding the mechanical loads, the mechanobiology of the different sources of cells encapsulated in the HA20/SF80 hydrogels in response to the mechanical compression and shear should be evaluated in future experiments by a cartilage bioreactor system as has been established by our group [45].

Using articular chondrocytes for autologous chondrocyte implantation encounters several limitations including donor site morbidity caused by cartilage harvesting [46].
Therefore, chondroprogenitor cells like MSCs have been proposed as alternative therapies. However, due to the heterogeneity of the MSCs population and development of hypertrophic phenotype, the clinical applications of MSCs have been limited [47,48]. Therefore, chondrocytes from other sources including nasal chondrocytes have been considered as candidates for cartilage tissue engineering approaches [49-51]. Previous clinical trials in post-traumatic cartilage lesions confirmed the feasibility and safety of the nasal chondrocytes implantation procedure [50]. Recent studies confirmed the possibility of using nasal chondrocytes in OA patients which not only could maintain the chondrogenic phenotype but also showed some anti-inflammatory effects. However, abundance of pro-inflammatory cytokines in the OA joint, necessitates the addition of other anti-inflammatory and anabolic compounds locally in the joint beside treatment with nasal chondrocytes. Therefore, in future studies, the effect of small molecules (VA and Epi C) on an *ex vivo* inflammatory model of nasal chondrocytes encapsulated in the HA20/SF80 hydrogels in a cartilage bioreactor system could be evaluated.
However, it was shown before that high donor variability in response to our inflammatory model and exposure to herbal small molecules should be considered. Therefore, identification of biomarkers to categorize the donors as 'responders' or 'non-responders' is important before testing new treatments *in vitro* or *ex vivo*. Therefore, as part of personalized medicine, a method should be developed to predict the outcome of treatment and reduce the risks of treatment failure.
Furthermore, development of an *in vivo* model of OA or osteochondral defect (OCD) for testing the injectable drug loaded or cell-laden hydrogels is envisioned. Primarily, the degradation rate, biocompatibility and the integration of the hydrogels with the host cartilage tissue should be

evaluated in small animal models like rats or rabbits. For further studies related to inflammatory OA or OCD, large animal models including sheep, pigs and horses are considered, due to the similarities of their articular cartilage structure to human which is more clinically relevant to the mechanical load on human joints (Chapter 5).

Also, due to the similarities between intervertebral disc nucleus pulposus (NP) cells and chondrocytes, several drugs which have shown anti-inflammatory or regenerative potential on cartilage have shown similar effects on intervertebral disc tissue [52]. Therefore, the effect of the hydrogel drug loaded VA and Epi C should be further investigated *in vitro* on NP cells and *ex vivo* on inflammatory disc tissue organ culture model [53].

Conclusions

In this thesis, we introduced novel small molecules with anti-inflammatory and anabolic effects for inhibition of inflammation and regeneration of damaged cartilage in OA joints. For this respect, after screening of 34 herbal compounds in an inflammatory model using human OA chondrocytes microtissues, VA, Epi C, PS, PCA, 4-HBA and 5-HMF showed anti-inflammatory and anti-catabolic effects and could inhibit further matrix degradation after induction of inflammation.

Furthermore, the selected compounds were assessed for their capacity to modulate the key catabolic and anabolic factors using several molecular analyses. After identification of the anti-inflammatory and anabolic properties of VA and Epi C, we selectively investigated the mechanism of action of these two most potent compounds. The IPA showed that in both treatment groups, osteoarthritic signaling pathways were inhibited. In the treatment group with VA, NF-κB signaling was inhibited through inhibition of IKK complex and attenuation of phosphorylation. Epi C showed a significant anabolic effect by increasing the expression of collagenous and non-collagenous matrix proteins. VA and Epi C with significant anti-inflammatory and anabolic properties could be potentially used in combination to treat or prevent joint OA. We also developed a tunable and injectable hydrogel to have a local drug delivery for VA and Epi C for regeneration of damaged cartilage. After enzymatic crosslinking of different concentrations of SF an HA, HA20/SF80 hydrogel showed the longest and the most sustained release profile for VA and Epi C over time, which is necessary for the long treatment

duration for OA joints. Also, we showed superior ECM production in HA20/SF80 chondrocyte-laden constructs. For future studies, to achieve a successful therapy, the combination of all mentioned approaches in an *ex vivo* cartilage organ culture model and in small and large animal models is envisioned.

References

1. Goldring, M.B.; Otero, M. Inflammation in osteoarthritis. *Curr Opin Rheumatol* **2011**, *23*, 471-478, doi:10.1097/BOR.0b013e328349c2b1.

2. Zhu, H.M.; Qin, L.; Garnero, P.; Genant, H.K.; Zhang, G.; Dai, K.; Yao, X.; Gu, G.; Hao, Y.; Li, Z., et al. The first multicenter and randomized clinical trial of herbal Fufang for treatment of postmenopausal osteoporosis. *Osteoporos Int* **2012**, *23*, 1317-1327, doi:10.1007/s00198-011-1577-2.

3. Wang, L.; Li, Y.; Guo, Y.; Ma, R.; Fu, M.; Niu, J.; Gao, S.; Zhang, D. Herba Epimedii: An Ancient Chinese Herbal Medicine in the Prevention and Treatment of Osteoporosis. *Curr Pharm Des* **2016**, *22*, 328-349, doi:10.2174/1381612822666151112145907.

4. Wang, F.; Shi, L.; Zhang, Y.; Wang, K.; Pei, F.; Zhu, H.; Shi, Z.; Tao, T.; Li, Z.; Zeng, P., et al. A Traditional Herbal Formula Xianlinggubao for Pain Control and Function Improvement in Patients with Knee and Hand Osteoarthritis: A Multicenter, Randomized, Open-Label, Controlled Trial. *Evid Based Complement Alternat Med* **2018**, *2018*, 1827528, doi:10.1155/2018/1827528.

5. Lee, C.J.; Wu, Y.T.; Hsueh, T.Y.; Lin, L.C.; Tsai, T.H. Pharmacokinetics and oral bioavailability of epimedin C after oral administration of epimedin C and Herba Epimedii extract in rats. *Biomed Chromatogr* **2014**, *28*, 630-636, doi:10.1002/bmc.3081.

6. Csaki, C.; Mobasheri, A.; Shakibaei, M. Synergistic chondroprotective effects of curcumin and resveratrol in human articular chondrocytes: inhibition of IL-1beta-induced NF-kappaB-mediated inflammation and apoptosis. *Arthritis research & therapy* **2009**, *11*, R165, doi:10.1186/ar2850.

7. Zeng, L.; Wang, W.; Rong, X.F.; Zhong, Y.; Jia, P.; Zhou, G.Q.; Li, R.H. Chondroprotective effects and multi-target mechanisms of Icariin in IL-1 beta-induced human SW 1353 chondrosarcoma cells and a rat osteoarthritis model. *Int Immunopharmacol* **2014**, *18*, 175-181, doi:10.1016/j.intimp.2013.11.021.

8. Kankala, R.K.; Lu, F.J.; Liu, C.G.; Zhang, S.S.; Chen, A.Z.; Wang, S.B. Effect of Icariin on Engineered 3D-Printed Porous Scaffolds for Cartilage Repair. *Materials (Basel)* **2018**, *11*, doi:10.3390/ma11081390.

9. Wang, P.; Zhang, F.; He, Q.; Wang, J.; Shiu, H.T.; Shu, Y.; Tsang, W.P.; Liang, S.; Zhao, K.; Wan, C. Flavonoid Compound Icariin Activates Hypoxia Inducible Factor-1alpha in Chondrocytes and Promotes Articular Cartilage Repair. *PLoS One* **2016**, *11*, e0148372, doi:10.1371/journal.pone.0148372.

10. Cao, H.J.; Li, C.R.; Wang, L.Y.; Ziadlou, R.; Grad, S.; Zhang, Y.; Cheng, Y.; Lai, Y.X.; Yao, X.S.; Alini, M., et al. Effect and mechanism of psoralidin on promoting osteogenesis and inhibiting adipogenesis. *Phytomedicine* **2019**, *61*, 152860, doi:10.1016/j.phymed.2019.152860.

11. van Loo, G.; Beyaert, R. Negative regulation of NF-kappaB and its involvement in rheumatoid arthritis. *Arthritis research & therapy* **2011**, *13*, 221, doi:10.1186/ar3324.

12. Kumar, S.; Boehm, J.; Lee, J.C. p38 MAP kinases: key signalling molecules as therapeutic targets for inflammatory diseases. *Nat Rev Drug Discov* **2003**, *2*, 717-726, doi:10.1038/nrd1177.

13. Loeser, R.F. Molecular mechanisms of cartilage destruction in osteoarthritis. *J Musculoskelet Neuronal Interact* **2008**, *8*, 303-306.

14. Kapoor, M.; Martel-Pelletier, J.; Lajeunesse, D.; Pelletier, J.P.; Fahmi, H. Role of proinflammatory cytokines in the pathophysiology of osteoarthritis. *Nature reviews. Rheumatology* **2011**, *7*, 33-42, doi:10.1038/nrrheum.2010.196.

15. Mariani, E.; Pulsatelli, L.; Facchini, A. Signaling pathways in cartilage repair. *International journal of molecular sciences* **2014**, *15*, 8667-8698, doi:10.3390/ijms15058667.

16. de Lange-Brokaar, B.J.; Ioan-Facsinay, A.; van Osch, G.J.; Zuurmond, A.M.; Schoones, J.; Toes, R.E.; Huizinga, T.W.; Kloppenburg, M. Synovial inflammation, immune cells and their cytokines in osteoarthritis: a review. *Osteoarthritis and cartilage* **2012**, *20*, 1484-1499, doi:10.1016/j.joca.2012.08.027.

17. Sellam, J.; Berenbaum, F. The role of synovitis in pathophysiology and clinical symptoms of osteoarthritis. *Nature reviews. Rheumatology* **2010**, *6*, 625-635, doi:10.1038/nrrheum.2010.159.

18. Scanzello, C.R.; Goldring, S.R. The role of synovitis in osteoarthritis pathogenesis. *Bone* **2012**, *51*, 249-257, doi:10.1016/j.bone.2012.02.012.

19. Hedbom, E.; Antonsson, P.; Hjerpe, A.; Aeschlimann, D.; Paulsson, M.; Rosa-Pimentel, E.; Sommarin, Y.; Wendel, M.; Oldberg, A.; Heinegard, D. Cartilage matrix proteins. An acidic oligomeric protein (COMP) detected only in cartilage. *J Biol Chem* **1992**, *267*, 6132-6136.

20. Xing, X.; Li, Z.; Yu, Z.; Cheng, G.; Li, D.; Li, Z. Effects of connective tissue growth factor (CTGF/CCN2) on condylar chondrocyte proliferation, migration, maturation, differentiation and signalling pathway. *Biochem Biophys Res Commun* **2018**, *495*, 1447-1453, doi:10.1016/j.bbrc.2017.11.190.

21. Fujisawa, T.; Hattori, T.; Ono, M.; Uehara, J.; Kubota, S.; Kuboki, T.; Takigawa, M. CCN family 2/connective tissue growth factor (CCN2/CTGF) stimulates proliferation and differentiation of auricular chondrocytes. *Osteoarthritis and cartilage* **2008**, *16*, 787-795, doi:10.1016/j.joca.2007.11.001.

22. Rigoglou, S.; Papavassiliou, A.G. The NF-κB signalling pathway in osteoarthritis. *The international journal of biochemistry & cell biology* **2013**, *45*, 2580-2584, doi:10.1016/j.biocel.2013.08.018.

23. Roman-Blas, J.A.; Jimenez, S.A. NF-κB as a potential therapeutic target in osteoarthritis and rheumatoid arthritis. *Osteoarthritis and cartilage* **2006**, *14*, 839-848, doi:https://doi.org/10.1016/j.joca.2006.04.008.

24. Yin, M.J.; Yamamoto, Y.; Gaynor, R.B. The anti-inflammatory agents aspirin and salicylate inhibit the activity of I(kappa)B kinase-beta. *Nature* **1998**, *396*, 77-80, doi:10.1038/23948.

25. Kong, D.; Yamori, T. ZSTK474 is an ATP-competitive inhibitor of class I phosphatidylinositol 3 kinase isoforms. *Cancer Sci* **2007**, *98*, 1638-1642, doi:10.1111/j.1349-7006.2007.00580.x.

26. Ghoreschi, K.; Laurence, A.; O'Shea, J.J. Selectivity and therapeutic inhibition of kinases: to be or not to be? *Nat Immunol* **2009**, *10*, 356-360, doi:10.1038/ni.1701.

27. Perkins, N.D. Integrating cell-signalling pathways with NF-kappaB and IKK function. *Nature reviews. Molecular cell biology* **2007**, *8*, 49-62, doi:10.1038/nrm2083.

28. Masuko, K.; Murata, M.; Yudoh, K.; Kato, T.; Nakamura, H. Anti-inflammatory effects of hyaluronan in arthritis therapy: Not just for viscosity. *International journal of general medicine* **2009**, *2*, 77-81.

29. Crivelli, B.; Perteghella, S.; Bari, E.; Sorrenti, M.; Tripodo, G.; Chlapanidas, T.; Torre, M.L. Silk nanoparticles: from inert supports to bioactive natural carriers for drug delivery. *Soft Matter* **2018**, *14*, 546-557, doi:10.1039/c7sm01631j.

30. Vepari, C.; Kaplan, D.L. Silk as a Biomaterial. *Progress in polymer science* **2007**, *32*, 991-1007, doi:10.1016/j.progpolymsci.2007.05.013.

31. Moreira Teixeira, L.S.; Feijen, J.; van Blitterswijk, C.A.; Dijkstra, P.J.; Karperien, M. Enzyme-catalyzed crosslinkable hydrogels: Emerging strategies for tissue engineering. *Biomaterials* **2012**, *33*, 1281-1290, doi:https://doi.org/10.1016/j.biomaterials.2011.10.067.

32. Wang, Y.; Blasioli, D.J.; Kim, H.J.; Kim, H.S.; Kaplan, D.L. Cartilage tissue engineering with silk scaffolds and human articular chondrocytes. *Biomaterials* **2006**, *27*, 4434-4442, doi:10.1016/j.biomaterials.2006.03.050.

33. Patel, J.M.; Wise, B.C.; Bonnevie, E.D.; Mauck, R.L. A Systematic Review and Guide to Mechanical Testing for Articular Cartilage Tissue Engineering. *Tissue engineering. Part C, Methods* **2019**, *25*, 593-608, doi:10.1089/ten.TEC.2019.0116.

34. Nicole R. Raia, B.P.P., Meghan McGill, Erica Palma Kimmerling,; Chiara E. Ghezzi, D.L.K. Enzymatically crosslinked silk-hyaluronic acid hydrogels. *Biomaterials* **2017**, *131*, 58-67.

35. Hasturk, O.; Jordan, K.E.; Choi, J.; Kaplan, D.L. Enzymatically crosslinked silk and silk-gelatin hydrogels with tunable gelation kinetics, mechanical properties and bioactivity for cell culture and encapsulation. *Biomaterials* **2020**, *232*, 119720, doi:https://doi.org/10.1016/j.biomaterials.2019.119720.

36. Discher, D.E.; Janmey, P.; Wang, Y.L. Tissue cells feel and respond to the stiffness of their substrate. *Science (New York, N.Y.)* **2005**, *310*, 1139-1143, doi:10.1126/science.1116995.

37. Vogel, V.; Sheetz, M. Local force and geometry sensing regulate cell functions. *Nature Reviews Molecular Cell Biology* **2006**, *7*, 265-275, doi:10.1038/nrm1890.

38. Lee, H.P.; Gu, L.; Mooney, D.J.; Levenston, M.E.; Chaudhuri, O. Mechanical confinement regulates cartilage matrix formation by chondrocytes. *Nature materials* **2017**, *16*, 1243-1251, doi:10.1038/nmat4993.

39. Sarem, M.; Arya, N.; Heizmann, M.; Neffe, A.T.; Barbero, A.; Gebauer, T.P.; Martin, I.; Lendlein, A.; Shastri, V.P. Interplay between stiffness and degradation of architectured gelatin hydrogels leads to differential modulation of chondrogenesis in vitro and in vivo. *Acta Biomater* **2018**, *69*, 83-94, doi:10.1016/j.actbio.2018.01.025.

40. Candrian, C.; Vonwil, D.; Barbero, A.; Bonacina, E.; Miot, S.; Farhadi, J.; Wirz, D.; Dickinson, S.; Hollander, A.; Jakob, M., et al. Engineered cartilage generated by nasal chondrocytes is responsive to physical forces resembling joint loading. *Arthritis & Rheumatism* **2008**, *58*, 197-208, doi:10.1002/art.23155.

41. Johnstone, B.; Alini, M.; Cucchiarini, M.; Dodge, G.R.; Eglin, D.; Guilak, F.; Madry, H.; Mata, A.; Mauck, R.L.; Semino, C.E., et al. Tissue engineering for articular cartilage repair--the state of the art. *Eur Cell Mater* **2013**, *25*, 248-267, doi:10.22203/ecm.v025a18.

42. Behrendt, P.; Ladner, Y.; Stoddart, M.J.; Lippross, S.; Alini, M.; Eglin, D.; Armiento, A.R. Articular Joint-Simulating Mechanical Load Activates Endogenous TGF-β in a Highly Cellularized Bioadhesive Hydrogel for Cartilage Repair. *The American journal of sports medicine* **2020**, *48*, 210-221, doi:10.1177/0363546519887909.

43. Li, Z.; Yao, S.; Alini, M.; Grad, S. Different response of articular chondrocyte subpopulations to surface motion. *Osteoarthritis and cartilage* **2007**, *15*, 1034-1041, doi:10.1016/j.joca.2007.03.001.

44. Li, Z.; Yao, S.J.; Alini, M.; Stoddart, M.J. Chondrogenesis of human bone marrow mesenchymal stem cells in fibrin-polyurethane composites is modulated by frequency and amplitude of dynamic compression and shear stress. *Tissue engineering. Part A* **2010**, *16*, 575-584, doi:10.1089/ten.TEA.2009.0262.

45. Grad, S.; Gogolewski, S.; Alini, M.; Wimmer, M.A. Effects of simple and complex motion patterns on gene expression of chondrocytes seeded in 3D scaffolds. *Tissue engineering* **2006**, *12*, 3171-3179, doi:10.1089/ten.2006.12.3171.

46. Tuan, R.S. A second-generation autologous chondrocyte implantation approach to the treatment of focal articular cartilage defects. *Arthritis research & therapy* **2007**, *9*, 109, doi:10.1186/ar2310.

47. Whitfield, M.J.; Lee, W.C.; Van Vliet, K.J. Onset of heterogeneity in culture-expanded bone marrow stromal cells. *Stem cell research* **2013**, *11*, 1365-1377, doi:10.1016/j.scr.2013.09.004.

48. Mueller, M.B.; Fischer, M.; Zellner, J.; Berner, A.; Dienstknecht, T.; Prantl, L.; Kujat, R.; Nerlich, M.; Tuan, R.S.; Angele, P. Hypertrophy in Mesenchymal Stem Cell Chondrogenesis: Effect of TGF-β Isoforms and Chondrogenic Conditioning. *Cells Tissues Organs* **2010**, *192*, 158-166, doi:10.1159/000313399.

49. Scotti, C.; Osmokrovic, A.; Wolf, F.; Miot, S.; Peretti, G.M.; Barbero, A.; Martin, I. Response of human engineered cartilage based on articular or nasal chondrocytes to interleukin-1beta and low oxygen. *Tissue engineering. Part A* **2012**, *18*, 362-372, doi:10.1089/ten.TEA.2011.0234.

50. Mumme, M.; Barbero, A.; Miot, S.; Wixmerten, A.; Feliciano, S.; Wolf, F.; Asnaghi, A.M.; Baumhoer, D.; Bieri, O.; Kretzschmar, M., et al. Nasal chondrocyte-based engineered autologous cartilage tissue for repair of articular cartilage defects: an observational first-in-human trial. *Lancet (London, England)* **2016**, *388*, 1985-1994, doi:10.1016/s0140-6736(16)31658-0.

51. Mumme, M.; Steinitz, A.; Nuss, K.M.; Klein, K.; Feliciano, S.; Kronen, P.; Jakob, M.; von Rechenberg, B.; Martin, I.; Barbero, A., et al. Regenerative Potential of Tissue-Engineered Nasal Chondrocytes in Goat Articular Cartilage Defects. *Tissue engineering. Part A* **2016**, *22*, 1286-1295, doi:10.1089/ten.TEA.2016.0159.

52. Lee, C.R.; Sakai, D.; Nakai, T.; Toyama, K.; Mochida, J.; Alini, M.; Grad, S. A phenotypic comparison of intervertebral disc and articular cartilage cells in the rat. *European spine journal : official publication of the European Spine Society, the European Spinal Deformity Society, and the European Section of the Cervical Spine Research Society* **2007**, *16*, 2174-2185, doi:10.1007/s00586-007-0475-y.

53. Lang, G.; Liu, Y.; Geries, J.; Zhou, Z.; Kubosch, D.; Südkamp, N.; Richards, R.G.; Alini, M.; Grad, S.; Li, Z. An intervertebral disc whole organ culture system to investigate proinflammatory and degenerative disc disease condition. *Journal of tissue engineering and regenerative medicine* **2018**, *12*, e2051-e2061, doi:10.1002/term.2636.

List of PhD-thesis Publications

1. Ziadlou R, Rotman S, Teuschl A, Salzer E, Barbero A, Martin I, Alini M, Eglin D, Grad S. **"Optimization of hyaluronic acid-tyramine/silk-fibroin composite hydrogels for cartilage tissue engineering and delivery of anti-inflammatory and anabolic drugs".** *Mater Sci Eng C Mater Biol Appl.* 2021 Jan;120:111701. doi: 10.1016

2. Kamali A, Ziadlou R, Lang G, Pfannkuche J, Cui S, Richards GR, Alini M, Grad S. **"Small molecules-based treatment approaches for intervertebral disc degeneration: Current options and future directions".** Review article. *Theranostics*. 2021 Jan 1;11(1):27-47. doi: 10.7150/thno.48987.

3. Ziadlou R, Barbero A, Stoddart M, Wang X, Qin L, Martin I, Alini M, Grad S. **"Anti-inflammatory and chondroprotective effects of Vanillic acid and Epimedin C in human osteoarthritic chondrocytes".** *Biomolecules,* 2020, 10, 932; doi:10.3390/biom10060932.

4. Meng X, Ziadlou R, Grad S, Alini M, Wen C, Lai Y, Qin L, Zhao Y, Wang X, **"Animal models of osteochondral defect for testing biomaterials".** Review Article. *Biochemistry Research International*. Volume 2020, Article ID 9659412.

5. Cao HJ, Li CR, Wang LY, Ziadlou R, Grad S, Zhang Y, Cheng Y, Lai YX, Yao XS, Alini M, Qin L, Wang XL. **"Effect and mechanism of Psoralidin on promoting osteogenesis and inhibiting adipogenesis"** *Phytomedicine*, 2019 Feb 4;61:152860. doi:10.1016/ j.phymed. 2019.152860. PMID: 31048126.

6. Ziadlou R, Barbero A, Martin I, Stoddart M, Wirth M, Li Z, Wang X, Qin L, Alini M, Grad S. **"Regulation of Inflammatory Response in Human Osteoarthritic Chondrocytes by Novel Herbal Small Molecules"** *Int J Mol Sci*. 2019 Nov 15;20(22). doi: 10.3390/ijms20225745. PMID: 31731767

Acknowledgements

The PhD has been a great experience that allowed me to grow both scientifically and on a personal level. I would have never been able to complete my doctoral studies without the assistance of some very great individuals, who I would like to thank in this section.

I wish to thank my supervisors Prof. Dr. Ivan Martin and Dr. Sibylle Grad for giving me the opportunity to do my PhD in their groups at the University hospital of Basel and AO Research Institute in Davos. I was able to generate this thesis with your great support.

Dear Ivan, during the project meetings that we had over the past years, I have received a lot of valuable input that have helped me to continue my path on the right track. Thanks a lot for being always responsive and supportive to discuss the issues.

Dear Sibylle, thanks a lot for always being supportive in the past years. You were always reachable to discuss any issue and you have been responsive for the problem solving. During our many meetings, you always had valuable points of view to improve the work which helped me to continue on the right path.

Much gratitude goes towards Prof. Dr. Mauro Alini, who as head of the Musculoskeletal Regeneration program gave me the opportunity to start my PhD in AO Research Institute in Davos. Thanks a lot for your support in terms of scientific feedback and advice. Your warm personality made the whole research program feel like a close-knit family. Thanks for creating a very pleasant work environment which made my stay very pleasant and I felt like I am at home in Davos.

I would like to express my gratitude to Dr. Laura Creemers, for being a member of my PhD committee. Thanks a lot for your valuable inputs on my project and your time for reading and assessing this doctoral thesis.

I would like to thank Prof. Dr. Andrea Barbero for his valuable inputs and guidance during past years. I learned a lot from you in each project meeting we had together and always your great suggestions were very beneficial for improvement of the thesis outcome.

I am very grateful to Prof. David Eglin, for his support and guidance in a very interesting project which I did next to my main PhD project. I could learn lots of new techniques and to get more familiar with the field of biomaterials and biomechanics.

I also would like to thank our Chinese partners Dr. Xinluan Wang and Prof. Dr. Ling Qin in Translational Medicine R&D Center, Chinese Academy of Science in Shenzhen (SIAT) and University of Hong Kong, for giving me the opportunity to visit their lab and the great collaboration that we had during past years.

I would also like to thank my many friends that I have met during my PhD. During my time in Davos and Basel I have made some wonderful friendships, and even though many of you are now scattered all over the world, I greatly appreciated our time together. I am sure that we will keep in touch in the years to come.

I would like to thank my family who has been a great support to me in many different regards and I am really grateful to them.

Finally, I would like to thank my husband for all the support that he gave me throughout the years of work that went into this thesis.

Reihane